FORMATION DAMAGE DUE TO CO_2 SEQUESTRATION IN SALINE AQUIFERS

A Dissertation

by

IBRAHIM MOHAMED MOHAMED

Submitted to the Office of Graduate Studies of
Texas A&M University
in partial fulfillment of the requirements for the degree of

DOCTOR OF PHILOSOPHY

Approved by:

Chair of Committee,	Hisham A. Nasr-El-Din
Committee Members,	Gioia Falcone
	Jerome J. Schubert
	Mahmoud El-Halwagi
Head of Department,	A. Daniel Hill

December 2012

Major Subject: Petroleum Engineering

ABSTRACT

Carbon dioxide (CO_2) sequestration is defined as the removal of gas that would be emitted into the atmosphere and its subsequent storage in a safe, sound place. CO_2 sequestration in underground formations is currently being considered to reduce the amount of CO_2 emitted into the atmosphere. However, a better understanding of the chemical and physical interactions between CO_2, water, and formation rock is necessary before sequestration. These interactions can be evaluated by the change in mineral content in the water before and after injection, or from the change in well injectivity during CO_2 injection. It may affect the permeability positively due to rock dissolution, or negatively due to precipitation.

Several physical and chemical processes cover the CO_2 injection operations; multiphase flow in porous media is represented by the flow of the brine and CO_2, solute transportation is represented by CO_2 dissolution in the brine forming weak carbonic acid, dissolution-deposition kinetics can be seen in the rock dissolution by the carbonic acid and the deposition of the reaction products, hydrodynamic instabilities due to displacement of less viscous brine with more viscous CO_2 (viscous fingering), capillary effects and upward movement of CO_2 due to gravity effect.

The objective of the proposed work is to correlate the formation damage to the other variables, i.e. pressure, temperature, formation rock type, rock porosity, water composition, sulfates concentration in the water, CO_2 volume injected, water volume injected, CO_2 to water volumetric ratio, CO_2 injection rate, and water injection rate.

In order to achieve the proposed objective, lab experiments will be conducted on different rock types (carbonates, limestone and dolomite, and sandstone) under pressure and temperature that simulate the field conditions. CO_2 will be used at the supercritical phase and different CO_2-water-rock chemical interactions will be addressed. Quantitative analysis of the experimental results using a geochemical simulator (CMG-GEM) will also be performed.

The results showed that for carbonate cores, maintaining the CO_2/brine volumetric ratio above 1.0 reduced bicarbonate formation in the formation brine and helped in minimizing precipitation of calcium carbonate. Additionally, increasing cycle volume in WAG injection reduced the damage introduced to the core. Sulfate precipitation during CO_2 sequestration was primarily controlled by temperature. For formation brine with high total dissolved solids (TDS), calcium sulfate precipitation occurs, even at a low sulfate concentration.

For dolomite rock, temperature, injection flow rate, and injection scheme don't have a clear impact on the core permeability, the main factor that affects the change in core permeability is the initial core permeability.

Sandstone cores showed significant damage; between 35% and 55% loss in core permeability was observed after CO_2 injection. For shorter WAG injection the damage was higher; decreasing the brine volume injected per cycle, decreased the damage. At higher temperatures, 200 and 250°F, more damage was noted than at 70°F.

DEDICATION

To my parents, my wife Aya, and my son Tamim, for their persistent love and spiritual support in my life.

ACKNOWLEDGEMENTS

I would like to take this opportunity to express my deepest gratitude and appreciation to my advisor and committee chair, Dr. Hisham A. Nasr-El-Din, for his continuous encouragement and especially for his academic guidance.

Appreciation is extended to the members of my committee, Dr. Gioia Falcone, Dr. Jerome J. Schubert, Dr. Mahmoud El-Halwagi, for their help.

I also would like thank my colleagues, Jia He and Salaheldin Elkatatny, for their help during my graduate study. Ms. K. Brady is acknowledged for proof reading this dissertation.

Finally, I would like to acknowledge the financial support of the Texas A&M U., the Texas Engineering Experiment Station of Texas A&M University and Crisman Institute for Petroleum Research. The facilities and resources provided by the Harold Vance Department of Petroleum Engineering of Texas A&M University are gratefully acknowledged.

TABLE OF CONTENTS

Page

LIST OF FIGURES

LIST OF TABLES

1. INTRODUCTION

Greenhouse gases (water vapor, carbon dioxide, methane, nitrous oxide, and ozone) (Karl and Trenberth, 2003), are the gases that are responsible for absorbing and emitting radiation within the thermal infrared range. Since the industrial era started in the 1750's the greenhouse gas levels in the atmosphere have been increasing. The global warming phenomena started to take place, due to the increase of the greenhouse gas concentrations in the atmosphere. Mitigation of global warming is necessary to keep the greenhouse gas concentrations at certain levels, and limit the increase of the global temperature.

The concentration of CO_2 has increased by 36% (EPA, 2008) since the 1750's, and the concentration is continuing to rise due to burning of fossil fuels and land-use change. Carbon capture and storage (CCS) has been proposed to mitigate the accumulation of CO_2 in the atmosphere. Although CO_2 is captured from a large point source and stored in an underground formation (depleted oil reservoir, water aquifer, or salt cavern), in order to reduce the effect of global warming, CO_2 has also been injected for various purposes, like in enhanced oil recovery (EOR), and enhanced coal bed methane (ECBM) recovery. Reduction in well injectivity, from 10 up to 100%, is always noted once CO_2 is injected into the reservoir (Grigg and Svec 2003).

CO_2 bathes through different reactions with the formation brine and formation rock (carbonate or sandstone). A summary of the important CO_2 chemical reactions with formation brine and formation rock is shown in **Table 1.1**. These reactions tend to

dissolve part of the formation rock and enhance the well productivity, due to increasing the near wellbore region permeability. Bicarbonate produced from most of these reactions is water soluble, but with continuous dissolution, bicarbonate concentration increases and starts to precipitate, causing formation damage and the loss of well injectivity (Izgec et al. 2005). The solubility of CO_2 depends on the incubation period of contact (Bahara and Liu 2008)

TABLE 1.1— CO_2 CHEMICAL REACTIONS WITH FORMATION BRINE AND DIFFERENT ROCK TYPE, (WELLMAN ET AL. 2003)

$CO_2 + H_2O \leftrightarrow H_2CO_3$
$CaCO_3 + H_2CO_3 \leftrightarrow Ca^{+2} + 2HCO_3^-$
$CaMg(CO_3)_2 + 2H_2CO_3 \leftrightarrow Ca^{+2} + Mg^{+2} + 4HCO_3^-$
$MgCO_3 + H_2CO_3 \leftrightarrow Mg^{+2} + 2HCO_3^-$
$Halite \leftrightarrow Na^+ + Cl^-$
$Anhydrite \leftrightarrow Ca^{+2} + SO_4^{-2}$

The primary factor that affects the formation injectivity during CO_2 injection is the formation rock type (carbonate or sandstone). The sandstone and carbonate systems initially performed similarly. This changed when, through dissolution of the rock matrix, a solution channel was formed in the limestone, creating a dominant flow path that significantly altered the flow behavior (Grigg et al. 2008). Increase in Ca^{2+}, Mg^{2+}, K^+, SO_4^{2-}, HCO^{3-}, and CO_2 concentrations were noticed during monitoring. The produced aqueous fluids and gases confirm the dissolution effect of the CO_2 injection (Raistrick et al. 2009).

1.1 Solubility of CO_2

Carroll et al. (1991) developed a correlation, based on experimental data, to calculate the solubility of CO_2 in water at a pressure below 1 MPa and temperature range between 273 and 433°K;

$$\ln(H) = -6.8346 + \frac{1.2817 * 10^4}{T} - \frac{3.7668 * 10^6}{T^2} + \frac{2.997 * 10^8}{T^3} \quad (1.1)$$

H = Henry's constant, MPa/molar fraction

T = temperature, °K

The effect of dissolved solids on the CO_2 solubility in water is studied by Enick and Klara (1989). They developed a correlation to calculate the solubility of CO_2 in water that is applicable at reservoir conditions, taking into consideration the effect of dissolved solids. They assumed that the solubility only depended on TDS regardless the salt type, Henry's constant for distilled water:

$$H^* = -5032.99 + 30.74113\,T - 0.052667\,T^2 + 2.630218 * 10^{-5} T^3 \quad (1.2)$$

Effect of total dissolved solids (TDS):

$$w_{CO_2} = w_{CO_2 w} * \begin{pmatrix} 1.0 - 4.893414 * 10^{-2} * TDS + \\ 0.1302838 * 10^{-2} * TDS^2 - 0.1871199 * 10^{-4} * TDS^3 \end{pmatrix} \quad (1.3)$$

Where;

H* = Henry's constant, bar/molar fraction

T = temperature, °K

T_R = reduced temperature (=T/Tc, where Tc is the critical temperature of water, 647°K)

TDS = total dissolved solids, weight percent

w_{co2w} = solubility of CO_2 in distilled water, weight fraction

w_{co2} = solubility of CO_2 in brine, weight fraction

The solubility of CO_2 in distilled water, and NaCl and $CaCl_2$ brines used in this study, at a pressure of 1300 psi and temperature of 200°F, was obtained from Nighswander et al. (1989), Duan et al. (2006), and Prutton and Savage (1945). Their work was specific for NaCl and $CaCl_2$ brines, while the solubility of CO_2 in $MgCl_2$ brine and seawater was calculated using Eq. 1.3.

1.2 WAG Injection of CO_2

CO_2 is usually stored in formations deeper than 2500 ft (Meggyesy et al 2008). At that depth, the pressure aids in keeping CO_2 in dense super critical fluid phase, as well as trapped in geological formations in four forms:

2. Structural and startigraphical trapping: the CO_2 is trapped as a mobile fluid by an impermeable cap rock that prevents it from moving upward (Bachu and Adams, 2003)
3. Residual CO_2 trapping: the CO_2 phase becomes disconnected and forms an immobile fraction, (Flett et al., 2004)
4. Solubility trapping: injected CO_2 dissolves in the brine, (Pruess and Garcia, 2003)
5. Mineral trapping: dissolved gases are precipitated as minerals, (Gunter et al., 1997)

Nghiem et al. (2009) stated that the two most important trapping mechanisms are residual gas trapping and solubility trapping, because the risk of gas escape from the cap rock or sealing fault is less.

Continuous CO_2 injection, simultaneous water and CO_2 injection (SWAG), and water alternating CO_2 injection (WAG) are three injection schemes that were used in this CO_2 injection project. This study will focus on WAG injection, because of the higher percentage of CO_2 being stored by the residual trapping under WAG injection (Juanes et al. 2006, Pentland et al. 2011). A simulation study run by Delshad et al. (2010) showed that the same mass of CO_2 injected at the average pressure, was less in WAG injection, which means more storage capacity was still available, while SWAG injection reduces the storage capacity and raises the reservoir pressure quickly.

1.3 Previous Work

CO_2 sequestration in carbonate aquifers showed either a permeability improvement or reduction. The change in rock properties is case dependent because it is related to distribution of pores, brine composition, and thermodynamic (Izgec et al. 2006). The precipitation process of dissolved material can impact the permeability, while a small change in porosity is observed (Grigg and Svec 2003). Permeability and porosity alterations showed similar trends at different temperatures (Izgec et al. 2005). The dissolution pattern was found to be dependent on the injection rate and brine composition; high flow rates give longer wormholes, while low flow rates lead to compact dissolution (Egermann et al. 2005).

Krumhansl et al. (2002) found that as the pressure increases, dissolution of calcite increases as well. Grigg and Svec (2003) found that CO_2 injection in carbonate rocks enhances the permeability of the core segment close to the inlet, due to wormhole formation, and that as moving toward the core outlet, the permeability will be reduced because of the damage due to calcium carbonate precipitation.

When the formation brine or the displacement brine contains SO_4^{2-} calcium sulfate will precipitate (Egermann et al. 2005). This reaction is governed by Eq. 3:

$$Ca^{2+} + SO_4^{2-} + xH_2O \rightarrow CaSO_4 \cdot xH_2O \quad (1.4)$$

Where x equal to 0 (anhydrite), ½ (hemihydrate), or 2 (gypsum).

Krumhansl et al. (2002) concluded that with continuous dissolution of calcite, calcium saturation will increase and calcium sulfate precipitation will take place inside the core. This kind of precipitation is temperature dependent. At temperatures lower than 40°C, gypsum is the stable form, while at higher temperatures, anhydrite is the stable product. Hemihydrate is a metastable phase (Meijer and Van Rosmalen 1984).

Several publications in literature have discussed the relative permeabilities for CO_2/brine systems (Dria et al. 2003, Bennion and Bachu 2006; 2008, Perrin et al. 2009). Their results showed that for lower core permeability, higher relative permeability for dense CO_2 was shown at residual water saturation (endpoint), and for the same carbonate formation, the lower the permeability, the less CO_2 can be injected into the formation. Grigg and Svec (2008) estimated that the removal of CO_2 saturation is more difficult and takes more time than establishing it.

Watts et al. (1982) reported that WAG injection of CO_2 in the Hilly Upland oil field, which was composed mainly of low permeability carbonate rock (permeability reported was 6.1 maximum, and less than 0.1 md minimum), caused an increase in the injection pressure. The static bottomhole pressure was 635 psi, CO_2 injection pressure was 1,252 psi at an injection rate of 70 RB/D, and water injection pressure was 1,850 psi at an injection rate of 7 B/D.

Pure carbonate formations that don't contain silicate or aluminosilicate minerals don't provide good mineral trapping for CO_2. Carbonate reactions tend to reach an equilibrium condition while the silicate reactions occur because of the higher reaction rate constant for carbonate minerals compared to silicates (Gunter et al. 2000). Grigg and Svec (2003) stated that no carbonate deposition was noted during WAG injection of CO_2 into dolomite cores, while significant carbonate was deposited downstream for limestone cores.

Injection of CO_2 in low pressure dolomite and sandy dolomite reservoirs (150 psi) did not affect well injectivity (Bardon et al. 1994). Morgenthaler et al. (1993) showed that CO_2 injection in the Permian Basin San Andres dolomite reservoir (95% dolomite, and 5% anhydrite) increased brine scaling tendency in the producing wells. Analyzing produced brines showed that there was an increase in calcium bicarbonate and calcium sulfate concentrations. Gypsum scaling is problematic at bottomhole conditions, while the scales at surface conditions are mostly calcite.

Grigg and Svec (2003) conducted coreflood studies on vuggy anhydritic dolomite and Indiana limestone rocks. Dissolution was noted in both rock types. For

dolomite, dissolution of anhydrite occurred during brine injection, while dolomite dissolution occurred during WAG injection. For limestone, calcium carbonate dissolution occurred during WAG injection.

Omole and Osoba (1983) tested the effect of CO_2 injection pressure on the interaction of CO_2 and dolomite cores. Different pressures were examined, dolomite cores with a diameter of 2.25 in. and lengths ranging between 3 and 9 in. were used, and the cores were initially saturated with 0.1 M NaCl. CO_2 was injected with an injection flow rate of 10 cm^3/hr, pressure ranged between 1000 and 2500 psig, and temperature was kept constant at 80°F. Their results showed that CO_2 dissolved the rock around the injection face, and increasing the pressure increases the rock dissolution. Dissolved carbonate will tend to precipitate along the flow bath as the pressure drops. Injection of CO_2 in deep saline carbonate aquifers will cause a reduction in the near wellbore porosity by 5-17% (Taberner et al. 2009)

Wellman et al. (2003) conducted a coreflood experiment using a core that had a mineral composition of 67% dolomite and 20% anhydrite. Experiments were run at a temperature of 38°C and back pressure of 13.79 Mpa. The total volume of CO_2 and brine injected was 145 liters. The results showed that the permeability increased from 30.6 to 200 md, while porosity increased from 13 to 21 vol%. Kamath et al. (1998) concluded that during WAG injection of CO_2 in dolomite formations, water injectivity was comparable to the initial waterflood injectivity, and increased as it dissolved the trapped CO_2, while the injectivity of CO_2 was higher than the initial waterflood injectivity.

Dissolution rate of dolomite and calcite rock, due to the reaction with CO_2, was studied by Pokrovsky et al. (2005; and 2009). They developed an empirical correlation to calculate calcite and dolomite dissolution rate at temperatures from 25 to 150°C, partial pressure of CO_2 (pCO_2) ranging between 10 and 50 atm, and 1 M NaCl solution as follows;

$$\log(K) = A + B\ x\ pCO_2 + C\ x\ (pCO_2)^2 \quad (1.5)$$

Where;

K = dissolution rate, $mol.cm^{-2}.s^{-1}$

A, B, and C = empirical parameters depend on temperature and pH

pCO_2 = partial pressure of CO_2, atm

The chemical reactions between carbonic acid and formation rock are much simpler in carbonate rock than in sandstone formations. In sandstone, the surface reaction rates are slow, and relatively uniform rock dissolution through the porous medium will result (Wellman et al. 2003). In carbonates, the surface reaction rates are higher, leading to nonuniform dissolution patterns, and wormhole channels will be created (Izgec et al. 2006).

Weyburn oil field in Canada is a sandstone reservoir in which CO_2 was used for EOR purposes. Monitoring of the produced brines showed an increase in $Ca^{2+,}$ Mg^{2+}, K^+, SO_4^{2-}, HCO^{3-}, and CO_2 concentrations, due to the dissolution of calcite, dolomite and K-feldspars (Raistrick et al. 2009).

The effect of the chemical reactions on sandstone permeability during CO_2 injection into sandstone formations has been studied by Sayegh et al. (1990). 5 wt%

NaCl brine saturated with CO_2 at 13.8 MPa was injected into sandstone cores from the Pembina Cardium reservoir, at 45°C. A reduction in core permeability was noted due to the dissolution of calcite and siderite, and migration of the fines, which were originally bonded to the rock by the carbonate cementing minerals. Nightingale et al. (2009) analyzed a sample from the reservoir rock before and after CO_2 injection, the analysis showed that a degradation of clay and feldspar grains, and a partial to complete removal of carbonate cements occurred, and residual clays were found in the rock sample after CO_2 injection.

Liu et al. (2003) concluded that in presence of CO_2, the dissolution of sandstone formations and the deposition of secondary minerals are enhanced by increasing the temperature. Fischer et al. (2010) conducted long term lab experiments on Stuttgart formation sandstone samples, at reservoir conditions (5.5 MPa, 40°C). The samples were mainly quartz and plagioclase with minor mineral phases, such as K-feldspar, hematite, muscovite, biotite, illite, chlorite and opaque. Analcime, dolomite and anhydrite are only found as cement phases. Dissolution of calcium-rich plagioclase, K-feldspar and anhydrite and precipitation of albite was observed. This is also confirmed by Wigand et al. (2009).

Precipitation of quartz, kaolinite, illite, chlorite, albite, siderite and Fe-chlorite were noted by Bertier et al. (2006). Their experiments confirmed that carbonate dissolution and precipitation occurred during CO_2 injection into sandstone rock, and reactions with Al-silicates were also observed.

Warner (1977) conducted a simulation study to address the effects of CO_2: brine volumetric ratio in WAG injection on the oil recovery from the Little Creek sandstone reservoir. The volumetric ratio examined in his study was 1:0 (continuous CO_2 injection), 1:1, 1:2, and 1:3. The results showed that increasing the volume of brine per cycle will increase the oil recovery. The chemical interaction between CO_2/rock/brine wasn't taken into consideration in his study.

1.4 Objectives

Literature review indicated that there is a chemical interaction between CO_2/water/rock. No study discussed the effect of different parameters, such as: pressure, temperature, injection flow rate, injection scheme, lithology, and rock heterogeneity on these interactions and how they affect the rock permeability. The objective of this study is to address the effects of the previous parameters on the formation rock during CO_2 injection into a saline aquifer. In order to achieve these objectives two main studies were conducted.

Coreflood study: The aim of this part of the study was to experimentally examine the dissolution/precipitation phenomena during CO_2 injection, and as a result, the change in core permeability. Core plugs from different rock types, i.e. Pink Desert limestone, Austin chalk, high permeability Indiana limestone, low permeability Indiana limestone, Silurian dolomite, and Berea sandstone.

Brines used in this study include, seawater, no sulfate seawater, high salinity formation brine, distilled water, and 1, 5, and 10 wt% NaCl, $CaCl_2$ and $MgCl_2$ brines.

Cores used in this study had dimensions of 6 in. length and 1.5 in. diameter. CO_2 was injected under supercritical conditions: pressure > 1071 psi and temperature above 88°F.

Simulation Study: A commercial geochemical simulator (CMG-GEM) was used to quantitatively confirm the experimental results. A field scale simulation will be run to study the effects of the examined parameter on the CO_2 trapping for a simple reservoir model.

2. EXPERIMENTAL STUDY

2.1 Test Design

The coreflood tests were designed to simulate WAG injection of CO_2 into saline aquifers. A slug of pure CO_2 (purity 99.8%) was used in the first half of the WAG cycle, while a slug of synthetic was injected in the second half. Different brines were used in this study, and tests were run at temperatures of 70, 100, 200, and 250°F. Back pressure was kept constant at 1300 psi for all experiments. Effluent samples were collected throughout the experiment; every 3 minutes during brine injection, while during CO_2 injection the first 2 samples were collected every 3 minutes, and the third sample at the end of the CO_2 half cycle.

2.2 Coreflood Setup

A Syringe Pump model ISCO 1000D was used to displace the fluids from the piston accumulators. Two stainless steel piston accumulators, with a capacity of 2 liters each, were used to store the synthetic brine and liquid CO_2. Swagelok valves model SS-41S21 were installed at the accumulator's outlet to control the fluids alternating during WAG injection. To monitor the pressure at the core inlet, a pressure gauge was installed at the coreholder inlet. A Phoenix Instruments Hassler type core holder was used to hold the core during the coreflood test. A Mity Mite backpressure regulator (S91W) was installed at the core outlet to maintain the outlet pressure at 1300 psi and keep the CO_2 in the supercritical phase.

Highly Saturated Nitrile (HSN) rubber sleeves were used to resist CO_2 diffusion into overburden fluids. An Enerpac P-392 hand pump was used to apply overburden pressure around the core; the overburden pressure was kept 500 psi higher than the core inlet pressure. A pressure transducer was used to measure the pressure drop across the core, and the data was sent through a data acquisition system to a computer that records the data through LabView software.

During injection, fluid was preheated in the lines by using a compact bench top CSC 32 series, installed on the coreholder upstream line, and the core was heated using heat jackets that were installed around the core holder. **Fig. 2.1** shows a schematic diagram of the coreflood setup.

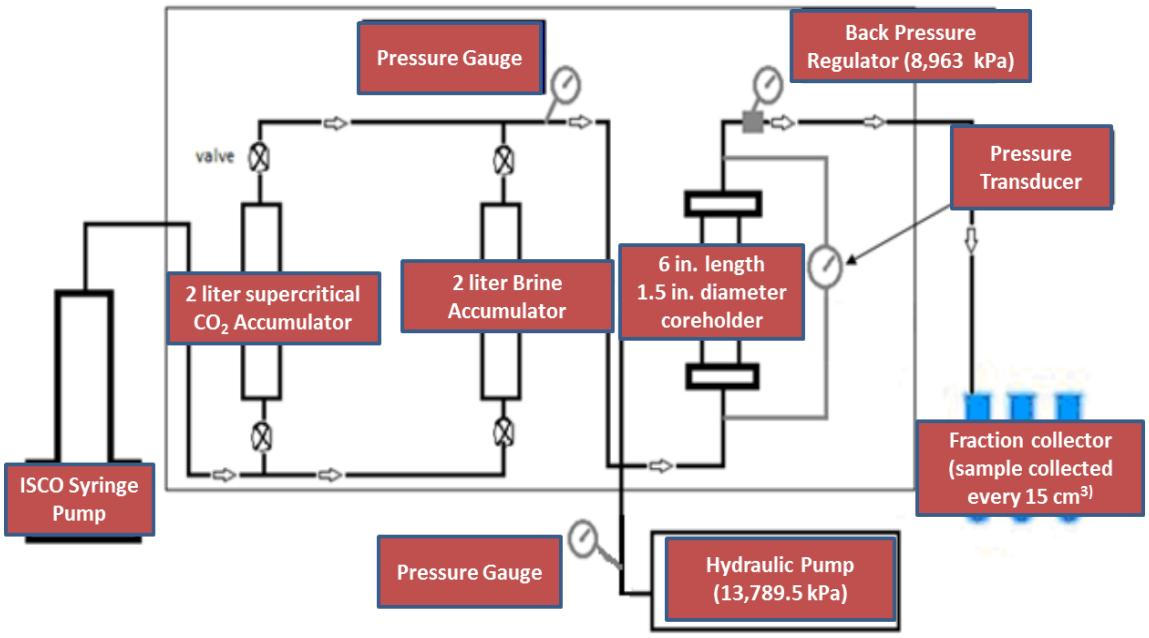

Fig. 2.1—Coreflood setup.

2.3 Core Preparation

Core rock from different locations and lithologies were used in this study. XRF analysis was run to define the elemental composition of these rocks. The cores were dried in an oven for 5 hours at 257°F. The cores were then saturated with brine. The cores were weighed dry, and saturated with brine. Pore volume and core porosity were calculated from the weight difference of the dry and saturated core.

2.4 Experimental Procedure

The core was placed inside the coreholder and brine was injected at room temperature, the pressure drop across the core was monitored and the stabilization pressure was used to calculate the permeability using Darcy's equation for linear and laminar flow. Then, heaters were turned on until the whole system was heated to the required temperature.

CO_2 was injected at a constant rate for a certain pore volume, followed by brine (one WAG cycle), until the total number of WAG cycles was injected. Once the system was cooled down, the permeability and porosity of the core was measured again the same way mentioned before. Composition of the core effluent samples was analyzed using Inductively Coupled Plasma Optical Emission Spectrometry (Optima 7000 DV ICP-OES). Sulfate concentration was measured using a SP600 Spectrophometer. The elemental composition of the precipitated particles was analyzed by XRD, XRF, and SEM. A new core was used for each experiment.

3. MODELING STUDIES

To confirm the experimental results, a simulation study was conducted to predict the experimental results in core scale using a commercial compositional simulator package (CMG-GEM). The input parameters are the core dimensions, injection schedule, relative permeability, capillary pressure, chemical kinetics of the chemical reactions between rock minerals, brine, and CO_2, and initial core properties (porosity and permeability). The simulator uses these data to calculate the change in core porosity across the core due to chemical reactions and pressure changes. The new porosity values were used by either Carman-Kozeny or power-law equations to predict the new permeability using an appropriate exponent. A detailed discussion about the calculations sequence is shown in this section.

A cylindrical core was divided into radial grid blocks with 5X20X20 blocks in the r, Θ, and z directions, respectively. Initially, the porosity and permeability were assumed to be constant for all grids.

3.1 Relative Permeability Calculations

Relative permeability (**Eqs. 3.1 and 3.2**) were adjusted to match the experimental pressure drop.

$$k_{rw} = k_{rwi}\left(\frac{S_w - S_{wi}}{1 - S_{wi}}\right)^{N_w} \tag{3.1}$$

$$k_{rCO2} = k_{rCO2i}\left(\frac{S_{CO2} - S_{CO2i}}{1 - S_{CO2i} - S_{wi}}\right)^{N_{CO2}} \tag{3.2}$$

Where;

k_{rw} = relative permeability to brine

k_{rwi} = relative permeability of brine at irreducible CO_2 saturation

k_{rCO2} = relative permeability to CO_2

k_{rCO2i} = relative permeability of CO_2 at irreducible brine saturation

S_w = brine saturation

S_{wi} = irreducible brine saturation

S_{CO2} = CO_2 saturation

S_{CO2i} = irreducible CO_2 saturation

N_w = brine exponent

N_{CO2} = CO_2 exponent

3.2 Capillary Pressure Calculations

Capillary pressure is a function of porosity, permeability, interfacial tension, and wetting-phase saturation. The model developed by El-Khatib (1995) was used to calculate the capillary pressure curves for the carbonate cores used in the present study, since this equation could be used for any kind of rock by adjusting the saturation exponent (b);

$$P_c = \frac{1}{\sqrt{2\tau}}\left(\frac{1}{\sqrt{2b+1}}\right)\left(\frac{(1 - S_{wi})^{b+0.5}}{(S_w - S_{wi})^b}\right)\left(\frac{\sigma \quad Cos\theta}{\sqrt{k/\phi}}\right) \tag{3.3}$$

Where;

b = saturation exponent

k = absolute permeability, m^2

P_c = capillary pressure, Pa

S_w = brine saturation

S_{wi} = irreducible brine saturation

τ = tortuosity

θ = contact angle

σ = interfacial tension, N/m

ϕ = porosity, volume fraction

For all rocks used in this study, the saturation exponent (b) used was 1.077, which is the average value proposed by El-Khatib (1995). The tortuosity values were calculated based on the core porosity by **Eq. 3.4** (Boving and Grathwohl 2001):

$$\tau = \phi^{-1.2} \tag{3.4}$$

Interfacial tension between CO_2 and seawater was obtained at the experimental conditions from Shariat et al. (2012) measurements. The irreducible water saturation (S_{wi}) was obtained from the coreflood experiments. Contact angle between CO_2 and brine was adjusted in order to match the experimental results.

3.3 Dissolution and Precipitation Calculations

The rate law for mineral dissolution and precipitation reactions (Sorensen et al. 2009):

$$r_\beta = k_\beta A_\beta \left[1 - \left(\frac{Q_\beta}{K_\beta} \right) \right] \tag{3.5}$$

Where;

$$k_\beta = k_{0\beta} \exp\left[-\frac{E_{a\beta}}{R} \left(\frac{1}{T} - \frac{1}{T_0} \right) \right] \tag{3.6}$$

A_β = reactive surface area for mineral β, m^2

$E_{a\beta}$ = activation energy for reaction of CO_2 with mineral β, J/mol

K_β = chemical equilibrium constant

$k_{0\beta}$ = rate constant of reaction of CO_2 with mineral β at reference temperature T_0, $mol/m^2.s$

k_β = rate constant of reaction of CO_2 with mineral β at temperature T, $mol/m^2.s$

Q_β = ion activity product

R = universal gas constant = 8.31 J/mol.°K

r_β = Reaction rate, $mole/m^2.s$

T = temperature, °K

The ratio (Q_β/K_β) is called the saturation index of the reaction. Dissolution occurs when this value is greater than 1.0, and precipitation takes place when this value is less than 1.0.

3.4 Porosity and Permeability Calculations

The porosity changes due to mineral dissolution and precipitation are governed by **Eqs. 3.7 and 3.8**:

$$\bar{\phi}^{*} \equiv \phi^{*} - \sum_{\beta=1}^{n_m} \left(\frac{N_\beta}{\rho_\beta} - \frac{N^{0}{}_\beta}{\rho_\beta} \right) \tag{3.7}$$

$$\phi = \bar{\phi}^{*} \left[1 + c_\phi (p - p^{*}) \right] \tag{3.8}$$

Where;

$c_ø$ = pores compressibility, kPa^{-1}

N_β = total moles of mineral β per bulk volume at the current time, mole

N^0_β = total moles of mineral β per bulk volume at the time 0, mole

p = current pressure, kPa

p^* = reference pressure, kPa

ϕ = porosity, fraction

$\bar{\phi}^{*}$ = reference porosity including mineral precipitation/dissolution, fraction

ϕ^{*} = reference porosity without mineral precipitation/dissolution, fraction

ρ_β = mineral molar density, mole

A change in porosity will yield a change in the absolute permeability. The power-law (**Eq. 3.9**) and Carman-Kozeny (**Eq. 3.10**) were used to calculate the permeability based on the initial and final permeabilities and porosities;

$$k = k_0 \left(\frac{\phi}{\phi_0} \right)^{n} \tag{3.9}$$

$$k = k_0 \left(\frac{\phi}{\phi_0} \right)^{m} \left(\frac{1 - \phi_o}{1 - \phi} \right)^{2} \tag{3.10}$$

Where n is the power-law exponent, and m is the Carman-Kozeny exponent. k and k_0 are the current and original permeabilities. ϕ and ϕ_0 are the current and original porosities.

4. PERMEABILITY ALTERNATION AND TRAPPING MECHANISMS DURING CO_2 INJECTION IN HOMOGENOUS LIMESTONE AQUIFERS: LAB AND SIMULATION STUDIES

Carbon dioxide sequestration in underground formations is being considered on a massive scale to reduce the amount of CO_2 emitted into the atmosphere. However, a better understanding of the chemical and physical interactions with formation fluids and rock is necessary before implementing sequestration in a depleted reservoir, aquifer, or during enhanced oil recovery operations. These interactions are affected by many parameters, including pressure, temperature, brine salinity, and CO_2 injection rate. They can be evaluated by the change in water composition before and after injection, or from the change in CO_2 injectivity over time. CO_2 may affect the permeability positively due to carbonate rock dissolution, or negatively due to precipitation of reaction products, mainly $CaCO_3$.

CO_2 dissolves in the formation brine, generating carbonic acid, which dissolves carbonate rock. Dissolution impacts brine composition, which affects solubility. Calcium carbonate may tend to precipitate with changing the concentration of bicarbonates. Precipitation may occur in either EOR operations or during primary CO_2 sequestration. Injectivity changes are a concern during EOR operations, while storage capacity and seal integrity are primary concerns during CO_2 sequestration. This chapter addresses experimentally and numerically the effects of the reservoir pressure, CO_2 volume, CO_2 to brine volumetric ratio, injection rate, and temperature on the

permeability of calcite aquifers and trapping mechanism of carbon dioxide during CO_2 sequestration.

4.1 Introduction

A coreflood study was conducted using limestone cores. CO_2 was injected under supercritical conditions at pressures of 700 and 1300 psi, and temperatures of 70, 100, and 200°F. Core effluent samples were collected and the concentrations of key ions were measured.

A numerical simulator (CMG-GEM) was used to confirm the experimental results. Power-law and Carman-Kozeny models were calibrated to predict the changes in permeability based on the changes in porosity. The chemical reaction that govern the reactions between CO_2 and calcite is given in **Table 1.1**

4.2 Materials

Cylindrical Pink Desert limestone cores with dimensions of 6 in. length and 1.5 in. diameter were used in all experiments. Core properties are given in **Table 4.1**. CO_2 with a purity of 99.8% was used to avoid introducing contaminants into the cores. A synthetic brine, **Table 4.2**, was used. It had total dissolved solids (TDS) of 35,884 ppm, pH 6.4, and a viscosity of 1.04 cp, at room temperature. Deionized water with a resistivity of 18.2 MΩ.cm at room temperature was used to prepare the synthetic brines. Reagent grade salts were used to prepare these brines.

Table 4.3 gives a summary of coreflood experiments, which were conducted to examine the effects of reservoir pressure, CO_2 volume, and CO_2 to brine volumetric ratio on the permeability changes.

Table 4.1— PROPERTIES OF THE PINK DESERT CORES.

Core #	Porosity (Vol%)	Permeability (md)
1	19.6	61.8
2	22.0	101.0
3	18.5	44.0
4	17.5	52.0
5	20.7	67.0
6	20.1	102.0
7	19.1	54.5
8	17.8	42.0
9	18.8	57.0
10	20.0	68.2
11	19.5	60.6
12	19.6	78.0
13	19.5	68.2
14	17.5	57.6
15	20.5	69.6
16	20.4	81.9
17	19.5	81.9
18	20.3	60.6
19	19.8	79.8
20	18.8	74.5

4.3 Results and Discussion

The reference case (back pressure = 1,300 psi, CO_2: brine volumetric ratio = 1:1, and CO_2 volume injected= 5 PV/cycle for 3 cycles) showed that there was a slight reduction in permeability and porosity: 2% reduction in permeability and 7% reduction

in porosity. Fig. 4.1 shows the pressure drop across the core during the sequestration experiment. Since CO_2 viscosity is 17 times lower than brine viscosity (CO_2 viscosity was 0.021 cp, while brine viscosity was 0.36 cp at the experiment conditions), it has higher mobility than brine. This explains the sudden increase in the pressure observed in Fig. 4.1 when alternating from CO_2 to brine, which indicated a lower mobility phase (brine) started to flow in the core displacing higher mobility phase (CO_2). As brine saturation increased, the pressure decreased, since the relative permeability to brine increased. The last cycle showed a gradual increase in the pressure drop across the core, which indicated that precipitation was taking place inside the rock. The final pressure drop was 7.5 psi, which was higher than the initial pressure (6 psi).

Table 4.2— CONCENTRATION OF KEY IONS IN SYNTHETIC BRINE.

Ion	Concentration (mg/l)
Cl^-	22,010
Na^+	12,158
Mg^{++}	1,315
Ca^{++}	401
Total Dissolved Solids	35,884

The viscosity of CO_2 was obtained from Fenghour et al. (1997) tables, while the viscosity of brine used in this study was calculated using **Eqs. 4.1** through **4.3**, Meehan (1980), at a temperature of 200°F and pressure of 1300 psi.

$$\mu_w = \mu_{wT}\left(0.9994 + 4.0295\times10^{-5}P + 3.1062\times10^{-5}P^2\right) \quad (4.1)$$

$$\mu_{wT} = \left(109.574 - 8.40564\, w_s + 0.313314\, w_s^2 + 8.72213\times10^{-3}\, w_s^3\right) T^{-D} \quad (4.2)$$

With

$$D = 1.12166 - 0.0263951\, w_s + 6.79461\times10^{-4}\, w_s^2 + 5.47119\times10^{-5}\, w_s^3 - 1.55586\times10^{-6}\, w_s^4 \quad (4.3)$$

Where;

P = pressure, psi

T = temperature, °F

w_s = weight percent of salt in brine

μ_w = brine viscosity at P and T, cp

μ_{wT} = brine viscosity at 14.7 psi and T, cp

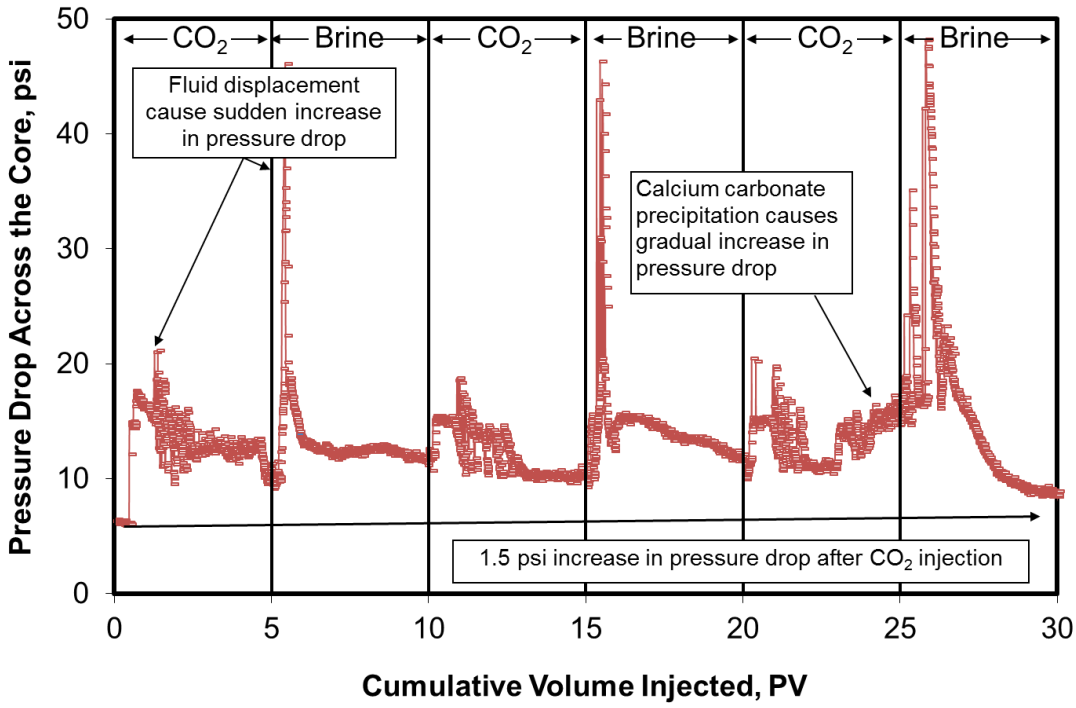

Fig. 4.1—Pressure drop across core #1 during CO_2 WAG injection (Reference case).

Table 4.3— SUMMARY OF COREFLOOD EXPERIMENTS							
Experiment	**CO_2 Volume per Cycle (Pore Volume)**	**No. of Cycles**	**CO_2 : Brine Volumetric Ratio**	**Back Pressure (psi)**	**Temperature (°F)**	**Rate (cm^3/min)**	**Case**
1	5.0	3	1.0 : 1.0	1300	200	2.0	Reference Case
2				700			Effect of Pressure
3	5.0	3	5.0 : 1.0	1300			Effect of Volumetric Ratio
4	5.0	3	2.0 : 1.0				
5	2.5	4	0.5 : 1.0				
6	1.0	15	1.0 : 1.0				Effect of CO_2 Volume/Cycle
7	3.0	5					
8	7.5	2					
9	15.0	1					
10	5.0	3			70	2.0	Effect of Temperature and Injection Rate
11						3.5	
12						5.0	
13						10.0	
14					100	2.0	
15						3.5	
16						5.0	
17						10.0	
18					200	3.5	
19						5.0	
20						10.0	

Capillary and gravity numbers are two dimensionless groups that were calculated to assess the effect of gravity and fluid viscosities on the flow behavior. The capillary number is the ratio of viscous force to capillary force, while the gravity number is the ratio of gravity force to viscous force (Zhou et al. 1994):

$$N_C = \frac{u_t \mu_w}{\sigma} \tag{4.4}$$

$$N_{gv} = \frac{\Delta\rho g k L}{H \mu_{CO2} u_t} \tag{4.5}$$

Where;

g = acceleration of gravity, m/s^2

H = height of the core, m

k = average permeability, md

L = length of the core, m

N_C = capillary number, dimensionless

N_{gv} = gravity number, dimensionless

u_t = total average Darcy flow velocity, m/s

μ_{co2} = CO_2 viscosity, cp

μ_w = brine viscosity. cp

σ = interfacial tension between CO_2 and brine, N/m

$\Delta\rho$ = density difference between CO_2 and brine, kg/m^3

When the capillary number is larger than 1×10^{-7} and the gravity number is less than 2, no gravity segregation will occur, and the flow will be dominated by viscous forces (Kuo et al. 2010). For the reference case (flow rate was 2 cm^3/min, brine density was 1.036 gm/cm^3, and CO_2 density was 0.2 gm/cm^3) using **Eqs. 4.4** and **4.5**, the N_C was 4.7×10^{-6} and the N_{gv} was 0.33, therefore the gravity effect can be neglected.

The concentration of calcium ions in the core effluent samples gave an indication about the reaction rate between CO_2/brine/rock. **Fig. 4.2** shows the concentration of calcium ions in the collected samples, and the pH value of these samples. The results show that the calcium concentration increased from the initial value of 401 to 2,300 ppm after CO_2 injection due to rock dissolution. Alternating to brine, the brine displaced CO_2

out of the core and the calcium concentration decreased to 1,100 ppm. Calcium concentration was always higher than the initial value, due to the presence of residual CO_2 inside the core. Applying material balance to calculate the amount of calcium that came out of the core by integrating the area under the calcium curve and above the initial calcium line, gave that the total collected calcium in the outlet samples as 0.64 g (the total calcium content for this core was 119.2 g) which represents 0.54 wt% of the total calcium content. pH value decreased as CO_2 was introduced into the rock due to the acidic nature of carbon dioxide, an increase in calcium concentration due to rock dissolution resulted in an increase in the pH value while CO_2 was still injected. pH value decreased again after switching to brine, due to the reduction in the calcium concentration in the solution.

Fig. 4.3 shows that the CT number of the Pink Desert limestone saturated with the synthetic brine with a composition; shown in **Table 4.2**, between 1,900 and 2,200. Scanning the core after the CO_2 was injected (**Fig. 4.4**) showed that injecting slugs of CO_2 and brine at a rate of 2 cm^3/min caused uniform dissolution occupied with small and short wormholes at the core inlet (Slice 1). Spots of a lower CT number (around 1500) appeared in slices 2, 3, and 4, that indicated change in the rock structure due to the double action of dissolution and precipitation because of CO_2 injection. These spots are shown by the light grey colored area in the upper left image in **Fig. 4.4**, the CT number of these spots decreases when moving toward the center of the spots and increases when moving toward the untouched rock, dissolved material in the center of the spot is directly precipitated around the dissolved area. These slices were followed by a region of

untouched rock (Slices 5 through 12). These spots appeared again from slice 13 to the end of the core, which agree with the literature in the terms that CO_2 injection in carbonate rocks enhances the permeability of the core segment close to the inlet due to wormhole formation, and that moving toward the outlet the permeability will be reduced because of the damage due to calcium carbonate precipitation (Grigg et al. 2005).

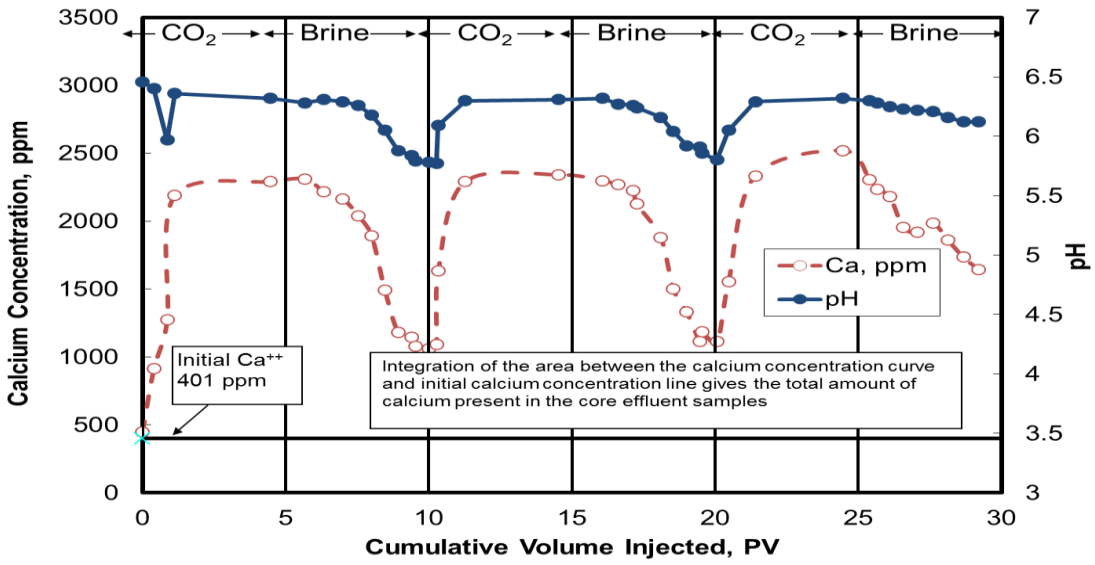

Fig. 4.2—Calcium concentration and pH during CO_2 WAG injection (Reference Case).

4.3.1 Effect of Pressure

A coreflood test was run to test the effect of pressure on the core permeability and porosity. The coreflood was run at the same conditions as the reference case, except that the back pressure regulator and CO_2 accumulator were set at 700 psi. This back pressure will result in gaseous CO_2 instead of supercritical CO_2 which was examined in the reference case.

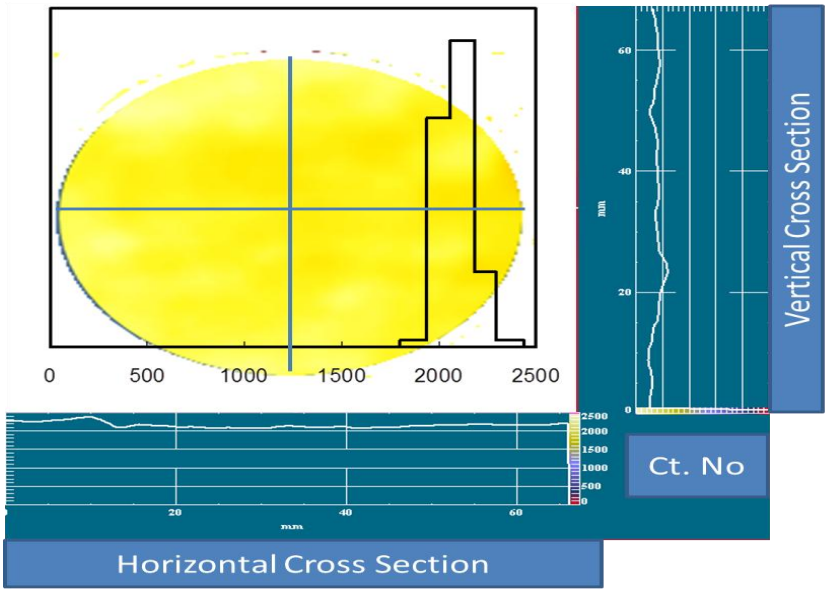

Fig. 4.3—Homogenous Pink Desert limestone cores have a CT No. between 1,900 and 2,200.

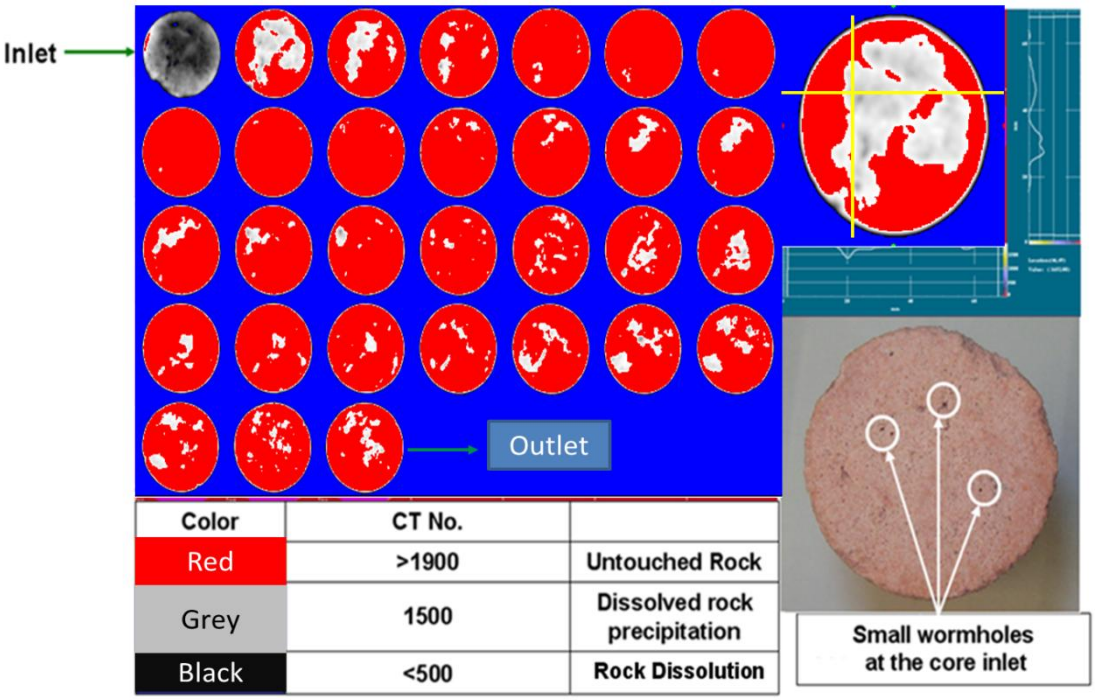

Color	CT No.	
Red	>1900	Untouched Rock
Grey	1500	Dissolved rock precipitation
Black	<500	Rock Dissolution

Fig. 4.4—CT scan for core #1 after CO_2 injection.

The results showed an enhancement in both permeability and porosity when injecting gaseous CO_2 instead of supercritical CO_2. **Fig. 4.5** shows the permeability and porosity divided by the original permeability and porosity for gaseous CO_2 injection and supercritical CO_2 injection experiments, because CO_2 solubility in the brine decreased from 11 to 8.5 mg CO_2/ g brine as the pressure decreased from 1300 to 700 psi. As a result, less rock was dissolved, which resulted in less precipitation at 700 psi.

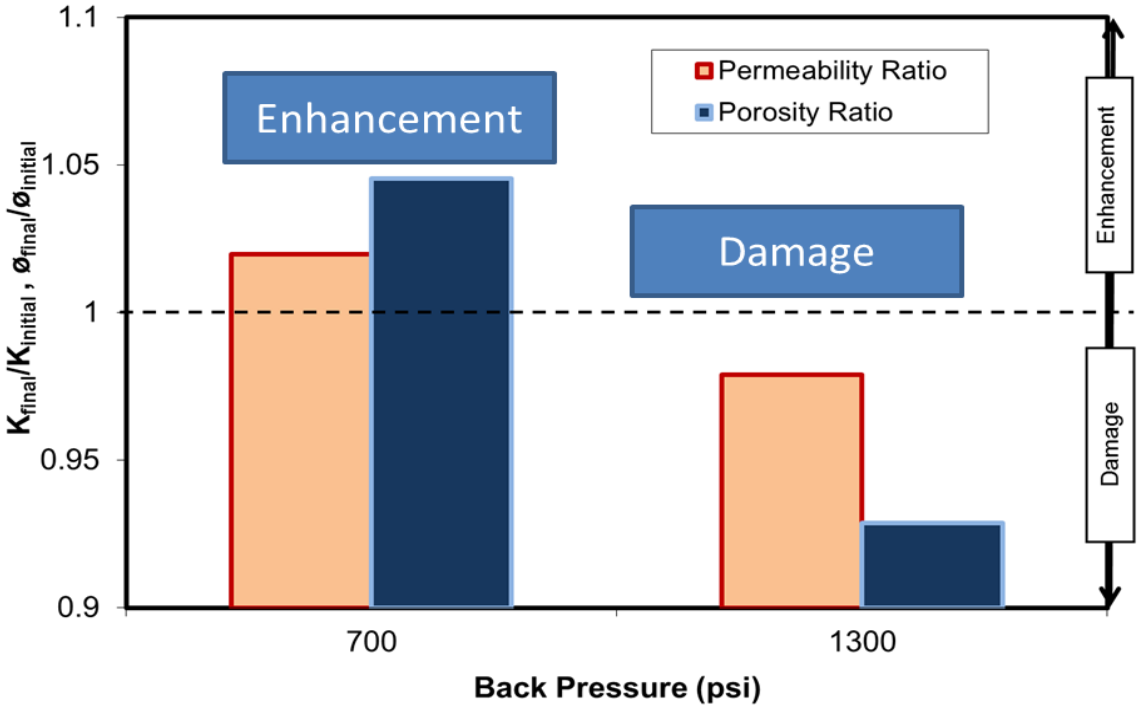

Fig. 4.5—Effect of back pressure on the permeability and porosity ratios after CO_2 WAG injection.

4.3.2 Effect of CO_2: brine Volumetric Ratio

Three coreflood tests were run to examine the effect of the volumetric ratio. CO_2 and brine were injected with volumetric ratios of 5:1, 2:1, and 0.5:1, besides the

reference case of 1:1. The experiments were run on three cycles of WAG. Total CO_2 volume injected (at P=1,300 psi, and T = 200°F) was kept constant for all experiments. 15 PV divided to 5 PV per each cycle, except for the last experiment (0.5 CO_2:1 brine), only 10 PV CO_2 injected divided to 2.5 PV/cycle for 4 cycles because of the pump capacity, which limited the experiment to a total fluid volume of 900 cm^3.

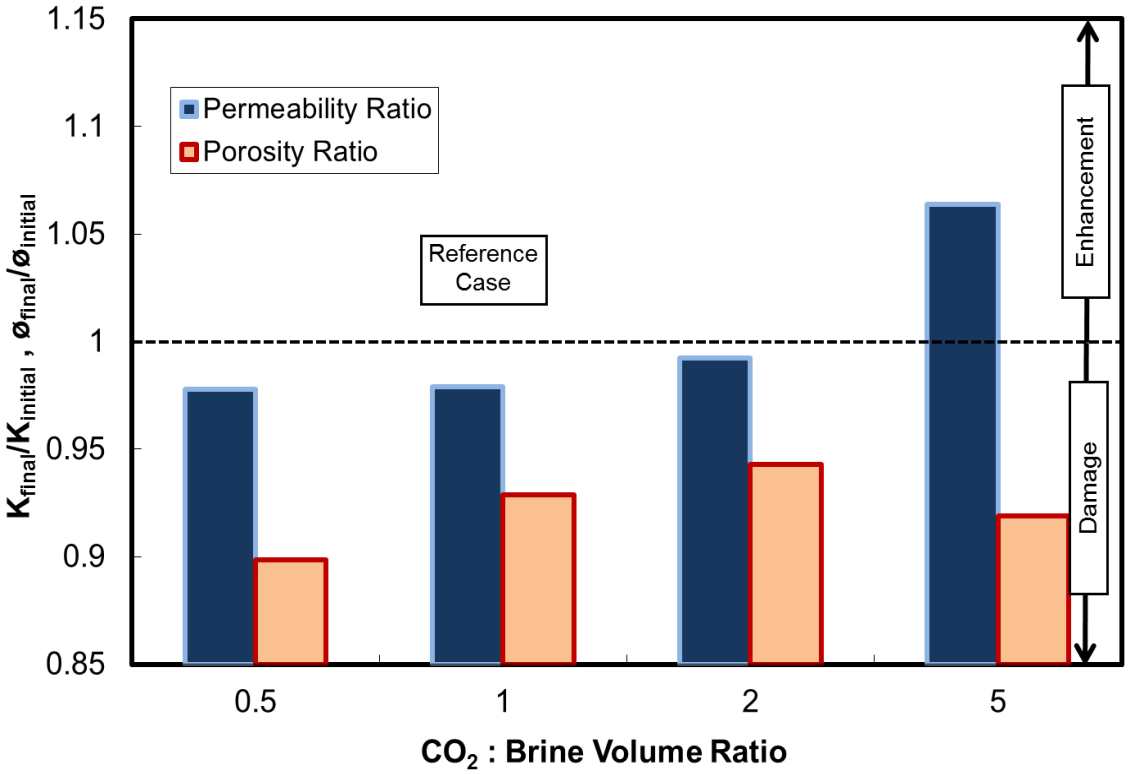

Fig. 4.6—Effect of volumetric ratio on the permeability and porosity ratios after CO_2 WAG injection.

Fig. 4.6 shows that as CO_2 to brine volume increased, less damage occurred to the rock, reflected by less permeability reduction, or, the more brine injected the more permeability reduction occurred. Porosity and permeability had the same behavior until

the CO_2: brine ratio was 2:1 then had more porosity loss introduced to the rock at CO_2: brine of 5:1. These results show that for the same CO_2 volume, more brine injected means more rock dissolution, which was followed by more precipitation and damage to the core.

4.3.3 Effect of CO_2 Volume/Cycle

Four coreflood tests were conducted to assess the effect of changing CO_2 volume per cycle. CO_2 was injected with volumes of 1, 3, 7.5 and 15 PV/cycle for 15, 5, 2, and 1 cycle, respectively. The results showed that injecting small PV/cycle CO_2 resulted in a significant loss in the formation porosity and permeability. **Fig. 4.7** shows that at 5 PV/cycle the damage was the lowest. As the PV/cycle decreased, the damage significantly increased, and as the PV/cycle increased the permeability decreased with a small rate, while the porosity increased continuously.

Fig. 4.8 shows the pressure drop across the core for the case where the CO_2 volume per cycle was 1 PV/cycle. The pressure increased gradually for each cycle until the tenth cycle; pressure increased from 12.5 psi during brine injection in the first cycle, to 33 psi at the tenth cycle at which a white solid material started to flow out of the core (**Fig. 4.9**). The pressure drop across the core decreased significantly to 17 psi during brine injection in cycle number 11. In this case, the contact time between brine and CO_2 was long, which enhanced rock dissolution. This was confirmed with the increase in calcium collected in the core effluent samples as the CO_2 volume/cycle decreased, and then more precipitation that built the pressure up. When the pressure drop across the core

was too high, the injected fluids started to sweep some of the precipitated calcium carbonate out of the core to open the path to flow and the pressure started to decrease again.

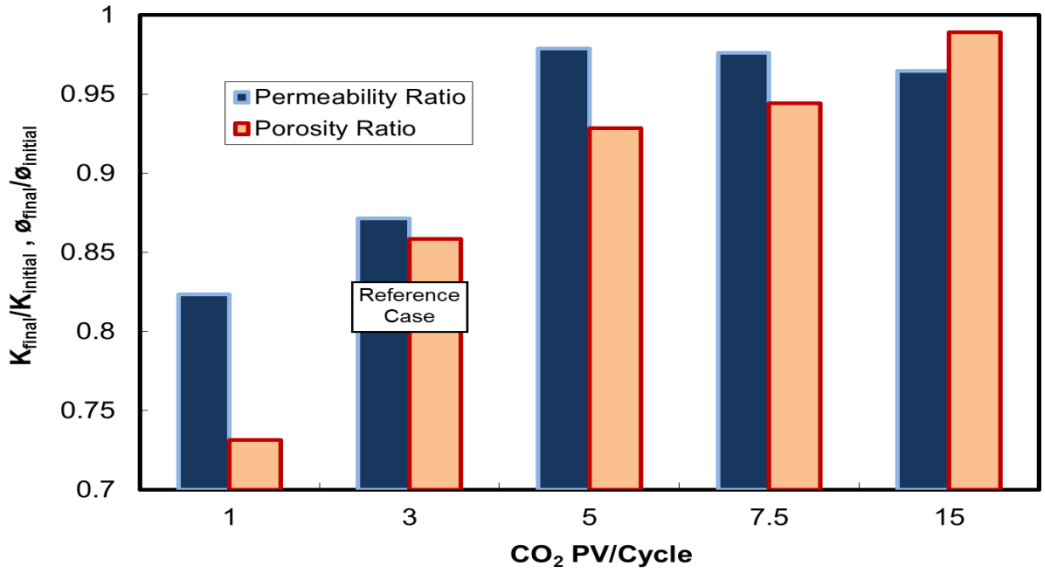

Fig. 4.7—Effect of CO_2 volume per cycle on the permeability and porosity ratios after CO_2 WAG injection.

4.3.4 Effect of Temperature

Three temperatures were examined: 70, 100, and 200°F. CO_2 solubility in brine decreases as temperature increases (Takasawa et al. 2010). As a result, increasing temperature adversely affects the amount of rock dissolved.

The solubility of calcium bicarbonate increases with increasing the temperature. Less precipitation of calcium carbonate occurred when temperature increased. **Fig. 4.10** shows that at higher temperatures, more permeability enhancement or less damage

occurred in the cores. The curves for 70, 100, and 200°F were almost parallel and moving upward as the temperature increased.

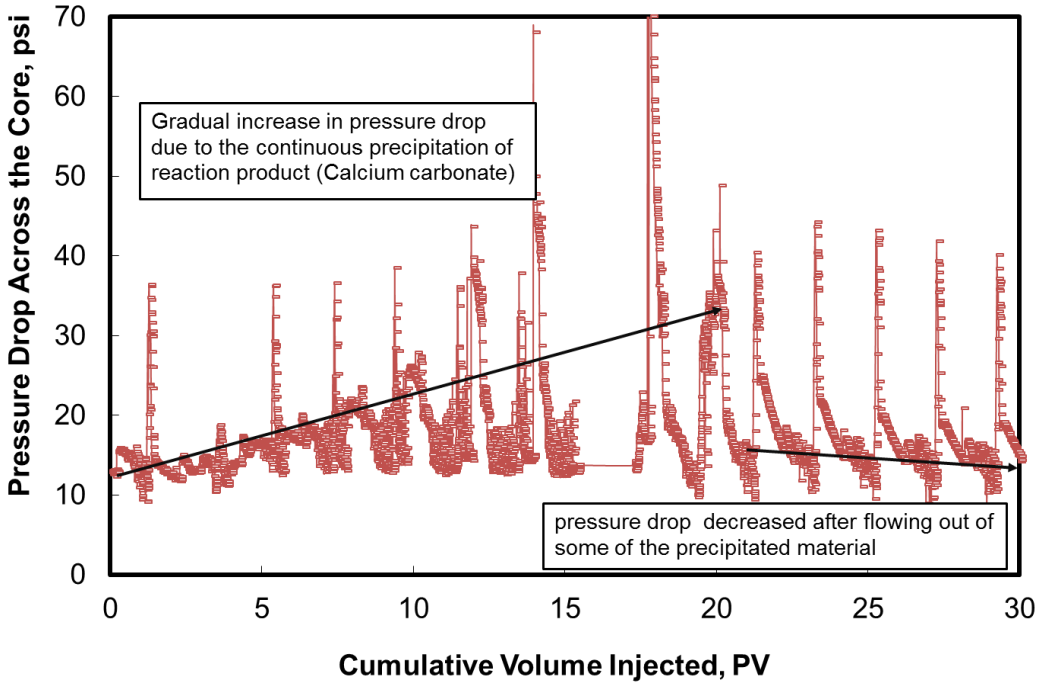

Fig. 4.8—Pressure drop across core #6 during CO_2 WAG injection.

The effect of temperature on the injection pressure drop across the core is shown in **Fig. 4.11**. It is clear that the higher the temperature, the lower the injection pressure during brine injection, because the brine viscosity decreases as the temperature increases. **Eqs. 4.1** and **4.2** give brine viscosities of 1.08, 0.74, and 0.36 cp at 1,300 psi and 70, 100 and 200°F, respectively, compared to the viscosity of 1.04 cp that was measured at room temperature and atmospheric pressure.

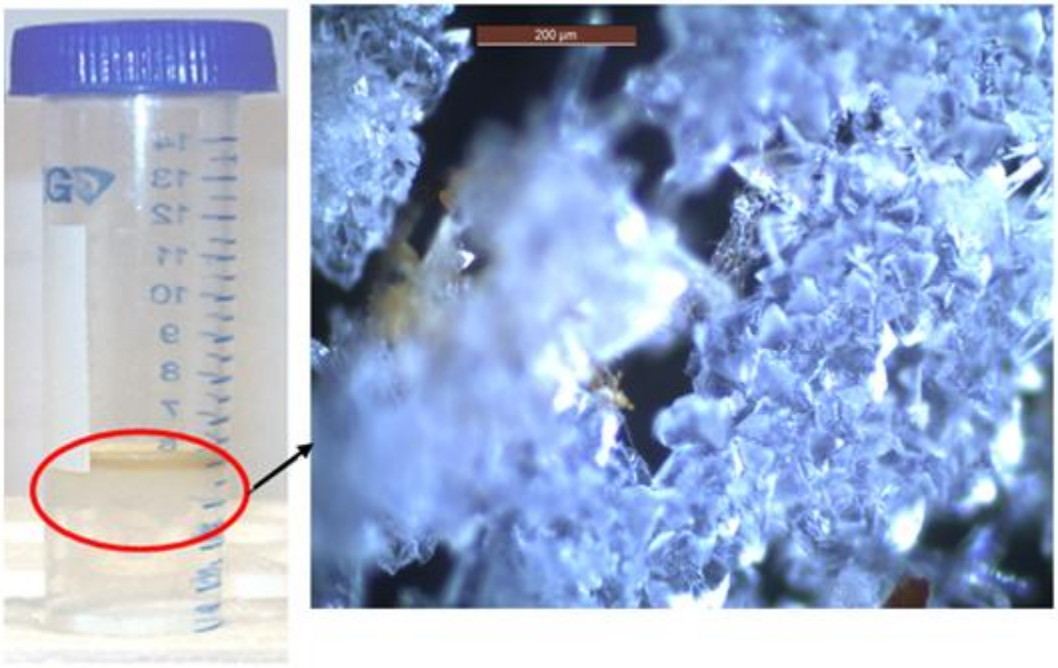

Fig. 4.9—Calcium carbonate noted in the core effluent samples, core #6.

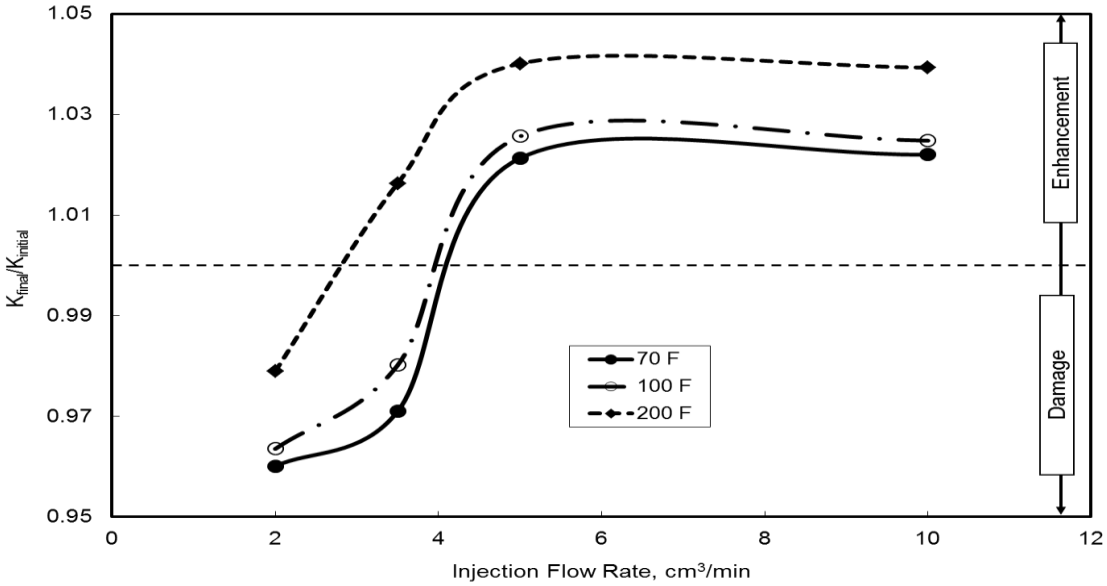

Fig. 4.10—Increasing the injection rate enhances the cores permeability, especially at high temperatures.

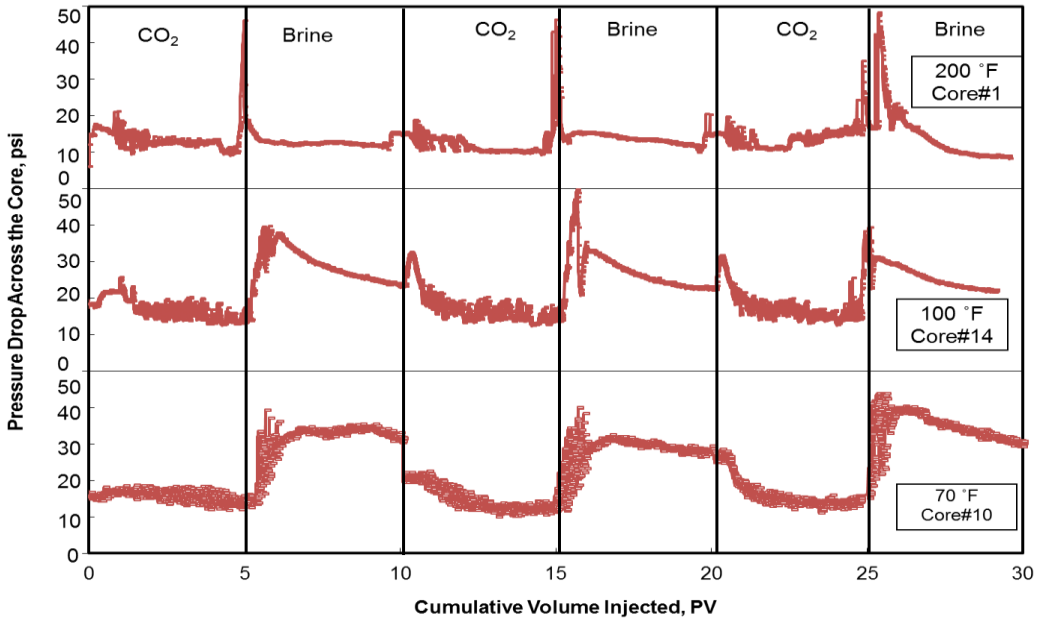

Fig. 4.11—Pressure drop across the core at injection rate of 2 cm^3/min and different temperatures.

During CO_2 injection, the pressure drop across the core decreased as the temperature increased (**Fig. 4.12**). CO_2 viscosities at pressures of 1,300 psi, and 70, 100, and 200°F are 0.086, 0.045, and 0.021 cp, respectively (Fenghour et al. 1997).

4.3.5 Effect of Injection Rate

Four injection rates were examined: 2, 3.5, 5, and 10 cm^3/min. At 10 cm^3/min, the contact time between CO_2 and brine, and the core rock was less. As a result, the amount of rock dissolved decreased as the injection rate was increased. Also, at higher injection rates brine has the ability to keep some of the precipitated material suspended and carry that precipitation out of the core. **Fig. 4.13** shows that at high injection rates (5 and 10 cm^3/min) a white precipitation was noted in the effluent sample just after

alternating from CO_2 to brine injection. This white precipitation was tested by concentrated hydrochloric acid (HCl): and this material was completely dissolved with HCl, which indicated that it was mainly calcium carbonate. **Fig. 4.14** shows a microscopic photo for the precipitated material collected in the effluent core samples. Calcium carbonate precipitated had a grain size ranging between 32 to 275 μm. These two mechanisms (lower contact time, and carrying the precipitated material out of the core) resulted in an increase in the permeability as the injection rate increases (**Fig. 4.10**).

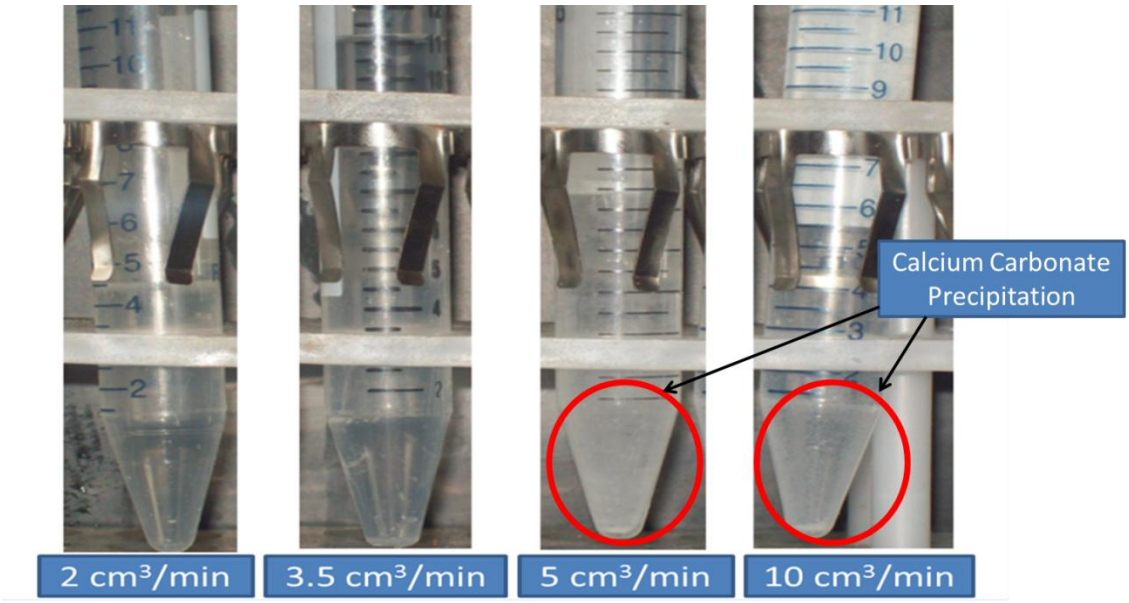

Fig. 4.12—Calcium carbonate was noted in the effluent samples just after alternating from CO_2 to brine at high flow rates.

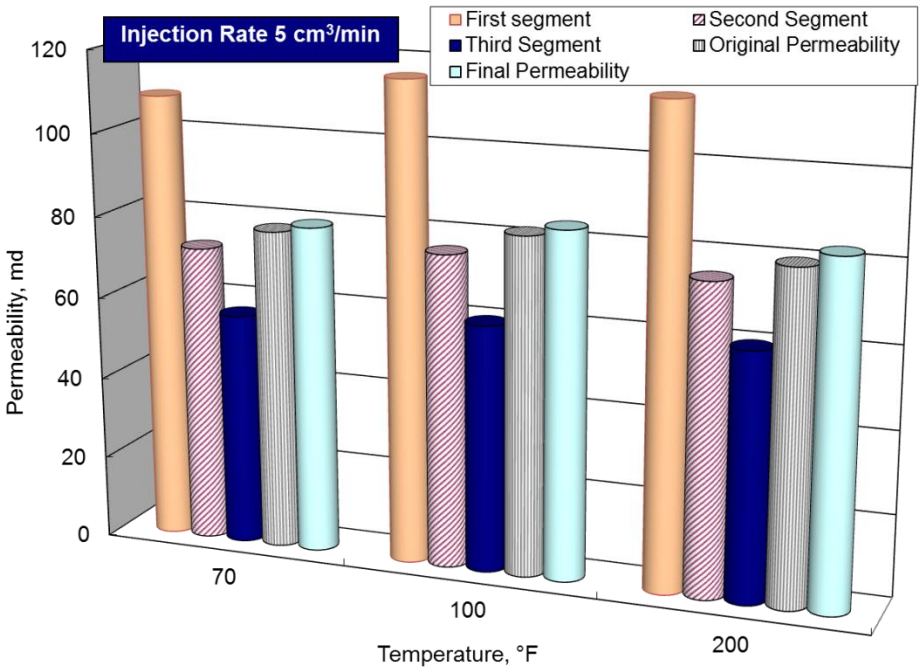

Fig. 4.13—Original and final core permeability, and the permeability distribution along the core length @ 5cm^3/min.

At low flow rates (2 cm^3/min) a reduction in the core permeability after CO_2 injection was always noted. Increasing the temperature and keeping the flow rate at the same value (2 cm^3/min) resulted in less permeability loss. Increasing the flow rate to 3.5 cm^3/min, the damage was still noted but with lower severity than in 2 cm^3/min rate, and again the permeability loss was less at higher temperature. At a temperature of 200°F, an enhancement in core permeability was noticed.

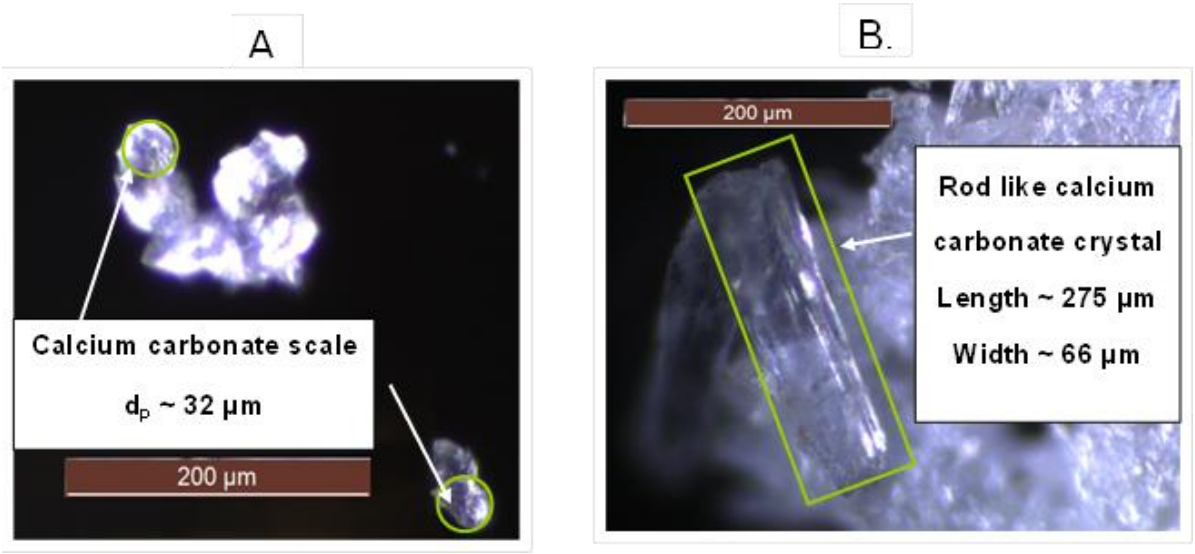

Fig. 4.14—Microscopic photo for precipitated calcium carbonate.

Increasing the injection rate to 5 cm^3/min caused an enhancement in core permeability at all temperatures in the range examined in this work. At an injection flow rate of 10 cm^3/min, the behavior was close to the behavior at 5 cm^3/min.

Although, core #16 had a higher initial permeability, it showed a higher pressure drop during brine injection in the first cycle because of the higher flow rate. Moving forward, core #16 showed a decreasing trend in the pressure drop, which indicated an increase in the core permeability. The pressure drop across core #15 almost had the same level for all cycles. Again the injection flow rate had no significant effect on the pressure drop during CO_2 injection because of the high mobility of carbon dioxide compared to brine mobility.

The results showed that for the cases examined in this study, the permeability change ranged between ±5%. The results were compared to results from previous work done by Grigg et al. (2005). They ran a coreflood test with injecting brine alternated with

CO_2 (WAG) on Indiana limestone at 2000 psig and 100°F and the permeability of the core was measured periodically.

4.3.6 Permeability Changes along the Core Length

The effect of CO_2 injection rate on the rock permeability was evaluated by the measurement of the core permeability before and after the experiment. Also, **Fig. 4.3** shows that Pink Desert limestone cores had a homogenous structure, the cores permeability is the same along the core length. Regardless of the temperature and injection rate, cutting down the cores into 3 pieces, each piece is 2 in. long. The measurements of the permeabilities of the three segments showed that the permeability of the first segment was always enhanced because of the dissolution of the rock, due to the reactions between carbonic acid and calcite rock. The damage started to show up from the second segment (the middle of the core) and increased moving farther from the injection face of the core. **Fig. 4.13** shows that the permeability distribution along the core length has the same trend for all temperatures examined. **Fig. 4.15** shows that first segment of the rock still shows enhancement in the permeability although the overall permeability of the core was reduced after CO_2 injection. The behavior that was observed for the 5 cm^3/min cores were repeated again at 2 cm^3/min, but with more damage being observed in the second and third segments.

4.4 Numerical Simulation Study

The compositional simulator (CMG-GEM) was used to predict a correlation between the change in core porosity and permeability. First, the permeability ratio results shown in the previous section (**Figs. 4.5, 4.6, 4.7, and 4.10**) were used to calibrate the model used by (CMG-GEM) for porosity and permeability relations, then a study was conducted at core scale. After calibrating the model, a simulation study at field scale was conducted to predict the change in reservoir porosity and permeability after CO_2 injection into a limestone aquifer, the amounts of CO_2 trapped by different trapping mechanisms were also calculated.

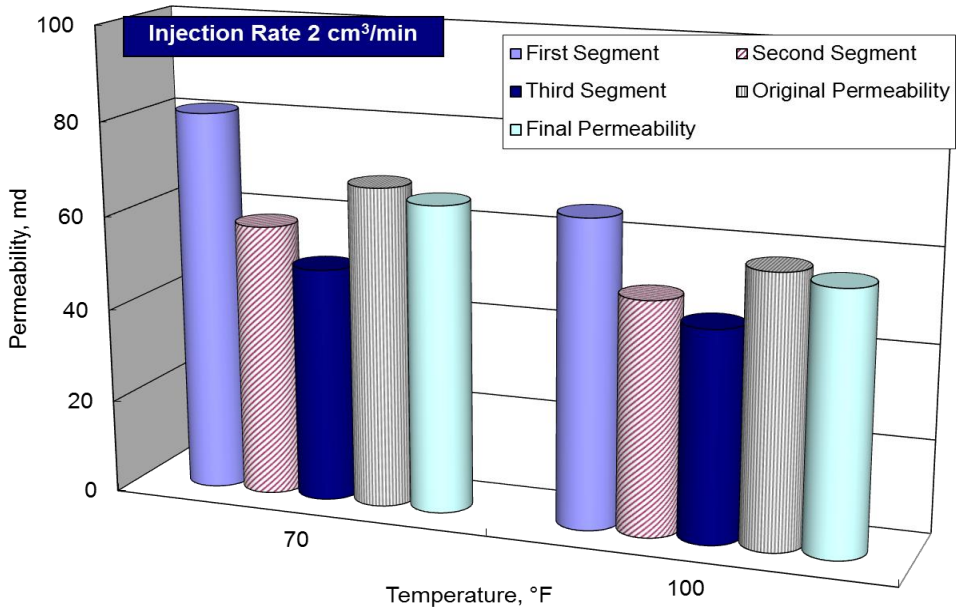

Fig. 4.15—Original and final core permeability, and the permeability distribution along the core length @ 2cm^3/min.

The kinetic rate parameters for CO_2 reaction with calcite was obtained from Svensson and Dreybrodt (1992), $A_\beta = 9.8\ cm^2/g$, $E_{a\beta} = 62.76$ KJ/mol., and $(Log_{10}\ k_{0\beta}) = -6.19$. Change in core permeability could be calculated by the change in porosity, two models were used to predict this relation, the power-law and Carman-Kozeny models, **Eqs. 3.9 and 3.10.**

4.4.1 Core Scale Simulations

Limestone cores used in this study were assumed to be formed completely from calcite mineral. The cylindrical cores were divided into radial grid blocks with 5X20X20 blocks in the r, Θ, and z directions, respectively. Initially, porosity and permeability were assumed to be constant for all grids. Relative permeability was adjusted to match the experimental pressure drop (**Eqs. 3.1 and 3.2**). Capillary pressure was calculated using, **Eq. 3.3**.

The twenty coreflood experiments conducted in this chapter (**Table 4.3**) were simulated, the exponents of power-law and Carman-Kozeny were calculated for each case (**Table 4.4**). The results showed that a different exponent was obtained for each core, ranging between 0.46 to 6.76, and from 0.07 to 6.07 for power-law and Carman-Kozeny models, respectively. The average value for the power-law exponent was 3.89, using this value to predict the permeability for all experiments gave acceptable results for final permeability. The average value for Carman-Kozeny exponent was 3.40.

Table 4.4— SUMMARY OF THE POWER-LAW AND CARMAN-KOZENY EXPONENTS					
Core	**Power-Law Exponent (n)**	**Carman-Kozeny Exponent (m)**	**Actual Final Permeability (md)**	**Final Permeability @ Average Power-Law Exponent**	**Final Permeability @ Average Carman-Kozeny Exponent**
1	2.79	2.48	60.5	59.98	60.07
2	1.07	0.4	103	110.9	111.24
3	6.15	5.67	46.8	45.71	45.71
4	0.49	0.07	51.6	48.92	48.97
5	2.1	1.76	65.5	64.7	64.7
6	3.69	3.19	84	83.13	83.08
7	5.38	4.97	47.5	49.2	49.3
8	3.28	2.86	41	40.81	40.83
9	5.1	4.65	55	55.47	55.48
10	5.16	4.66	65.5	66.18	66.17
11	3.25	2.76	58.52	58.48	58.48
12	3.18	2.68	79.66	80.03	80.03
13	2.09	1.6	69.7	71.04	71.04
14	5.49	5.06	55.5	56.12	56.15
15	3.42	2.94	68.22	68.07	68.07
16	5.62	5.11	84	83.34	83.35
17	4.55	4.06	84	83.68	83.69
18	6.76	6.04	61.63	60.16	60.3
19	5.17	4.53	83	81.39	81.6
20	3.09	2.59	77.43	78.45	78.46
Arithmetic Average	**3.89**	**3.40**			

Fig. 4.16 shows the porosity and permeability distribution across core #1 (long WAG cycles) and core #6 (short WAG cycles), the increase in core porosity and

permeability were calculated near the core inlet, and damage was noted as moving away from the core inlet. More damage was predicted by the simulator for core #6 compared to core #1.

A comparison between the permeability distribution along the core measured in the lab and calculated by the simulator is given in **Fig. 4.17**. Close to the core inlet, the permeability measured in the lab was higher than the permeability calculated by the simulator. Away from the core inlet, the measured permeability is lower than the calculated one. During CO_2 injection into carbonate rock, the enhancement in permeability occurred due to the dissolution of carbonate rock, which increased the pore volume and formed wormholes as shown in **Fig. 4.4**, while the damage occurred due to precipitation of calcium carbonate, which reduced the porosity and plugged the core throats. The simulator doesn't capture the wormhole formation and pore throat plugging, it only captures the change in core porosity, and causes the difference between the measured and calculate results. Using the power-law or Carman-Kozeny equation can give an estimation for the overall change in core permeability, but doesn't give a detailed distribution of permeability along the core.

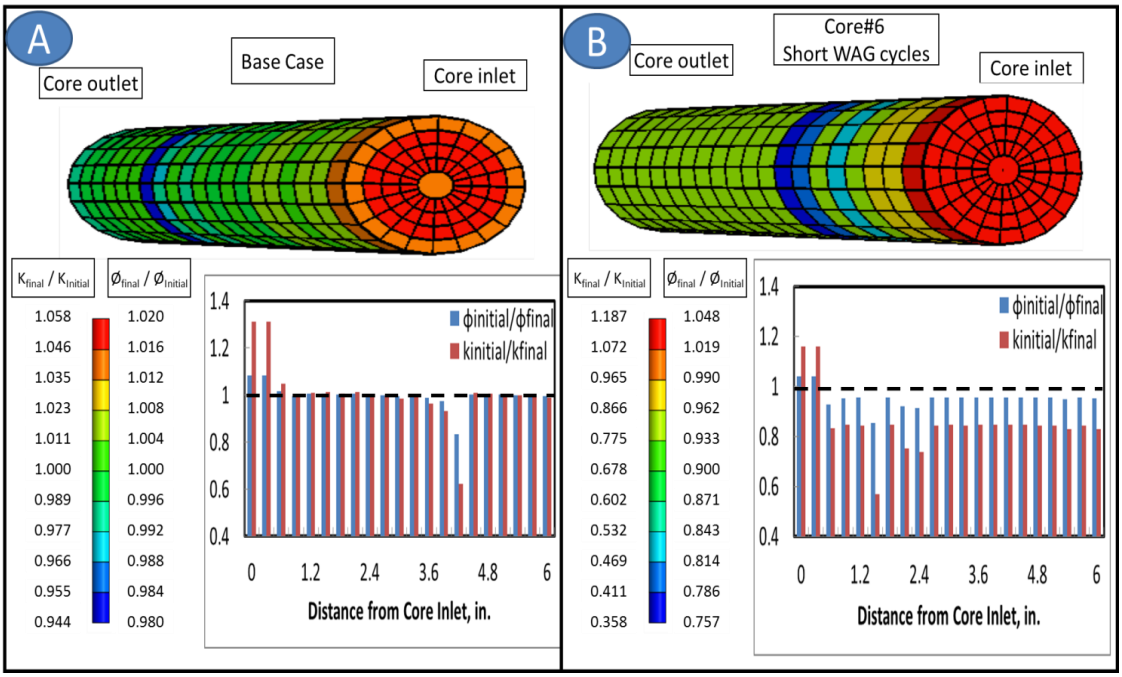

Fig. 4.16—Change in porosity and permeability as predicted by the reservoir simulator (CMG-GEM), A) core #1, B) core #6

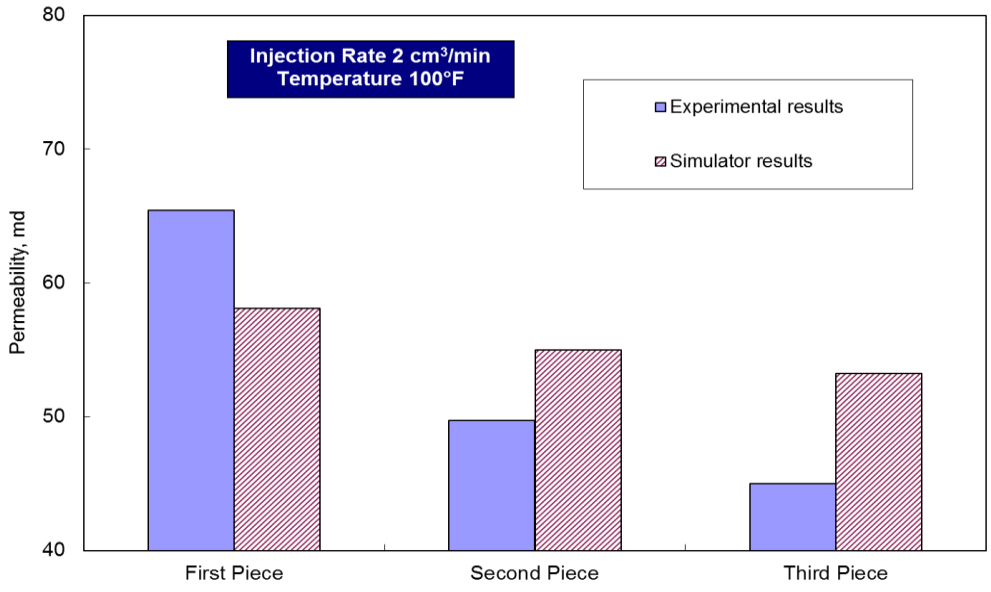

Fig. 4.17—Permeability distribution along core #14, comparison between experimental and simulation results.

4.4.2 Field Scale Simulations

The homogenous saline aquifer model used in this study is the modified benchmark CO_2 injection introduced by Dahle et al. (2009). The aquifer extension is 10 km in both x and y dimensions, with a thickness of 50 m, the aquifer top is at a depth of 8200 ft. Aquifer temperature is 163°F and the porosity = 0.15. The aquifer has a permeability of 100 md in the horizontal direction with k_z/k_h = 0.3 at a normal pore pressure gradient of 0.465 psi/ft at initial conditions.

The aquifer was divided into Cartesian grid blocks with 35X35X8 blocks in x, y, and z directions. A CO_2 injection well was completed at the center of the aquifer with perforating at the bottom of the aquifer. Injection was conducted at constant bottomhole pressure of 5740 psi (equivalent to a fracture pressure gradient of 0.7 psi/ft). The simulator ran for 30 years of CO_2 injection, and 500 years after injection to monitor the movement of CO_2 and the changes in trapping mechanisms. Four injection scenarios were tested to compare different injections schemes;

a) Continuous CO_2 injection at constant bottomhole pressure
b) WAG injection, each cycle composed of 3 weeks of CO_2 injection and one week of brine injection (short WAG cycles)
c) WAG injection, each cycle composed of 9 months of CO_2 injection and 3 months of brine injection (long WAG cycles)
d) SWAG injection, with brine injection flow rate of 100 m^3/day, while CO_2 injected at constant bottomhole pressure of 5740 psi.

Fig. 4.18 shows the amount of CO_2 injected for each injection scenario, more CO_2 was injected for the continuous CO_2 injection scenario (2.7 M. ton) with no brine injected. For the two WAG injection scenarios the mass of CO_2 injected was (1.9 M.ton) with 748,000 m^3 brine injected for short WAG cycles, and 810,000 for long WAG cycles. The least amount of CO_2 was injected when SWAG injection was conducted (1.3 m. ton) with total brine volume of 1,100,000 m^3.

Figs. 4.19-4.22 show the distribution of free CO_2 and dissolved CO_2 inside the aquifer during CO_2 injection and 500 after CO_2 injection stops, the change in porosity and permeability was also shown for different injection scenarios. For all cases, changes in porosity and permeability occurred just around the wellbore, and negligible changes (less than 1%) beyond wellbore blocks. For continuous CO_2 injection, reduction in permeability was noted above the perforations with maximum reduction in permeability of 2 md. For both WAG injection scenarios, a small increase in permeability was noted around the perforations (1 md), maximum damage above the perforation zone was 4 md. For SWAG case, damage was noted around the wellbore; maximum damage was observed around the perforations (1.5 md). It is clear that the changes in porosity and permeability are minor and don't have a significant effect, maximum damage noted was less than 5%, because of the fast reaction rates of CO_2 with limestone and the reaction reaching equilibrium very quickly. The figures show that, with time, free CO_2 tends to migrate to the top of the aquifer and more CO_2 is trapped in the dissolved phase.

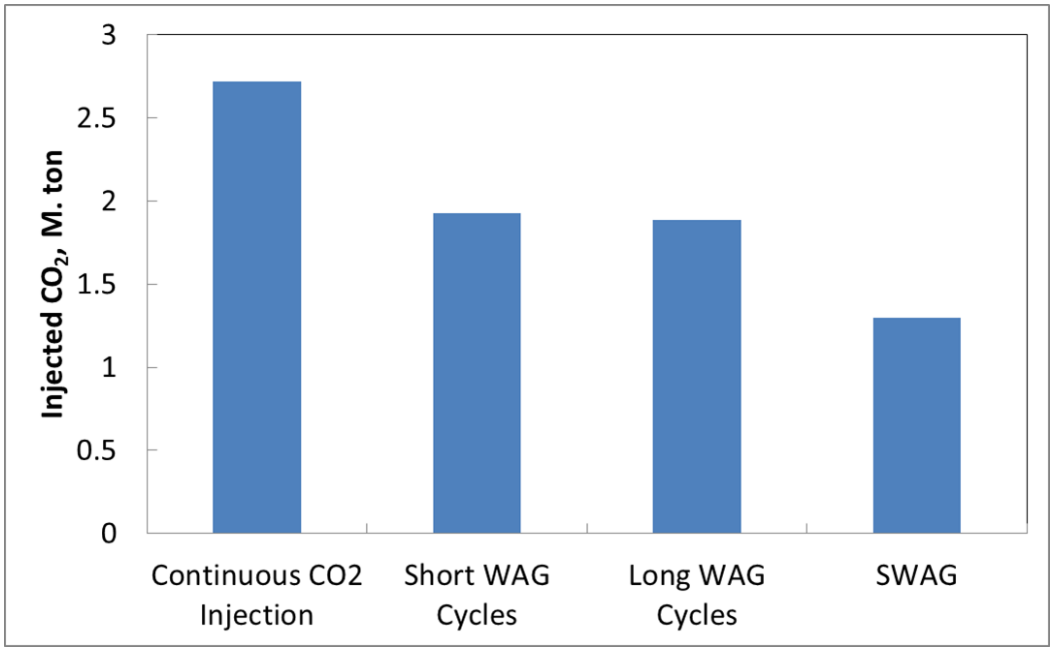

Fig. 4.18—Mass of injected CO_2 for each scenario.

Four main trapping mechanisms controls the storage of CO_2 in saline aquifers; 1) structural trapping, 2) solubility trapping, 3) residual phase trapping, and 4) mineral trapping. **Fig. 4.23** shows the contribution of each mechanism to store CO_2 for all injection scenarios proposed in this study.

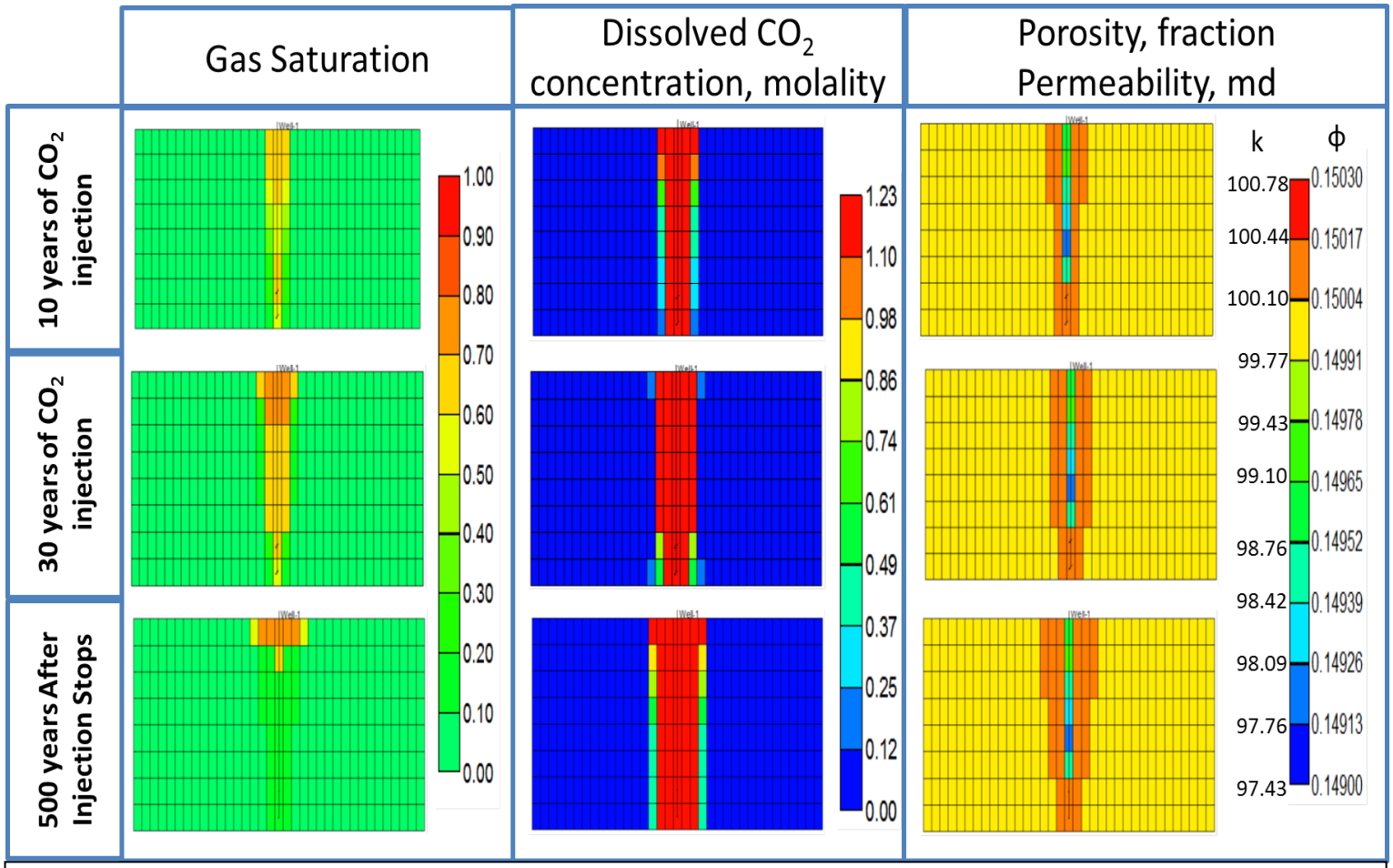

Fig. 4.19— Distribution of porosity, permeability and the free and dissolved CO_2 in the aquifer after 10 years of CO_2 injection, at the end of injection, 500 years after injection stops, continuous CO_2 injection scenario.

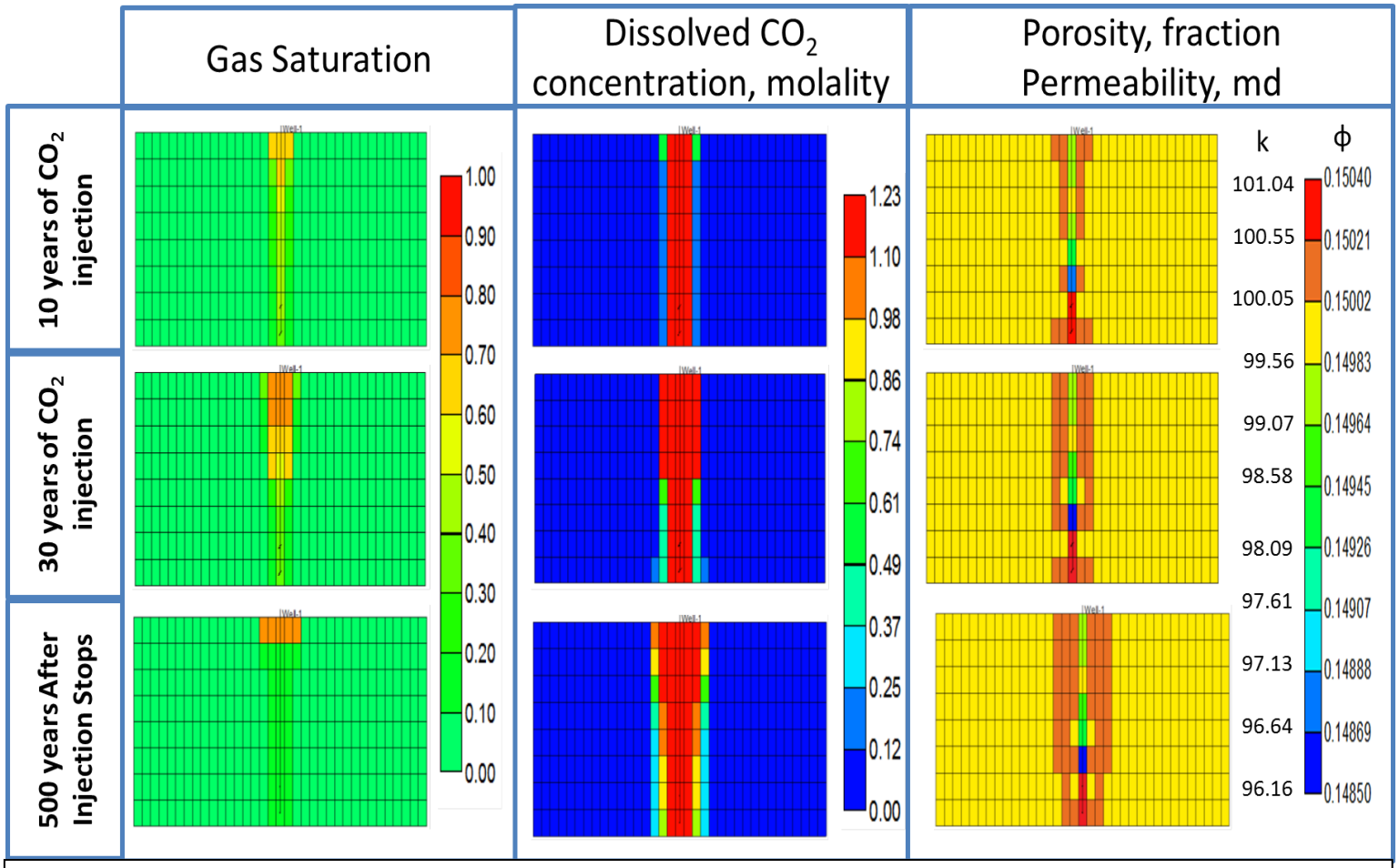

Fig. 4.20— Distribution of porosity, permeability and the free and dissolved CO_2 in the aquifer after 10 years of CO_2 injection, at the end of injection, 500 years after injection stops, short WAG cycles scenario.

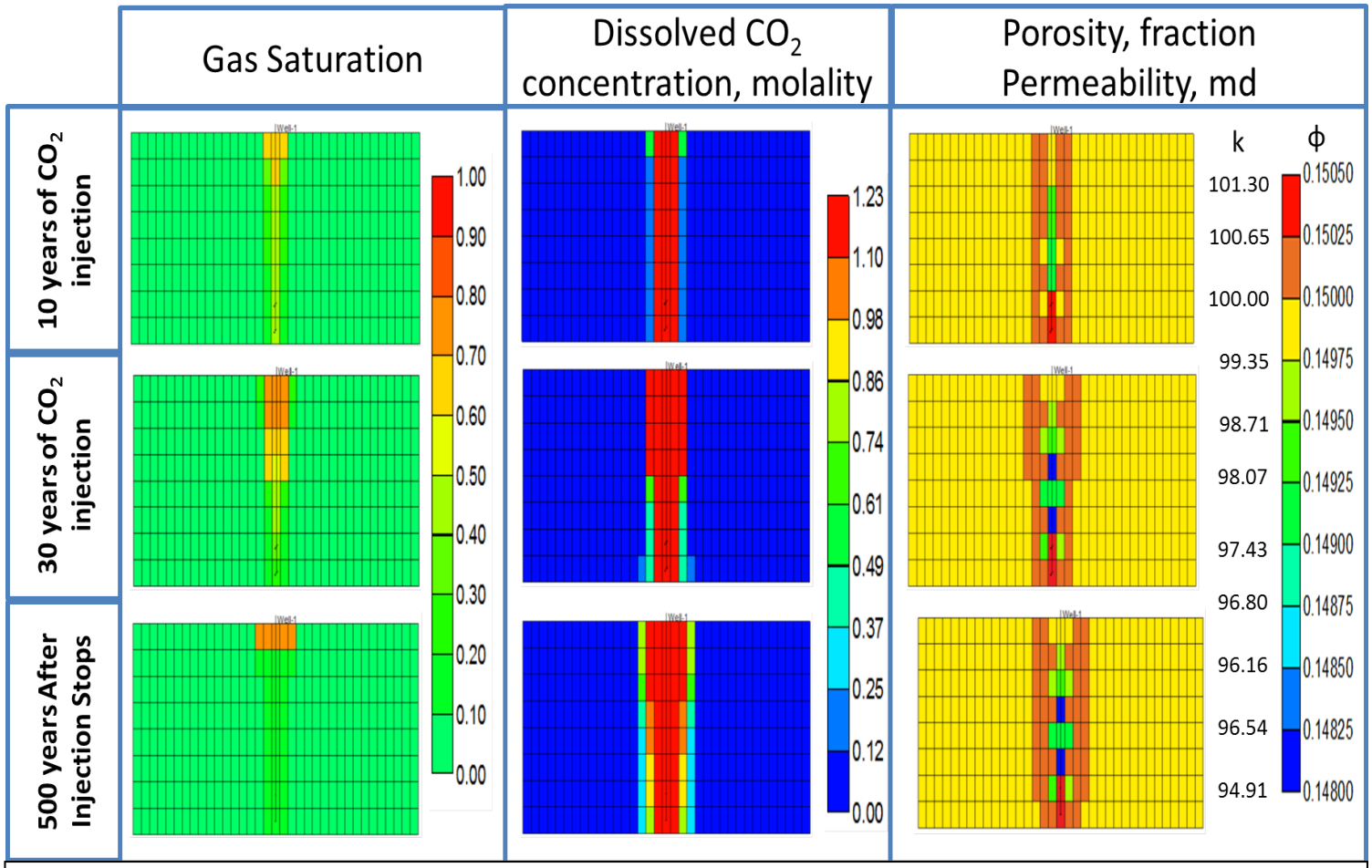

Fig. 4.21—Distribution of porosity, permeability and the free and dissolved CO_2 in the aquifer after 10 years of CO_2 injection, at the end of injection, 500 years after injection stops, long WAG cycles scenario.

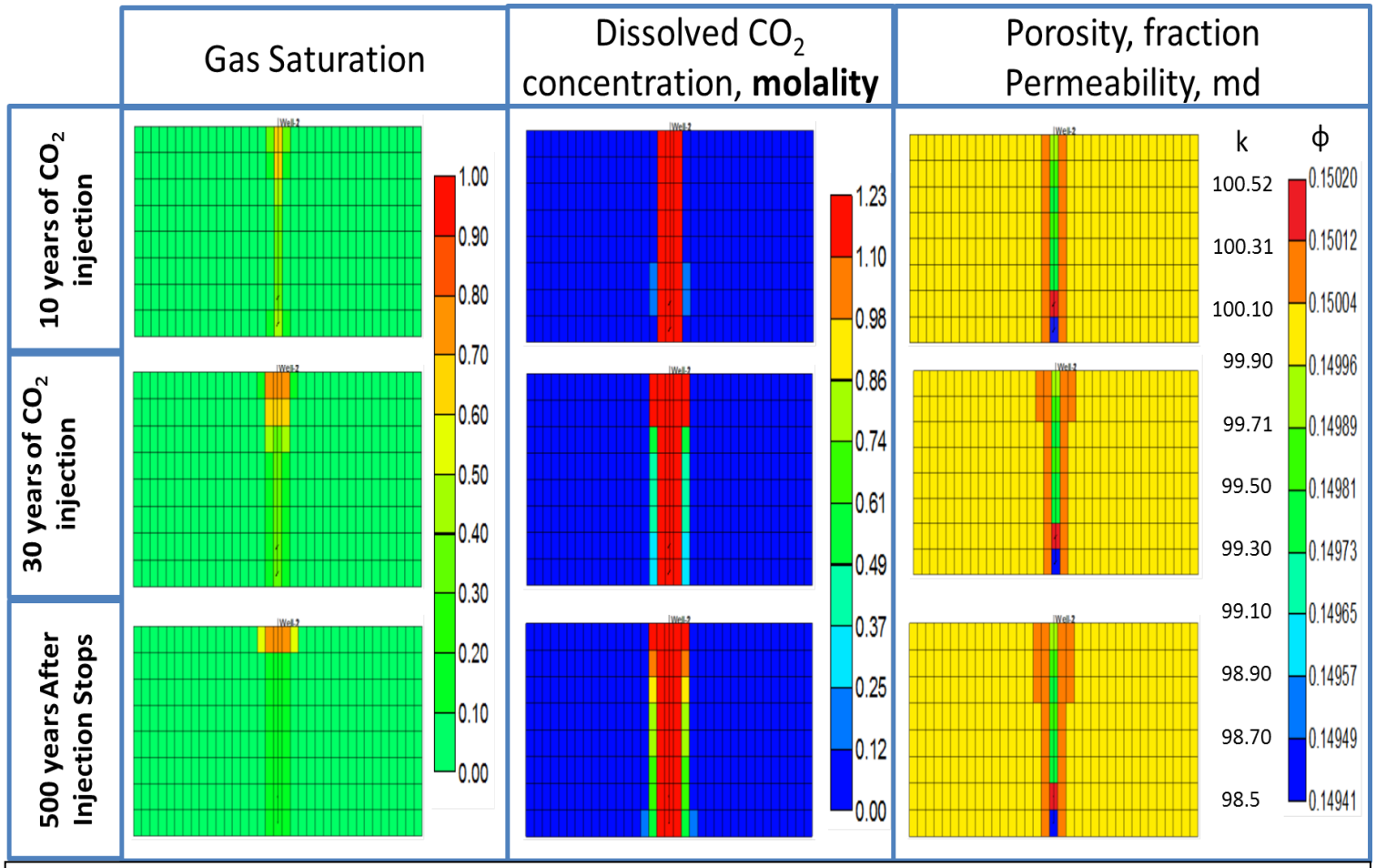

Fig. 4.22—Distribution of porosity, permeability and the free and dissolved CO_2 in the aquifer after 10 years of CO_2 injection, at the end of injection, 500 years after injection stops, SWAG cycles scenario.

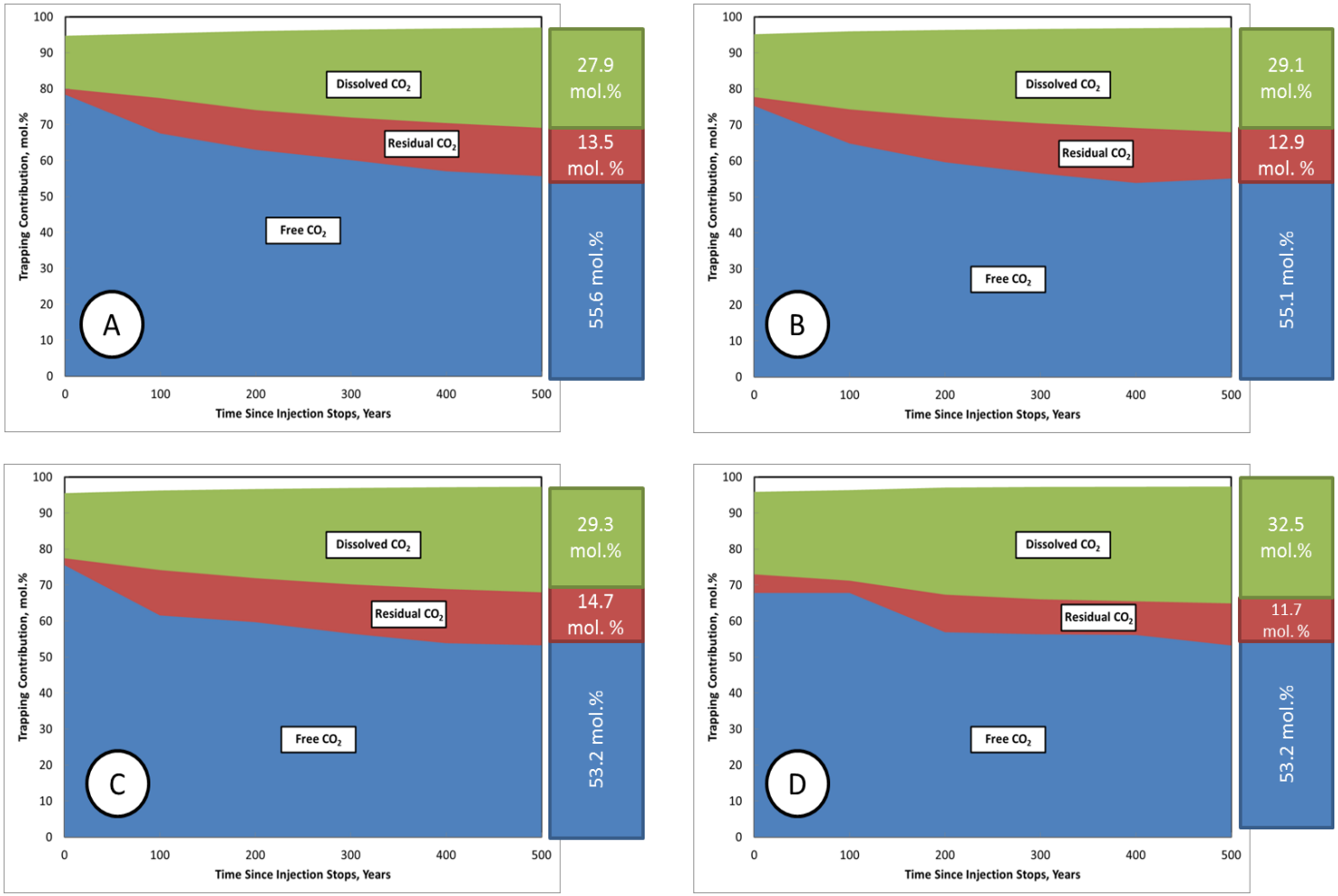

Fig. 4.23— Trapped phases during CO_2 injection into saline carbonate aquifer; A) continuous CO_2 injection, B) short WAG cycles, C) long WAG cycles, and D) SWAG injection

The main trapping mechanism is the structural trapping shown by the amount of free gas present in the reservoir, it contributes more than 50 mol% for all cases. The figures showed that amount of free gases decreases with time, due to upward migration of CO_2 because of the gravity difference, leaving behind CO_2 trapped in residual phase, also more CO_2 is dissolved in water with time. CO_2 trapped in residual trapping mechanisms bathes through two stages; firstly, increased, due to migration of free gases, then decreased, due to the solubility in brine as shown in **Fig. 4.23B**.

Continuous gas injection had the most amount of CO_2 trapped in the free phase (55.6 mol%). Short WAG injection had the highest level of residual gas trapping of 15.5 mol% after 400 years of injection stops, which decreased to 12.9 mol% after another 100 years due dissolution in brine. Dissolved phase trapping was enhanced by SWAG injection (32.5 mol%) when compared to other injection scenarios. Carbonate aquifers are a poor place for mineral trapping of CO_2 because the reactions reach equilibrium very quickly, the results showed that mineral trapping represents less than 3% for all proposed injection scenarios.

5. EFFECT OF BRINE COMPOSITION ON CO_2/LIMESTONE ROCK INTERACTIONS DURING CO_2 SEQUESTRATION

The primary factor that affects well performance during CO_2 injection, is the rock type (carbonate or sandstone). The solution channel was formed in the limestone, creating a dominant flow path that significantly altered the flow behavior. Increases in Ca^{2+}, Mg^{2+}, HCO^{3-}, and CO_2 concentrations were noticed during monitoring, and the produced aqueous fluids and gases confirms the dissolution effect noted during CO_2 injection. Brine salinity and composition play a key role in the chemical reaction between CO_2/water/rock during CO_2 sequestration, since the total dissolved solids (TDS) affects the solubility of CO_2 in brines.

The effects of pressure, temperature, injection flow rate, CO_2 volume injected per cycle, and CO_2 : water volumetric ratio on the carbonate core permeability during WAG injection of CO_2 was discussed in the previous chapter. Sodium sulfate was excluded from the seawater composition in these studies. The objective of this chapter is to study the effect of the brine composition on the chemical reactions between CO_2 and formation during WAG injection of CO_2 into a limestone aquifer, and the impact of flow rate and temperature, on the final permeability. NaCl, $CaCl_2$, and $MgCl_2$ were tested at various concentrations (0, 1, 5, and 10 wt%). The reaction kinetics was also obtained using a compositional simulator (CMG-GEM) for each brine used in the current study.

5.1 Introduction

CO_2 is an acidic gas that dissolves in formation brine forming a weak carbonic acid. Carbonic acid dissolves carbonate rocks forming calcium bicarbonate, **Eqs. 5.1-5.2**;

$$H_2O + CO_2 \leftrightarrow H_2CO_3 \quad (5.1)$$

Reaction of carbonic acid with calcite;

$$CaCO_3 + H_2CO_3 \leftrightarrow Ca^{2+} + 2HCO_3^- \quad (5.2)$$

When the formation brine or the displacement brine contains SO_4^{2-}, calcium sulfate will precipitate (Egermann et al. 2005). This reaction is governed by Eq. 1.4:

$$Ca^{2+} + SO_4^{2-} + xH_2O \rightarrow CaSO_4 \cdot xH_2O \quad (1.4)$$

Where x equal to 0 (anhydrite), ½ (hemihydrate), or 2 (gypsum).

A coreflood study was conducted using limestone cores. CO_2 was injected at a pressure greater than 1300 psi and temperatures of 70 and 200°F. CO_2 and brines were injected in WAG cycles at injection rates of 2 and 5 cm^3/min. Seawater and formation brine were used in this study. Core effluent samples were collected and the concentrations of calcium, magnesium, sodium, and sulfate ions were measured. Core permeability was measured before and after the experiment.

A commercial compositional simulator was used to simulate the coreflood experiments at the lab conditions. The reaction rate constant of CO_2 with calcite at different brine compositions was adjusted to match the calcium concentration obtained in the lab.

5.1.2 Solubility of Calcium Sulfate

Solubility of calcium sulfate in brines is mainly controlled by the hydration state of its molecule. The solubility is also affected by temperature and brine salinity. The first solubility plot of calcium sulfate was published by Partridge and White (1929), their results showed that the solubility of anhydrite and hemihydrate in distilled water decreases as temperature increases. While gypsum solubility in distilled water increases as temperature increases up to 38°C, at higher temperatures solubility of gypsum decreases as temperature increases.

Meijer and Van Rosmalen (1984) used a computer program developed by Marshall and Sulsher (1968) to calculate the solubility of calcium sulfate in seawater, their results showed that the solubility in seawater is higher than the solubility in distilled water, although temperature has the same effect on the solubility of calcium sulfate for both cases. Solubility of calcium sulfate decreases at salt concentrations of brine twice the salt concentrations of seawater (Flint 1967).

5.1.3 Reaction Kinetics

Different values for rate constant of reaction of CO_2 with calcite at reference temperature (k_o) were reported in the literature (Alkattan et al. 1998). A summary of k_o and E_a used in previous studies with different brine compositions is given in **Table 5.1** Log(k_o) ranged from -8.94 at a low salinity brine with TDS of 395 mg/l (Lee and Morse 1999), to -1.69 for a high salinity formation brine with TDS of 232,000 mg/l (Bacon et al. 2009).

5.2 Materials

Calcite cores (Pink Desert limestone), with a length of 6 in. and a diameter of 1.5 in., were used in this study. The cores had a permeability that ranged from 56 to 100 md. Core properties are summarized in **Table 5.2**.

TABLE 5.1—LIST OF KINETIC RATE PARAMETERS FOR REACTIONS BETWEEN CO_2 AND LIMESTONE.

Reference	Log(k_o) (mol/m^2.sec)	Ea (KJ/mol*°K)	Reference Temperature (°C)	Brine Composition Ion	Brine Composition Conc. mg/l
Gaus et al. (2005)	-6.35		37	Al	9.47E-04
				Ba	1.72
				C	0.83
				Ca	7093.88
				Cl	16982.08
				Fe	0.02
				K	5.55
				Mg	269.79
				Na	2436.92
				S	15.42
				Si	7.08
Bacon et al. (2009)	-1.69	23.5	54	Na	55152.53
				Mg	3038.13
				Al	0.01
				SiO_2	7.21
				K	18258.91
				Ca	30240.00
				Mn	2.20
				Fe	0.56
				Cl	125007.98
				SO_4	158.50
				HCO_3	134.24
Sorensen et al. (2009)	-6.19	62.76	25	10 wt% NaCl	

TABLE 5.1—CONTINUED

Reference	Log(k_o) mol/m^2.sec	Ea KJ/mol*°K	Reference Temperature °C	Brine Composition Ion	Conc. mg/l
Lee and Morse (1999)	-8.94		25	Na	91.60
				Ca	40.00
				Cl	141.37
				HCO_3	122.00
Wellman et al. (2003)	-2.00		25	Na	16,575.65
				SO_4	629.21
				Mg	631.93
				Cl	29,993.41
				Ca	1,824.00
Knauss et al. (2005)	-6.19	62.7	25	Al	8.70E-04
				Ba	59.18
				Sr	109.44
				Ca	2,211.64
				Fe	36.28
				K	414.21
				Mg	461.82
				Na	40,845.98
				SiO_2	24.11
				Cl	68,757.94
				SO_4	10.32
Cantucci et al. (2009)	-5.81	23.5	25	Na	42,990.93
				K	2,502.29
				Ca	39.48
				Mg	0.16
				HCO_3	447.25
				Cl	63,815.76
				HS	3,261.04
				SO_4	4.44
				Li	2.57
				Sr	46.88
				Si	10.44
				Al	1.84E-03

TABLE 5.1—CONTINUED

Reference	Log(k_o) mol/m^2.sec	Ea KJ/mol*°K	Reference Temperature °C	Brine Composition Ion	Conc. mg/l
Xu et al. (2006)	-6.19	62.76	25	Ca	7,284.00
				Mg	112.05
				Na	27,886.63
				K	2,807.26
				Fe	0.08
				Cl	60,979.50
				SiO_2	210.30
				HCO_3	457.63
				SO_4	194.05
				Al	1.53E-04
				Pb	2.07E-07
Wigand et al. (2009)	-1.69	23.5	25	Al	0.08
				SiO_2	4.27
				Ca	275.48
				Fe	17.98
				K	64.00
				Mg	39.01
				Mn	47.03
				Zn	1.83
				Li	0.02
				Sc	0.16
				Cu	0.95
				Rb	0.07
				Sr	0.44
				Cd	0.02
				Pb	0.02

CO_2 (99.8% pure) was used in this study to avoid introducing contaminants into the core. Different synthetic brines were used; the first one was equivalent to seawater excluding Na_2SO_4, the second brine composition was equivalent to seawater, and the third one was equivalent to formation brine from the Middle East. The compositions of the three brines are given in **Table 5.3**. Pure salt brines that are composed of NaCl, $MgCl_2$, or $CaCl_2$, at concentrations of 1, 5, and 10 wt%. The brines densities were

measured at room temperature using a DMA4100 density meter, and a psl 1643/02 capillary viscometer was used to measure the viscosity of these brines.

TABLE 5.2—PROPERTIES OF THE PINK DESERT CORES.		
Core #	**Porosity (vol%)**	**Permeability (md)**
1	19.6	61.8
2	21.9	50.0
3	18.9	56.52
4	19.8	79.8
5	22.4	77.0
6	22.4	68.2
7	19.6	57.5
8	27.1	96.0
9	24.1	77.0
10	24.4	99.0
11	24.4	99.0
12	25.9	93.5
13	24.7	91.0
14	26.9	85.0
15	26.2	80.0
16	23.6	72.0
17	24.8	93.0

Seventeen coreflood experiments were conducted in this study. The experiments were run at temperatures of 70 and 200°F, and injection flow rates of 2 and 5 cm^3/min were used. A summary of the coreflood experiments is given in **Table 5.4**.

TABLE 5.3—CONCENTRATION OF KEY IONS, AND PROPERTIES OF SYNTHETIC BRINES.			
Ion	**Seawater Without Sulfate**	**Seawater**	**Formation Brine**
Cl^-	22,010*	22,010	143,285
SO_4^{--}	0	2,850	108
Na^+	12,158	12,158	51,187
Mg^{++}	1,315	1,315	4,264
Ca^{++}	401	401	29,760
TDS mg/l	35,884	38,734	228,604
Viscosity @ 70°F (cp)	1.040	1.045	1.70
Density @ 70°F (g/cm^3)	1.0260	1.0266	1.1640
pH value @ 70°F (g/cm^3)	6.4	6.4	6.9

*all unites are expressed in mg/l.

5.3 Results and Discussion

Three cycles of CO_2 alternating brine were injected in all experiments. For core #1 a synthetic seawater without Na_2SO_4 was used, while for core #2, the synthetic seawater with Na_2SO_4 was injected.

TABLE 5.4—A SUMMARY OF COREFLOOD EXPERIMENTS.			
Experiment	**Temperature (°F)**	**Injection flow rate of CO_2 and brine (cm^3/min)**	**Brine Injected**
1	200	2	Seawater without Sulfate
2	200	2	Seawater
3	70	2	Seawater
4	200	5	Seawater without Sulfate
5	200	5	Seawater
6	200	2	Formation Brine
7	70	2	Formation Brine
8	200	5	Distilled Water
9	200	5	1 wt% NaCl
10	200	5	5 wt% NaCl
11	200	5	10 wt% NaCl
12	200	5	1 wt% $CaCl_2$
13	200	5	5 wt% $CaCl_2$
14	200	5	10 wt% $CaCl_2$
15	200	5	1 wt% $MgCl_2$
16	200	5	5 wt% $MgCl_2$
17	200	5	10 wt% $MgCl_2$

A comparison between the concentration of calcium ions in the core effluent samples for both experiments, and the concentration of sulfate for core #2 are shown in **Fig. 5.1**. For core #1, calcium concentration increased during CO_2 injection, due to the reaction between carbonic acid and limestone. A reduction in calcium concentration is observed during brine injection, due to the reduction in CO_2 saturation inside the core, which limits the amount of dissolved rock. Core #2 showed the same increasing behavior during CO_2 injection, while during seawater injection a slight increase in

calcium concentration was observed in the beginning, and then a sharp decrease started to take place. Total calcium collected can be calculated by integrating the area under the calcium concentration curve shown in **Fig. 5.1**. When seawater was injected, the total amount of calcium collected decreased from 0.64 g for core #1, to 0.45 g for core #2. It is clear that using seawater in CO_2 WAG injection limited the maximum calcium level to 1,780 mg/l; the calcium concentration of the injected seawater was 401 mg/l, compared to 2,300 mg/l when the brine didn't contain sodium sulfate.

Sulfate concentration decreased during CO_2 injection and increased during water injection as CO_2 saturation decreased inside the core. The sulfate concentration was always less than its concentration in seawater, which was 2850 mg/l. The integration of the area between the sulfate curve and initial sulfate level line, gave a total amount of sulfate precipitated of 0.08 g, which is 5.3 % of the total injected sulfate. The total amount of sulfate injected was 1.5 g.

No significant change in the core permeability was observed after WAG injection of CO_2 in carbonate rock. Permeability changed from 61.8 to 60.5 md for core #1. However, the presence of sulfate in seawater caused some damage after WAG injection of CO_2. For core #2, the original permeability was 50 md, and final permeability was 43 md.

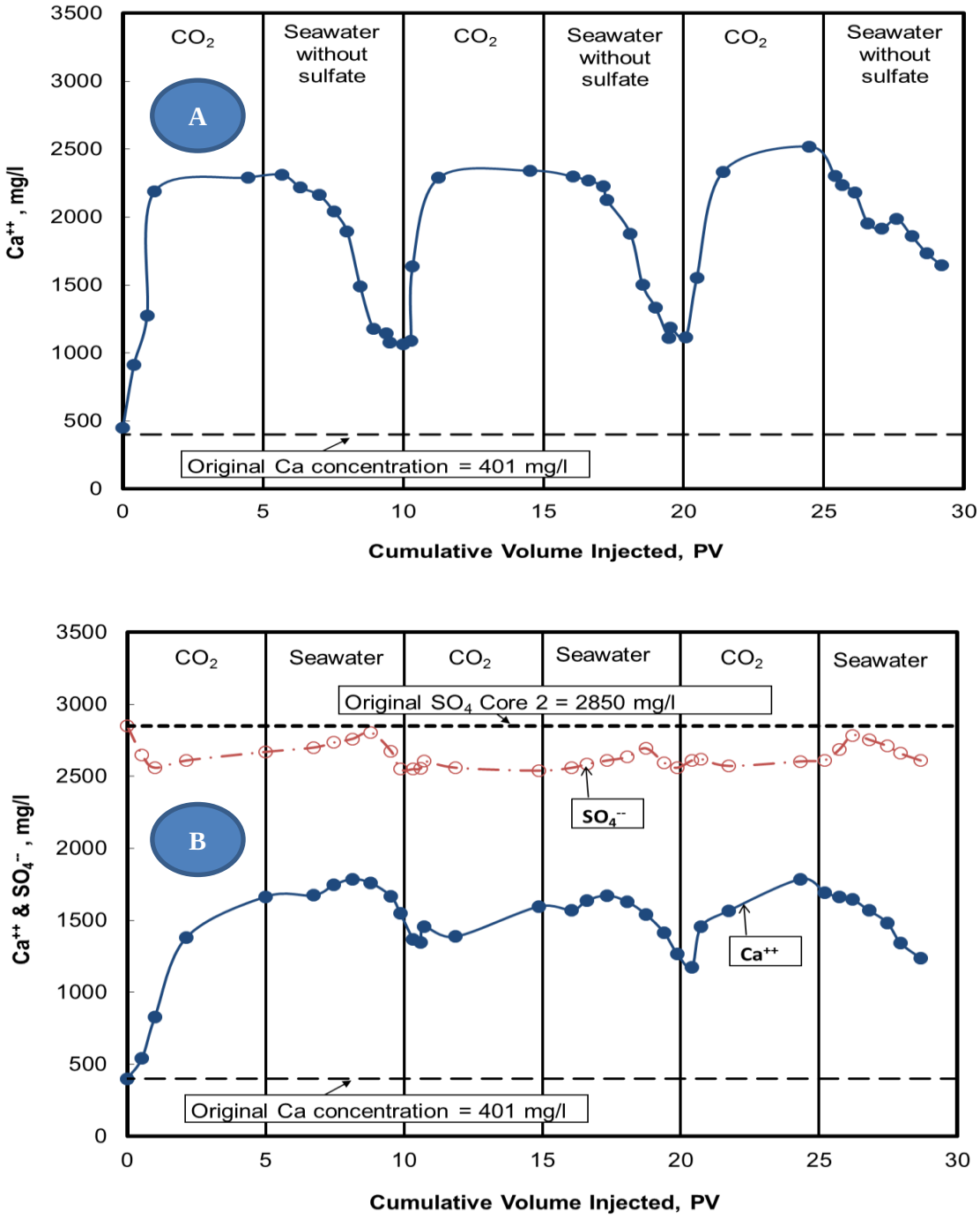

Fig. 5.1—Calcium and sulfate concentrations in the core effluent samples at a rate of 2 cm^3/min, and 200°F.

5.3.1 Effect of Temperature

Coreflood #2, which was run at 200°F, was compared with core #3 which was run at 70°F. The solubility of calcium sulfate in seawater is given by Flint (1967) and Linnikov and Podbereznyi (1995), since gypsum is the stable calcium sulfate form at temperatures less than 40°C (104°F) and anhydrite is the stable form at higher temperatures. Anhydrite solubility at 200°F is compared to the solubility of gypsum at 70°F and was found to be less than half, 0.42 wt% for gypsum and 0.195 wt% for anhydrite. Less damage is expected and less sulfate will be precipitated at lower temperatures.

The concentrations of calcium and sulfate in the core effluent sample for core #3 are given in **Fig. 5.2**. More calcium was collected in this experiment than in core #2. It reached 2590 mg/l during CO_2 injection, comparing to 1780 mg/l in core #2. Also, there was almost no change in the sulfate level for the first two WAG cycles, the last cycle only showed some decrease in the SO_4 concentration.

The total calcium collected in the core effluent sample for core #3 was 0.75 g. The increase in calcium collected was due to the higher solubility of calcium sulfate at 70°F, and the higher solubility of CO_2 in brine at this temperature.

Although the core effluent sample showed that at 70°F there was 0.046 g loss in the sulfate injected, the total sulfate present in the injected seawater was 1.4 g. The permeability of this core increased from 56.5 to 60.6 md.

Two temperatures were examined in this study, the results showed that at lower temperature (70°F) the solubility of calcium sulfate and CO_2 in seawater is higher, and

more calcium carbonate dissolved which resulted in an increase in the core permeability. At higher temperature (200°F) the solubility of calcium sulfate and CO_2 in seawater is less, that will cause more precipitation and less calcium carbonate dissolution, which resulted in more damage noted to the core.

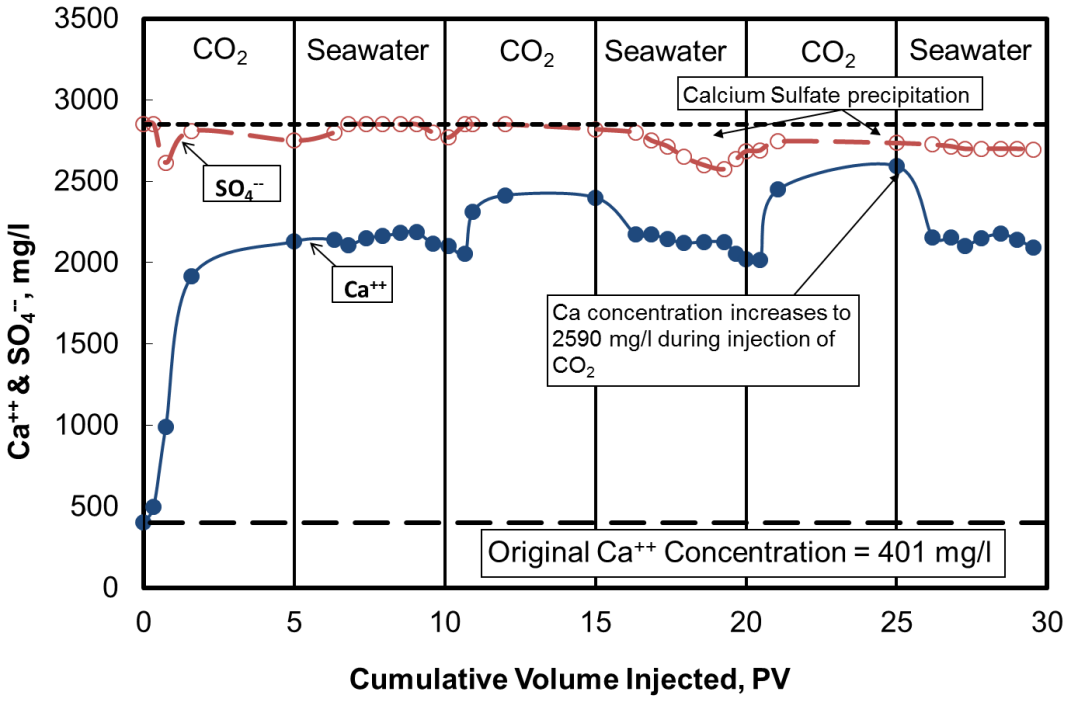

Fig. 5.2—Calcium and sulfate concentrations in the core effluent samples at a rate of 2 cm^3/min, and 70°F. core #3.

5.3.2 Effect of Injection Flow Rate

In this study two flow rates were examined, 2 and 5 cm^3/min. A flow rate of 2 cm^3/min was discussed briefly in the previous section. Two coreflood experiments were

run at 5 cm^3/min, core #4 was run with no sulfate in the injected brine, and core #5 with sulfate in seawater composition, both conducted at 200°F.

The same behavior observed at a rate 2 cm^3/min (**Fig. 5.1**) was repeated again at rate 5 cm^3/min, and the absence of SO_4^{-2} in the injected brine increased the amount of calcium collected in the effluent core samples. Total calcium collected for core #4 was 0.58 g, while 0.375 g was collected from core #5. The measurements of sulfate concentrations showed that less sulfate precipitated at 5 than at 2 cm^3/min. The total amount of precipitated sulfate for core #5 was 0.039 g, compared to 0.08 g for core #2. It is also noted, that in the first two cycles, sulfate concentration went up to 3000 mg/l, which is above the original sulfate level (2850 mg/l). This indicated that some of the precipitated sulfate was swept out of the core by the high velocity brine injected in the core.

Precipitation of calcium sulfate was also evaluated by the change in the core permeability. For core #5, the permeability decreased from 77 to 69 md; while it increased from 79.8 to 83 md for core #4.

The injection flow rate of CO_2 doesn't have a significant effect on the cores permeability after WAG injection of CO_2. The same behaviors were noted when CO_2 was injected at 2 and 5 cm^3/min.

5.3.3 Effect of Brine Salinity

The TDS of seawater used was 38,734 mg/l, and the formation brine was 228,604 mg/l (Alotaibi et al. 2010). Formation brine composition and properties are

shown in **Table 5.2**. Cores #6 and #7 were both flooded with CO_2 alternating formation brine. The temperatures used were 200 and 70°F for cores #6 and #7, respectively.

A significant amount of calcium was collected when formation brine was used in CO_2 WAG injection, compared to seawater (Cores #1 and #2). Calcium concentration increased from 29,760 mg/l originally to 60,000 mg/l at 200°F, and 42,000 mg/l at 70°F (**Figs. 5.3 and 5.4**). The total calcium collected from core #6 was 6.9 g, which was 15 times more than the calcium collected from core #2. 4.2 g of calcium was collected from core #7. Again, calcium concentration increased during CO_2 injection, and decreased during brine injection. The effect of each salt (NaCl, $CaCl_2$, and $MgCl_2$) will be addressed in next sections.

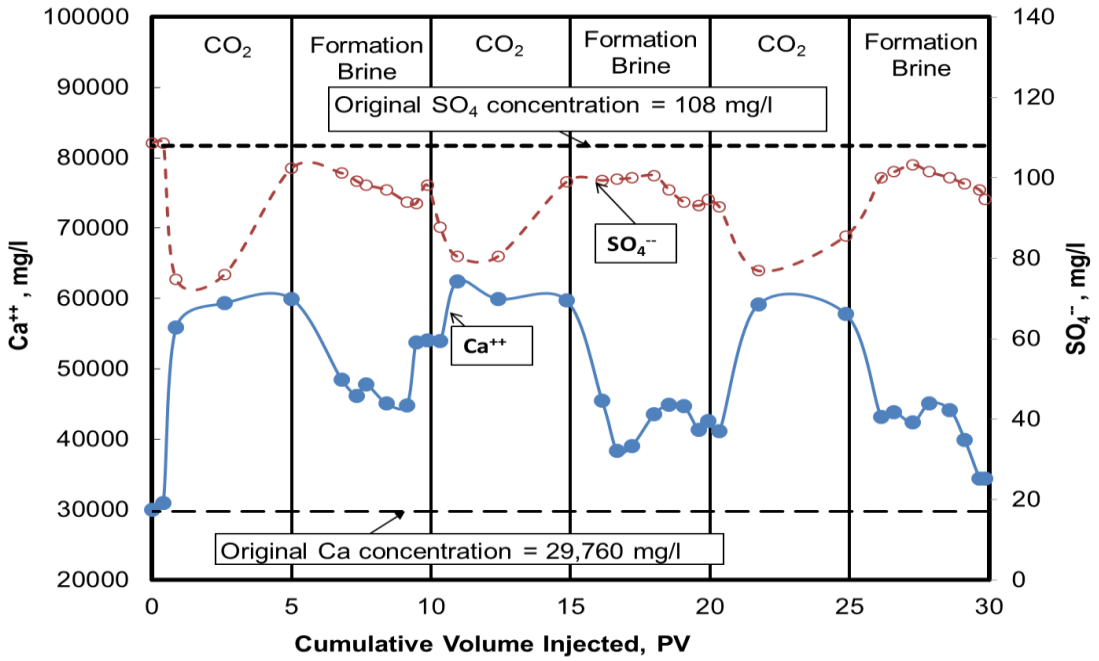

Fig. 5.3—Calcium and sulfate concentrations in the core effluent samples when formation brine was injected at 200°F, core #6.

At lower temperatures (core #7), more sulfate precipitated, compared to core #6 (higher temperature), since formation brine initially contains only 108 mg/l SO_4^{-2}. The precipitated sulfate in both cases was very small and had no significant impact on the core permeability, the main mechanism that affected the core permeability was the precipitation of calcium carbonate because of the high concentration of the calcium in the formation water, due to rock dissolution. The permeability of core #6 decreased from 68.2 to 64 md, while for core #7, it increased from 57.5 to 63 md.

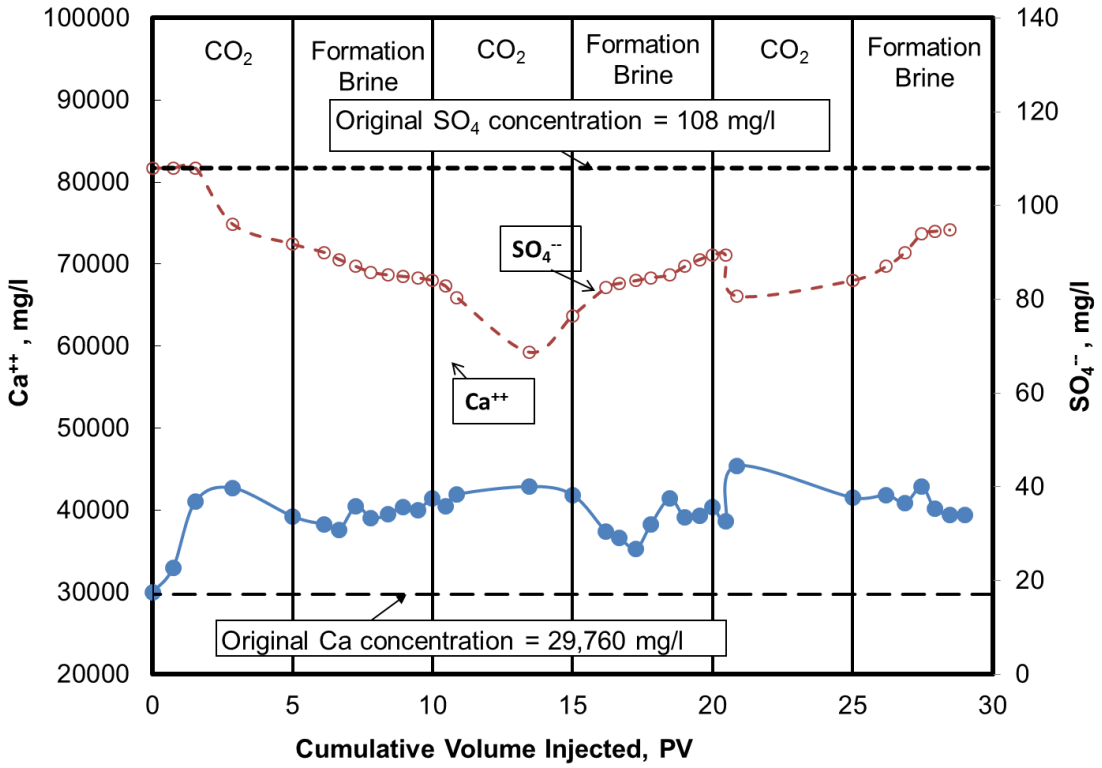

Fig. 5.4—Calcium and sulfate concentrations in the core effluent samples when formation brine was injected at 70°F, core #7.

Table 5.5 summarizes the change in the cores permeability, and **Fig. 5.5** gives a brief summary of the total calcium collected in the core effluent samples and total sulfate precipitated for each experiment for cores #1-7.

TABLE 5.5—EFFECT OF BRINE COMPOSITION ON THE CORE PERMEABILITY AFTER CO_2 WAG INJECTION

Core	$K_{initial}$ (md)	K_{final} (md)	Ratio	Injection Conditions	Brine
1	61.8	60.5	0.98	2 cm^3/min 200°F	Seawater without sulfate
2	50	43	0.86		Seawater
3	56.5	60.6	1.07	2 cm^3/min 70°F	Seawater
4	79.8	83	1.04	5 cm^3/min 200°F	Seawater without sulfate
5	77	69	0.90		Seawater
6	68.22	64	0.94	200°F	Formation Brine
7	57.5	63	1.10	70°F	

5.3.4 Effect of Distilled Water (DI Water)

Calcium concentration increased during CO_2 injection from 0 to 1080 mg/l due to rock dissolution, a reduction in calcium concentration was observed during water injection to 500 mg/l. The behavior was repeated each cycle, with a slight change in the calcium concentration values. The maximum value was 1184 and 1070 mg/l, and the minimum value was 300 and 530 mg/l for the second and third cycles, respectively.

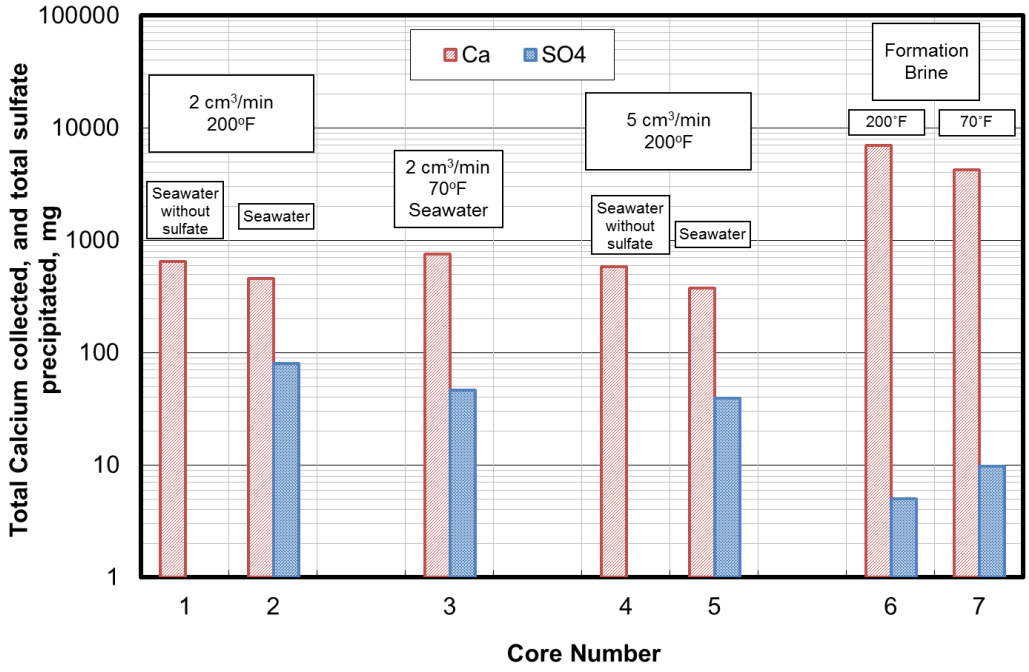

Fig. 5.5—Percent of calcium collected to the total calcium originally present in each core, and percent of sulfate precipitated in each core.

The total calcium collected for this core is 0.353 g. A reduction in core permeability from 96 to 90 md was observed after CO_2 injection.

5.3.5 Effect of NaCl Brines

Three coreflood experiments were run at NaCl concentrations of 1, 5, and 10 wt%. Measuring the permeability for these cores before and after CO_2 injection, showed no change in permeability.

For 1 wt% NaCl brine, the maximum calcium concentration was almost the same as when distilled water was used (**Fig. 5.6**). The minimum calcium concentration was 300 and 1000 mg/l for distilled water and 1 wt% NaCl brine, respectively.

Although the solubility data showed that less CO_2 will be dissolved with increasing TDS, the results showed that more calcium was collected when using 5 wt% NaCl brine, compared to 1 wt% NaCl brine (**Fig. 5.7**). When the concentration of sodium chloride was increased to 10 wt%, a slight reduction in calcium concentration was observed in the core effluent samples compared to 5 wt%, but still higher than the concentration collected with 1 wt% NaCl brine.

The maximum calcium concentrations were 1276, 1841, and 1700 mg/l, while the total calcium collected was 0.436, 0.635, and 0.54 g for 1, 5, and 10 wt% NaCl brine, respectively.

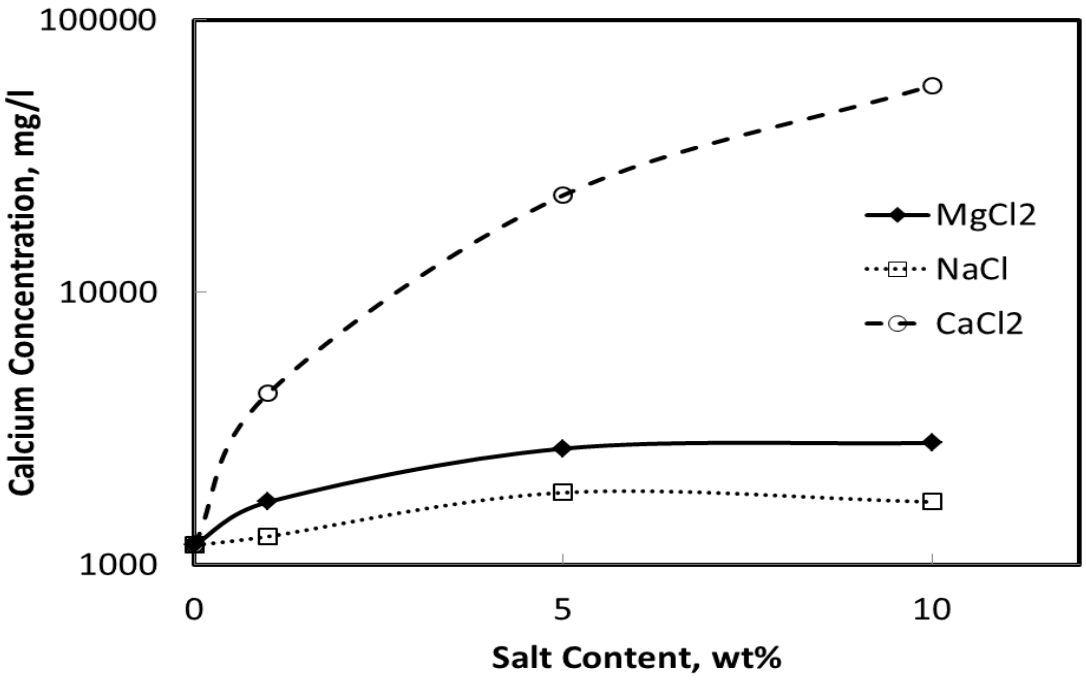

Fig. 5.6—Calcium concentration in the core effluent samples.

5.3.6 Effect of $CaCl_2$ Brines

Fig. 5.6 shows that for 1 wt% $CaCl_2$ brine, the maximum calcium concentration increased from 3100 mg/l initially to 4256 mg/l. This was an increase of 1156 mg/l, which was equal to the increase of calcium concentration when distilled water was used.

A significant increase in the calcium concentration in the core effluent samples was observed when increasing the concentration of calcium chloride in the injected brine. For 5 wt% $CaCl_2$ brine the calcium increased from 15,504 to a maximum concentration of 22,792, with a 7,288 mg/l increase in calcium concentration. When doubling calcium chloride concentration to 10 wt%, calcium increased from 31,008 to 57,000 mg/l, with 26,000 mg/l increase in calcium concentration.

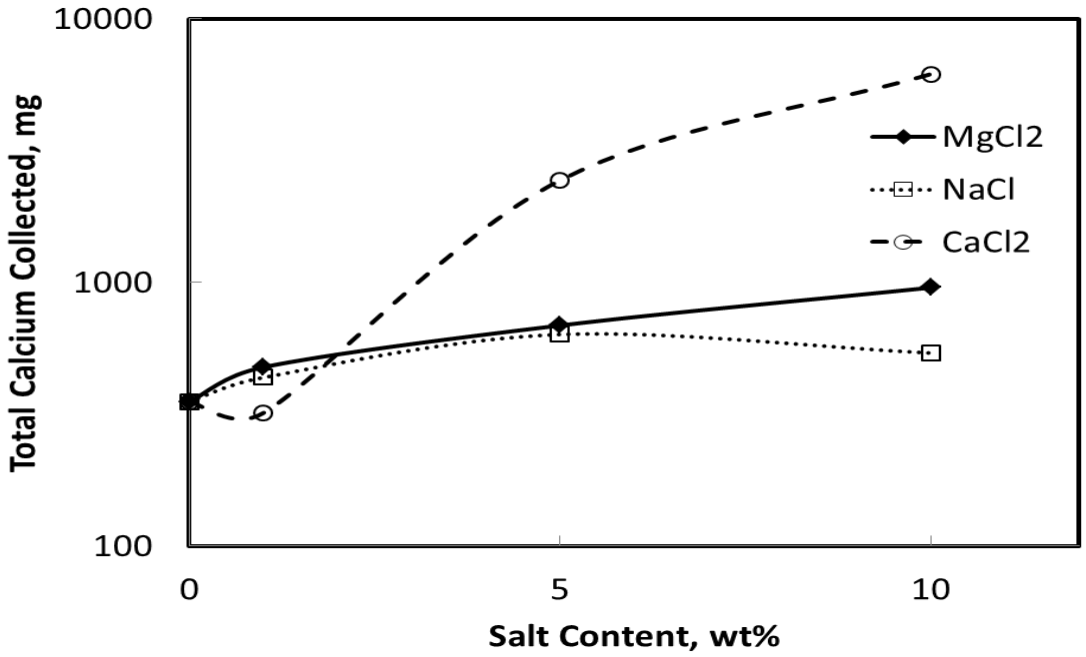

Fig. 5.7—Total calcium collected in the core effluent samples.

Total calcium collected was 0.32, 2.44, and 6.17 g for 1, 5, and 10 wt% $CaCl_2$ brine, respectively. (**Fig. 5.7**).

The ratio of the final core permeability to the initial permeability is given in **Fig. 5.8**. An enhancement in core permeability, of 6.5 %, was noted when 1 wt% $CaCl_2$ brine was injected, compared to 7 % loss in permeability when distilled water was used. At higher calcium chloride concentrations, 5 and 10 wt%, a permeability reduction of 14 % occurred after CO_2 injection.

5.3.7 Effect of $MgCl_2$ Brines

To examine the effect of magnesium chloride on the core permeability during CO_2 sequestration, three coreflood experiments were run. **Fig. 5.6** shows that with increasing the concentration of $MgCl_2$ in the injected brine, more calcium was collected in the core effluent samples. The maximum calcium detected in the samples was 1764, 2686, and 2843 mg/l for 1, 5, and 10 wt% $MgCl_2$ brine, respectively. Total calcium collected was 0.477, 0.687, and 0.956 g, as shown in **Fig. 5.7**. Magnesium concentration was the same for all core effluent samples.

Fig. 5.8 shows that as magnesium chloride concentration increased, the damage introduced to the cores was still close: 4, 5, and 8 % loss in the core permeability for 1, 5, and 10 wt% $MgCl_2$ brine, respectively.

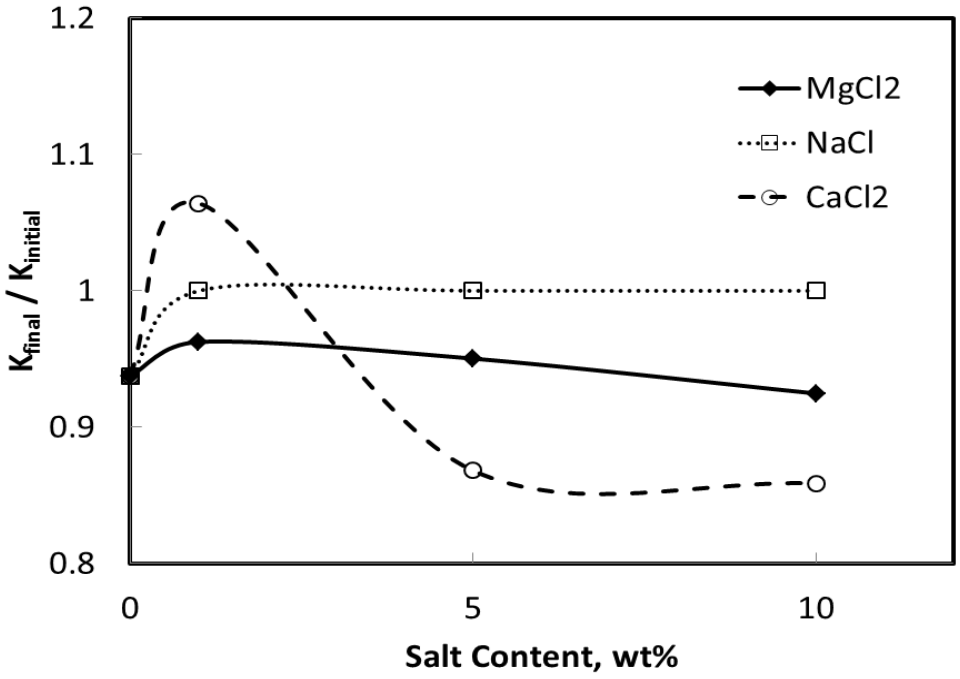

Fig. 5.8—Change in cores permeability when different salt concentrations of $CaCl_2$ brine were injected in CO_2 WAG injection.

5.4 Calculation of Maximum Calcium Concentration

Calcium concentration present in the core effluent sample gives an indication about the reactions between CO_2/rock/brine. A correlation to calculate the maximum calcium concentration in the core effluent samples was developed using the experimental results obtained in this study as follows;

$$C_{Ca} = 18533.2 - 9.66861x10^{7} w_{co2}^{2} + 1069.71 C_{NaCl} - 44.1245 C_{NaCl}^{2} + 3849.85 C_{CaCl2} + 234.52 C_{CaCl2}^{2} + 1321.04 C_{MgCl2} - 58.4118 C_{MgCl2}^{2} - 14239 w_{co2} TDS \quad (5.3)$$

Where;

C_{Ca} = Maximum calcium concentration in core effluent samples, mg/l

C_{NaCl} = concentration of NaCl in brine, wt%

C_{CaCl2} = concentration of $CaCl_2$ in brine, wt%

C_{MgCl2} = concentration of $MgCl_2$ in brine, wt%

TDS = Total dissolved solids, wt%

w_{CO2} = Solubility of CO_2 in brine, weight fraction

The solubility of CO_2 in distilled water, NaCl and $CaCl_2$ brines used in this study, at a pressure of 1300 psi and temperature of 200°F, was obtained from Nighswander et al. (1989), Duan et al. (2006), and Prutton and Savage (1945), respectively. Their work was specified for NaCl and $CaCl_2$ brines, while the solubility of CO_2 in $MgCl_2$ brine was calculated using **Eq. 1.3** and given in **Table 5.6**. **Eq. 5.3** is developed based on the results of coreflood experiments conducted at a pressure of 1300 psi, and 200°F, and is valid for NaCl, $CaCl_2$, and $MgCl_2$ brines.

TABLE 5.6—CO_2 SOLUBILITY AT 1300 PSI AND 200°F

Salt Concentration, wt%	**0%**	**1%**	**5%**	**10%**
Brine Composition	**CO_2 Solubility, weight fraction**			
NaCl	0.0134	0.0130	0.0115	0.0098
$CaCl_2$		0.0130	0.0115	0.0096
$MgCl_2$		0.0128	0.0105	0.0083

Eq. 5.3 was applied to the experiment run on core #1. The brine composition was 2.879 wt% NaCl, 0.111 wt% $CaCl_2$, and 0.515 wt% $MgCl_2$. Ca^{++} calculated is 2249 mg/l, while the measured value was 2290, 2300, and 2500 for the first, second and third cycles, respectively.

Another case where **Eq. 5.3** was applied, and gave acceptable results (an error less than 4%), was the experiment run on core #4. This formation brine had a salt composition of 12.9 wt% NaCl, 8.23 wt% $CaCl_2$, 1.67 wt% $MgCl_2$, and 0.016 wt% Na_2SO_4. The effect of sodium sulfate salt was ignored, since its concentration is very small. The calculated calcium concentration was 57,825 mg/l, while the measured value was 60,000 mg/l.

5.5 Simulation Studies

The experimental results showed that the kinetics of the reaction between CO_2 and limestone rock is a function in the brine composition. A compositional simulator (CMG-GEM) was used to predict the reaction rate constant between CO_2 and limestone for each brine used based on the calcium concentration measured in the core effluent samples. A field scale simulation was also run to address the effect of brine composition on the permeability distribution during WAG injection of CO_2.

The simulator input is the injection schedule, CO_2 and brine relative permeability, capillary pressure between CO_2 and injected brine, chemical kinetics of the chemical reactions, initial porosity and permeability, and the core dimensions.

To calculate the relative permeability curves, the irreducible water saturation and the critical saturation of CO_2 were obtained from the coreflood experiments to be 0.25 and 0.15, respectively. Relative permeabilities were calculated using **Eqs. 3.1-3.2**. the end points permeability and the exponents were adjusted to match the pressure drop obtained in the lab;

0.35 = relative permeability to brine at irreducible CO_2 saturation

0.05 = relative permeability to CO_2 at irreducible brine saturation

0.25 = irreducible brine saturation

0.15 = irreducible CO_2 saturation

5.5.1 Core Scale Simulation

The cylindrical cores were divided into radial grids with 5X20X20 blocks in the radial coordinates r, Θ, and z directions, respectively. The initial permeability and porosity were assumed constant for all grid blocks, cores initial porosity and permeability are shown in **Table 5.2**.

The simulator uses **Eqs. 3.5** and **3.6** to predict the dissolution and/or precipitation rate for calcium carbonate during the reaction with CO_2. In this study, the activation energy of 62.7 KJ/mole.°K, and reactive surface area of 9.5 cm^2/g were used for all cases (Svensson and Dreybrodt 1992). In order to simulate the calcium concentration obtained in the experimental study, the reaction rate constant was found ($\log(k_{25})$) to be in the range between -9.2 (for DI water case) and -6.2 (for 5 wt% $CaCl_2$ brine case). A summary for the reaction rate constant for all cases is given in **Table 5.7**. It is clear that

at a higher salt content the reaction rate constant increases, and a larger value was obtained for $CaCl_2$ brines than $MgCl_2$ brines, and a smaller value was obtained for NaCl brines. The simulation failed at high calcium concentration cases (10 wt% $CaCl_2$ and formation), no reaction rate constant could be predicted for these cases.

The simulator also has the capability to predict the change in core permeability due to the dissolution and precipitation reactions. The change in core porosity was calculated using **Eqs. 3.7 and 3.8**, while permeability was calculated using the Carman-Kozeny equation based on the initial and final porosity.

The permeability and porosity change distribution across the core calculated by CMG-GEM for cores #4 and 5 are shown by **Figs. 5.9** and **5.10**, respectively. The Carman-Kozeny exponents used in these calculations were 4.53 when seawater without sulfate injected with CO_2 during WAG injection, and 7.82 in seawater case as shown in Chapter 8.

Fig. 5.9 shows that for core #4 an enhancement in the permeability was noted close to the core inlet until 1.5 in. from the core inlet; more increase in the permeability was noted each cycle. Behind this region, damage was noted to the core outlet, and the damage increased with the number of WAG cycles. Seawater in CO_2 WAG injection causes a reduction in core permeability throughout the core length, with more damage close to the core inlet due to calcium sulfate precipitation (**Fig. 5.10**). The damage increases as more WAG cycles were injected.

TABLE 5.7—A SUMMARY OF THE REACTION RATE CONSTANT FOR EACH BRINE USED IN THIS STUDY			
Brine	**Log (k_{25}) mol/m^2.sec**	**Maximum Calcium Concentration Measured mg/l**	**Maximum Calcium Concentration Simulated mg/l**
DI Water	-9.20	1,184	1,168
1 wt% NaCl	-9.08	1,276	1,264
5 wt% NaCl	-7.38	1,841	1,788
10 wt% NaCl	-7.30	1,700	1,724
1 wt% $MgCl_2$	-7.3	1,764	1,776
5 wt% $MgCl_2$	-7.05	2,686	2,672
10 wt% $MgCl_2$	-6.55	2,843	2,832
1 wt% $CaCl_2$	-7.72	[a]4,256	4,276
5 wt% $CaCl_2$	-6.20	[b]22,792	23,000
Seawater without sulfate	-6.70	[c]2,300	2,240
Seawater	-6.46	1,780	1,800

a initial calcium concentration = 3,100 mg/l
b initial calcium concentration = 15,504 mg/l
c initial calcium concentration = 401 mg/l

The overall core permeability after WAG injection for cores #4 and #5 are given in **Fig. 5.11**. Most of the change in permeability occurs during the first WAG cycle, the permeability after the second and third WAG cycle was almost the same as after the first

cycle. A good match between the permeability measured in the lab and calculated by the simulator was also shown in **Fig. 5.11**.

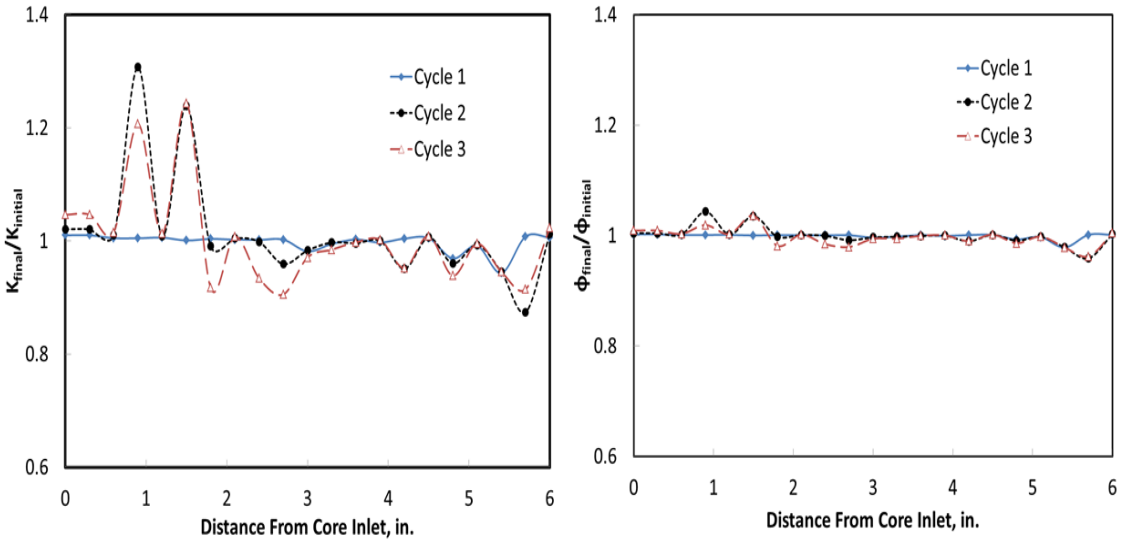

Fig. 5.9—Permeability and porosity distribution at the end of each WAG cycle when WAG injection of CO_2 and seawater without sulfate conducted for core #4

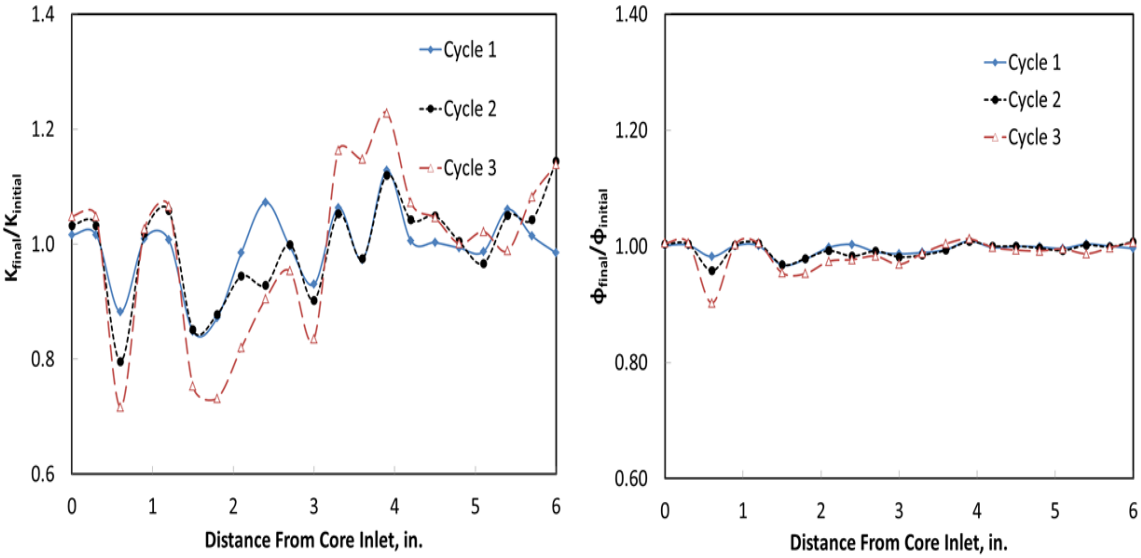

Fig. 5.10—Permeability and porosity distribution at the end of each WAG cycle when WAG injection of CO_2 and seawater conducted for core #5

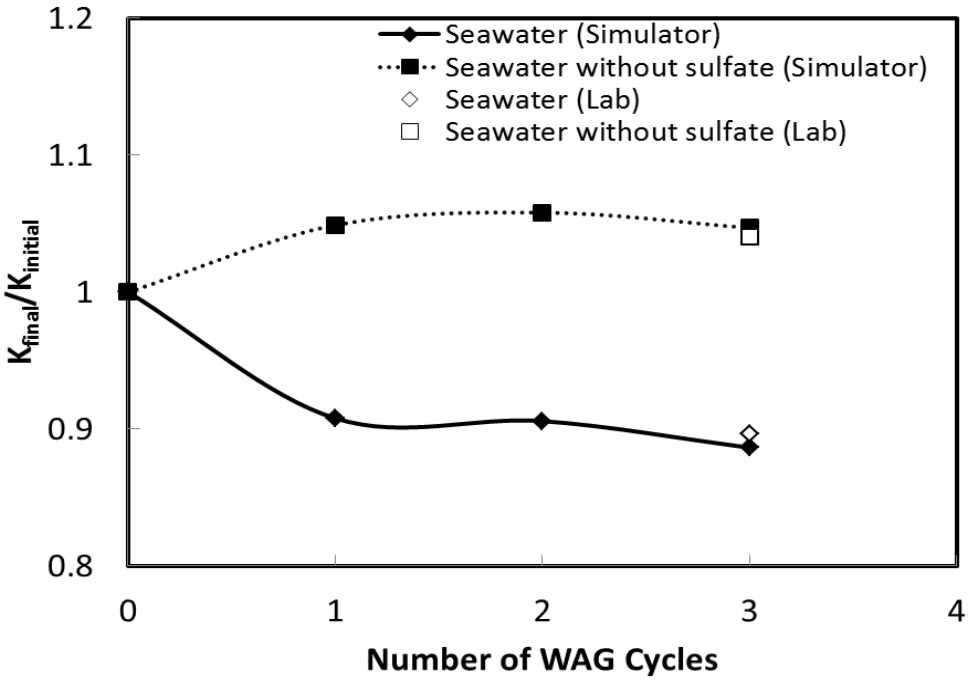

Fig. 5.11—Comparison between the permeability data obtained from the simulator and measured in the lab for cores #4 and #5.

5.5.2 Field Scale Simulation

Simulation in field scale was conducted based on the reaction kinetics obtained from the core scale simulations. The aquifer model is a homogenous saline aquifer with dimensions of 10 km X 10 km X 50 m in x, y, and z directions, respectively. The aquifer is 2500 m deep with a temperature of 163°F. The porosity is 0.15, horizontal permeability of 100 md, and vertical permeability of 33 md. The aquifer was initially at a normal pore pressure gradient of 0.465 psi/ft (Dahle et al. 2009).

The aquifer was divided into Cartesian grids with 11X11X8 blocks in x, y, and z directions, with refining the grids into smaller blocks as we move toward the injector

(**Fig. 5.12**). The injection well was completed at the center of the aquifer. Injection was conducted at a constant bottomhole pressure of 5740 psi (equivalent to a fracture pressure gradient of 0.7 psi/ft). The simulator ran for 30 years of CO_2 injection, and 1400 years after injection (the maximum number of time steps reached) to monitor the movement of CO_2 and the changes in trapping mechanisms. The aquifer was initially saturated with formation brine with the composition given in **Table 5.3**. WAG injection of CO_2 was conducted, each cycle composed of 9 months of CO_2 injection and 3 months of brine injection. Three brine compositions were tested;

a) DI Water

b) Seawater without sulfate

c) Seawater

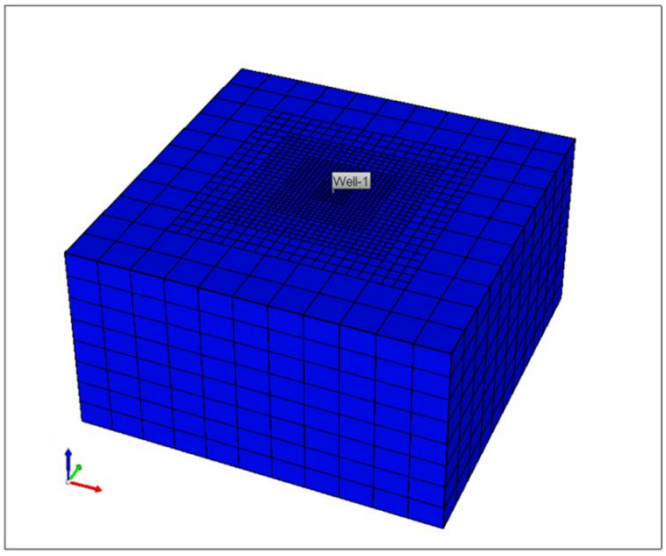

Property	Value
length	10 km
width	10 km
thickness	50 m
depth	2500 m
T	163°F
ϕ	0.15
k_h	100 md
k_v	33 md

Fig. 5.12—Aquifer model used in the simulation study.

The amount of CO_2 injected for each case was almost the same. The cumulative CO_2 injected was 2.7 M. ton with 809,448 m^3 DI water for the first case, 2.63 M. ton with 794,844 m^3 seawater without sulfate for the second case, and 2.63 M. ton with 790,931 m^3 seawater for the third case. The values give storage efficiency of 0.5% (total volume of CO_2 injected at reservoir conditions divided by the total pore volume of the aquifer, which equals 750,000,000 m^3).

The permeability and porosity distribution in the aquifer during WAG injection of CO_2 and 1400 years after injection stops are shown by **Figs. 5.13-5.15**, dissolved calcium and calcium sulfate concentration (for the seawater case) are also shown in these figures. The main changes in the permeability occurred within the wellbore block grids, beyond these blocks a minor change in porosity and permeability was noted.

For the DI water case (**Fig. 5.13**) no damage was observed (no precipitation occurred). The dissolved calcium concentration shows that the maximum calcium concentration was 580 mg/l because of the small reaction rate constant (-9.2) as shown in **Table 5.7**. The maximum increase in the permeability was 3 md around the wellbore region.

WAG injection of CO_2 and seawater without sulfate caused a 5 md loss in the permeability around the wellbore (**Fig. 5.14**) after 10 years of injection due to the precipitation calcium carbonate. At the end of injection (after 30 years) the damage reduced due to the rock dissolution, the final reduction in permeability was only 2 md. The maximum dissolved calcium concentration was 2000 mg/l. The enhancement in

permeability in the DI water case and damage in the seawater without sulfate case was still insignificant, the change in permeability didn't exceed 5%.

More damage was observed in WAG injection of CO_2 with seawater, 10 md losses in permeability after 10 years of injection was established, due to the precipitation of calcium sulfate. **Fig. 5.15** shows that reaction governed by **Eq. 1.4** occurred in this case and the calcium sulfate concentration increased to 560 mg/l.

Fig. 5.16 shows the contribution of each trapping mechanism to keep CO_2 in place over time. **Table 5.8** shows that the brine composition doesn't affect the trapping contribution of each trapping mechanism, the values are close for the three cases tested in this study.

Most of CO_2 was trapped as a free phase, it contributes more than 40 mol% after 1400 years since the injection stopped. **Fig. 5.16** shows that the amount of free gases decreases with time, due to upward migration of CO_2 because of the gravity difference, leaving behind CO_2 trapped in residual phases; also more CO_2 is dissolved in water with time.

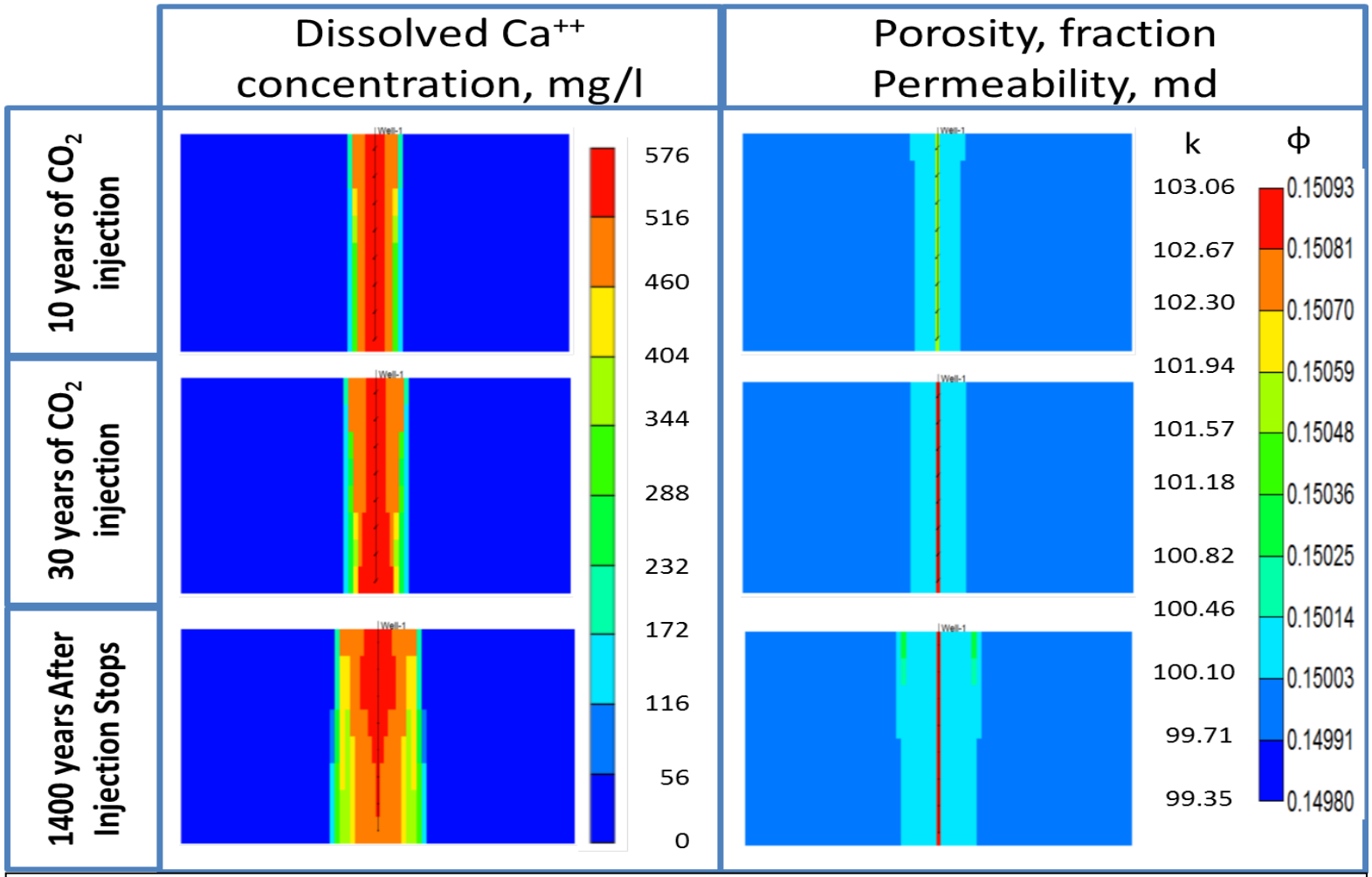

Fig. 5.13—Distribution of porosity, permeability and the dissolved calcium in the aquifer after 10 years of WAG injection of CO_2 and DI water, at the end of injection, and 1400 years after injection stops.

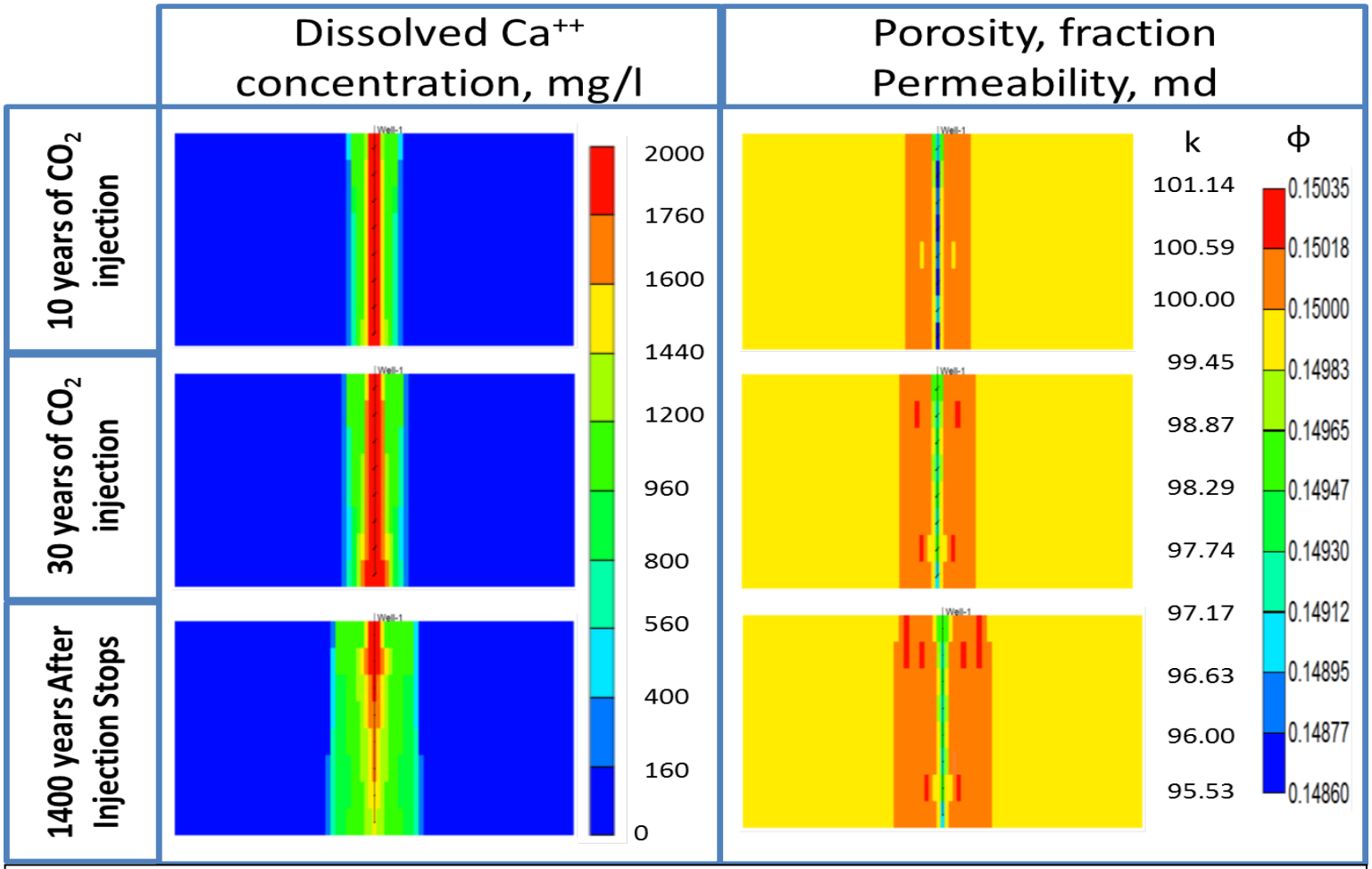

Fig. 5.14—Distribution of porosity, permeability and the dissolved calcium in the aquifer after 10 years of WAG injection of CO_2 and seawater without sulfate, at the end of injection, and 1400 years after injection stops.

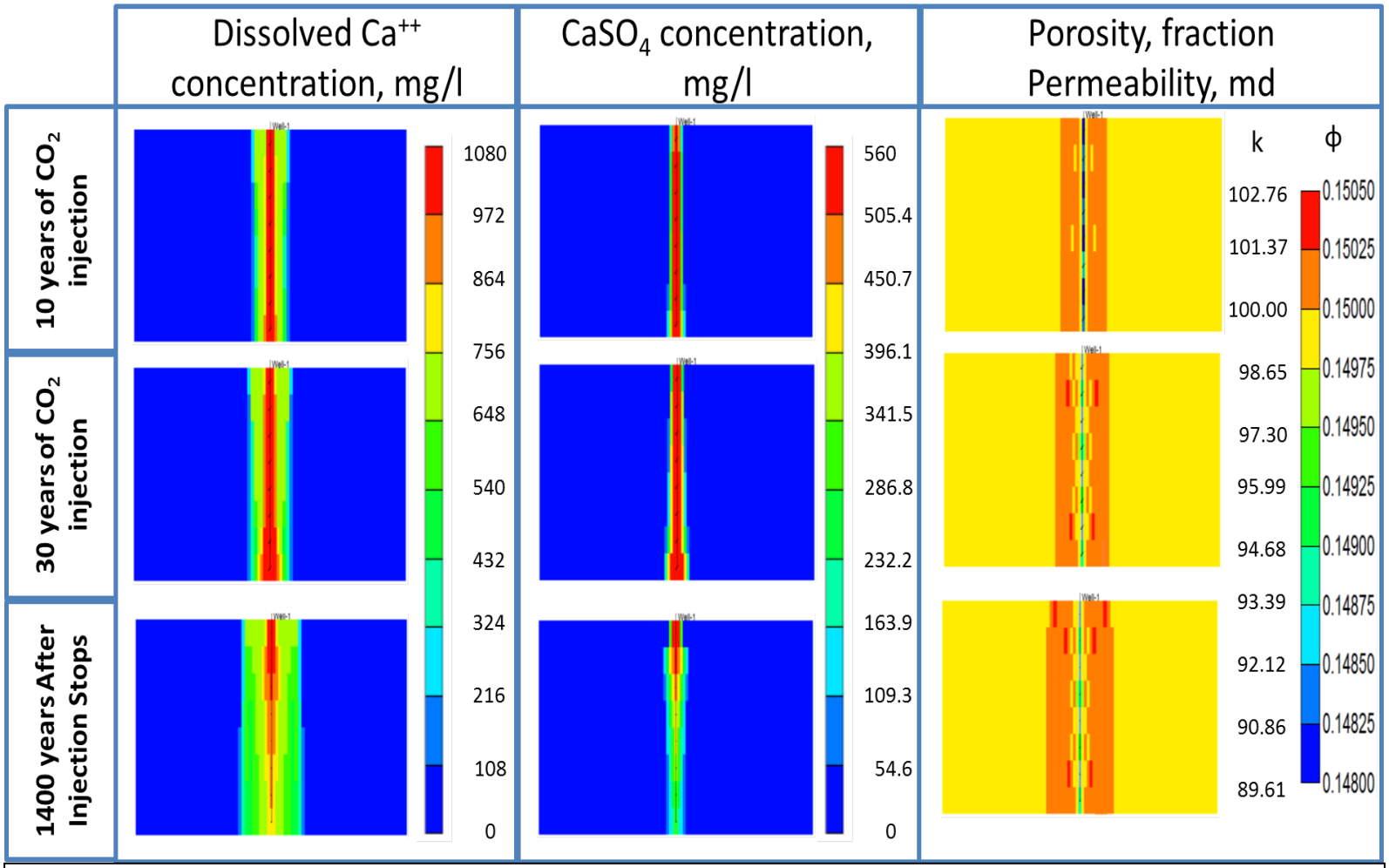

Fig. 5.15—Distribution of porosity, permeability and the dissolved calcium in the aquifer after 10 years of WAG injection of CO_2 and seawater, at the end of injection, and 1400 years after injection stops.

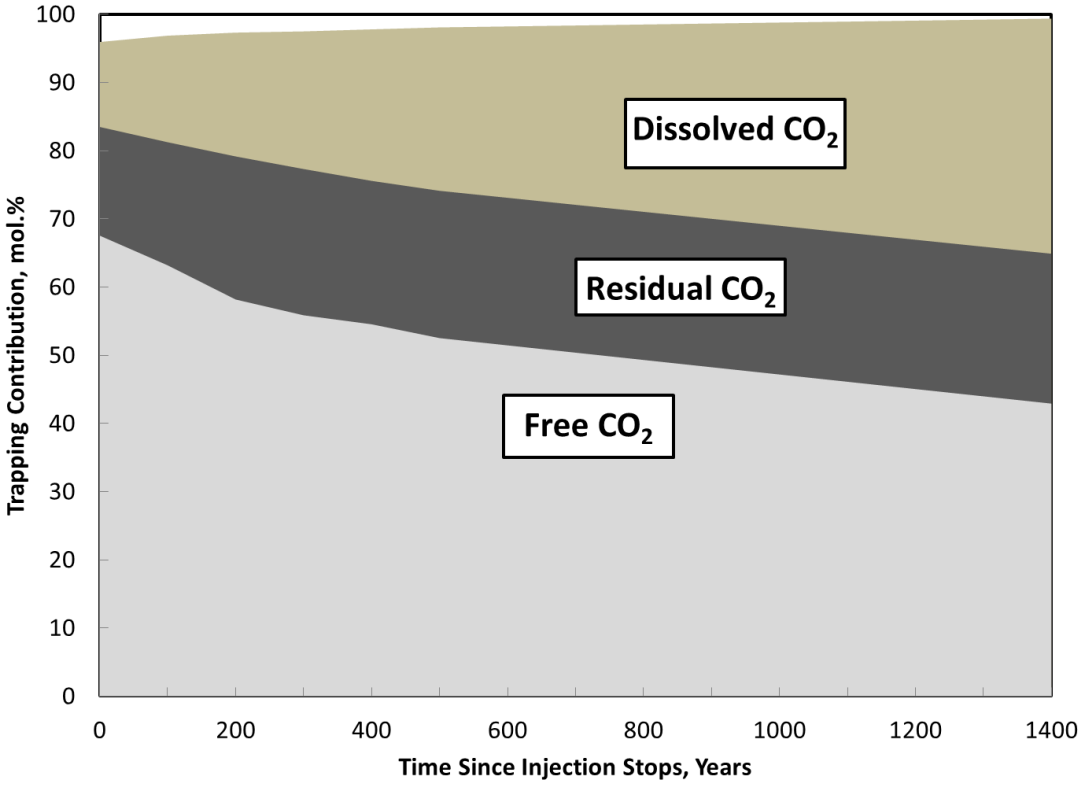

Fig. 5.16— Trapped phases after WAG injection of CO_2 and seawater without sulfate into saline carbonate aquifer

TABLE 5.8—TRAPPED PHASES AFTER WAG INJECTION OF CO_2 INTO SALINE CARBONATE AQUIFER

Brine Composition	0 years after injection stops			1400 years after injection stops		
	Free CO_2 mol%	Residual CO_2 mol%	Dissolved CO_2 mol%	Free CO_2 mol%	Residual CO_2 mol%	Dissolved CO_2 mol%
DI Water	67.55	15.94	12.45	42.91	21.98	34.47
Seawater without Sulfate	68.33	15.23	12.38	43.77	21.64	33.90
Seawater	68.55	15.48	12.41	43.73	21.77	34.05

6. CARBON DIOXIDE SEQUESTRATION IN DOLOMITE ROCK

Dolomite rock is carbonate rock that contains more than 50 wt% dolomite mineral ($CaMg(CO_3)_2$), calcite mineral ($CaCO_3$) and anhydrite form the remaining percent, non-carbonate phases may also be present (Warren 2000). Dolomite formations are usually heterogeneous, different kinds of permeability and porosity can be identified in the dolomite including: (1) intercrystal, (2) vug, (3) moldic, (4) intracrystal, (5) fracture, and (6) intraparticle porosity (Mathis and Sears 1984). Reduction of well injectivity ranging between 40% and 50% is usually noted during WAG CO_2 injection in dolomite formations (Grigg and Svec 2003).

Injection of CO_2 into dolomite formations will dissolve the reservoir rock creating wormholes and increase the reservoir heterogeneity (Graue and Blevins 1978). A minor enhancement in the formation porosity will result from this dissolution.

This chapter addresses the effect of the temperature, injection rate, brine composition, and injection scheme on the damage generated in the formation due to CO_2 injection.

6.1 Introduction

The chemical reactions between CO_2, formation brine, and dolomite is governed by **Eq. 6.1:**

$$CaMg(CO_3)_2 + 2H_2CO_3 \leftrightarrow Ca^{2+} + Mg^{2+} + 4HCO_3^- \quad (6.1)$$

A coreflood study was conducted using dolomite cores. CO_2 was injected under supercritical conditions at a pressure of 1,300 psi, and at temperatures ranging from 70 to 200°F, and injection rates of 2.0, 3.5 and 5.0 cm^3/min. Core effluent samples were collected and the concentrations of calcium and magnesium ions were measured. Core permeabilities were measured before and after the experiment to evaluate the damage generated.

6.2 Materials

Silurian dolomite used in this study is heterogeneous vuggy dolomite rock (**Fig. 6.1**) that contains small percent of silicate minerals (98 wt% dolomite and 2 wt% feldspars). Cores cut in cylindrical shapes with dimensions of 6 in. length and 1.5 in. diameter were used in all experiments. X-ray fluorescence (XRF) was used to determine rock composition **Table 6.1**, rock composition is 97.5% dolomite, presence of Si, Al, K, and Na indicated that clays and/or feldspar are present, also a small iron concentration is noted. Core properties are given in **Table 6.2**. CO_2 used with a purity of 99.8% to avoid introducing contaminants into the cores. A synthetic brine, **Table 4.2**, was used. It had total dissolved solids (TDS) of 35,884 ppm, pH 6.4, and a viscosity of 1.04 cp at room temperature. Deionized water with a resistivity of 18.2 MΩ.cm at room temperature was used to prepare the synthetic brines. Reagent grade salts were used to prepare these brines.

CO_2 was injected as a liquid phase at 70°F, or as a supercritical phase at 200 and 250°F. A summary of coreflood experiments is given in **Table 6.3**.

Fig. 6.1—Vuggy Silurian dolomite core.

TABLE 6.1—BULK COMPOSITION OF SILURIAN DOLOMITE		
Element	**wt%**	**mol %**
O	51.46	59.55
C	12.69	19.561
Ca	21.18	9.786
Mg	12.79	9.743
Na	1.26	1.014
Si	0.2	0.13
Al	0.16	0.112
Fe	0.1	0.034
Cl	0.09	0.045
K	0.05	0.024
Sn	0.01	0.002

6.3 Results and Discussion

In this study, 20 coreflood experiments were run to examine the effect of different parameters on the core permeability during CO_2 injection. The coreflood

experiment that was conducted on the core #1 was considered as a reference case and all the other cases were compared to this one.

TABLE 6.2—PROPERTIES OF THE SILURIAN DOLOMITE CORES.

Core #	Permeability (md)	Total Magnesium Content (g)	Total Calcium Content (g)
1	182	83.06	50.15
2	190	82.82	50.00
3	192	80.71	48.73
4	96	85.04	51.34
5	233	81.73	49.34
6	192	82.16	49.61
7	102	84.75	51.17
8	117	83.41	50.36
9	65.5	86.88	52.45
10	164	82.62	49.88
11	147	83.59	50.47
12	165	82.93	50.07
13	211	81.32	49.10
14	234	82.16	49.61
15	218	82.64	49.90
16	218	80.71	48.73
17	164	82.79	49.98
18	136	83.45	50.38
19	218	81.54	49.23
20	122	84.92	51.27

Core #1 experiment was run at temperature of 200°F and injection flow rate of 5 cm^3/min. Five pore volumes of CO_2 were injected in each cycle for three WAG cycles of CO_2 and brine injected, the CO_2 volume was equal to brine volume in each cycle, five pore volumes of CO_2 were injected in each cycle. Initial core permeability was 182 md. Capillary and gravity for this case were calculated using the equation introduced by

Zhou et al. (1994) and found to be 1.17 $x10^{-5}$ and 0.39, respectively. No fluid segregation will occur inside the core.

TABLE 6.3—SUMMARY OF COREFLOOD EXPERIMENTS.						
Core #	**CO_2 Volume per Cycle (Pore Volume)**	**No. of Cycles**	**CO_2 : Brine Volumetric Ratio**	**Rate (cm^3/min)**	**Temperature °F**	**Case**
1	5	3	1:1	5	200	Reference case
2	5	3	1:1	5	250	Effect Temperature and Flow Rate
3	5	3	1:1	5	Room	
4	5	3	1:1	2	200	
5	5	3	1:1	2	250	
6	5	3	1:1	2	Room	
7	5	3	1:1	10	200	
8	5	3	1:1	10	250	
9	5	3	1:1	10	Room	
10	5	3	1:1	3.5	200	
11	5	3	1:1	3.5	250	
12	5	3	1:1	3.5	Room	
13	1	15	1:1	5	200	Effect of CO_2 Volume/Cycle
14	3	5	1:1	5	200	
15	7.5	2	1:1	5	200	
16	15	1	1:1	5	200	
17	5	3	2:1	5	200	Effect of CO_2: Water Volumetric Ratio
18	5	3	5:1	5	200	
19	15	0	1:0	5	200	
20	5	2	1:2	5	200	

Fig. 6.2 shows the pressure drop profile during WAG injection for core #1. Initially 3.5 PV of the brine was injected until pressure stabilized at 5.2 psi. Alternating to carbon dioxide, CO_2 started to displace the brine and the pressure increased to 30 psi,

as the CO_2 saturation inside the core increased, the pressure drop across the core decreased. The average pressure drop during CO_2 injection at irreducible water saturation was 13.5 psi. Several factors govern the flow of CO_2 in carbonate rock, including multiphase flow in porous media (brine and CO_2), solute transportation, dissolution-deposition of the formation rock, hydrodynamic instabilities due to displacement of more viscous brine with less viscous CO_2, capillary effects, and upward movement of CO_2 due to gravity. These factors might cause a disturbance in the pressure drop profile shown in **Fig. 6.2**. Alternating to brine, the pressure disturbance was still noted for 1.25 PV, most of the CO_2 was displaced out of the core and the pressure stabilized at 17.2 psi.

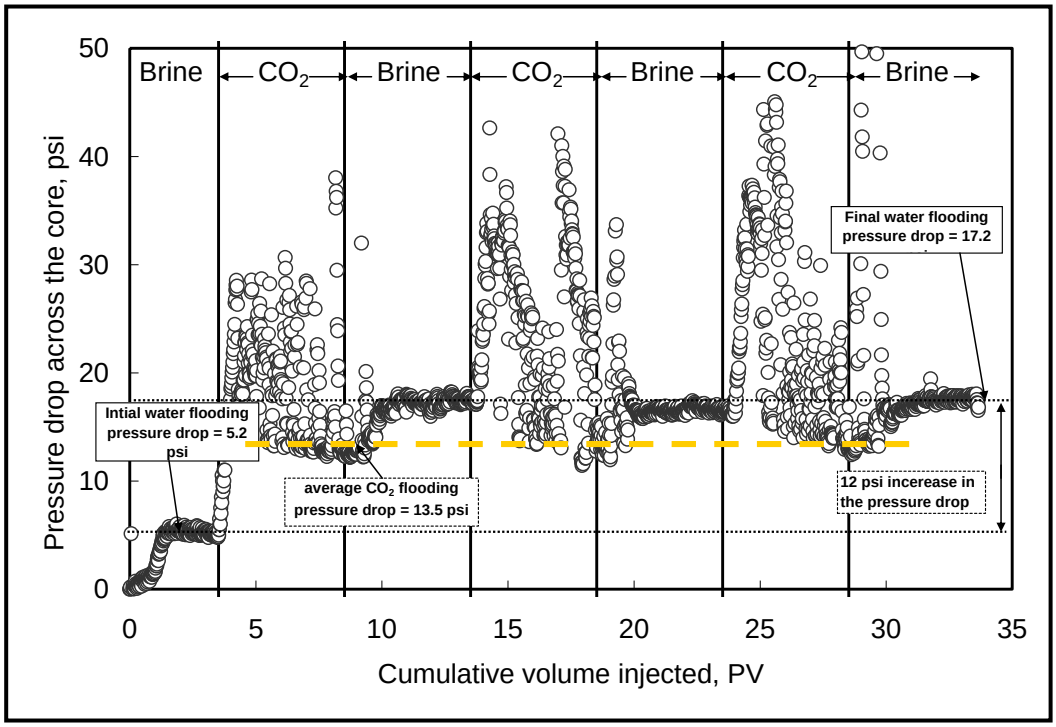

Fig. 6.2— Pressure drop across the core #1, T =200°F, injection flow rate = 5 cm^3/min

The dissolution of dolomite rock by the reaction with carbonic acid was expected to increase the core permeability, but the core permeability decreased from 182 to 100 md (45% loss in the permeability). The rock composition showed that a small percent (2.5%) of silicate minerals (feldspars and/or clays) are present (**Table 6.1**). Although it is a small percent but it had a significant effect on the rock permeability. Damaging chemical reactions occurred between the feldspar and carbonic acid;

1) Reaction with calcic plagioclase (Knauss et al. 2005)

$$2NaCa_{0.5}Al_2Si_2O_8 + 2H_2O + 3CO_2 \rightarrow 2NaAlCO_3(OH)_2 + 4SiO_2 + CaCO_3 + Al_2O_3 \quad (6.2)$$

Another reaction with plagioclase (Gaus et al. 2005)

$$5Na_{0.8}Ca_{0.2}Al_{1.2}Si_{2.8}O_8 + 5CO_2 + 6H_2O \rightarrow 10SiO_2 + 4NaAlCO_3(OH)_2 + CaCO_3 + Al_2Si_2O_5(OH)_4 \quad (6.3)$$

2) Reaction with chlorite (Mito et al. 2008)

a) Clinochlore

$$(Mg_5Al)(AlSi_3)O_{10}(OH)_8 + 10H^+ \rightarrow 5Mg^{2+} + 2Al(OH)_3 + 3H_4SiO_4 \quad (6.4)$$

b) Chamosite

$$(Fe_5Al)(AlSi_3)O_{10}(OH)_8 + 10H^+ \rightarrow 5Fe^{2+} + 2Al(OH)_3 + 3H_4SiO_4 \quad (6.5)$$

6.3.1 Analysis of Core Effluent Samples

Core #1 was CT scanned completely saturated with brine before and after the coreflood experiment. CT scan image for the core before CO_2 injection is shown in **Fig. 6.3A**. The core is heterogeneous, the CT number of the matrix ranged between 2100 and

2600 (2100 is represented by the green color, and 2600 is represented by red color in **Fig. 6.3**), several vugs were observed along the core length. **Fig. 6.3B** is the CT scan image after CO_2 injection, no wormholes formed in the core, the dissolution was uniform throughout the core. Comparing Figs. 6.3A, and 6.3B, a reduction in the CT No. was noted by reducing the areas of the red colored zones, which indicated rock dissolution. No precipitation was detected using the CT scan. This proposed that the damage introduced to the core due to blocking the pore throat by the scale resulted from different chemical reactions between CO_2 and the rock.

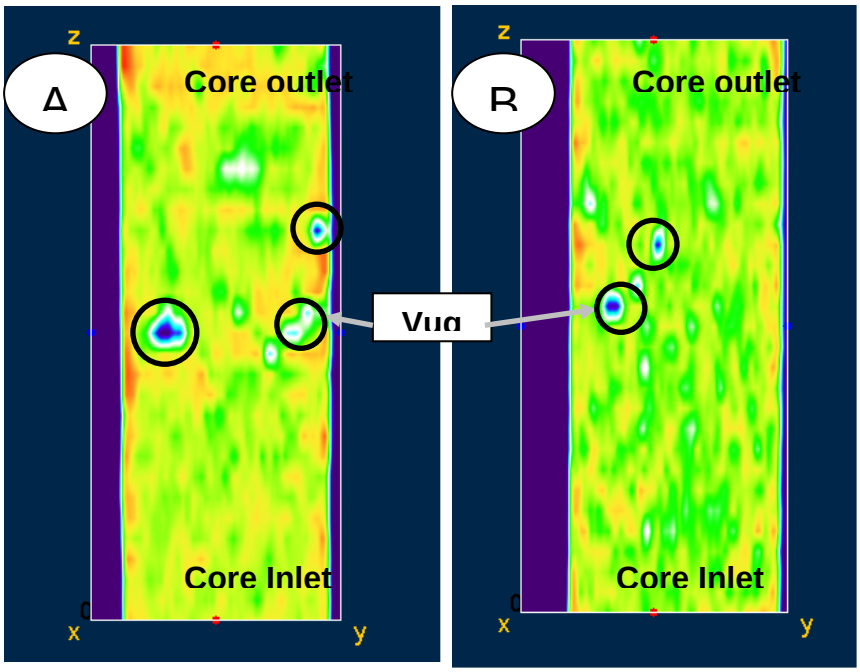

Fig. 6.3—CT scan images for core #1 (A) CT scan image before CO_2 injection. (B) CT scan image after CO_2 injection.

Core effluent samples were collected during the experiment. White scale particles were observed in the core effluent sample (**Fig. 6.4A**). The color of these

particles turns to red with time (**Fig. 6.4B**). The scale particles were separated from the effluent samples, X-ray diffraction (XRD) and XRF analyses were run to analyze the scale. XRD of the scale particles showed that the scale was mainly aragonite, Kitano et al. (1979) stated that the presence of Magnesium ions in a parent solution inhibit calcite formation and favor aragonite formation. Also, some calcite magnesian ($Mg_{0.13}Ca_{0.87}CO_3$) was noted; calcite magnesian precipitation is common in calcium bicarbonate solution that contains magnesium ions and has the symbols $Mg_xCa_{1-x}CO_3$ where x is the mole fraction of the Mg and increases as Mg concentration increases in the solution (Kitano et al. 1979; Jimenez-Lopez et al. 2006). XRF analysis is shown in **Table 6.4**, the mole ratio of carbon to calcium was 1:1, which indicated that magnesium was neither precipitated in magnesite nor dolomite form, and precipitated in the form of calcite magnisan or was associated with the silicate minerals. The mole ratio of calcium to magnesium was 1.65:1. The presence of Al, Si, and Fe supports that the reaction between CO_2 and silicate minerals occurred during CO_2 flooding. The concentration of iron was 7.3 wt% and that explains the red color observed in the core effluent samples.

The concentration of calcium and magnesium ions in the core effluent samples are given in **Fig. 6.5**. It shows that the concentrations of calcium and magnesium increased during the CO_2 half cycle from 402 and 1315 to 685 and 1522 mg/l, respectively. During the brine half cycle, the concentration decreased as the carbonic acid was diluted by increasing the brine saturation inside the core. The amount of calcium and magnesium dissolved from the rock could be calculated by the integration of the area under calcium and magnesium curves. The total calcium and magnesium

collected in the samples was 49.6 and 46.6 mg or 0.0012 and 0.0019 moles, respectively. Which are 0.06 wt% of the total calcium, and 0.09 wt% of the total magnesium initially present in the core. The mole ratio of calcium to magnesium was 0.645:1.0. Comparing the composition of the precipitated scales to the water composition, more calcium was present in solid phase, and more magnesium dissolved in the brine.

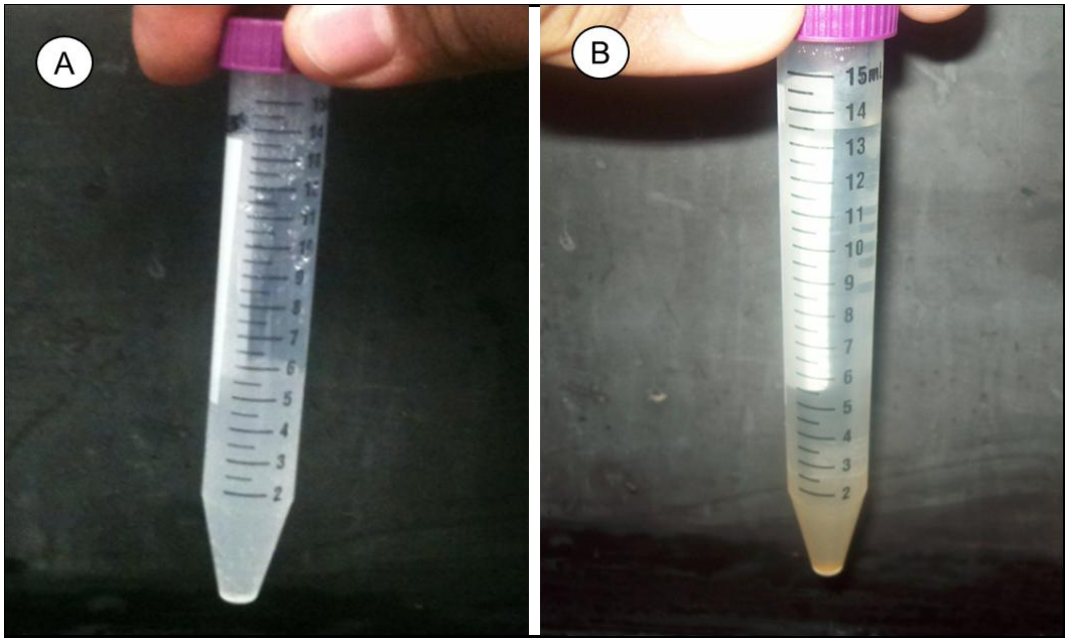

Fig. 6.4—Core effluent sample (A) directly after collected. (B) one day after collected.

After CO_2 flooding, the inlet and outlet parts of the core were analyzed by XRF. **Table 6.5** shows that a reduction in the magnesium concentration at the inlet part associated with increase in calcium concentration occurred. Close to the core outlet, the change in rock composition was negligible.

TABLE 6.4—COMPOSTION OF THE SCALE PARTICLES		
Element	**wt%**	**mol %**
O	45.96	60.08
C	6.01	10.46
Ca	20.03	10.45
Mg	7.39	6.35
Si	7.56	5.63
Al	4.84	3.75
Fe	7.31	2.74
Cl	0.91	0.53

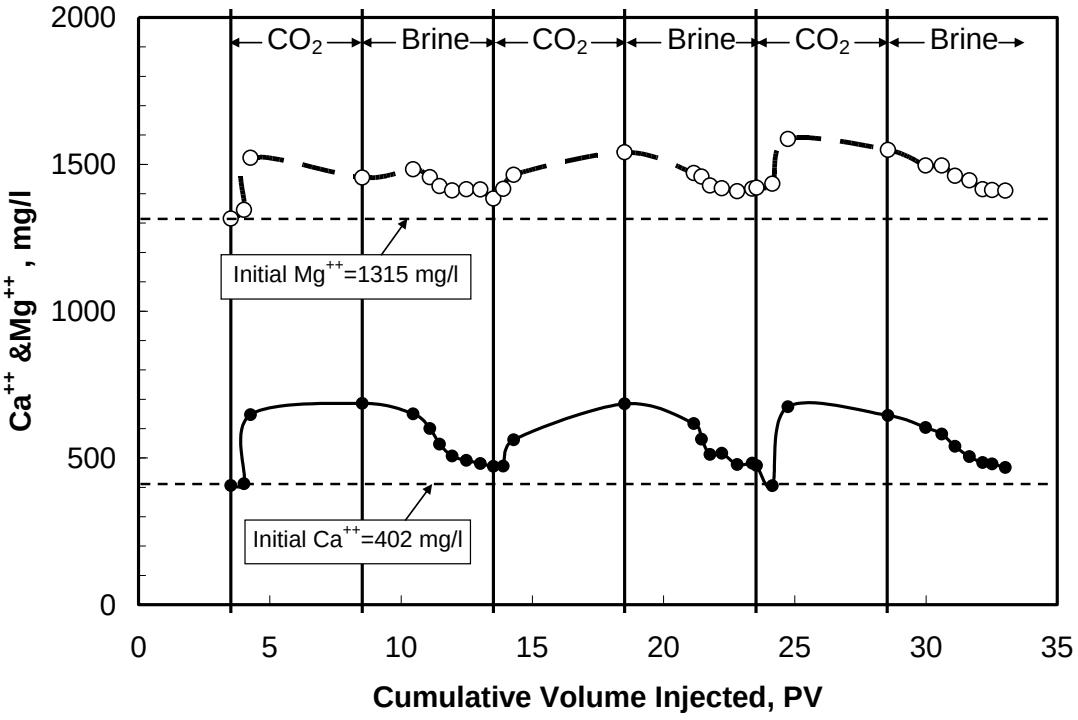

Fig. 6.5—Concentration of Ca^{++} and Mg^{++} in the core effluent samples, core #1

TABLE 6.5—COMPOSION OF THE INLET AND OUTLET OF THE DOLOMITE CORE AFTER CO_2 INJECTION			
Element	Concentration wt%		
	Fresh Core	Core Inlet	Core Outlet
O	51.46	51.1	51.45
C	12.69	12.6	12.71
Ca	21.18	23.3	21.72
Mg	12.79	11.3	12.51
Na	1.26	0.69	0.83
Si	0.2	0.29	0.17
Al	0.16	0.2	0.15
Fe	0.1	0.15	0.16
Cl	0.09	0.21	0.19
K	0.05	0.16	0.1
Sn	0.01	0.01	0.01

6.3.2 Effect of Injection Flow Rate

Four injection flow rates were examined in this study 2, 3.5, 5 and 10 cm^3/min. **Fig. 6.6** shows that for the same cumulative volume injected (30 PV), as the injection flow rate increased, the amount of calcium and magnesium dissolved was slightly reduced, since the reaction time decreased, the experiment was 1.5 hrs long at injection rate of 10 cm^3/min and 8 hrs long at flow rate of 2 cm^3/min. More magnesium than calcium was noticed in the core effluent samples for all flow rates examined in this study, with mole ratio of calcium to magnesium decreased as the flow rate was increased (**Fig. 6.7**).

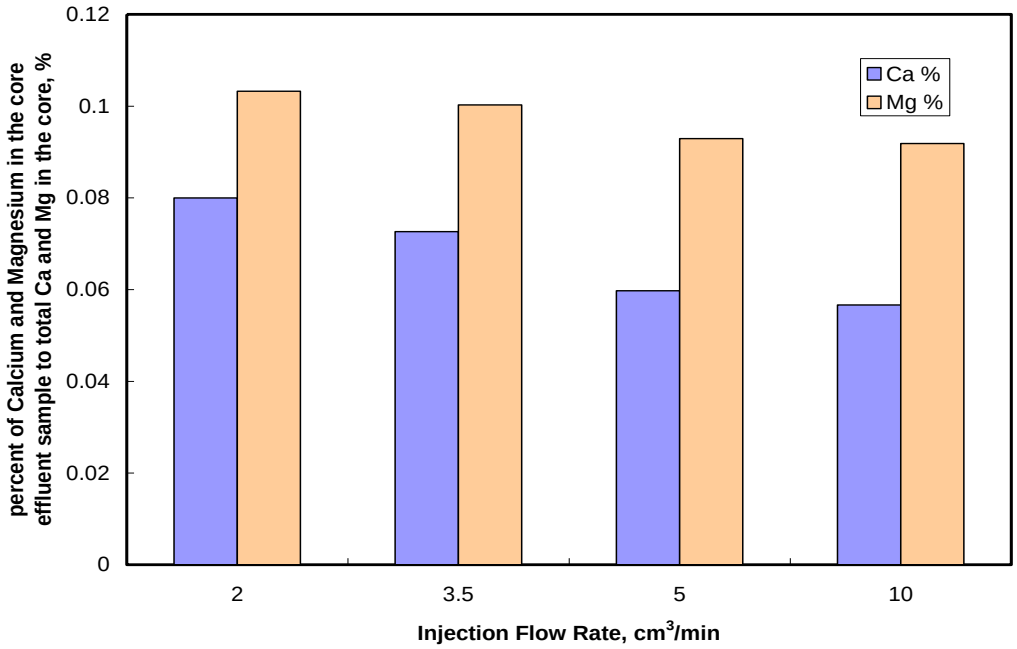

Fig. 6.6—Effect of injection flow rate on the percent of calcium and magnesium collected to total calcium and magnesium originally present in the core.

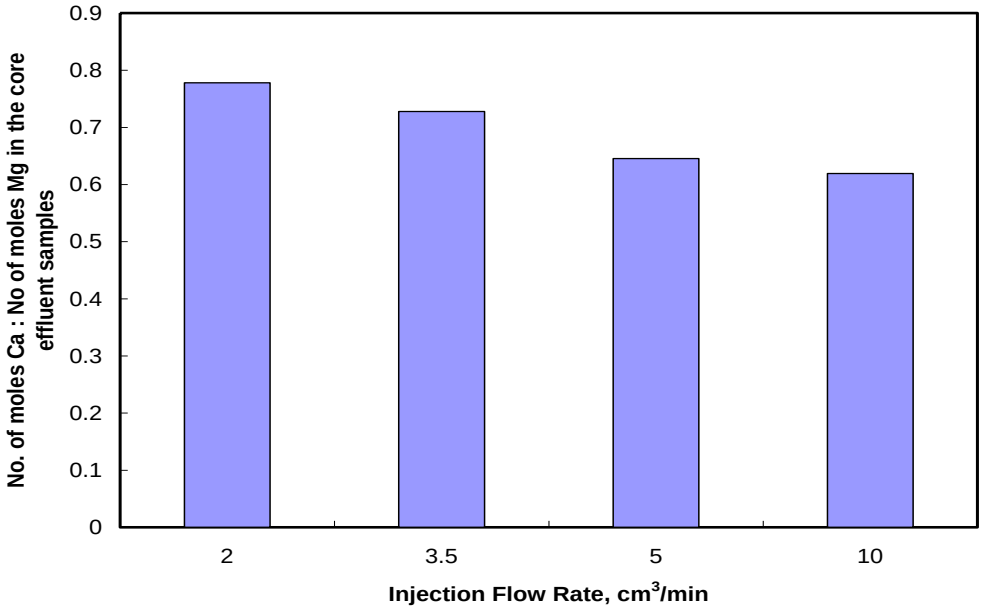

Fig. 6.7—Effect of injection flow rate on the Ca : Mg ratio noted in the core effluent samples.

The pressure drop profile across core #4 (T = 200°F and injection rate = 2 cm^3/min) is given in **Fig. 6.8**. More damage was introduced to the core for each WAG cycle. The pressure drop across the core for the initial brine flooding was 2 psi, pressure drop increased to 20.3 psi during brine half cycle for the first WAG cycle, and to 24.8 psi for the second cycle, the final pressure drop for the last cycle was 31 psi. The relative permeabilities were 0.039, 0.031, 0.022 for CO_2, and 0.19, 0.15, and 0.12 for the brine, for the first, second and third WAG cycle, respectively.

Regardless the injection flow rate the reduction in core permeability was observed at all flow rates. **Fig. 6.9** shows that there is no clear correlation between the injection flow rate and change in the core permeability. More damage was noted at flow rates of 2 and 5 cm^3/min, while less damage was introduced to the cores at 3.5 and 10 cm^3/min.

Although, for the injection flow rates of 2 and 5 cm^3/min, the damage ratio was very close 0.54 and 0.55, respectively. The pressure drop profile showed that for 2 cm^3/min the damage gradually increased from WAG cycle to another and that gave the step like pressure drop profile (**Fig. 6.8**). At injection flow rate of 5 cm^3/min most of the damage took place during the first WAG cycle, the pressure drop was found to be similar for the 3 WAG cycles shown in **Fig. 6.2**.

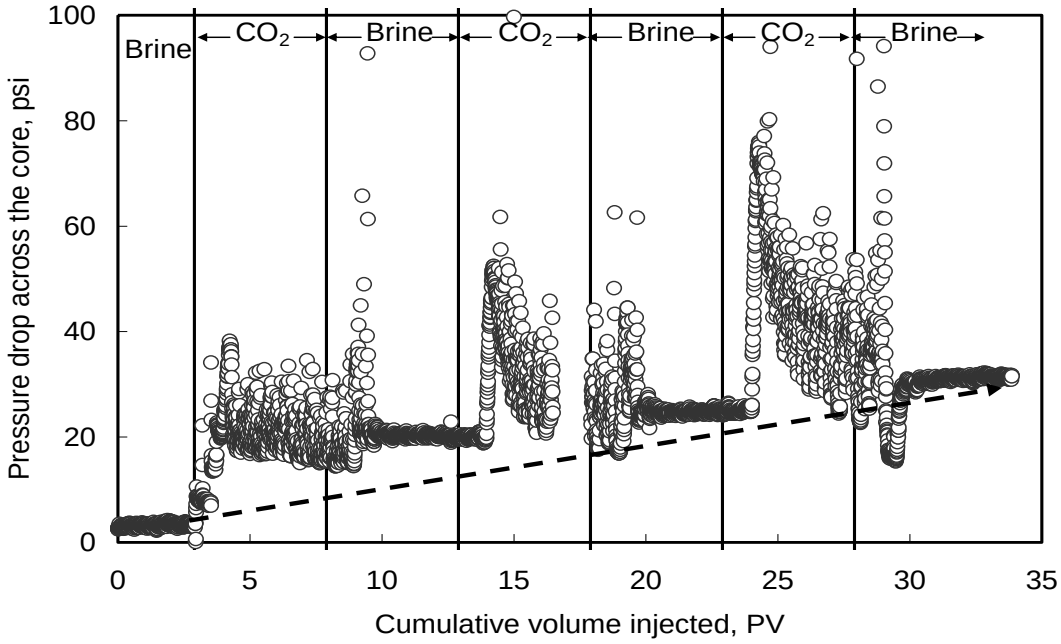

Fig. 6.8—Pressure drop across the core #1, T =200°F, injection flow rate = 2 cm^3/min.

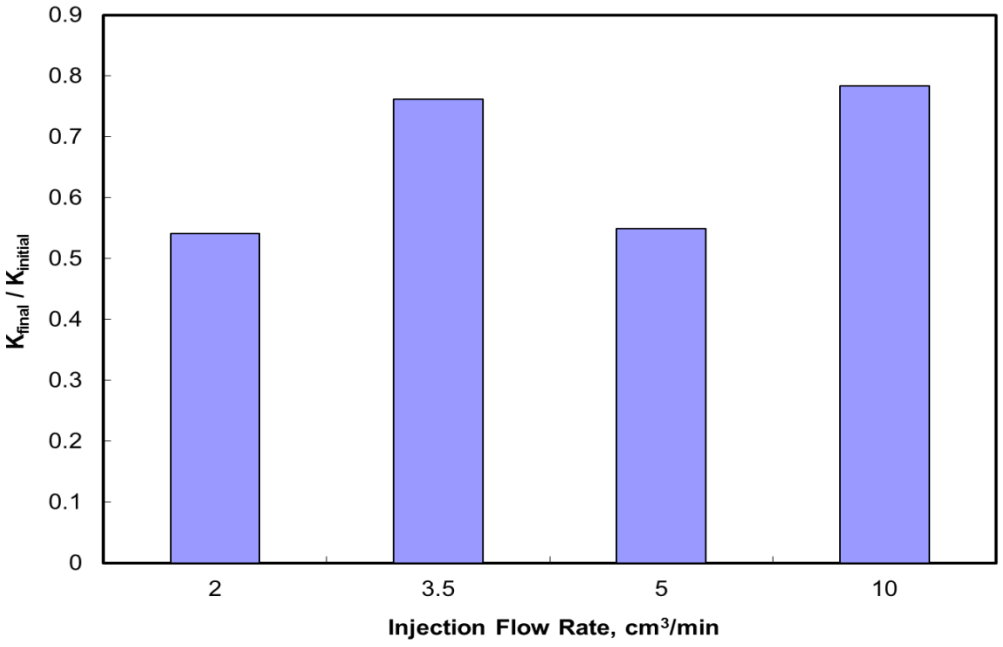

Fig. 6.9—Change in core permeability vs. the change in injection flow rate, 200°F.

6.3.3 Effect of Temperature

The coreflood experiments were run under three different temperatures: 70, 200, and 250°F. There was no clear trend that describes the effect of the temperature on the core permeability. The change in core permeability was different for different flow rates (**Fig. 6.10**). At injection flow rate of 2 cm^3/min, more damage was introduced to the core at 200°F, than at 70 and 250°F. At injection rate of 3.5 cm^3/min the damage decreased as the temperature increased. At higher flow rates, 5 and 10 cm^3/min, the damage was the same at temperatures of 200 and 250°F. At temperature of 70°F, more damage was observed at flow rate of 5 cm^3/min, and less damage was noted at 10 cm^3/min.

Dissolution rate of dolomite rock due to the reaction with CO_2 where studied by Pokrovsky et al. (2005; and 2009). They developed an empirical correlation to calculate calcite and dolomite dissolution rate at temperatures from 25 to 150°C, partial pressure of CO_2 (pCO_2) ranged between 10 and 50 atm, and 1 M NaCl solution as follows;

$$\log(K) = A + B\ x\ pCO_2 + C\ x\ (pCO_2)^2 \tag{6.6}$$

Where;

K = dissolution rate, $mol.cm^{-2}.s^{-1}$

A, B, and C = empirical parameters depend on temperature and pH

pCO_2 = partial pressure of CO_2, atm

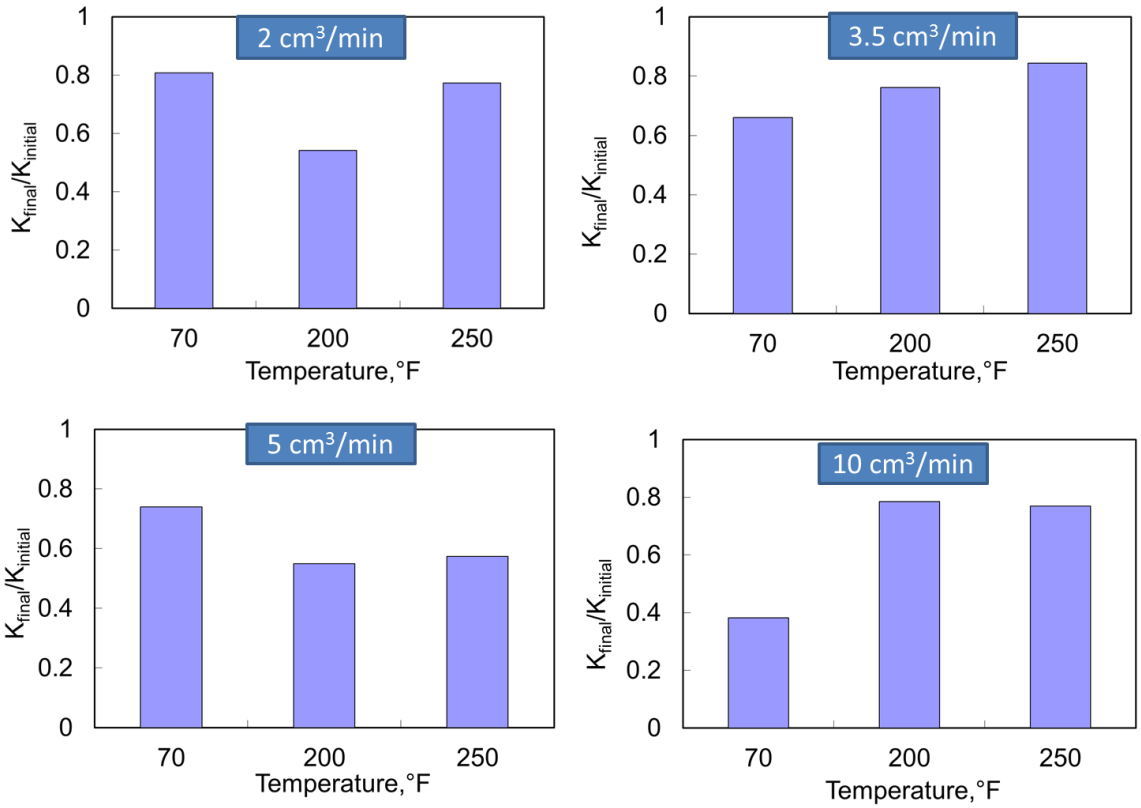

Fig. 6.10—Change in core permeability vs. the change temperature for different flow rates.

Although the dissolution rate of dolomite with CO_2 increases as temperature increased, the dissolution rates calculated by **Eq. 6.6** are $1.6X10^{-10}$, $1.9X10^{-9}$, and $2.4X10^{-9}$ mole.cm^{-2}.s^{-1} at 70, 200, and 250°F, respectively. Less calcium and magnesium were dissolved from the cores (**Fig. 6.11**), the reason is the CO_2 solubility in brine decreases as temperature increases, and that decreased the reaction rate. The mole ratio of calcium to magnesium increased and became closer to unity as the temperature increased (**Fig. 6.12**). Because of increasing the solubility of calcium bicarbonate in brine with increasing temperature, less calcium will precipitate.

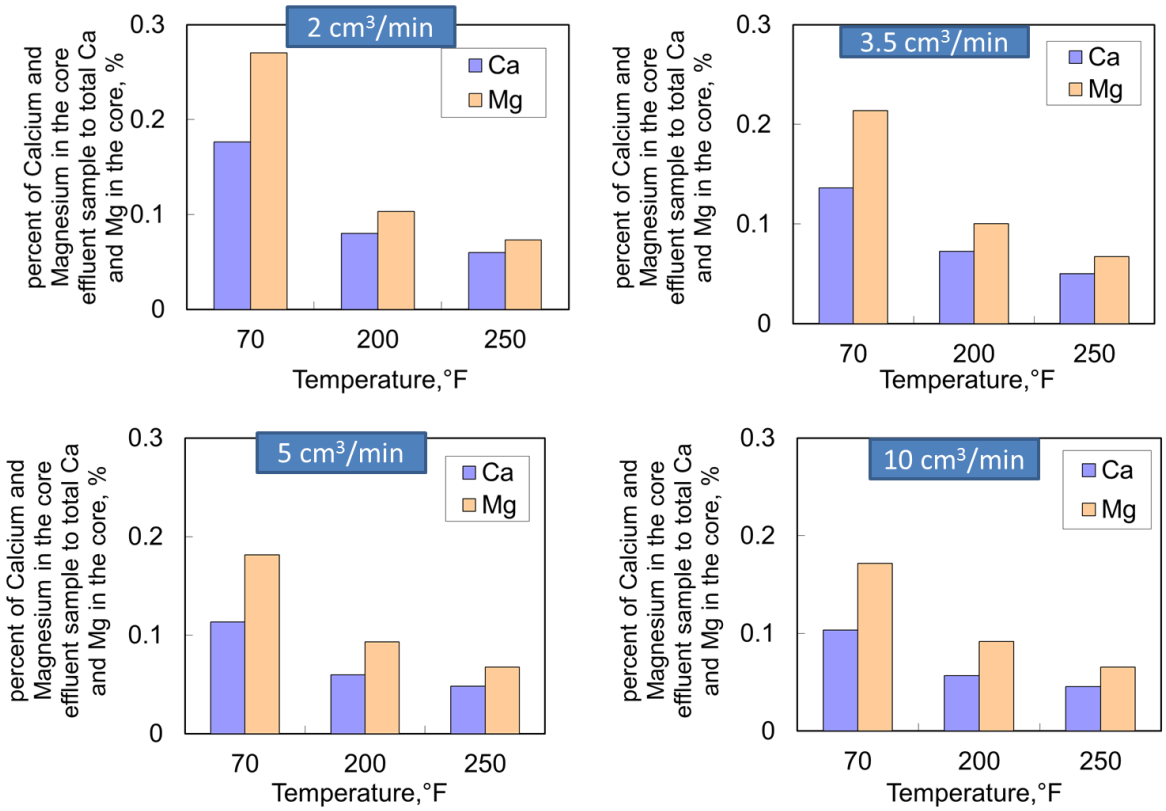

Fig. 6.11—Effect of temperature on the percent of calcium and magnesium collected to total calcium and magnesium originally present in the core.

6.3.4 Effect of WAG Cycle Volume

Five experiments were conducted to study the effect of the WAG cycle volume on the core permeability during CO_2 injection in dolomite aquifers. As the WAG cycle volume increased, the number of cycles decreased to keep the cumulative volume injected constant for all experiments (30 PV).

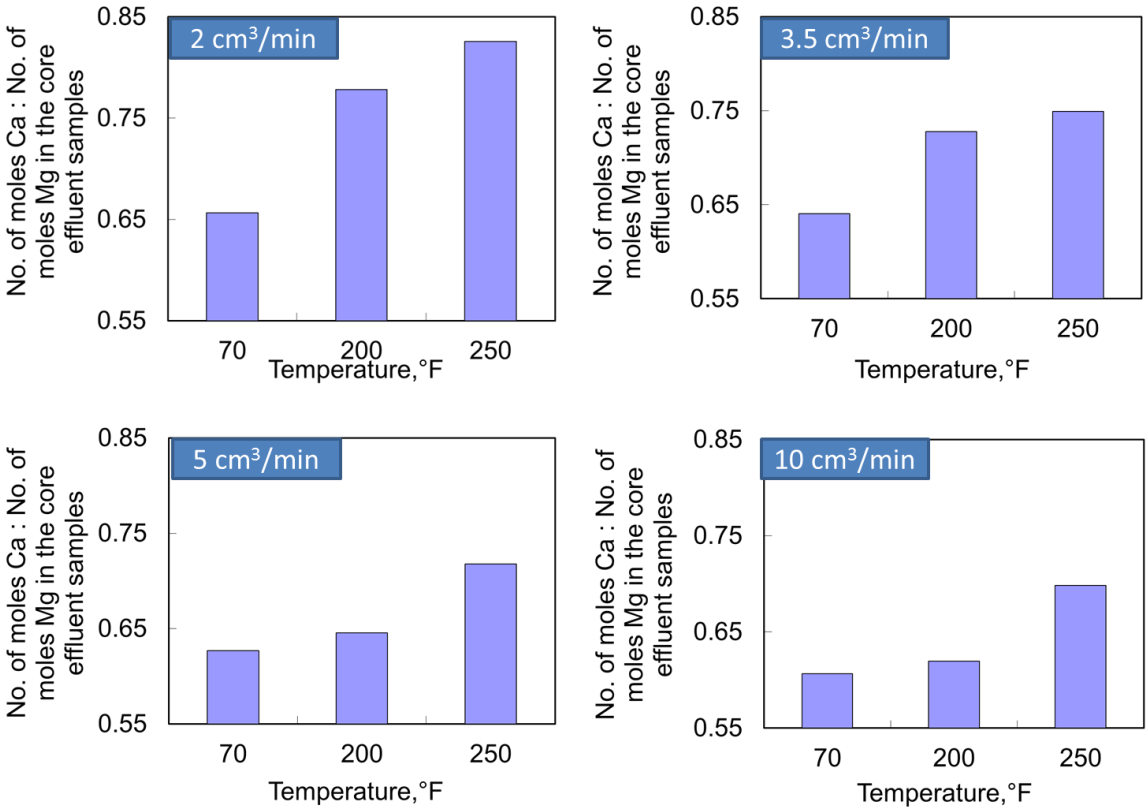

Fig. 6.12—Effect of temperature on the Ca : Mg ratio noted in the core effluent samples.

Fig. 6.13 shows that there was still no correlation between the cycle volume and change in core permeability, the damage increased as the WAG cycle become shorter, until WAG cycle volume of 10 PV (3 cycles were injected). At shorter cycles less damage was noted.

For shorter cycles, more calcium and magnesium were observed in the core effluent samples (**Fig. 6.14**), since the interface between brine and CO_2 occurred more frequently inside the core, the interface occurred 30 times for a 15 cycle experiment, and only 2 times for a one cycle experiment. For shorter WAG cycles, Ca to Mg mole ratio

increased (**Fig. 6.15**) and became close to unity at WAG cycle length of 2 PV (15 cycle were injected).

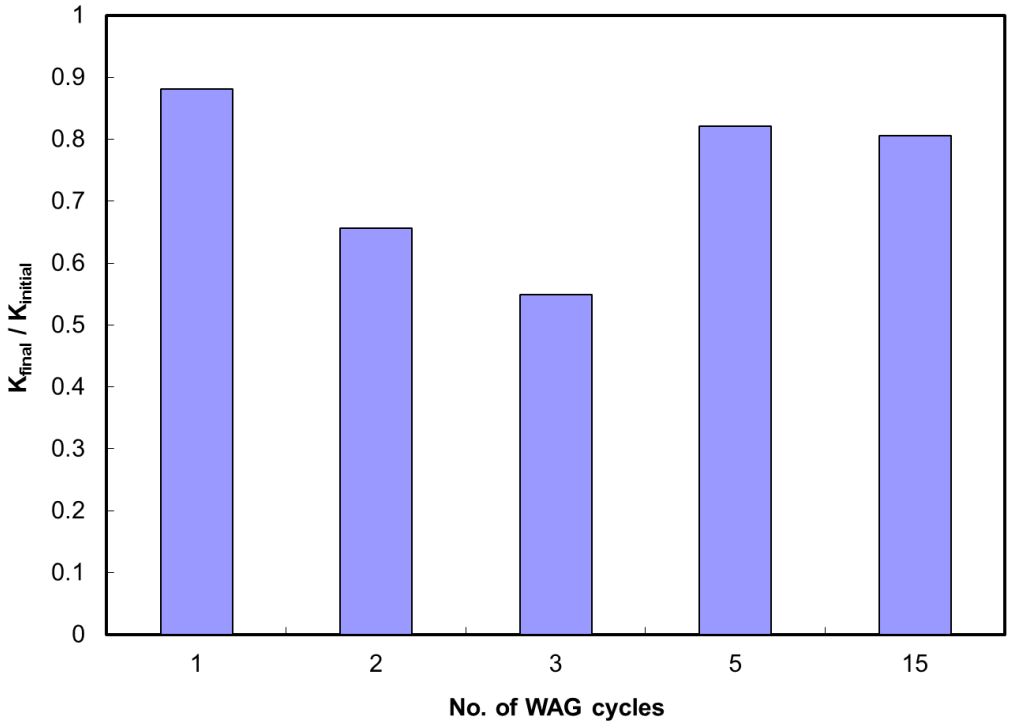

Fig. 6.13—Change in core permeability vs. the change in WAG cycle volume.

6.3.5 Effect of Brine:CO_2 Volumetric Ratio

Five experiments were conducted to study the effect of the brine to CO_2 volumetric ratio on the core permeability during CO_2 injection in dolomite aquifers. The brine to CO_2 volumetric ratio of zero represents the continuous gas injection case.

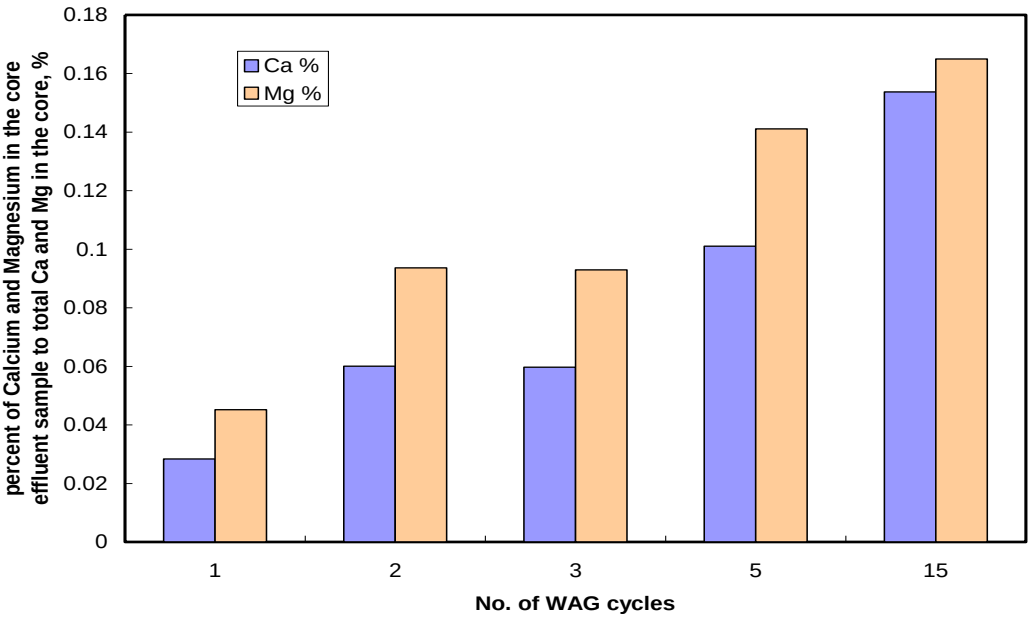

Fig. 6.14—Effect of WAG cycle volume on the percent of calcium and magnesium collected to total calcium and magnesium originally present in the core.

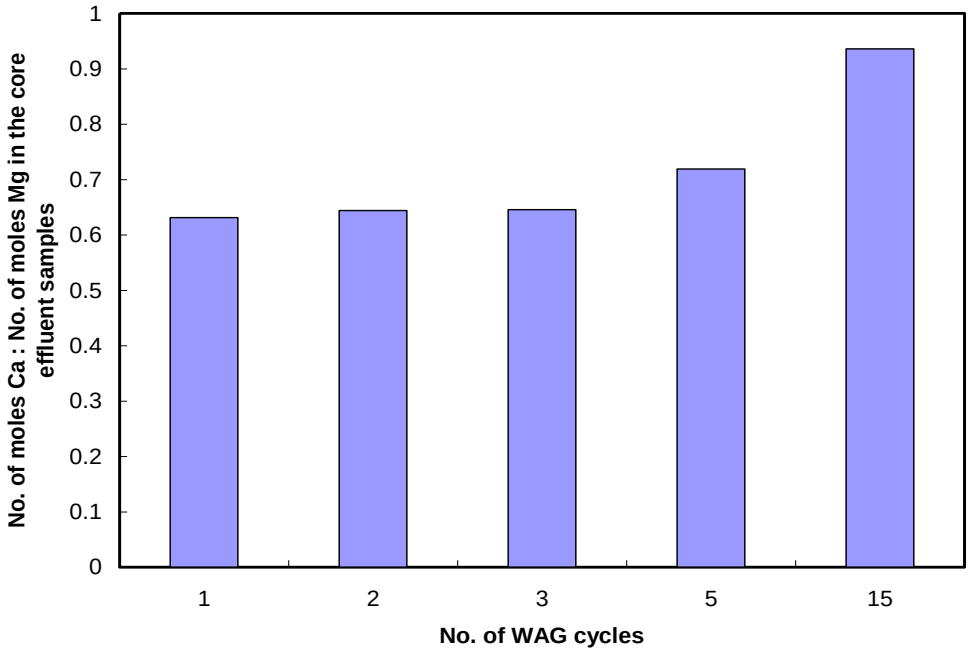

Fig. 6.15—Effect of WAG cycle volume on the Ca : Mg ratio noted in the core effluent samples.

Fig. 6.16 shows that as the brine:CO_2 volume increased, the damage increased. Except for the last case where the volumetric ratio was 2, the damage is less than the previous cases. No obvious relation between volumetric ratio and change in permeability was shown in this figure. The case where the volumetric ratio was 1:5 is the only case in this study that showed an enhancement in the permeability after CO_2 injection.

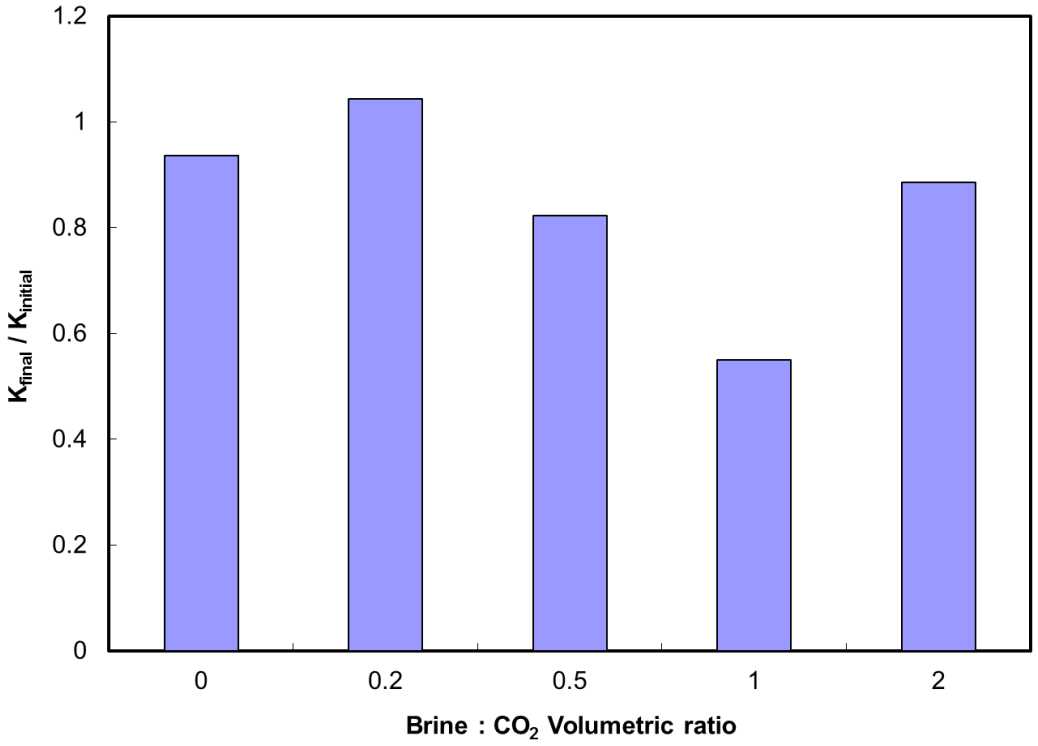

Fig. 6.16—Change in core permeability vs. the volumetric ratio.

Increasing the brine to CO_2 volume, more calcium and magnesium were observed in the core effluent samples (**Fig. 6.17**), **Fig. 6.18** shows the effect of volumetric ratio on the Ca to Mg mole ratio.

For the 20 cores that were used in this study, a plot of the cores initial permeability vs. the cores final permeability was drawn (**Fig. 6.19**). This figure shows that the only factor that affects the change in the core permeability is the initial core permeability. The higher the initial core permeability, the higher the final core permeability.

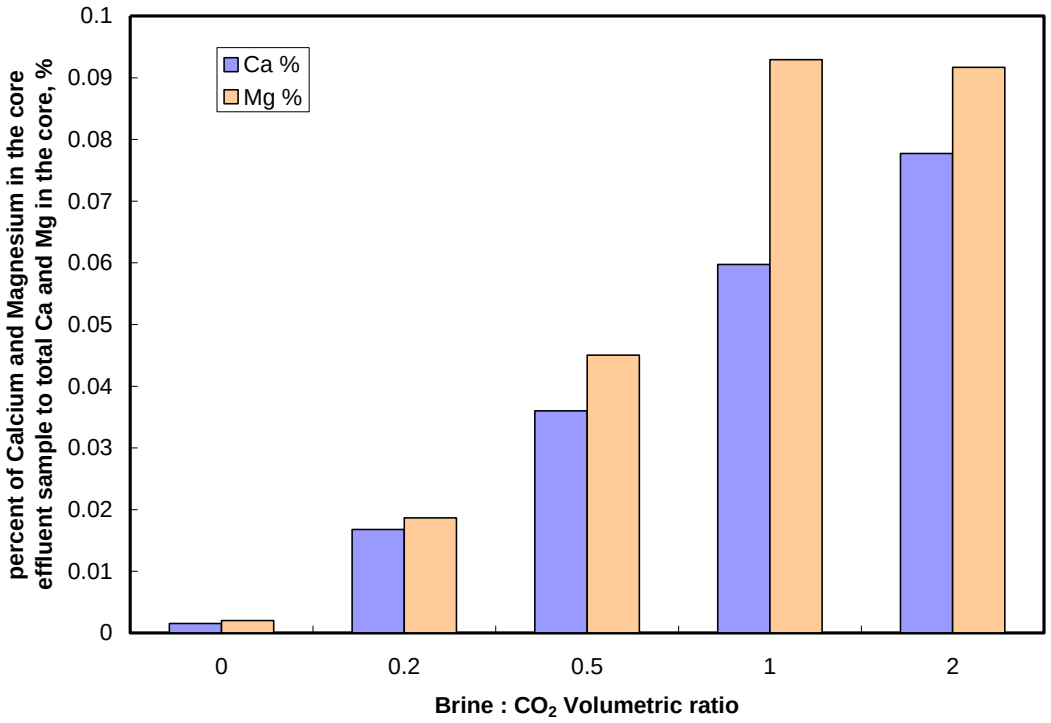

Fig. 6.17—Effect of volumetric ratio on the percent of calcium and magnesium collected to total calcium and magnesium originally present in the core.

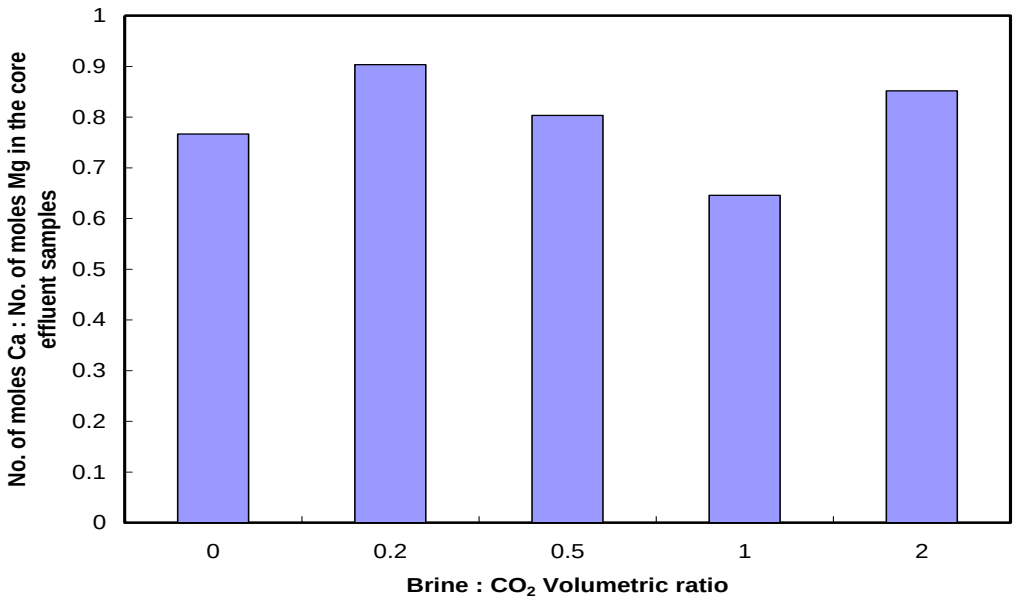

Fig. 6.18—Effect of volumetric on the Ca : Mg ratio noted in the core effluent samples.

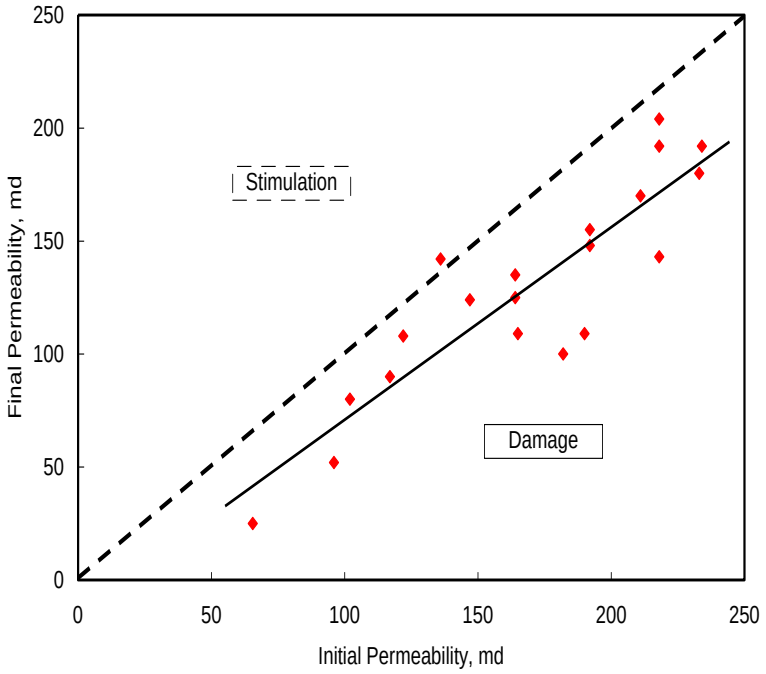

Fig. 6.19—Relationship between the initial cores permeability and final cores permeability

7. CARBON DIOXIDE SEQUESTRATION IN SANDSTONE AQUIFERS: HOW DOES IT AFFECT PERMEABILITY?

Most sandstone formations are composed of quartz particles bonded together by cementing materials, carbonates, silica and clays. The chemical reactions between carbonic acid and formation rock are much simpler in carbonate rock than in sandstone formations. In sandstones, the surface reaction rates are slow, and relatively uniform rock dissolution through the porous medium will be resulted (Wellman et al. 2003). In carbonates, the surface reaction rates are higher, leading to nonuniform dissolution patterns, and wormhole channels will be created (Izgec et al. 2006).

CO_2 will potentially cause formation damage when injected in sandstone formations, due to the precipitation of reaction products that are generated by the reaction between carbonic acid and different clays and feldspars, which often exist in sandstone formations.

Several parameters affect these interactions including pressure, temperature, brine composition, CO_2 injection rate, and overall injection scheme. This chapter addresses the effect of the temperature and injection scheme on the permeability reduction generated in the sandstone cores due to CO_2 injection.

7.1 Introduction

Weyburn oil field in Canada is a sandstone reservoir where CO_2 was used for EOR purposes. Monitoring of the produced brines showed an increase in Ca^{2+}, Mg^{2+}, K^{+},

SO_4^{2-}, HCO^{3-}, and CO_2 concentrations due to the dissolution of calcite, dolomite and K-feldspars (Raistrick et al. 2009).

The effect of the chemical reactions on the sandstone permeability during CO_2 injection into sandstone formations has been studied by Sayegh et al. (1990). 5 wt% NaCl brine saturated with CO_2 at 13.8 MPa was injected into sandstone cores from Pembina Cardium reservoir at 45°C. A reduction in core permeability was noted due to the dissolution of calcite and siderite and migration of the fines, which was originally bonded to the rock by the carbonates cementing minerals. Nightingale et al. (2009) analyzed a sample from the reservoir rock before and after CO_2 injection, the analysis showed that a degradation of clay and feldspar grains, and a partial to complete removal of carbonate cements occurred, and residual clays were found in the rock sample after CO_2 injection.

Liu et al. (2003) concluded that in the presence of CO_2 dissolution of sandstone formation and the deposition of secondary minerals is enhanced by increasing the temperature. Fischer et al. (2010) conducted long term lab experiments on Stuttgart Formation sandstone samples at reservoir conditions (5.5 MPa, 40°C). The samples were mainly quartz and plagioclase with minor mineral phases, such as K-feldspar, hematite, muscovite, biotite, illite, chlorite and opaque. Analcime, dolomite and anhydrite are only found as cement phases. Dissolution of calcium-rich plagioclase, K-feldspar and anhydrite and precipitation of albite was observed. This is also confirmed by Wigand et al. (2009).

Precipitation of quartz, kaolinite, illite, chlorite, albite, siderite and Fe-chlorite were noted by Bertier et al. (2006). Their experiments confirmed that carbonate dissolution and precipitation occurred during CO_2 injection into sandstone rock. Reactions with Al-silicates were also observed.

A coreflood study was conducted using Berea sandstone cores. CO_2 was injected under supercritical conditions at a pressure of 1,300 psi, and at temperatures ranging from 70 to 250°F at injection flow rate of 5.0 cm^3/min. Core effluent samples were collected and the concentrations of calcium, potassium, magnesium, aluminum, iron, and silicon ions were measured. Precipitated material collected in the effluent samples were analyzed using XRD and XRF. Core permeabilities were measured before and after the experiment to evaluate the damage generated. A compositional simulator tool (CMG-GEM) was used to confirm the experimental results obtained in this study by predicting the change in core permeability and defining the location of precipitation of the reaction products between CO_2 and the Berea sandstone cores.

7.2 Test Design

The coreflood tests were designed to simulate WAG injection of CO_2 into saline sandstone aquifers. A slug of pure CO_2 (purity 99.8%) in the first half of the WAG cycle, while a slug of synthetic brine with TDS of 35.884 ppm (**Table 4.2**) were injected in the second half. To study the effect of CO2:brine volumetric ratio, the ratio was controlled to be 1:2, 1:1, 2:1, and 5:1, beside the continuous CO_2 injection (1:0).

Different WAG cycle volumes were tested by keeping the volumetric ratio at 1:1 and changing the half cycle volume to be 1, 3, 5, 7.5, and 15 PV.

Tests were run at temperatures of 70, 200, and 250 °F. Back pressure was kept constant at 1300 psi for all experiments. Core effluent samples were collected throughout the experiment, every 3 minutes during brine injection, while during CO_2 the first 2 samples were collected every 3 minutes, and the third sample at the end of CO_2 half cycle. A summary of the coreflood tests is shown in **Table 7.1**.

TABLE 7.1—SUMMARY OF COREFLOOD EXPERIMENTS

Core #	CO_2 Volume per Cycle (Pore Volume)	No. of Cycles	CO_2 : Brine Volumetric Ratio	Injection Flow Rate (cm^3/min)	Temperature (°F)	Permeability (md)	Case
1	5	3	1:1	5	200	55.5	Reference case
2	15	0	1:0	5	200	86	Continuous CO_2 Injection
3	5	3	1:1	5	70	45	Effect of Temperature
4	5	3	1:1	5	250	81	
5	1	15	1:1	5	200	81	Effect of CO_2 Volume/Cycle
6	3	5	1:1	5	200	86	
7	7.5	2	1:1	5	200	65	
8	15	1	1:1	5	200	81	
9	5	3	2:1	5	200	63	Effect of CO_2: brine Volumetric Ratio
10	5	3	5:1	5	200	42	
11	5	2	1:2	5	200	80	

7.3 Possible Reactions between Berea Sandstone and CO_2

Mineral composition of Berea sandstone was shown by conducting XRD analysis, the results showed that the rock was composed of 79.61 wt% quartz, 7.21 wt% kaolinite, and 4.11 wt% illite. Mahmoud et al. 2011 stated that dolomite, calcite, potassium feldspar, and chlorite are also present in Berea sandstone. An XRF analysis was conducted to confirm the presence of these minerals (**Table 7.2**). The presence of calcium and magnesium confirmed that dolomite and calcite were present, potassium confirmed the presence of potassium feldspar, and iron confirms the presence of chlorite.

TABLE 7.2—BULK COMPOSITION OF BEREA SANDSTONE AS DETERMINED BY XRF

Element	wt%	mol.%
O	51.456	65.319
Si	31.995	23.137
Ca	5.023	2.546
Al	3.159	2.378
S	2.914	1.846
C	1.508	2.550
Fe	1.060	0.385
K	1.041	0.541
Mg	0.663	0.554
Na	0.620	0.547
Ti	0.346	0.147
Zr	0.064	0.014
Mn	0.036	0.013
Ba	0.032	0.005
Cu	0.020	0.006
Nd	0.016	0.002
Sn	0.013	0.002

The possible chemical reactions during CO_2 injection into Berea sandstone can be summarized as follow;

1) Reaction with kaolinite (Li et al. 2005)

$$Al_2Si_2O_5(OH)_4 + 6H^+ \leftrightarrow 2Al^{3+} + 2H_4SiO_4 + H_2O \quad (7.1)$$

2) Reaction with calcite and dolomite (Wellman et al. 2003)

$$CaCO_3 + CO_2 + H_2O \leftrightarrow Ca^{2+} + 2HCO_3^- \quad (5.2)$$

$$CaMg(CO_3)_2 + 2CO_2 + 2H_2O \leftrightarrow Ca^{2+} + Mg^{2+} + 4HCO_3^- \quad (6.1)$$

3) Reaction with potassium feldspar (Pauwels et al. 2007)

$$2KAlSi_3O_8 + CO_2 + 2H_2O + Ca^{2+} \rightarrow 2K^+ + 4SiO_2 + CaCO_3 + Al_2Si_2O_5(OH)_4 \quad (7.2)$$

4) Reaction with chlorite (Mito et al. 2008)

Clinochlore

$$(Mg_5Al)(AlSi_3)O_{10}(OH)_8 + 10H^+ \rightarrow 5Mg^{2+} + 2Al(OH)_3 + 3H_4SiO_4 \quad (6.4)$$

Chamosite

$$(Fe_5Al)(AlSi_3)O_{10}(OH)_8 + 10H^+ \rightarrow 5Fe^{2+} + 2Al(OH)_3 + 3H_4SiO_4 \quad (6.5)$$

5) Reaction with illite

$$K_{0.6}Al_2Mg_{0.25}(Al_{0.3}Si_{3.5}O_{10})(OH)_2 + 8H^+ \rightarrow 0.6K^+ + 0.25Mg^{2+} + 2.3Al^{3+} + 3.5SiO_2(aq.) \quad (7.3)$$

6) Reaction quartz (Wellman et al. 2003)

$$SiO_2 \leftrightarrow SiO_2(aq.) \quad (7.4)$$

7.4 Results and Discussion

Core #1 experiment is the reference case in this study, 3 WAG cycles of CO_2 and brine were injected. Brine and CO_2 half cycle volumes were the same and equal to 5 PV. The fluids were injected at constant injection flow rate of 5 cm^3/min at 200°F. Core #1 initial permeability was 55.5 md.

To assess the effect of gravity and fluid viscosities on the flow behavior, capillary and gravity numbers are two dimensionless groups that were calculated. The capillary number is the ratio of viscous force to capillary force, while the gravity number is the ratio of gravity force to viscous force. Zhou et al. (1994). Gravity number for this case was 0.119 and the capillary number was 1.17×10^{-5}, the flow was dominated by viscous forces and gravity segregation was negligible.

Pressure drop across the core is shown in **Fig. 7.1**. Initial pressure drop across the core was 26 psi. Alternating to CO_2, the pressure drop initially increased when CO_2 starts to displace brine; with increasing CO_2 saturation inside the core, the pressure drop decreased to an average value of 19 psi, and the pressure peak was increasing each cycle. Alternating to brine, a sharp increase in the pressure was initially noted due to the displacement of less viscous fluid (CO_2) by a more viscous fluid (brine), more increase in pressure was noted in the second cycle and reached the maximum in the third cycle (155 psi). Increasing the brine saturation inside the core, the pressure decreased until stabilization at a value that was always higher than the initial water flooding pressure; 28, 30, and 32 psi for the first, second, and third cycle, respectively.

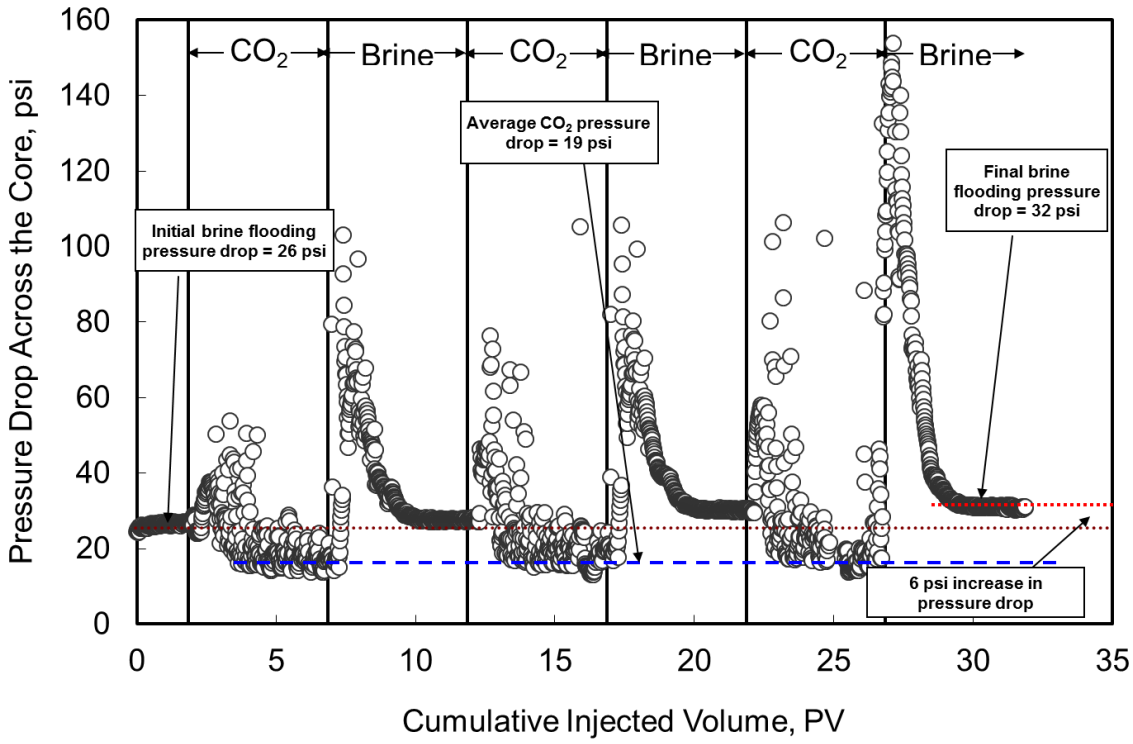

Fig. 7.1—Pressure drop across core #1, T = 200°F, injection flow rate = 5 cm^3/min.

The permeability of core #1 decreased from 55.5 to 30 md (46% loss in permeability). Core effluent samples collected after CO_2 injection had white particles, after a few hours the color turned to red, HCl dissolved these particles and altered the color to yellow (**Fig. 7.2**), which indicates that there was iron collected in the samples.

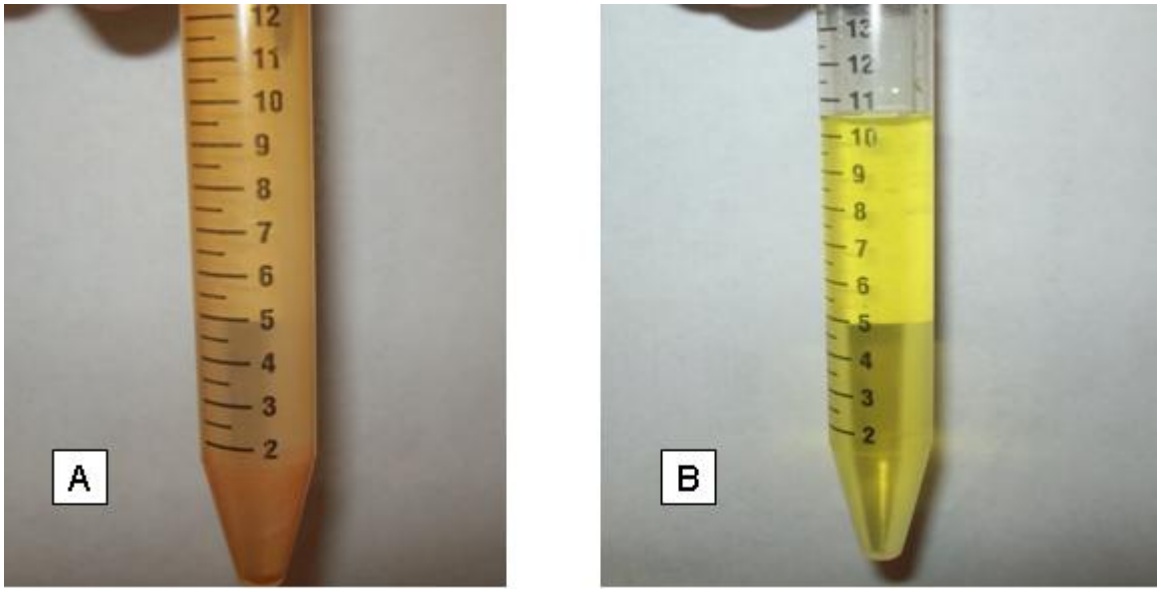

Fig. 7.2— A) Core effluent sample after one day shows the precipitation of iron oxides and calcium carbonate. B) Core effluent sample after adding HCl, iron dissolved to form iron chloride

Filtration of the core effluent and running an XRF analysis on the collected particles showed that the precipitated materials are mainly calcium and iron (**Table. 7.3**). XRD analysis showed that the main minerals present were aragonite ($CaCO_3$) and magnetite (Fe_3O_4). SEM analysis of the precipitated solids showed three different compounds present (**Fig. 7.3**), 1) calcium carbonate that has a relatively larger particle size compared to the other compounds, 2) iron oxides, the small particle shown in **Fig. 7.3**, and 3) clays, the particles were invisible at this magnification (1500 X).

The concentrations of calcium, magnesium, aluminum, iron, silicon, and potassium were measured in the core effluent. **Fig. 7.4** shows that calcium and magnesium concentrations increased during the CO_2 half cycle from 401 and 1,315 to 620 and 1,530 mg/l, respectively, due to the reaction between CO_2 and carbonate

minerals (calcite and dolomite), and decreased during the brine half cycle due to the dilution of the carbonic acid. Total calcium collected was 46.8 mg, while the total magnesium was 47.5 mg.

TABLE 7.3—COMPOSITION OF PRECIPITATED PARTICLES AS DETERMINED BY XRF		
Element	**wt%**	**mol.%**
O	59.674	76.687
Ca	11.477	5.888
Fe	19.566	7.204
C	3.443	5.894
Si	3.276	2.398
Al	2.363	1.801
S	0.200	0.128

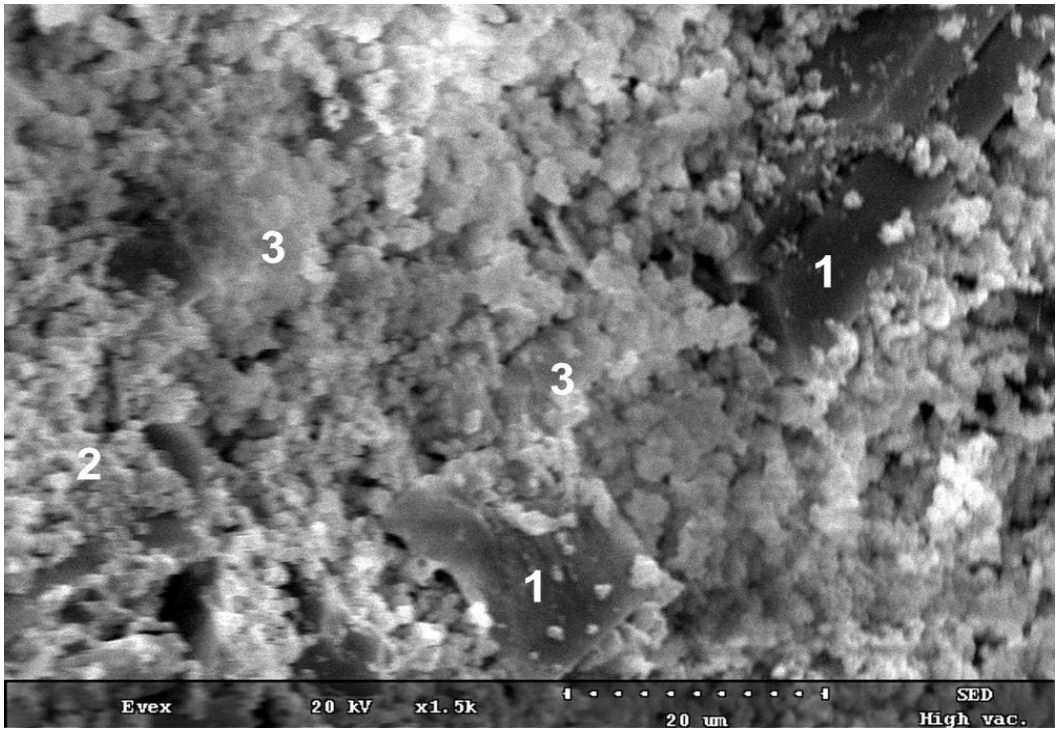

Fig. 7.3—SEM photomicrograph of the precipitated particles 1) calcite, 2) magnetite, 3) clays.

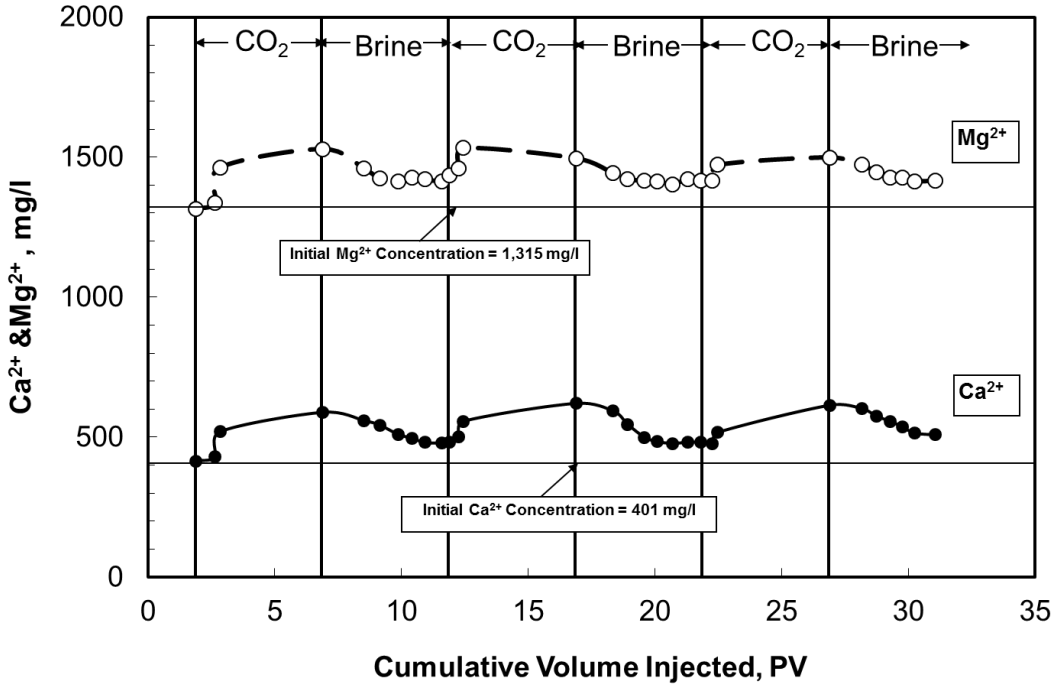

Fig. 7.4—Concentrations of Ca^{++} and Mg^{++} in the core effluent samples, core #1

Traces of silicon and iron dissolved in the core effluent (**Fig. 7.5**); maximum silicon concentration was 36 mg/l, while maximum iron concentration was 32 mg/l. No aluminum dissolved in the core effluent fluids, it was only observed in the precipitated particles.

The inlet and outlet parts of the core were analyzed using XRF, the analysis showed that there was a reduction in the calcium concentration from 5.023 wt% in the fresh core to 2.45 wt% in the inlet face due to dissolution of calcium carbonate. The concentration of calcium increased to 7.393 wt% in the outlet face due to the precipitation of calcium carbonate again. Iron also showed that same behavior but with a smaller percentage of reduction at the inlet face and increasing at the outlet (**Table 7.4**).

The experiment was repeated at the same conditions in a core with an initial permeability of 47 md to confirm the results, magnesium and calcium curves were the same and a final permeability of 25.5 md was obtained after CO_2 injection; 46% reduction in permeability, which was the same result obtained from core #1.

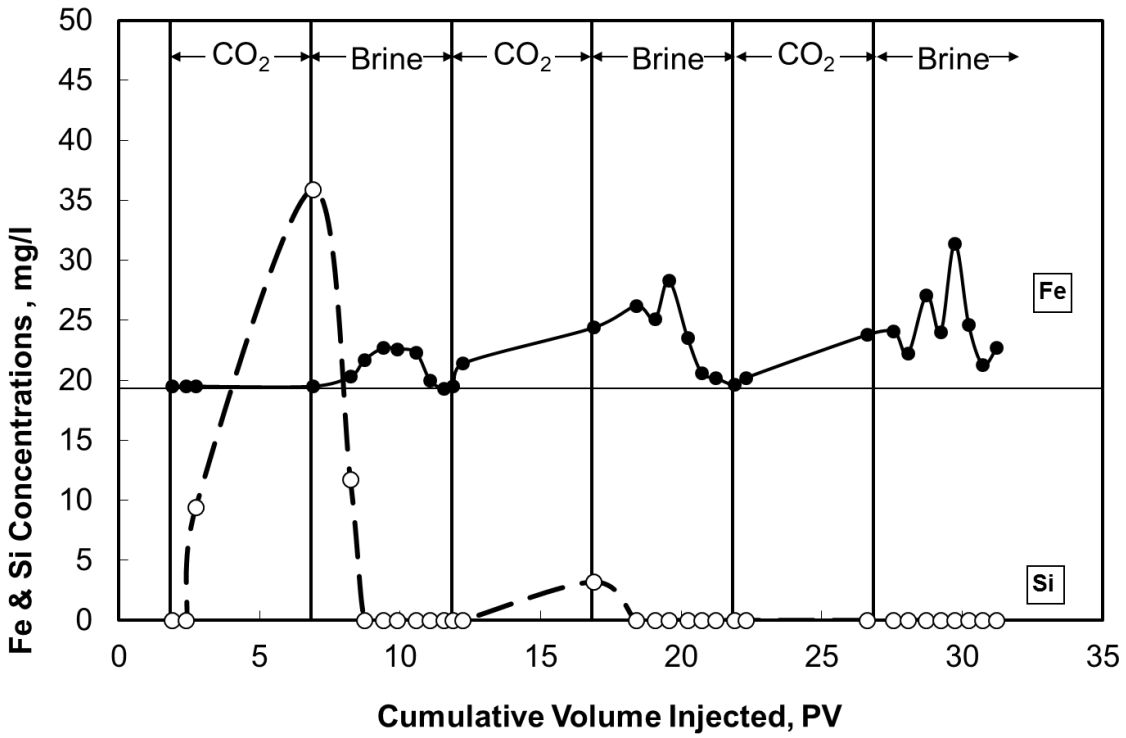

Fig. 7.5—Concentrations of Fe and Si in the core effluent samples, core #1

7.4.1 Continuous CO_2 Injection

Core #2 brine was injected initially until pressure stabilized, then 15 PV of CO_2 was injected continuously at an injection flow rate of 5 cm^3/min and temperature of 200°F. A reduction in core permeability from 86 to 53 md was observed (39% reduction in core permeability). Also the damage in this case is less than the damage observed

after WAG injection (core #1) but it is still significant. Total calcium and magnesium collected in the core effluent samples were 2.4 and 2.5 mg, respectively.

TABLE 7.4—COMPOSITION OF THE INLET AND OUTLET FACES OF THE BEREA SANDSTONE CORE AFTER CO_2 INJECTION AS DETERMINED BY XRF

Element	Concentration wt%		
	Fresh core	Core Inlet	Core Outlet
O	51.456	50.953	51.833
Si	31.995	37.661	31.243
Ca	5.023	2.450	7.393
Al	3.159	3.414	1.975
S	2.914	0.069	0.235
C	1.508	0.737	2.286
Fe	1.060	1.047	1.341
K	1.041	1.299	1.126
Mg	0.663	0.840	1.665
Na	0.620	0.868	0.264
Ti	0.346	0.400	0.315
Zr	0.064	0.077	0.124
Mn	0.036	0.032	0.077
Ba	0.032	0.036	0.040
Cu	0.020	0.017	0.026
Nd	0.016	0.023	0.034
Sn	0.013	0.015	0.022

Fig. 7.6 shows the pressure drop across core #2. Cycles of gradual increase in pressure followed by a sudden drop were observed during CO_2 flow. The suggested mechanism that explains this behavior is that the increase in pressure is caused by the damage introduced by migration of fines that originally attached to the dissolved carbonate cementing material, and/or the precipitation of the reaction products formed by the chemical reactions between CO_2 and different minerals. These particles

participated at the pore throat forcing CO_2 to move to the smaller pores that were occupied with brine, a sudden increase in the pressure drop was observed due to the displacement of brine by CO_2 from the smaller pores; displacing brine from these pores will open up a new path for CO_2 to flow through, so the pressure decreased again. This mechanism was explained in **Fig. 7.7**.

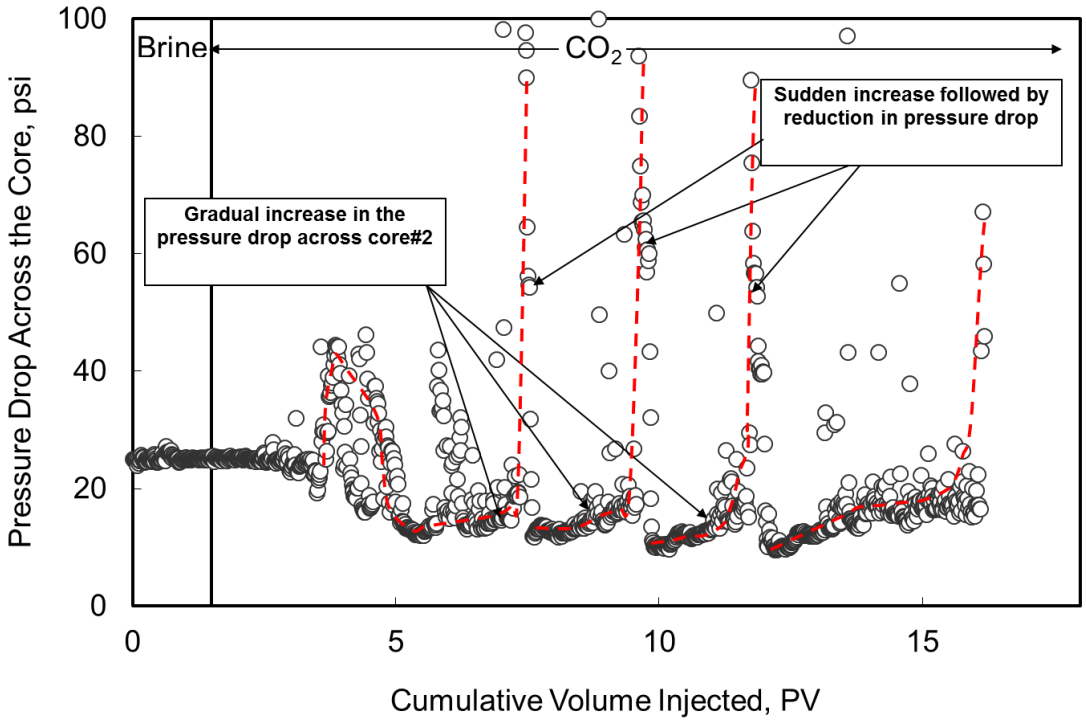

Fig. 7.6—Pressure drop across the core #2, T =200°F, injection flow rate = 5 cm^3/min.

7.4.2 Effect of WAG Cycle Volume

The effect of the volume of the WAG cycle was examined by conducting coreflood experiments with changing the volume of CO_2 injected per cycle, to keep the

cumulative CO_2 volume constant the number of cycles increased as the volume of CO_2 injected each cycle was decreased. Experiments conducted with 1, 3, 5, 7.5, and 15 PV CO_2 per cycle were injected for 15, 5, 3, 2, and 1 cycles, respectively, besides the continuous CO_2 injection case (core #2). Volumetric ratio was 1:1 at injection flow rate of 5 cm3/min and temperature 200°F.

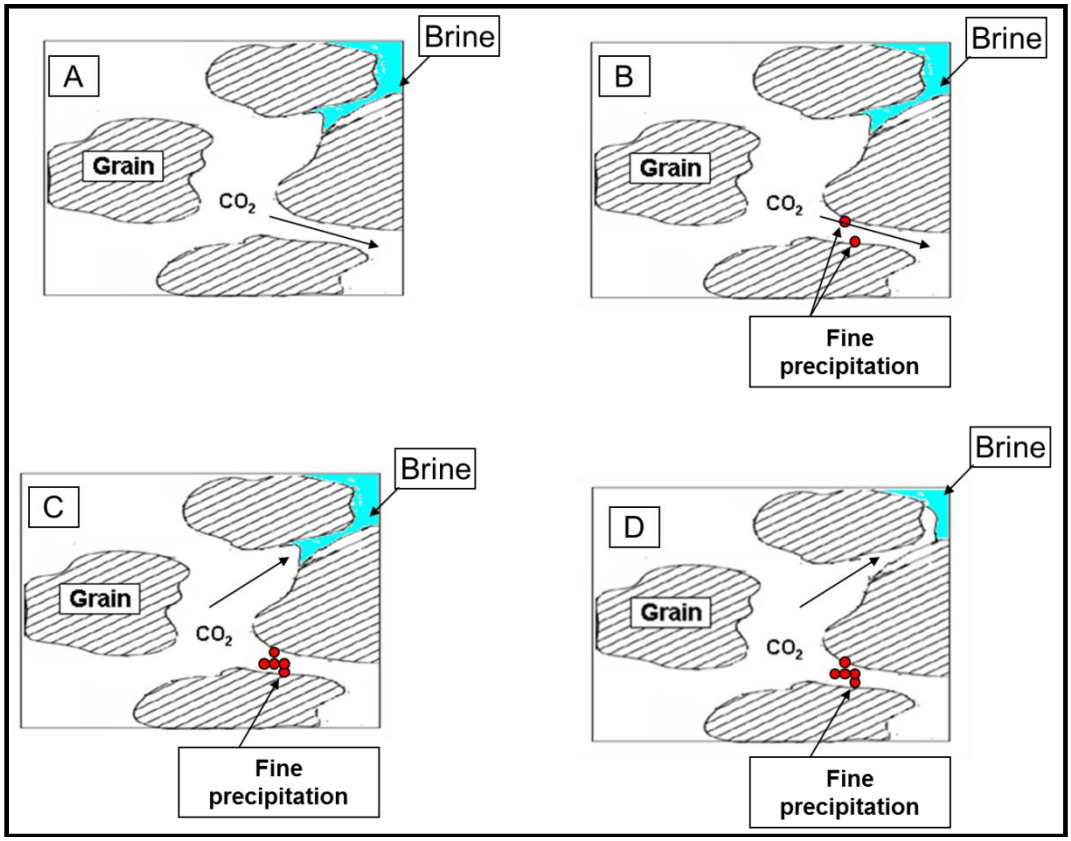

Fig. 7.7—A) CO_2 flowing in the larger pore throats and brine trapped in smaller pores, B) fines produced due to the reactions between CO_2 and formation rock precipitate at the pore throat generate more resistance to CO_2 flow (gradual increase in pressure drop), C) with continuous precipitation, CO_2 will be diverted into the smaller pore throats trying to displace the brine (Sudden increase in pressure drop), D) CO_2 displaced brine and started to flow in the smaller pores (reduction in pressure drop).

Fig. 7.8 shows that when injecting shorter WAG cycle, more damage was introduced to the sandstone cores. The least damage was related to the continuous gas injection, and the most damage was observed when injecting 1 PV CO_2 per cycle (55% loss in permeability). The number of WAG cycles increased as the CO_2 volume per cycle decreased in order to inject the same volume of CO_2, that increased the contact time with CO_2 and brine, which enhanced the reactions with the core rock that might explain why more damage occurred when decreasing the WAG cycle length.

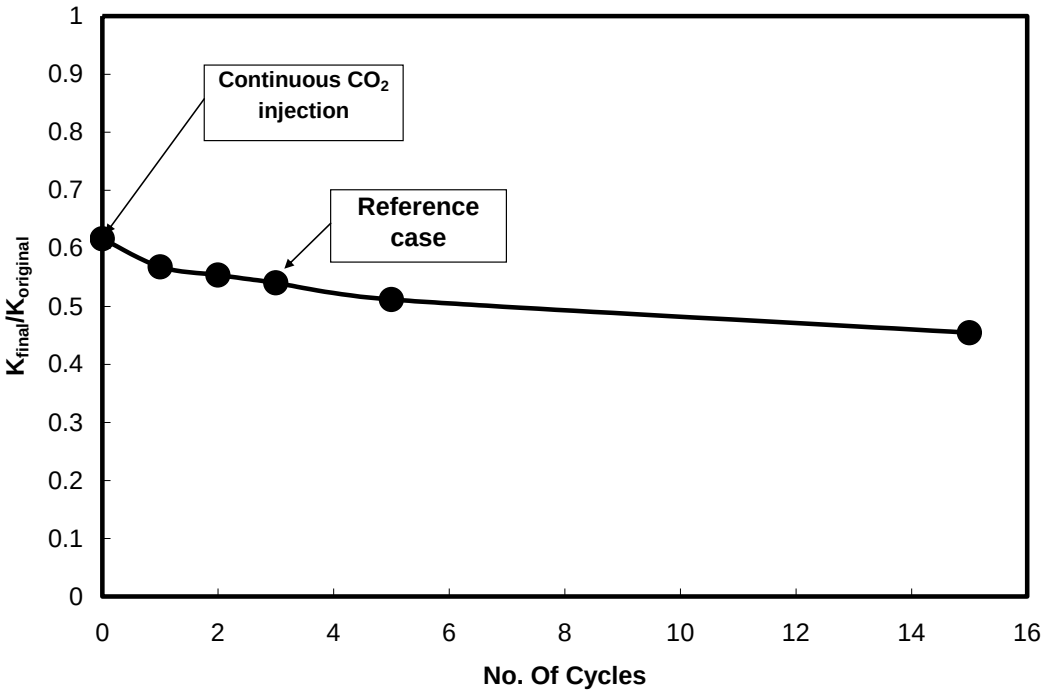

Fig.7.8—Effect of WAG cycle volume on the permeability ratio (final/original).

Fig. 7.9 shows the total calcium and magnesium collected in the core effluent sample. Increasing the number of WAG cycles injected increases the contact time

between CO_2 and brine and enhances the reactions between the fluid and the rock. As a result, more calcium and magnesium were collected in the core effluent samples.

7.4.3 Effect of CO_2 : Brine Volumetric Ratio

CO_2 : brine volumetric ratio of 1:1, 2:1, 5:1, and 1:2 were examined in this study. The change in core permeability is given in **Fig. 7.10**. Increasing the CO_2 : brine volumetric ratio reduces the damage due to less contact between CO_2 and brine, which limited the chemical reactions with the rock.

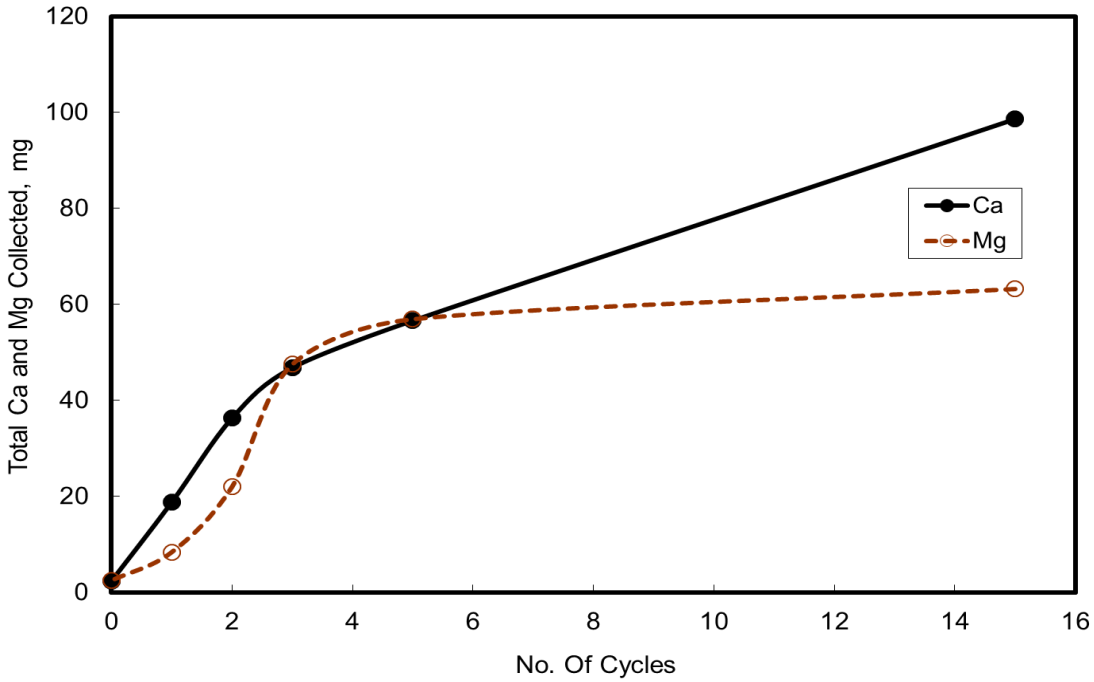

Fig. 7.9—Effect of WAG cycle volume on the total calcium and magnesium collected in the core effluent samples.

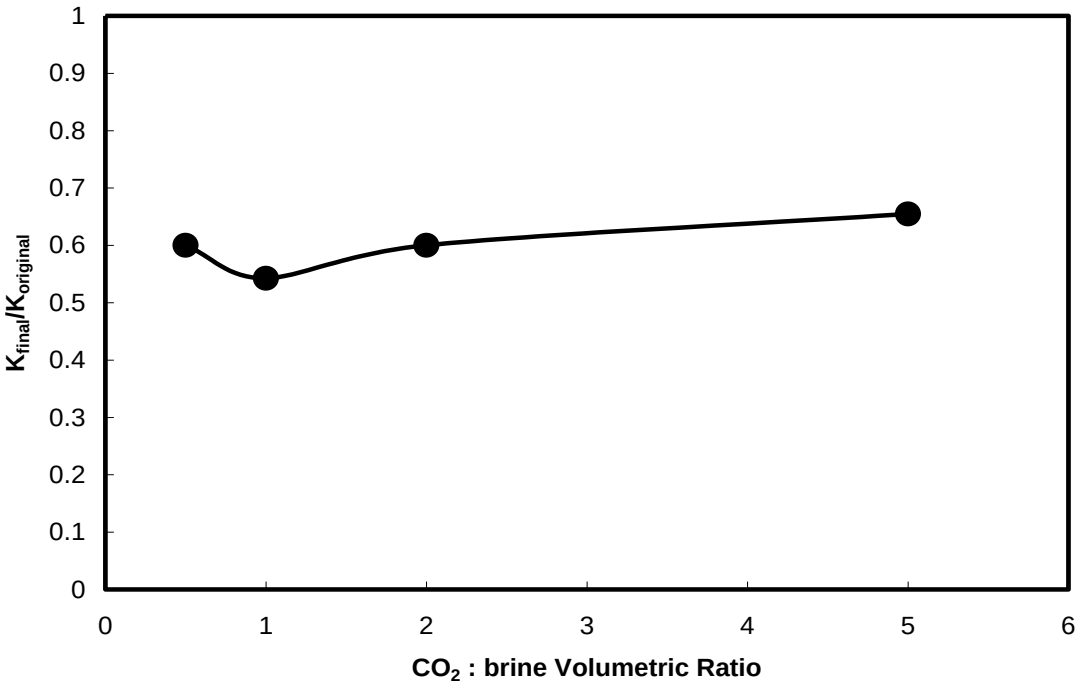

Fig. 7.10—Change in the core permeability vs. change in CO_2 : brine volumetric ratio.

Core #11 was conducted with volumetric ratio of 1:2 for 2 cycles because the pump volume was limited to 900 cm^3, the CO_2 half cycle was 5 PV, while the brine half cycle was 10 PV. Total calcium and magnesium collected at a volumetric ratio of 1:2 is less than 1:1 because less CO_2 was injected at volumetric ratio of 1:2 (**Fig. 7.11**). Less calcium and magnesium were collected in the core effluent samples at high volumetric ratios.

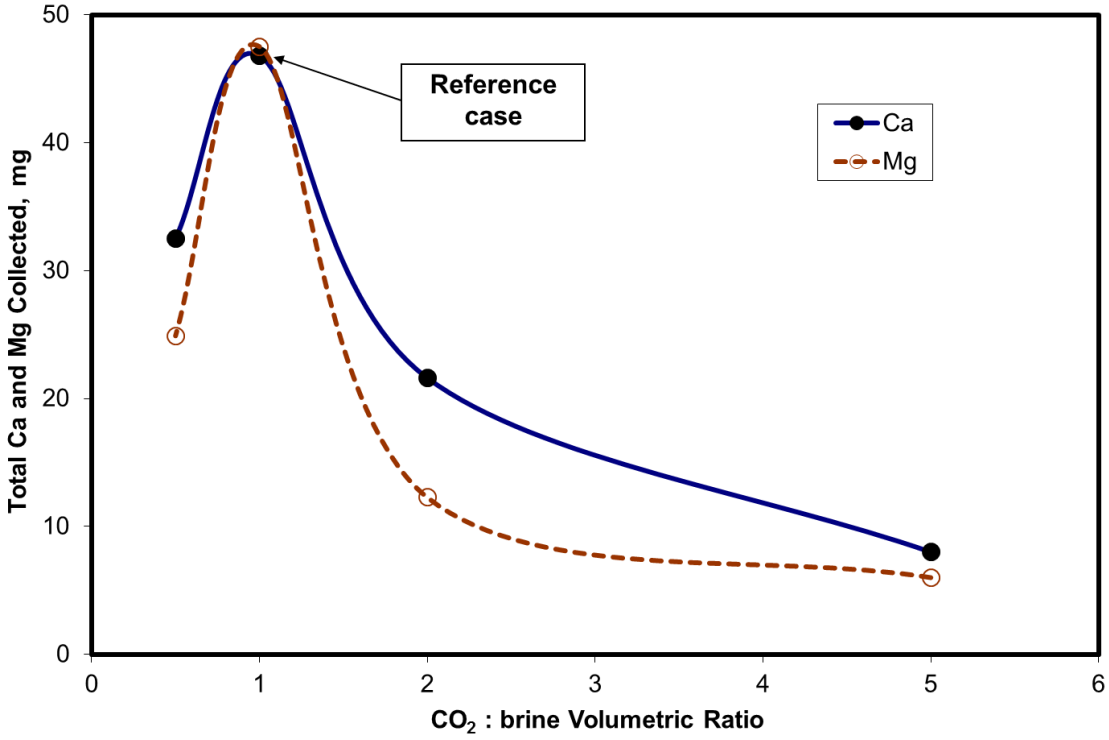

Fig. 7.11—Effect of CO_2 : brine volumetric ratio on the total calcium and magnesium collected in the core effluent samples.

7.4.4 Effect of Temperature

The experiment in this study was conducted at three different temperatures 70, 200, and 250°F. **Fig. 7.12** shows that at higher temperatures, more damage was introduced to the cores. The reaction rate between carbonates and carbonic acid increases at higher temperatures (Pokrovsky et al. 2009). Less calcium and magnesium were collected in the core effluent sample at lower temperatures (**Fig. 7.13**). Enhancement in the dissolution of carbonate minerals, fine migration of the particles attached by these carbonates, will be more severe. This might explain the damage increasing with the temperature increase.

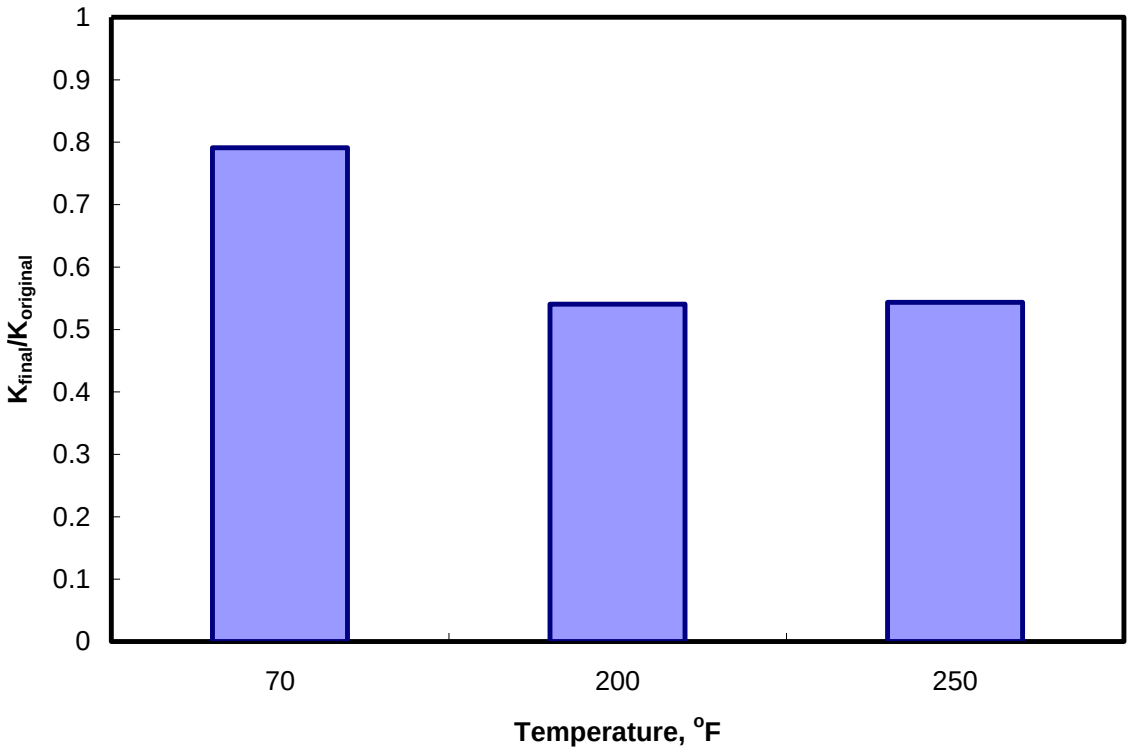

Fig. 7.12—Effect of temperature on the permeability ratio (final/original).

7.5 Modeling Studies

A compositional simulator software (CMG-GEM) was used to simulate the coreflood experiments and to predict the change in core permeability due to CO_2 injection. The objective of the simulation study is to find an appropriate equation that predicts the change in the core permeability based on the change in porosity resulting from the chemical reactions between CO_2 and different minerals present in Berea sandstone.

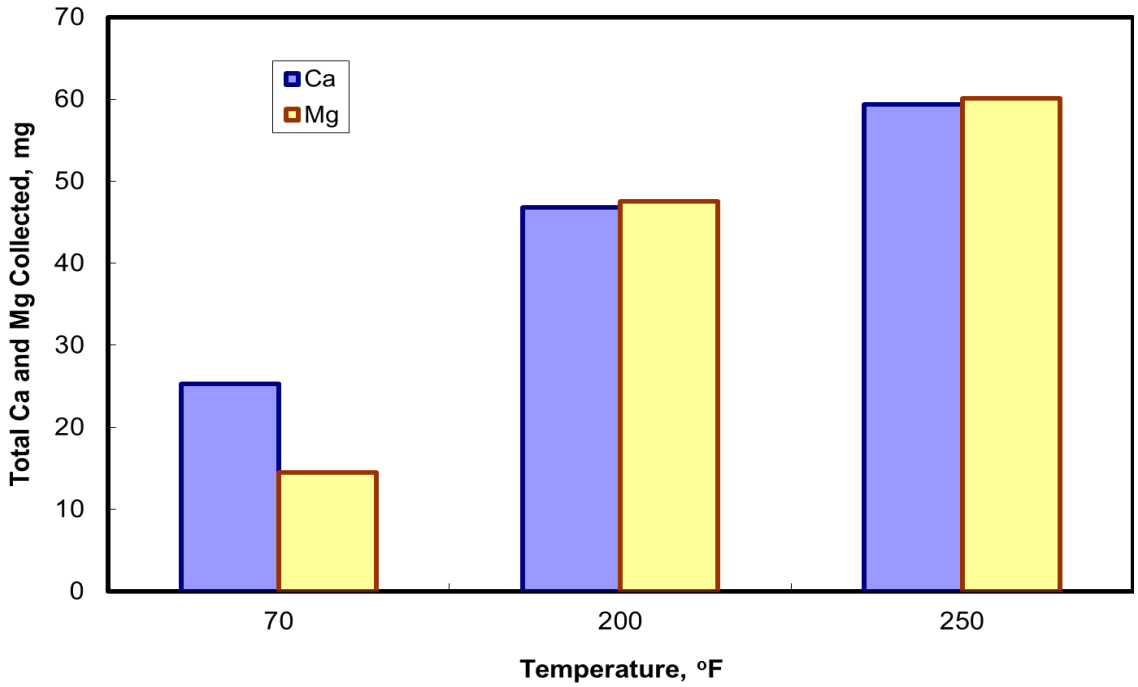

Fig. 7.13—Effect of temperature on the total calcium and magnesium collected in the core effluent samples.

The core was gridded into 2000 blocks (5X20X20 blocks in the r, Θ, and z directions, respectively). The initial porosity and permeability were assumed to be constant for all grids. Relative permeability for CO_2 and brine was calculated using **Eqs. 3.1-3.2**:

The irreducible brine and CO_2 saturation were obtained from the coreflood experiments to be 0.25 and 0.2, respectively. The permeability end points and the exponents were adjusted to match the pressure drop across the core obtained in the lab and the pressure drop calculated by the simulator. The values used for relative permeability end points are 0.1 and 0.4, while for exponents they are 5.0 and 2.0 for CO_2 and brine, respectively.

Capillary pressure between CO_2 and brine for Berea sandstone is calculated using **Eq. 3.3**. The contact angle value used in this study is 50°. The tortuosity is calculated using **Eq. 3.4**. The rate law for mineral dissolution and precipitation reactions calculated using **Eqs. 3.5-3.6**. The reaction kinetics used in this study are given in **Table 7.5**. The porosity changes due to mineral dissolution and precipitation are governed by **Eqs. 3.7-3.8.**

TABLE 7.5—LIST OF KINETIC RATE PARAMETERS FOR REACTIONS BETWEEN CO_2 AND DIFFERENT MINERALS

Mineral	Reactive Surface Area cm^2/g	$Log_{10}\ k_{0\beta}$ $mol/m^2.s$	Activation Energy KJ/mole	Reference Temperature °C	Reference
Calcite	9.8	-6.19	62.76	25	Svensson and Dreybrodt (1992)
Dolomite	9.8	-8.90	62.76	25	Xu and Pruess (2004)
Chlorite	9.8	-12.52	88.00	25	Xu et al. (2006)
Illite	$6.68\ X\ 10^5$	-12.78	35.00	25	Xu et al. (2006)
K-Feldspar	9.8	-12.41	38.00	25	Xu et al. (2006)
Kaolinite	$1.95\ X\ 10^5$	-13.16	22.20	25	Xu et al. (2006)
Quartz	9.8	-14.00	87.70	25	Xu et al. (2006)

7.5.1 Numerical Simulation

Fig. 7.14 shows the change in porosity of core #1 predicted by the simulator after WAG injection of CO_2 due to the dissolution and precipitation of calcite mineral. The calcite mineral dissolution occurred at the core inlet until 4.5 in. resulted in increasing the rock porosity at this region, while precipitation and reduction in porosity occurred from this point to the core outlet. The permeability of core #1 measured in the lab reduced from 55.5 md to 30 md, the source of damage at the zone of porosity increased is the pore plugging by fines, while at the porosity reduction zone the damage occurred by the pore plugging and precipitation of reaction products.

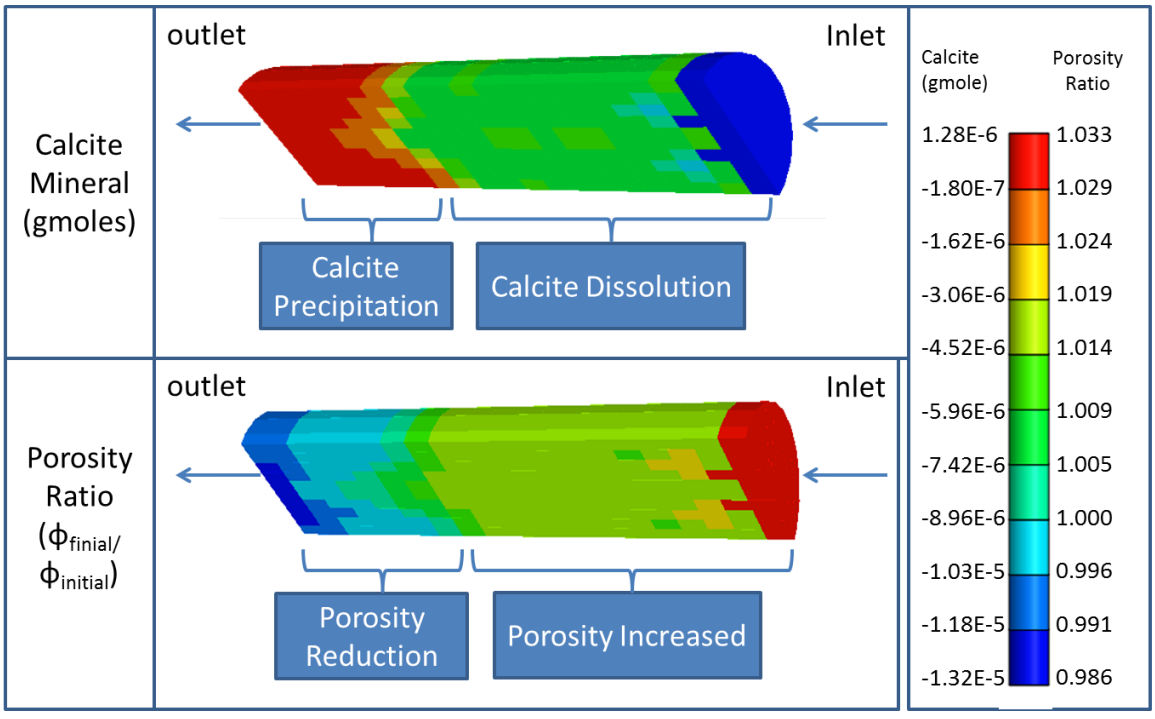

Fig. 7.14—Calcite dissolution and precipitation, and change in core porosity after WAG injection of CO_2, core #1

Several equations were used to predict the change in permeability based on the change in rock porosity, including: power-law (**Eq. 3.9**), Carman-Kozeny (**Eq. 3.10**), and modified Van Baaren's equations (Vernik 2000). Power-law and Carman-Kozeny equations couldn't predict the change in permeability for sandstone cores, since the overall porosity of the cores increased after CO_2 injection these equations predict an enhancement of the core permeability which is not true.

Van Baaren's equation is a function in porosity, grain size, and rock sorting (**Eq.7.5**);

$$k = 10\ D_d^2\ \phi^{3.64+f}\ C^{-3.64} \tag{7.5}$$

Where;

D_d = particle diameter, μm

ϕ = porosity, fraction

f = Archie cementation exponent

C = sorting coefficient ranging from 0.7 in very well sorted to 1.0 in poorly sorted sediments

The modified Van Baaren's equation used in this study is the same as **Eq. 7.5,** except that the particle size is replaced by the initial core permeability. The sorting coefficient used in this study is 0.75. Modified Van Baaren's equation (**Eq. 7.6**);

$$k = 14.67\ k_0^2\ \phi^{3.64+f} \tag{7.6}$$

The Archie cementation exponent (f) was adjusted to match the permeability measured in the lab. For core #1, the permeability calculated matched the measured permeability at f of 1.35. **Fig. 7.15A** shows the calculations of the permeability across

core #1 after WAG injection after each WAG cycle. The figure shows that the damage occurred across the core from the inlet to the outlet. Comparing the porosity and permeability data conclude that in the zone that shows increase in the porosity, the permeability increases with number of WAG cycles, because more cementing materials dissolved enlarging the pore diameter. The zone of porosity reduction shows more damage accumulated each WAG cycle because of more precipitation taking place, **Fig. 7.15B** shows a slight linear increase in the overall permeability of the core each WAG cycle.

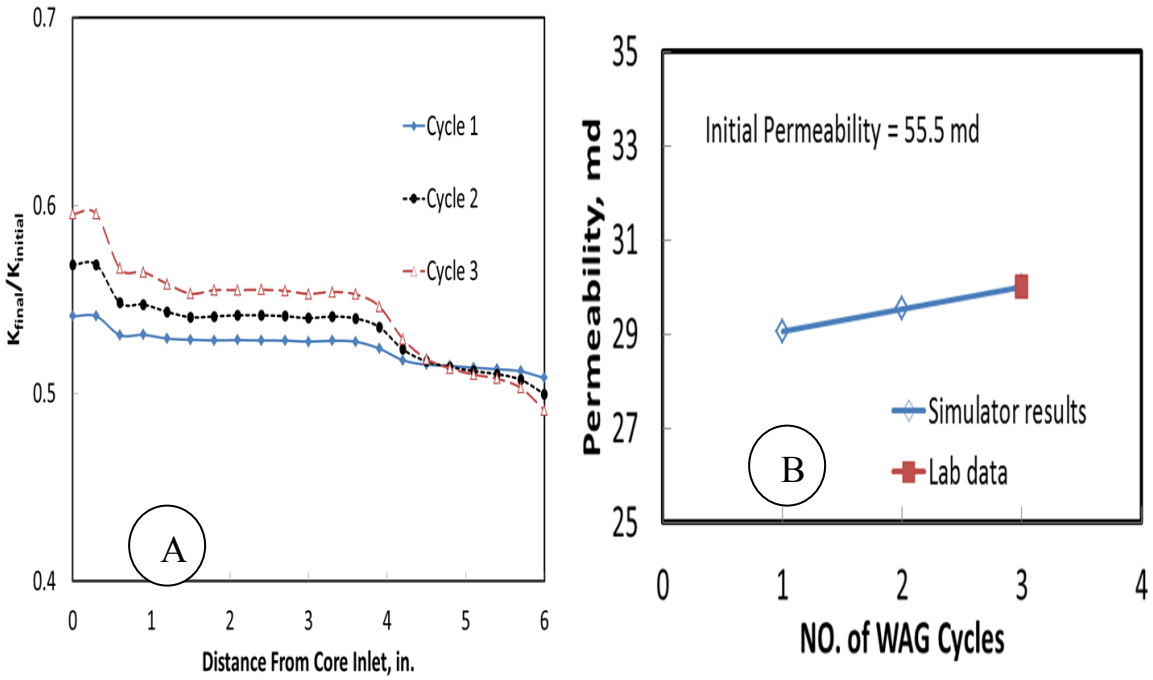

Fig 7.15—Change in core permeability after WAG injection of CO_2 into core #1: A) permeability distribution across the core after each WAG cycle, B) overall permeability of the core after each WAG cycle

The simulation for core #1 was extended to 100 WAG cycles to study the change in permeability for a larger volume of CO_2 injected. **Fig. 7.16A** shows that enhancement in the permeability close to the core inlet occurred after injecting 50 WAG cycles, extension of the enhanced zone to 4.0 in. from the core inlet after 100 WAG cycles injected. **Fig. 7.16B** shows that the permeability trend is increasing with increasing number of WAG cycles, but the original permeability was never restored; the final permeability after 100 WAG cycles injected is 0.72 of the original permeability. These results agree with the experimental results obtained by Sayegh et al. (1990). They concluded that for Pembina Cardium sandstone cores flooded with carbonated brine, the permeability dropped initially to a minimum value, and then the permeability steadily rose again and reached 70 to 85% of the original value.

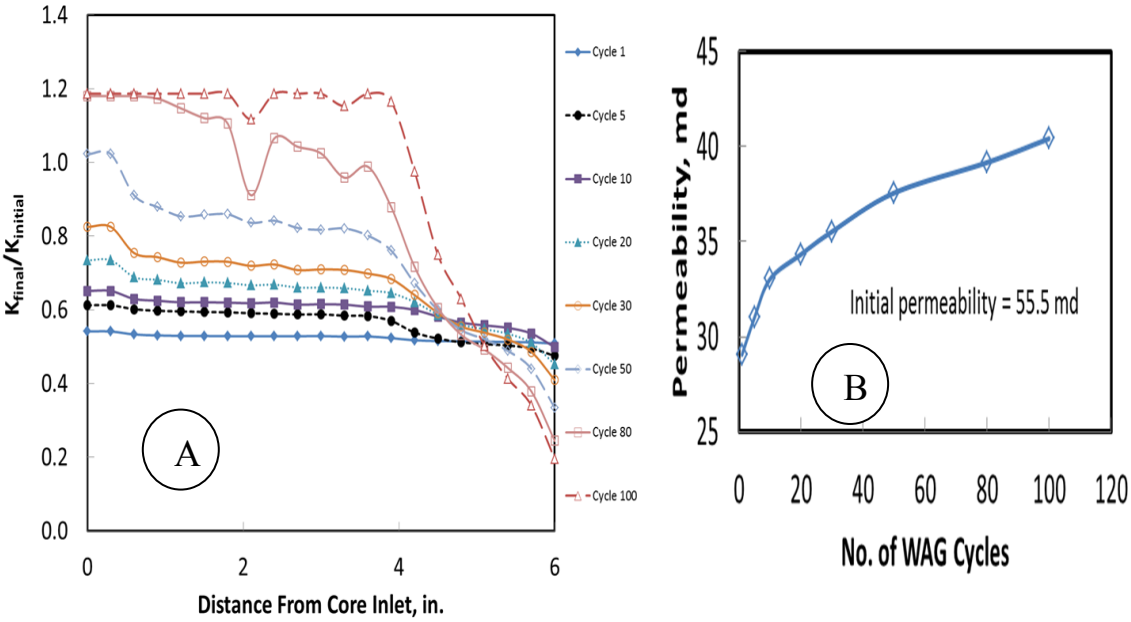

Fig 7.16—Change in core permeability after WAG injection of CO_2 into core #1 after injection of 100 WAG cycle of CO_2 : A) permeability distribution across the core, B) overall permeability of the core after each WAG cycle.

In the continuous CO_2 injection case (**Fig. 7.17**), an increase in the core porosity occurred through the core length. No calcite precipitation was predicted because of minimizing the contact time between brine and CO_2 in this case. The Archie cementation exponent for the continuous CO_2 injection experiment that matches the lab results is 1.511.

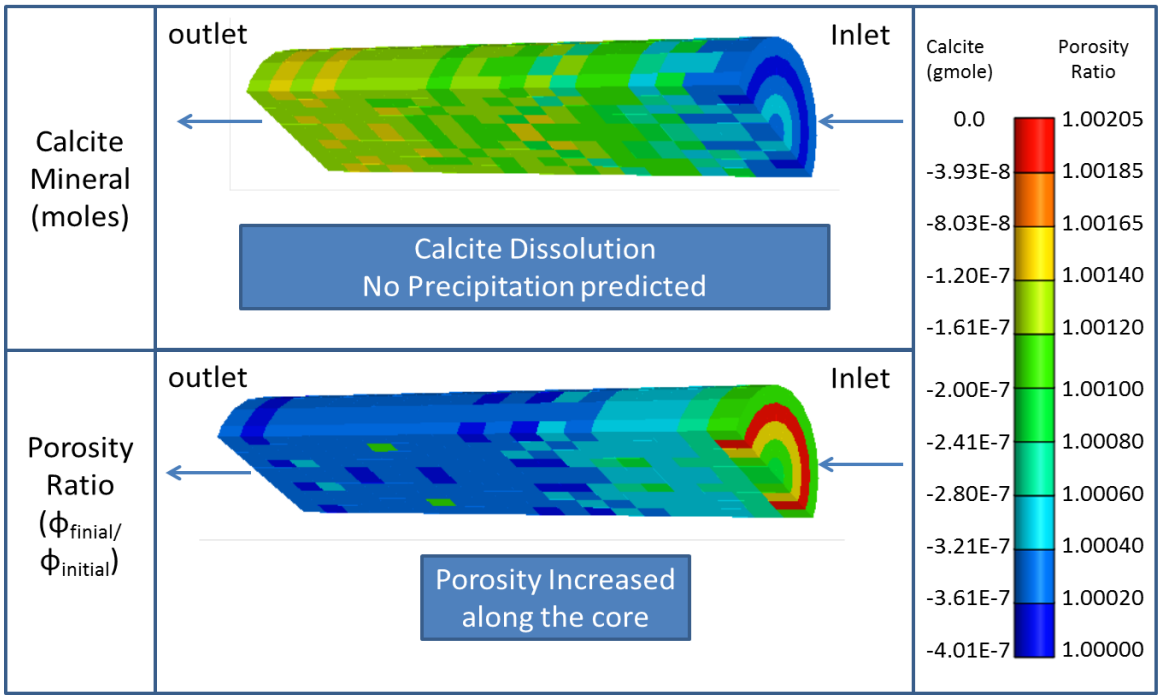

Fig. 7.17—Calcite dissolution and change in core porosity after continuous CO_2 injection, core #2

For short WAG cycle cases (core #5, 1 PV CO_2 injected per WAG cycle for 15 cycle), the zone with increase in porosity is shorter compared to the core #1. This zone propagated with WAG cycle from 1 in. after first cycle, to 3 in. after cycle number 15. The calcite precipitation occurs early in the core (**Fig. 7.18**) because of increasing the

contact time between CO_2 and brine. When 15 WAG cycles were injected this resulted in repeating the interface between brine and CO_2 30 times; for core #1 the interface repeated 6 times (3 WAG cycles), and for core #1 the interface occurred only once (continuous CO_2 injection).

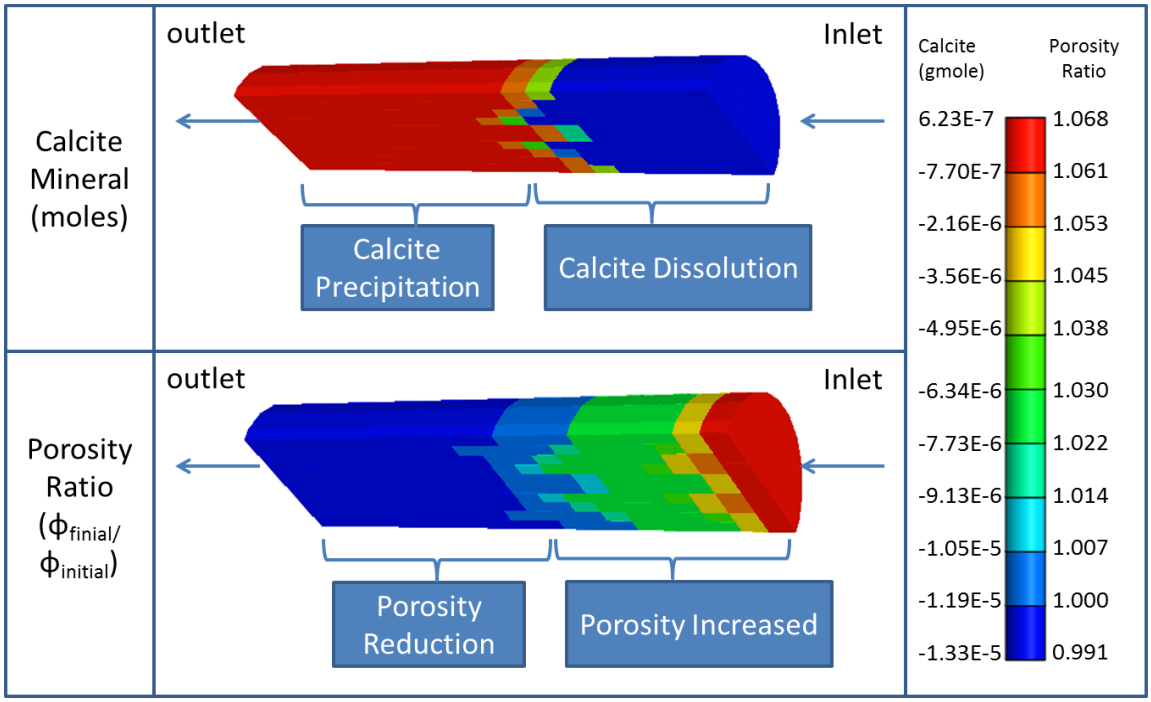

Fig. 7.18—Calcite dissolution and precipitation, and change in core porosity after WAG injection of CO_2, core #5

The Archie cementation exponent for core #5 that predicts a reduction in the core permeability from 81 to 36.8 md is 1.7. The permeability distribution after each WAG cycle is shown by **Fig. 7.19A**, the same trend noted for core #1 was noted again for core #5, the permeability increases with number of WAG cycles close to the core inlet, and

decreases close to the core outlet. **Fig. 19B** shows a slight linear increase in the overall permeability of the core each WAG cycle.

To address the effect of core length, a case was run to simulate a 20 in. core with the same conditions as core #1 (3 WAG cycles with 5 PV CO_2 injected each cycle, and the CO_2:brine volumetric ratio 1:1 at 200°F, and back pressure of 1300 psi). No precipitation was predicted in this case and the porosity increased through the core length (**Fig. 7.20**). From the comparison between the simulation 6 in. core and 20 in. cores, a conclusion can be obtained that the actual CO_2 volume injected is the critical factor that defines the location of the precipitated calcite, not the pore volume of CO_2. **Fig. 7.21** shows a reduction in the core permeability, with a small increase in the core permeability each WAG cycle.

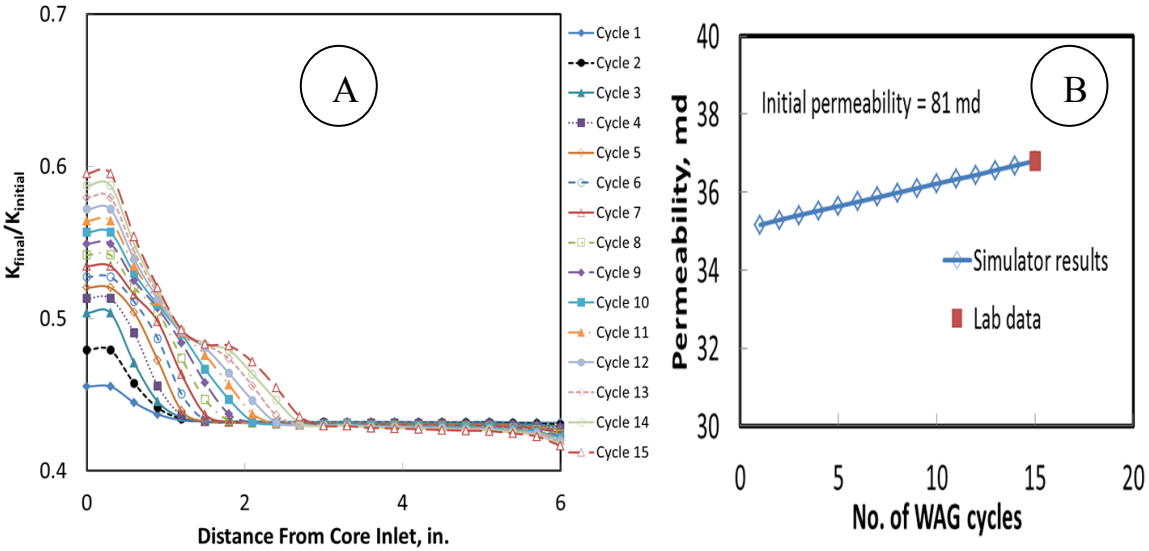

Fig 7.19— Change in core permeability after WAG injection of CO_2 into core #5: A) permeability distribution across the core after each WAG cycle, B) overall permeability of the core after each WAG cycle.

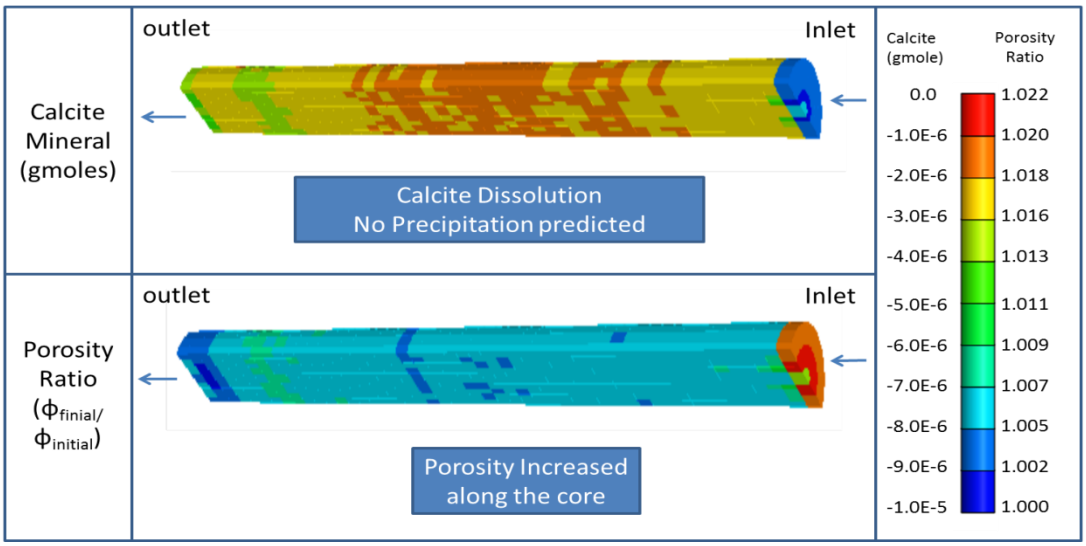

Fig. 7.20—Calcite dissolution and change in core porosity after 3 WAG cycles injected for a 20 in core.

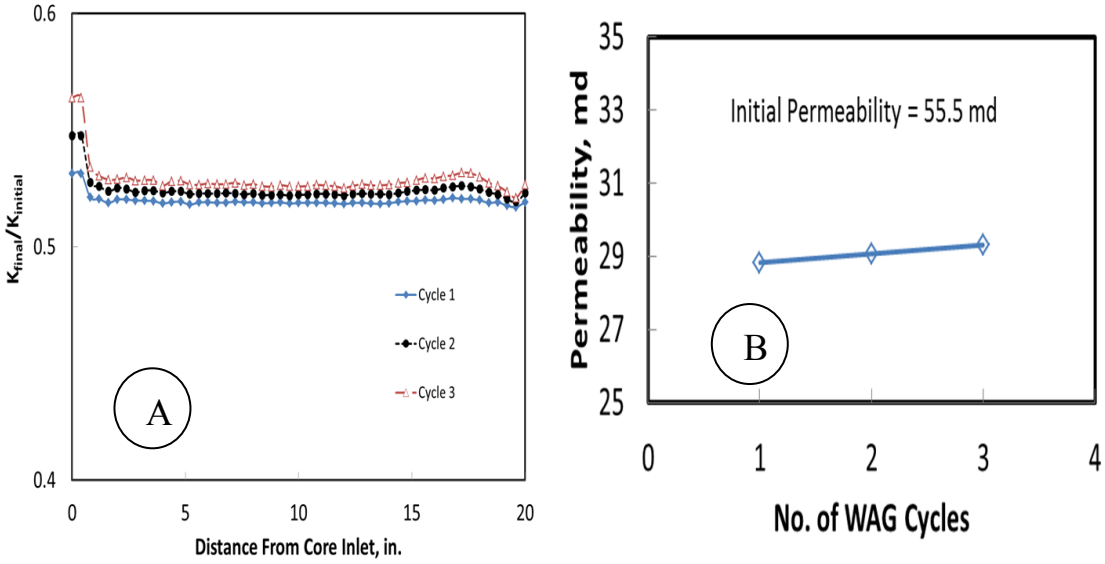

Fig 7.21—Change in core permeability after WAG injection of CO_2 into 20 in. core after injection of 3 WAG cycle of CO_2: A) permeability distribution across the core, B) overall permeability of the core after each WAG cycle

TABLE 7.6—SUMMARY OF THE ARCHIE CEMENTATION EXPONENT				
Core	**Archie Cementation Exponent (*f*)**	**Actual Final Permeability (md)**	**Final Permeability Calculated @ Average Exponent**	**Error %**
1	1.350	30.0	26.6	11.3%
2	1.511	53.0	61.0	15.1%
3	1.017	35.6	18.5	48.0%
4	1.580	44.0	56.3	28.0%
5	1.700	36.0	56.7	57.5%
6	1.660	44.0	63.9	45.3%
7	1.430	36.0	36.4	1.1%
8	1.540	46.0	55.2	20.0%
9	1.350	38.0	33.5	11.8%
10	1.034	27.5	14.7	46.5%
11	1.512	48.0	55.1	14.8%
Arithmetic Average	1.426			

A summary with the Archie cementation exponent for all coreflood experiments run in this study is given in **Table 7.6**. The values ranged from 1.017 to 1.7, with an average value of 1.426. The calculation of permeability is very sensitive to the f value. Permeability calculated using the average f gives error up to 57.5%. The Archie cementation exponent is case dependent and changes with changing the experimental conditions (pressure, temperature, injection scheme, core permeability, and porosity).

8. FORMATION DAMAGE DUE TO CO_2 SEQUESTRATION IN DEEP SALINE CARBONATE AQUIFERS: LAB AND MODELING STUDIES

CO_2 injection in carbonate formations causes a reduction in the well injectivity, due to precipitation of the reaction products between CO_2/rock/brine. The precipitated material includes sulfate and carbonate scales. The homogeneity of the carbonate rock, in terms of mineralogy and rock structure, is an important factor that affects the behavior of permeability changes during CO_2 injection.

Limestone rocks that were tested in this study were homogenous, and included: Pink Desert limestone and Austin chalk, which are mainly calcite. Silurian dolomite (composed of 98% carbonate minerals, and 2% silicate minerals) and Indiana limestone were the heterogeneous rock used and had vugs.

In this chapter, the effect of CO_2/WAG injection on permeability and porosity of various carbonate cores is examined using a coreflood study. Synthetic seawaters with/without sulfate were used in the WAG process to assess potential precipitation of calcium sulfate and its effect on permeability. Finally, modeling studies were conducted to predict experimental results and determine permeability and porosity variations across the cores.

8.1 Introduction

Change in well injectivity is a well-known problem in CO_2 injection wells, either in enhanced oil recovery or sequestration projects (Grigg and Svec 2003). Well

injectivity changes, due to relative permeability effects occurring by multiphase flow, and chemical reactions between CO_2/brine/rock.

The risk of water blockage, resulting from the trapping of water in the pore throat is high, in low permeability water-wet formations (Nasr-El-Din et al. 2002). Water blockage occurs when water blocks the macro pores, especially in low permeability reservoirs. Water saturation close to irreducible water saturation has a small effect on permeability; higher water saturations have a more pronounced effect on the permeability since the larger pores are filled with water (Gruber 1996).

Torn et al. 2012 ran a simulation study to address the feasibility of CO_2 injection into different formations, CMG-GEM model was used in their study by ignoring the geochemical process, the capillary pressure was also ignored in their study.

Coreflood experiments were conducted to compare the behavior of the permeability loss between these rocks. CO_2 was injected with the water alternating gas (WAG) technique. Different brines were examined including seawater and seawater without sulfate. The experiments were run at a back pressure of 1300 psi, a temperature of 200°F, and an injection rate of 5 cm^3/min. A compositional simulator tool (CMG-GEM) was used to confirm the experimental results obtained in this study.

8.2 Test Design

The coreflood tests were designed to simulate WAG injection of CO_2 into saline carbonate aquifers. A slug of CO_2 (purity 99.8%) was injected in the first half of the WAG cycle, while a slug of a synthetic brine was injected in the second half. Two brines

were used in this study, the first one was seawater without sulfate with total dissolved solids (TDS) of 35.884 ppm, or the second one was seawater with TDS 38,734 ppm (**Table 5.3**). Tests were run at 200°F, and back pressure was kept constant at 1300 psi for all experiments. Core effluent samples were collected throughout the experiment; every 3 minutes during brine injection, while during CO_2 injection the first 2 samples were collected every 3 minutes, and the third sample at the end of the CO_2 half cycle.

TABLE 8.1—BULK COMPOSITION OF CARBONATE CORES USED IN THIS STUDY.

Element	Concentration, wt%				
	Pink Desert Limestone	**Austin Chalk**	**High Permeability Indiana Limestone**	**Low Permeability Indiana Limestone**	**Silurian Dolomite**
O	47.80	47.90	47.90	47.70	51.46
Ca	39.70	39.60	39.70	38.50	21.18
C	11.90	11.90	11.90	11.50	12.69
Si	0.12	0.17	0.18	0.83	0.20
Mg	0.08	0.12	-	0.39	12.79
Al	0.07	0.08	0.09	0.23	0.16
Fe	0.04	0.03	0.12	0.18	0.10
S	0.03	0.01	0.02	0.05	-
K	0.02	-	-	0.12	0.05
Na	-	-	-	-	1.26
Sr	0.02	0.04	0.02	0.02	-
Mn	-	0.01	0.01	0.04	-
Sn	0.01	0.01	0.01	0.01	0.01
Total	99.80	99.86	99.96	99.57	99.90

Carbonate rock from different locations and lithologies were used in this study including; Pink Desert limestone, Austin chalk, high permeability Indiana limestone, low permeability Indiana limestone, and Silurian dolomite (**Fig. 8.1**). XRF analysis was run

to define the elemental composition of these rocks (**Table 8.1**). A summary of the coreflood tests is given in **Table 8.2**.

TABLE 8.2—SUMMARY OF THE COREFLOOD EXPERIMENTS.

Core	Rock Type	Injected Brine	Initial Core Permeability (md)
PD1	Pink Desert Limestone	Seawater Without Sulfate	79.8
PD2		Seawater	77.0
AC1	Austin Chalk	Seawater Without Sulfate	3.4
AC2		Seawater	4.9
HKI1	High Permeability Indiana limestone	Seawater Without Sulfate	102.0
HKI2		Seawater	71.0
LKI	Low Permeability Indiana Limestone	Seawater Without Sulfate	2.52
SD1	Silurian Dolomite	Seawater Without Sulfate	182.0
SD2		Seawater Without Sulfate	35
SD3		Seawater Without Sulfate	2.7

8.3 Results

8.3.1 Pink Desert Limestone

Two experiments were run to examine CO_2 WAG injection in Pink Desert limestone cores; one using seawater without sulfate (PD1), and the other one using seawater (PD2). Calcium and sulfate concentrations in the core effluent samples are shown in **Fig. 8.2**. Comparing the two calcium curves showed that PD1 had a higher calcium concentration compared to PD2 because of calcium sulfate precipitation in the case of PD2. The sulfate concentration curve for PD2 showed a reduction in the sulfate concentration in the core effluent. Integrating the area between the calcium concentration curve and initial calcium concentration line in **Fig. 8.2** gives the total amounts of calcium collected from PD1 and PD2 to be 0.58 and 0.375 g, respectively. 0.039 g of sulfate was lost due to calcium sulfate precipitation.

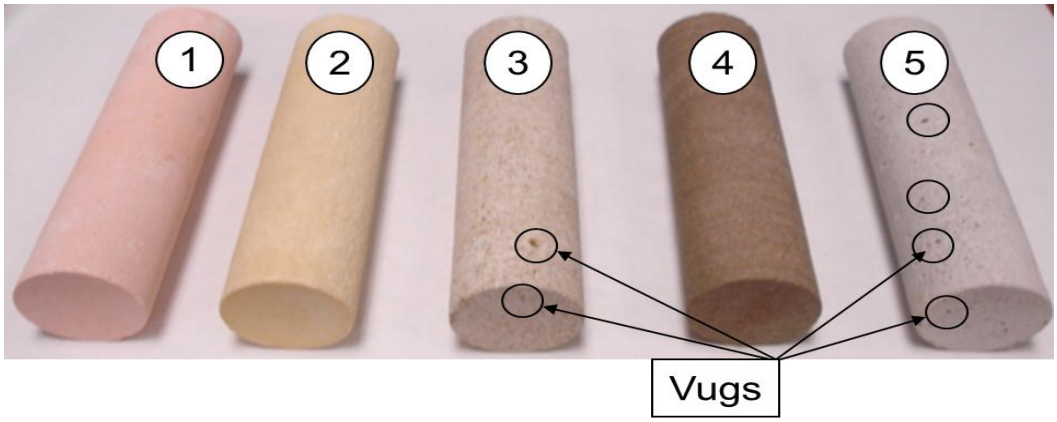

Fig. 8.1—Cores used in this study with dimensions of 6 in. length and 1.5 in. diameter. Homogenous cores 1) Pink Desert limestone, 2) Austin chalk, 3) High Permeability Indiana limestone. Heterogeneous cores with vugs with diameter ranges between 2 and 4 mm 4) Low Permeability Indiana limestone, and 5) Silurian dolomite.

pH value for the core effluent samples ranged between 6.3 and 5.8 depending on the calcium concentration. As the calcium concentration increases, the pH value increases. Precipitated particles collected in the core effluent were analyzed using SEM. For PD1 calcium carbonate precipitated (**Table 8.3**). Analysis of the precipitated particles from PD2 showed that the composition was 1) 51.83.0% Oxygen, 2) 35.71% Calcium, 3) 10.34% Carbon, 4) 1.15% Magnesium, and 5) 0.97% Sulfur (**Fig. 8.3**). PD1 showed a slight increase in the core permeability from 79.8 to 83 md, while a reduction in the core permeability was noted for PD2, from 77 to 69 md.

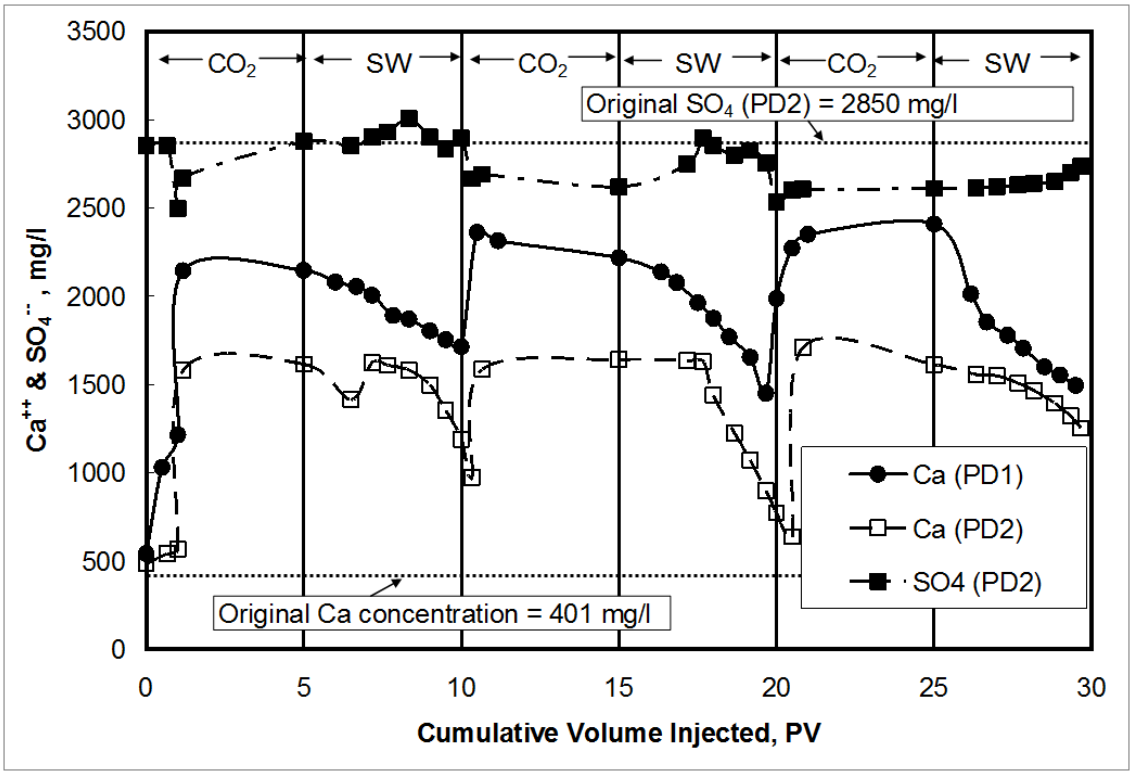

Fig. 8.2—Calcium concentration in the core effluent samples for core PD1 (WAG with seawater without sulfate injected), and calcium and sulfate concentrations for core PD2 (WAG with seawater injected).

TABLE 8.3—ELEMENTAL COMPOSITION OF PRECIPITATED MATERIAL IN CORE EFFLUENT SAMPLES.								
Element	**Concentration, wt%**							
	PD1	**PD2**	**AC1**	**AC2**	**HKI1**	**HKI2**	**LKI**	**SD**
O	50.13	51.83	54.33	55.00	51.12	52.15	47.84	45.96
Ca	38.25	35.71	34.27	33.56	36.58	35.60	32.99	6.01
C	10.62	10.34	10.27	9.91	10.96	10.58	17.60	20.03
Mg	1.00	1.15	1.14	1.14	1.33	0.77	0.71	7.39
Si	-	-	-	-	-	-	-	7.56
Al	-	-	-	-	-	-	-	4.84
Fe	-	-	-	-	-	-	-	7.31
S	-	0.97	-	0.39	-	0.53	0.49	-
Total	100.00	100.00	100.00	99.99	99.99	99.63	99.63	99.10

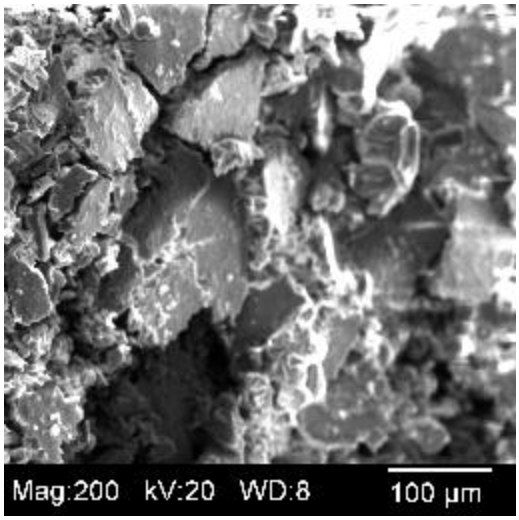

Fig. 8.3—SEM photomicrograph of calcium carbonate ($CaCO_3$) particles noted in the core effluent samples, Pink Desert limestone.

8.3.2 Austin Chalk

Austin chalk is a homogenous low permeability limestone rock. Two cores were used in this study, AC1 with a permeability of 3.4 md, and AC2 with a permeability of 4.9 md. Three WAG cycles were injected into each core; CO_2 followed by seawater

without sulfate injected to AC1, and CO_2 followed by seawater for AC2. Both cores had the same pressure drop behavior during WAG injection; the pressure drop across AC2 is shown in **Fig. 8.4**. Initially, the seawater flooding pressure drop stabilized at 125 psi. Alternating to CO_2, there was a slight increase followed by a reduction in the pressure drop, due to higher CO_2 mobility compared to seawater (under the experiment conditions, the viscosity of CO_2 was less than seawater viscosity by orders of magnitude of 17). Alternating to seawater, a sharp increase in the pressure drop was noted, after injecting 3.5 PV, the pressure drop started to decrease. The same behavior was repeated each cycle, with an increasing pressure level, the final seawater flooding pressure drop was 85 psi higher than the initial pressure. CO_2 saturation at the end of the CO_2 half cycle was 67.0 %, and the final seawater saturation at the end of the seawater half cycle was 89.7 %.

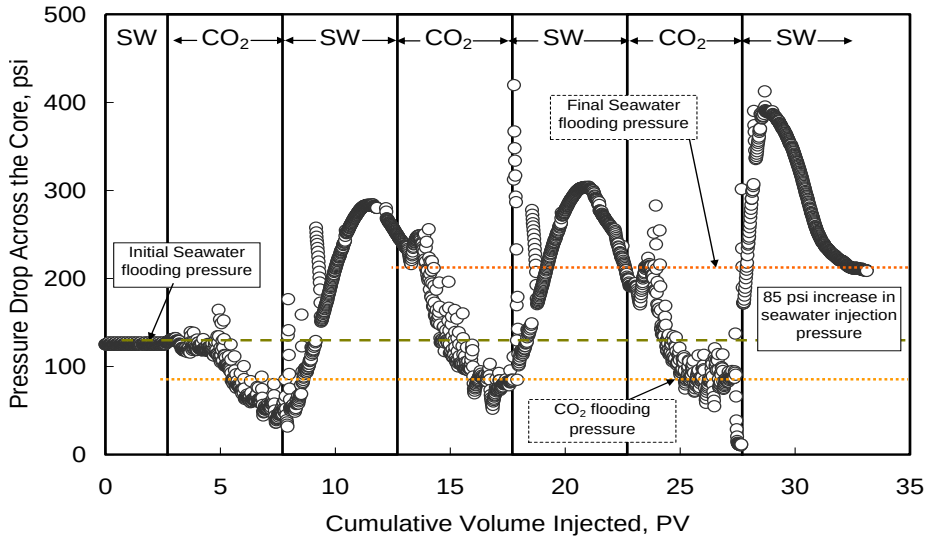

Fig. 8.4—Pressure drop across core AC2 during CO_2 and seawater WAG injection.

Fig. 8.5 shows the concentrations of calcium and sulfate in the core effluent samples for cores AC1 and AC2. The curves were similar to the results obtained for Pink Desert limestone, the presence of sulfate reduced the calcium concentration in the core effluent samples from 2100 for AC1, to 1700 mg/l for AC2; also, a reduction in the sulfate concentration was noted due to the precipitation of calcium sulfate. **Fig. 8.6** shows the SEM analysis for the precipitated particles collected in the core effluent samples, the solid precipitated for cores AC1 and AC2 was mainly aragonite ($CaCO_3$); some sulfur (0.39 wt%) was detected with the precipitated particles collected from core AC2, from the precipitation of calcium sulfate.

Permeability reduction was observed for the two cores, with more damage occurring to AC2. The permeability of AC1 decreased from 3.4 to 3.29 md, and for AC2, decreased from 4.9 to 4.5 md.

8.3.3 High Permeability Indiana Limestone

High permeability Indiana limestone cores were heterogeneous with the presence of vugs (**Fig. 8.1**). The permeability of the cores used in this study was 102.0 and 71.0 md, for cores HKI1 and HKI2, respectively. The pressure drop profile showed that the pressure stabilized quickly after alternating from seawater to CO_2, and vice versa, CO_2 flooding pressure was always less than seawater flooding pressure; final seawater flooding pressure was 3 psi higher than the initial pressure (**Fig. 8.7**). Saturations of CO_2 at the end of the CO_2 half cycle were 60 %, and for seawater 71 %.

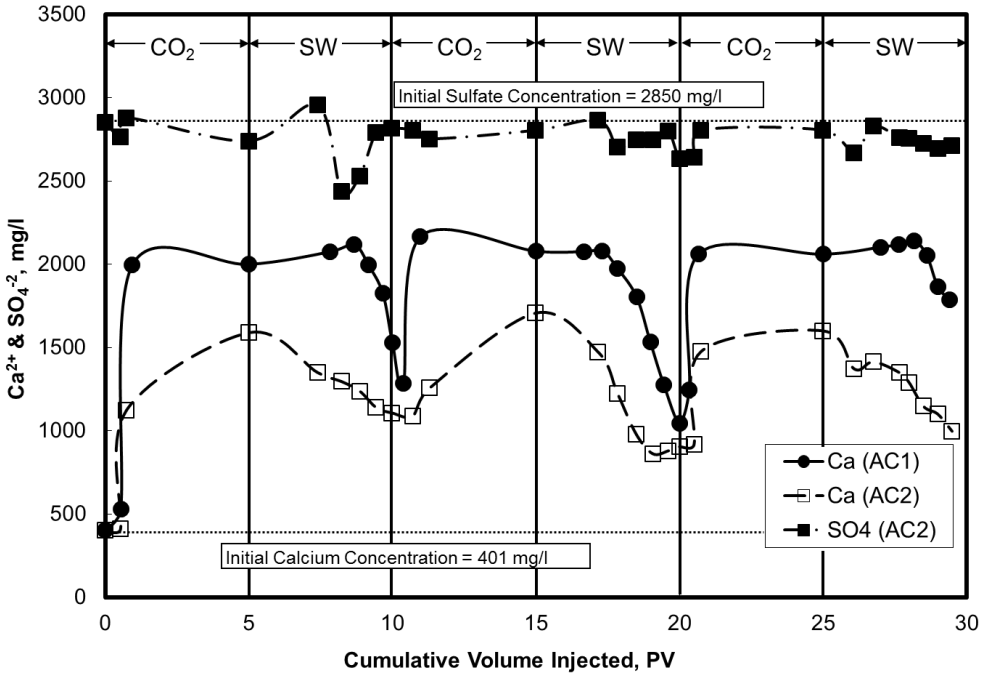

Fig. 8.5—Calcium concentration in the core effluent samples for core AC1 (WAG with seawater without sulfate injected), and calcium and sulfate concentrations for core AC2 (WAG with seawater injected).

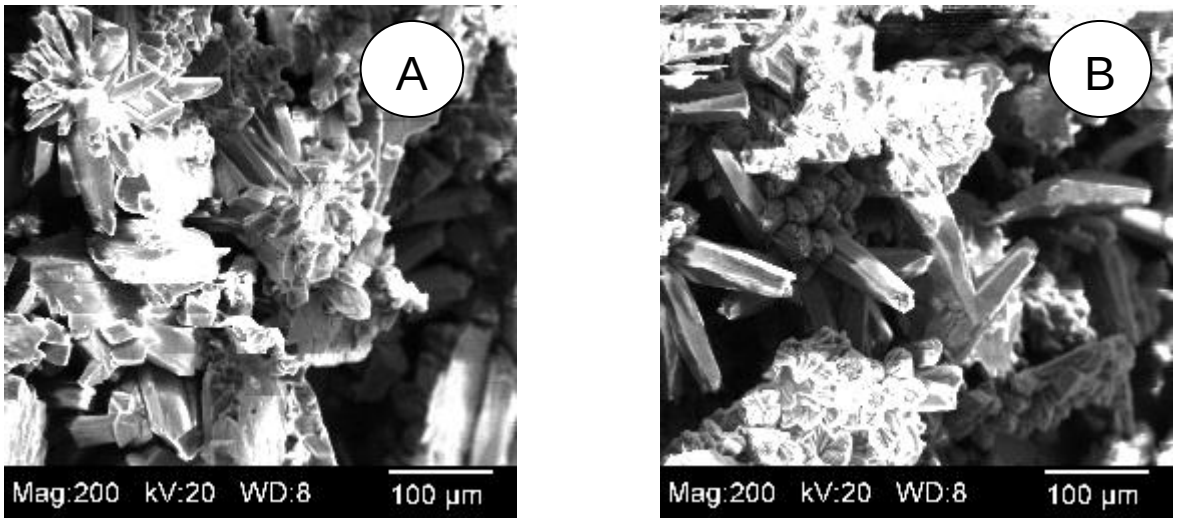

Fig. 8.6—SEM photomicrograph of calcium carbonate ($CaCO_3$) particles noted in the core effluent samples for cores, A) AC1, and B) AC2.

Analysis of the core effluent samples showed similar behavior to Pink Desert limestone and Austin chalk; the presence of sulfate decreased the concentration of calcium in the effluent samples, due to calcium sulfate scale precipitation inside the core (**Fig. 8.8**). The precipitated particles were a combination of calcite and aragonite (both are $CaCO_3$), with some sulfates noted in the precipitated particles collected from the HKI2 effluent samples (**Fig. 8.9**).

Both cores had a final permeability less than the original permeability after CO_2 injection; HKI1 had a reduction in permeability from 102 to 84 md, and HKI2 had damage that caused permeability to be reduced from 71 to 41.5 md.

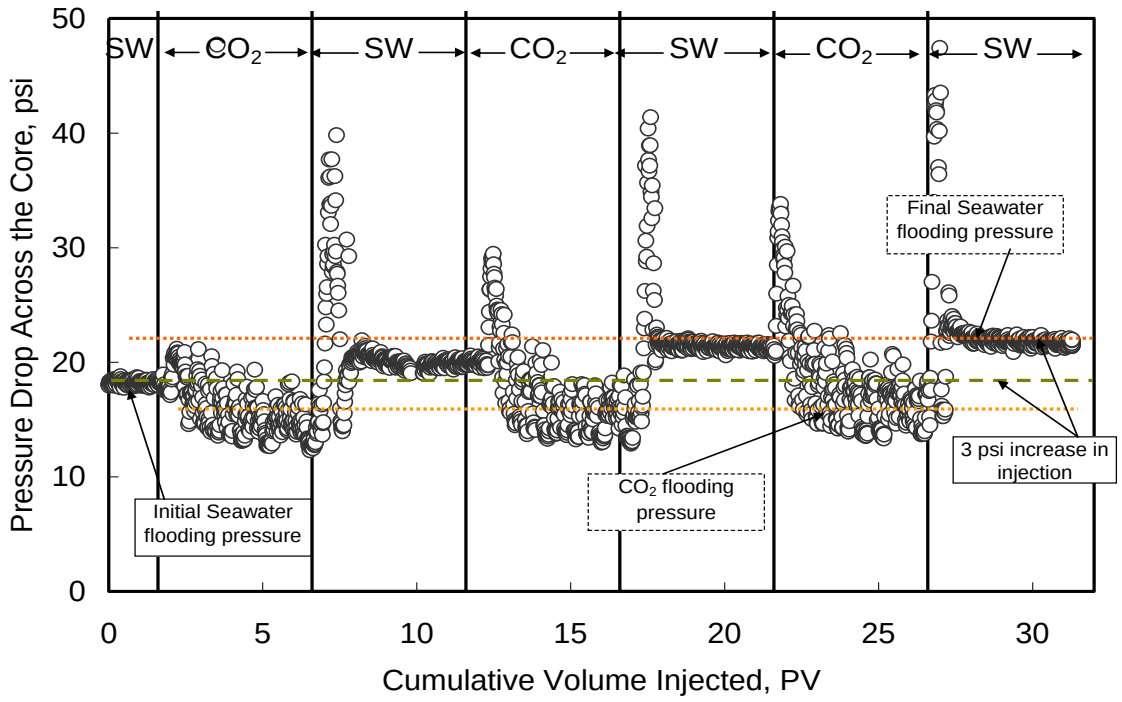

Fig. 8.7—Pressure drop across core HKI2 during CO_2 and seawater WAG injection.

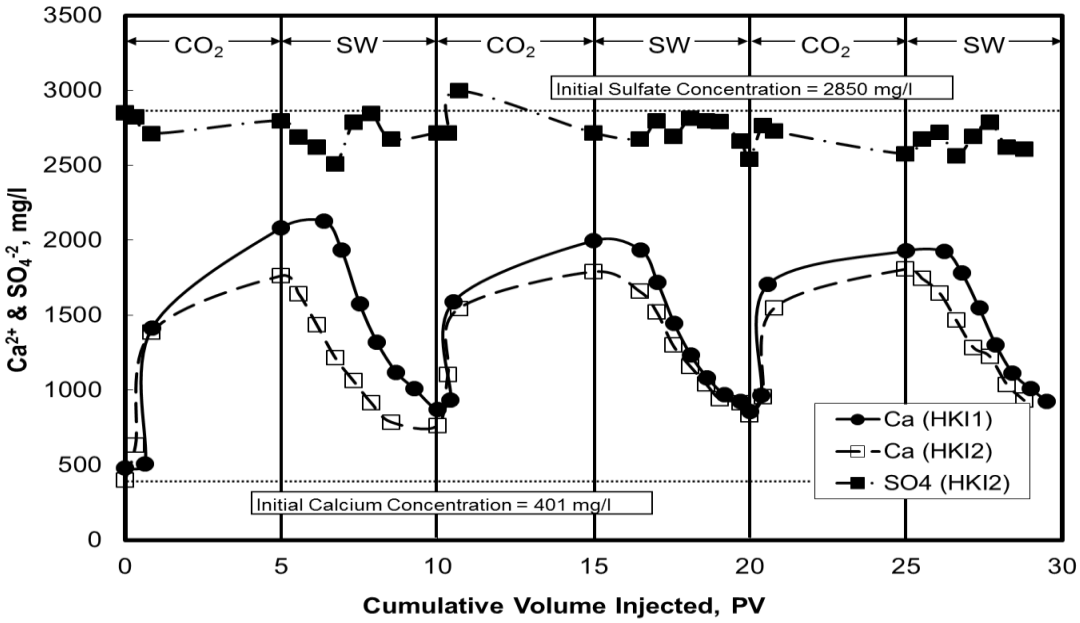

Fig. 8.8—Calcium concentration in the core effluent samples for core HKI1 (WAG with seawater without sulfate injected), and calcium and sulfate concentrations for core HKI2 (WAG with seawater injected).

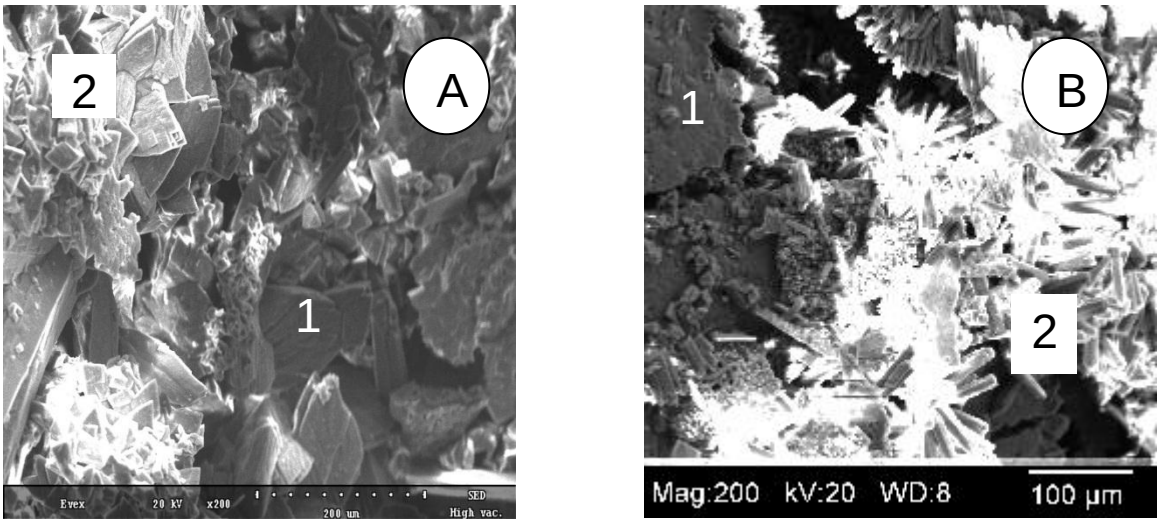

Fig. 8.9—SEM photomicrograph of the precipitated particles in the core effluent samples, XRD showed that the precipitated particles are two forms of calcium carbonate 1) Calcite, 2) Aragonite. Cores, A) HKI1, and B) HKI2.

8.3.4 Low Permeability Indiana Limestone

The XRF analysis of the low permeability Indiana limestone cores showed that some silicon and aluminum exist in the composition of this rock (**Table 8.1**), which indicates the presence of silicate minerals (clays and/or feldspars). The initial core permeability was 2.52 md. **Fig. 8.10** shows the pressure drop across core LKI during CO_2 and seawater without sulfate, during WAG injection. The pressure drop profile showed that the seawater flooding pressure increased from 670 to 970 psi in the first WAG cycle. The experiment stopped at the second WAG cycle during the seawater half cycle when the pressure drop reached 1070 psi; no more water could be injected after this point since the pump reached the maximum pressure limit (2300 psi). CO_2 injection pressure in the two cycles was less than seawater flooding pressure. Saturation of CO_2 inside the core was 66.0 % at the end of the CO_2 half cycle. The final seawater saturation for the first WAG cycle was 92.0 %.

Fig. 8.11 shows the calcium concentration in the core effluent samples for the two WAG cycles injected in this experiment. The figure shows that the maximum calcium concentration for the LKI core is less than the maximum calcium concentration obtained for the other limestone cores examined in this study. The analysis of the precipitated particles in the core effluent samples showed that these particles were composed of smaller particles of calcium carbonate, compared to the precipitated particles collected from the other carbonate cores (**Fig. 8.12**). A reduction in the core permeability occurred, from 2.52 to 1.7 md.

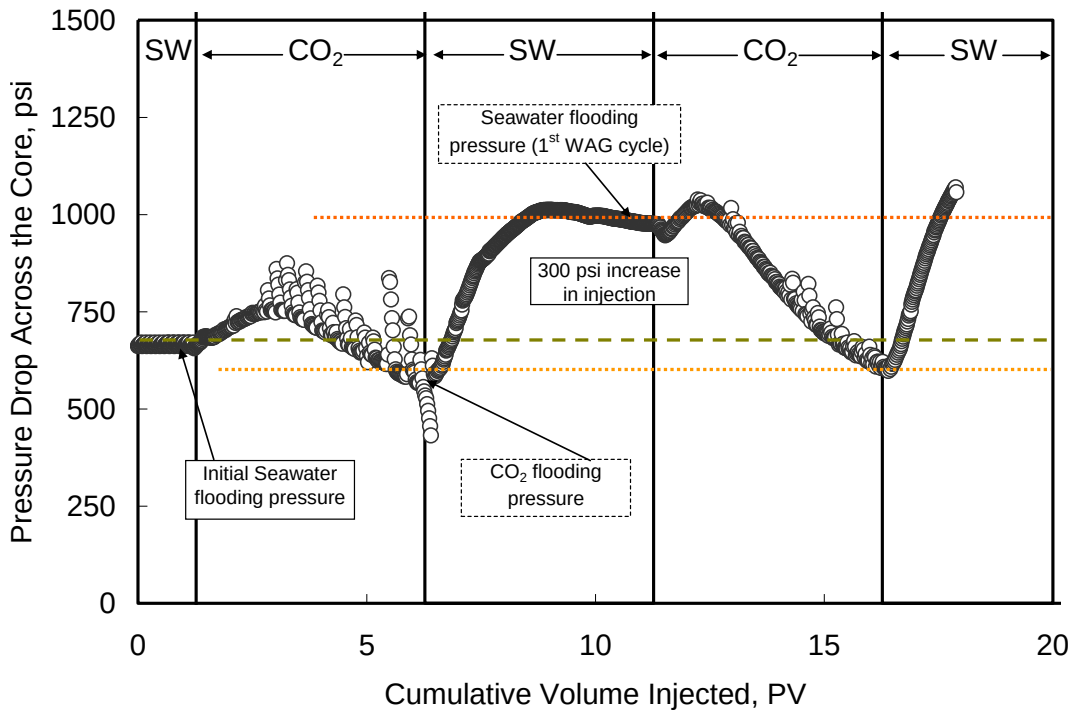

Fig. 8.10—Pressure drop across core LKI during CO_2 and seawater without sulfate WAG injection.

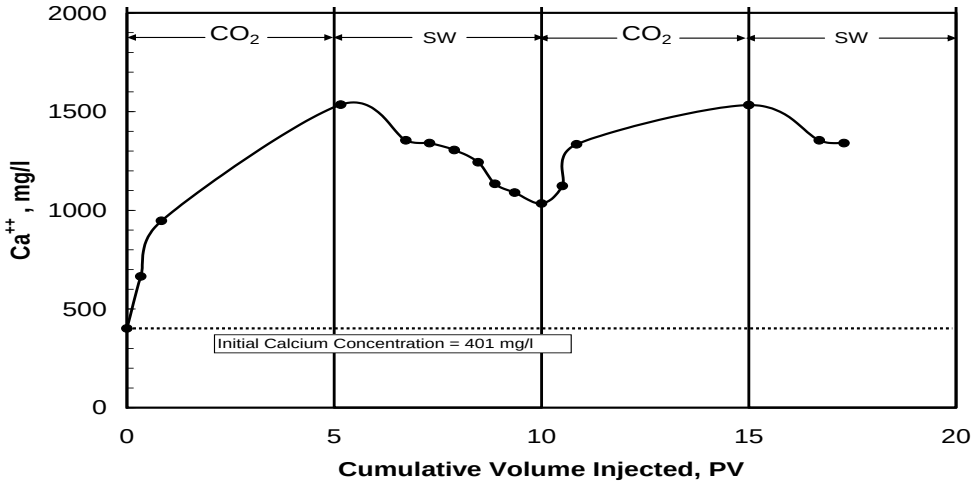

Fig. 8.11—Calcium concentration in the core effluent samples, Low Permeability Indiana limestone.

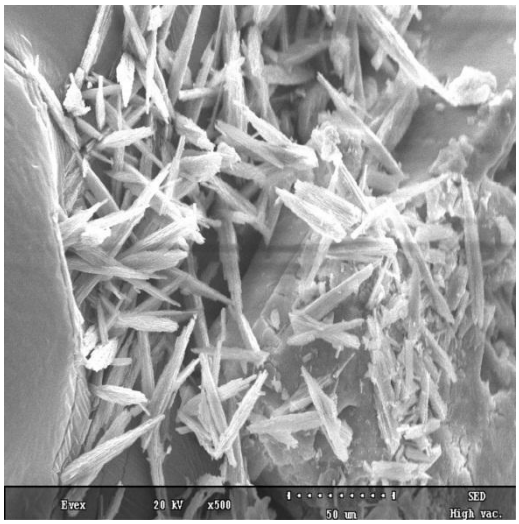

Fig. 8.12—SEM photomicrograph of calcium carbonate ($CaCO_3$) particles noted in the core effluent samples, LKI.

8.3.5 Silurian Dolomite

Silurian dolomite rock is a heterogeneous carbonate rock with many vugs existing in its structure. Three cores were tested in this study, with permeability varying from 182.0 md for SD1, 35 md for SD2, and 2.7 md for SD3. XRF analysis of the rock (**Table 8.1**) showed that besides calcium and magnesium, small amounts of sodium, iron, silicon and aluminum were also present (Si and Al are the main cations that form clays and feldspars).

The pressure drop profiles for cores SD1, and SD3 are given in **Figs. 8.13** and **8.14**, respectively. For SD1, the pressure drop increased just after introducing two phase flow into the core; the pressure was always higher than the initial seawater flooding pressure. CO_2 flooding pressure was 8.3 psi higher than initial seawater flooding pressure, while final seawater flooding pressure was 12 psi higher than the initial one.

Core SD3 also showed an increase in the pressure drop just after the injection of CO_2; the pressure was always higher than injection pressure, with CO_2 injection pressure higher than seawater injection pressure. The experiment stopped at the second cycle, since the pump reached the pressure limit and no more CO_2 could be injected. Since SD1 has a higher permeability, that indicated larger pore size comparing to SD3, which allowed the generated scales (due to the reaction between CO_2/fluid/rock) to bathe through. For SD3, the scales generated each WAG cycle tend to plug more pores and increase the pressure drop across the core.

Fig. 8.15 shows the concentrations of the calcium and magnesium in the core effluent for cores SD1, SD2 and SD3. It is clear that the absolute permeability of the core doesn't have any effect on the chemical reactions between the fluids and the rock, calcium and magnesium levels were very close for the three experiments. Reddish particles were collected from the core effluent samples, XRD analysis of these precipitated particles showed that it was mainly aragonite with some magnisian calcite. XRF analysis showed that silicon, aluminum, and iron were also present, which explained the red color of these particles. Elemental analysis of SEM confirmed the presence of these cations, but since these cations are found in clay and iron oxide forms, which are smaller than calcium carbonate compounds, the SEM photo micrograph just showed the aragonite and magnisian calcite (**Fig. 8.16**). Core permeability decreased from 182.0, 35.0, and 2.7 md to 100.0, 20.0, and 2.2 md, respectively.

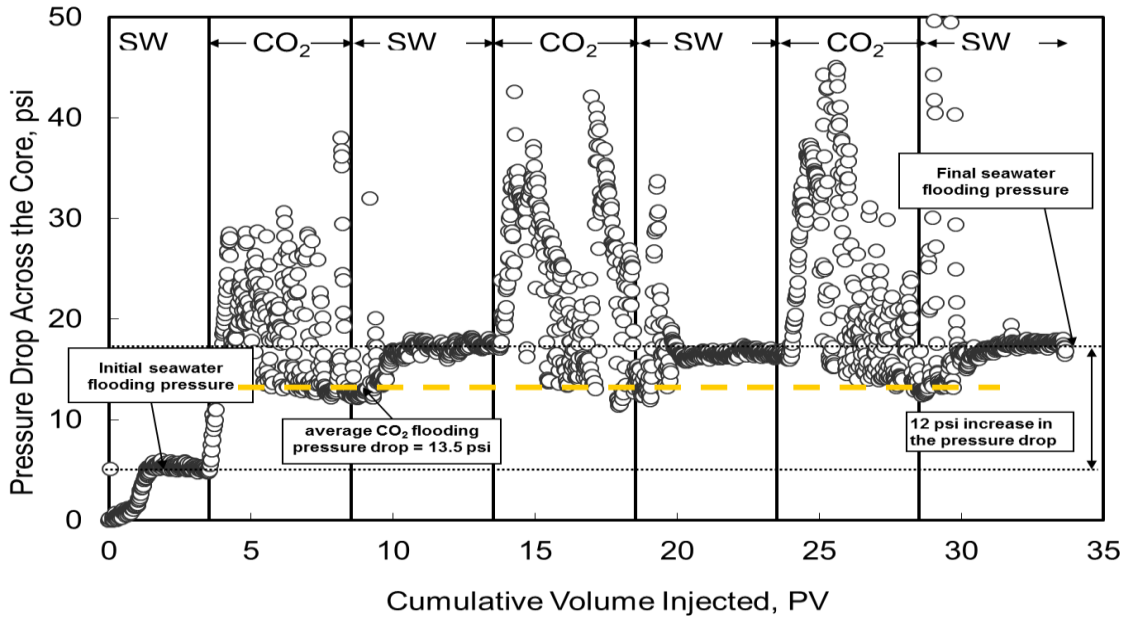

Fig. 8.13—Pressure drop across core SD1 during CO_2 and seawater without sulfate WAG injection.

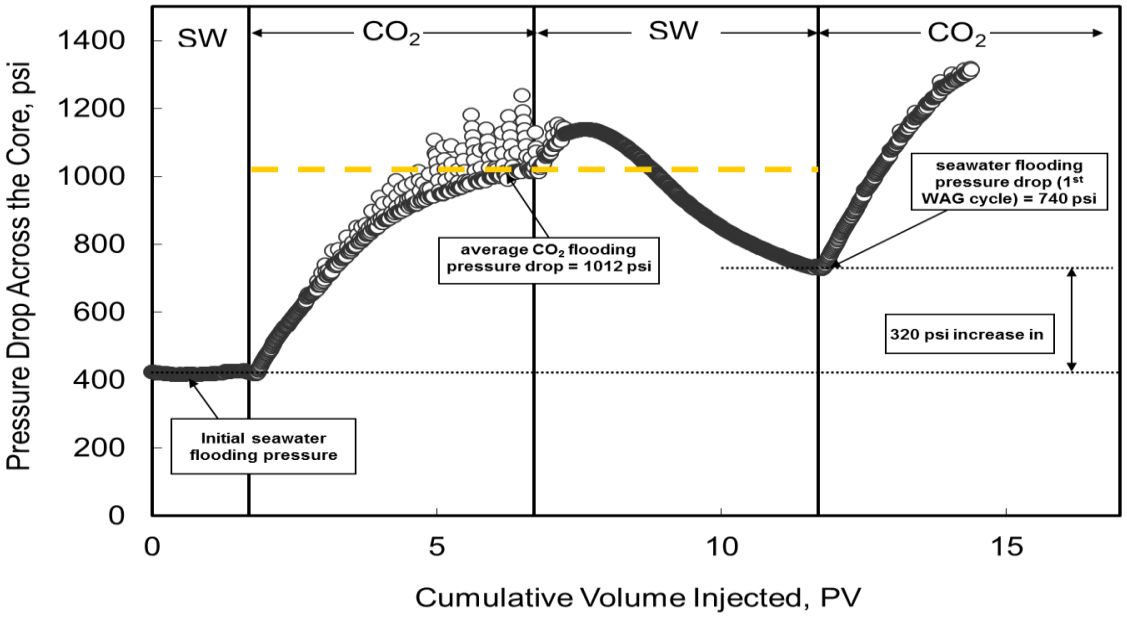

Fig. 8.14—Pressure drop across core SD3 during CO_2 and seawater without sulfate WAG injection.

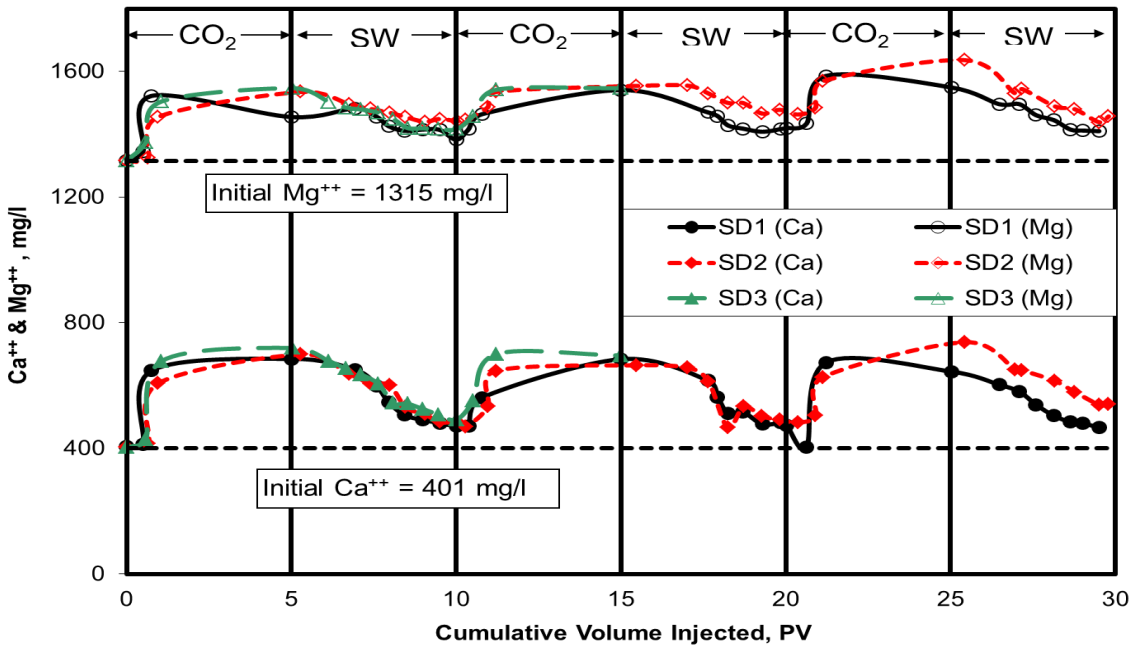

Fig. 8.15—Calcium and magnesium concentrations in the core effluent samples, Silurian dolomite.

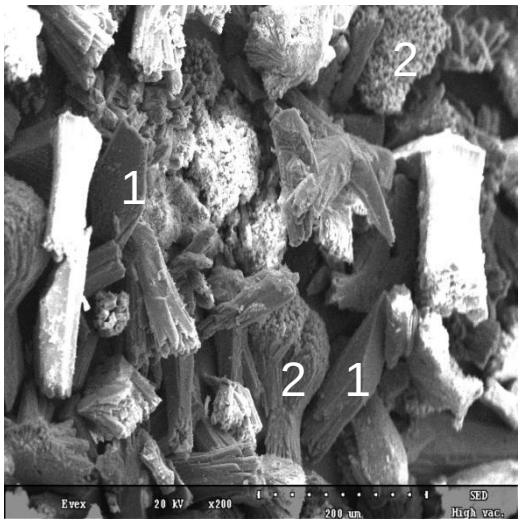

Fig. 8.16—SEM photo micrograph of the precipitated particles in the core effluent samples, SD1. XRD showed that the precipitated particles are; 1)Magnisian Calcite ($Mg_{0.13}Ca_{0.87}CO_3$), 2) Aragonite ($CaCO_3$).

8.4 Discussion

The results showed that all the carbonate cores had the same chemical behavior, regardless of the core initial permeability. Calcium concentrations were almost the same for all limestone cores used in this study, except for low permeability Indiana limestone, the calcium concentration was less. XRF indicated more silicon and aluminum were present in low permeability Indiana limestone, compared to the other limestone rocks, indicating that more silicate mineral was present, which has a slower reaction rate with carbonic acid compared to carbonates (Gaus et al. 2008). The same calcium and magnesium concentration levels were observed in the core effluent for the three dolomite cores used in this study.

A summary of the ratio of final permeability to initial permeability for all experiments run in this study, is given in **Fig. 8.17**. The results showed that for homogenous rock (Austin chalk and Pink Desert limestone), less damage occurred to the cores when compared to heterogeneous ones (high permeability Indiana limestone and Silurian dolomite). Due to the rock heterogeneity, CO_2 will tend to flow through the larger pores and bypass the smaller ones. Most of the chemical reaction will occur in the larger pores, which leads to the dissolution/precipitation actions that will occur there, and that might explain why more damage occurred to the heterogeneous rock.

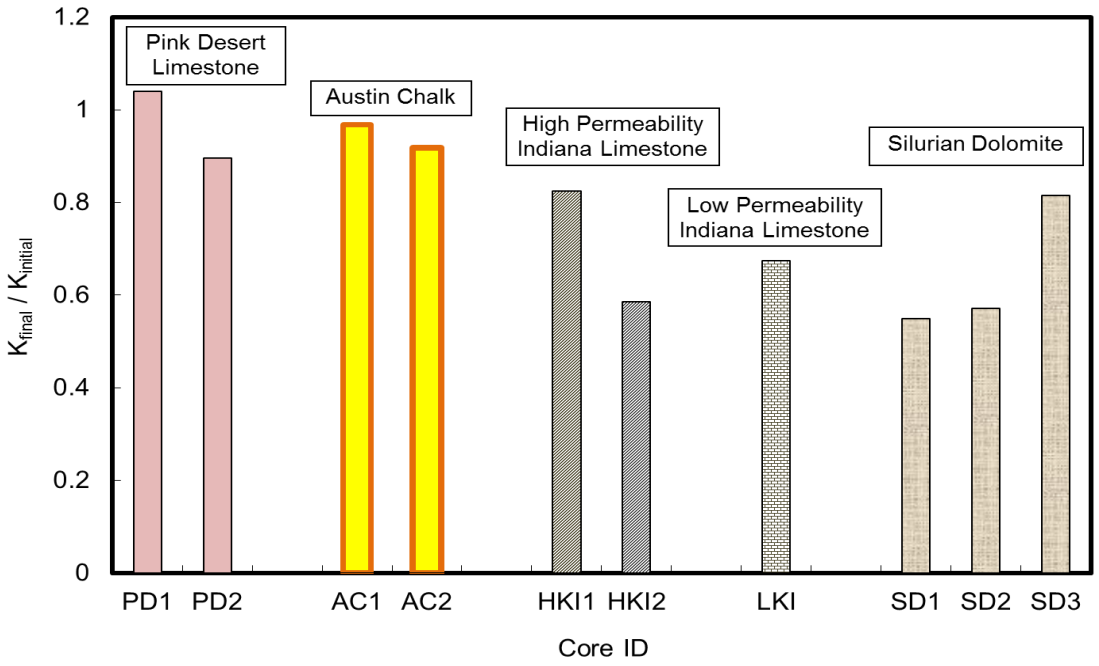

Fig. 8.17—Absolute permeability after WAG divided by the initial core permeability.

The permeability results of WAG injection of CO_2 and seawater for homogenous carbonate cores (Pink Desert limestone and Austin chalk) were compared to the permeability results for SWAG injection obtained by Egermann et al. (2005). At the same injection flow rate, more damage was observed for SWAG injection (15%) because of the longer contact time between CO_2 and seawater comparing to WAG injection. The loss in permeability observed for cores PD2 and AC2 were 10% and 8%, respectively. Egermann et al. (2005) results also showed an increase in the damage level with decreasing the injection flow rate, 35% reduction in the core permeability at injection flow rate of 0.03 cm^3/min.

Using permeability data, average pore diameter can be calculated using the approach developed by Talash and Crawford (1964). Another approach is to take the square root of the permeability in md; the result is the average pore diameter in microns (Dick et al. 2000). The second approach was used for pore size calculation, because of the simplicity of this approach and the results of both approaches are pretty close. The calculations showed that for homogenous rock (Pink Desert limestone and Austin chalk) a small reduction in the pore diameter was observed; while for heterogeneous rock (Indiana limestone and Silurian dolomite) there was more reduction in the pore diameter. **Fig. 8.18** shows a good correlation between the final and the logarithm of the initial average pore size.

To confirm the correlation between the initial and final pore diameter, data from earlier publications was used for coreflood experiments run under different conditions: temperature, pressure, brine composition, and injection flow rate, using Pink Desert limestone and Silurian dolomite (**Fig. 8.19**). The data showed that the correlation between the final and the logarithm of the initial average pore size doesn't exist. Instead, two linear correlations were observed, one for the homogenous and low permeability cores, and the other one for heterogeneous and sandstone cores. Low permeability cores tend to behave like homogenous rock, since only small pores are available for fluid to flow through; while for heterogeneous rock, both large and small pores exist. Fluid tends to flow through the high permeability passage, and the chemical reactions are localized there which decreases the permeability due to the dissolution/precipitation actions. Sandstone behaves like heterogeneous rock, because of the heterogeneous composition

of sandstone, different clays, feldspars, and cementing materials are present in the sandstone structure, which reacts with CO_2 and causes the precipitation of the reaction products that damage the cores (Sayegh et al. 1990).

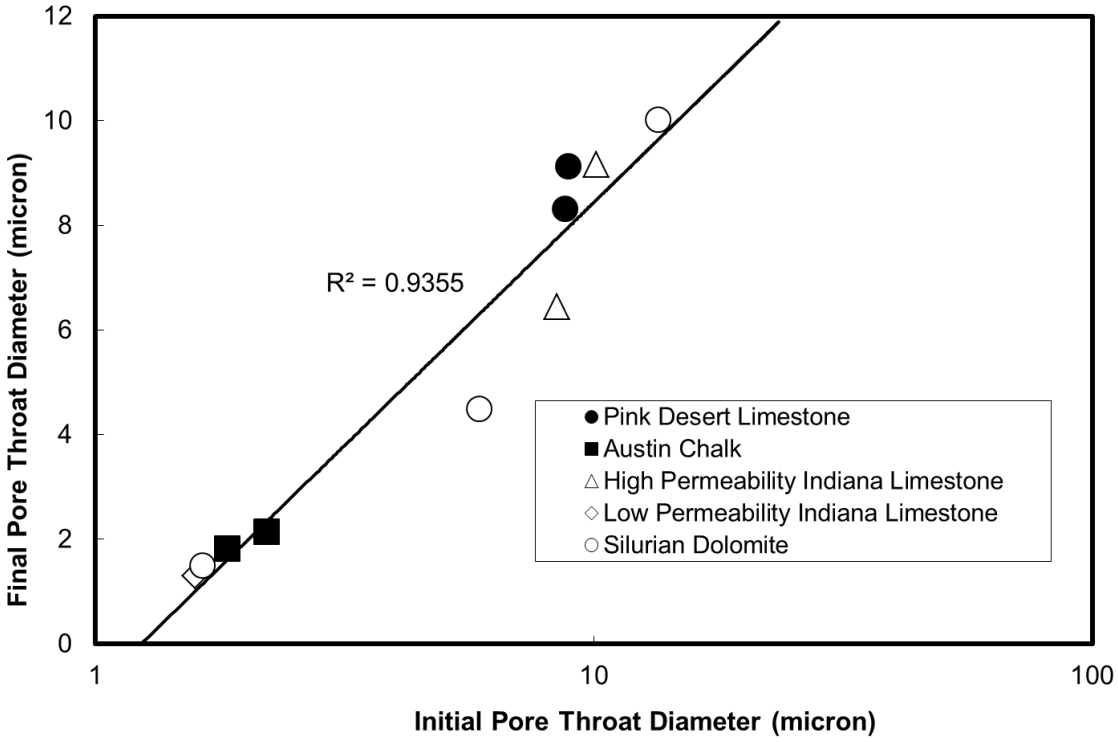

Fig. 8.18—A semi-log Correlation between initial and final average pore throat diameter were obtained for the ten experiments run in this study.

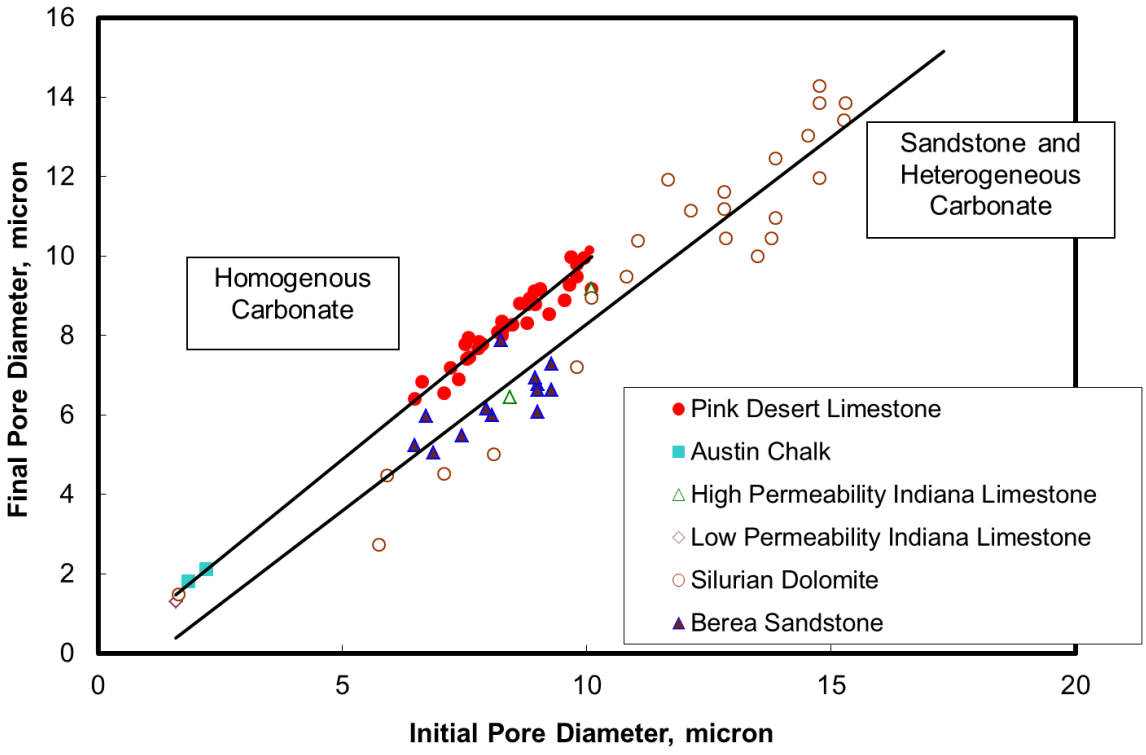

Fig. 8.19—Correlation between initial and final average pore diameter for homogenous and heterogeneous carbonate, and sandstone cores.

8.4.1 Effect of Two-Phase Flow

The experimental results showed that the change in the absolute permeability, due to CO_2 injection was not always a concern, especially for homogenous cores. The final permeability was a few percent off the original one. However, introducing two phase flow into the core (water and CO_2) will cause an increase in the injection pressure due to the capillary pressure effect, which has a more pronounced effect in low permeability rocks. Although the permeability of core AC2 decreased by only 8%, **Fig. 8.4** shows the one phase flow (seawater) pressure drop was 125 psi; this pressure increased to a maximum pressure of 391 psi at the third WAG cycle, due to the capillary

pressure effect. Cores LKI and AC3 also showed an increase in the pressure drop to a level where no more fluid could be injected using the same pump.

Bennion and Bachu (2006) stated that for CO_2 and water systems, the lower permeability rock has a higher relative permeability to CO_2 at end points, than the higher permeability rock. The pressure data obtained in this study showed that for lower permeability cores, the increase in CO_2 injection pressure was more pronounced, due to the high capillary pressure resulting from smaller pore size.

8.5 Modeling Studies

To confirm the experimental results, a simulation study was conducted to predict the experimental results in core scale using a commercial compositional simulator package (CMG-GEM). The input parameters are the core dimensions, injection schedule, relative permeability, capillary pressure, chemical kinetics of the chemical reactions between rock minerals, brine, and CO_2, and initial core properties (porosity and permeability). The simulator uses these data to calculate the change in core change in porosity across the core due to chemical reactions and pressure changes. The new porosity values were used by either Carman-Kozeny or power-law equation to predict the new permeability using an appropriate exponent. A detailed discussion about the calculation sequence is shown in this section.

A cylindrical core was divided into radial grid blocks with 5X20X20 blocks in the r, Θ, and z directions, respectively. Initially, the porosity and permeability were assumed to be constant for all grids. Relative permeability (**Eqs. 3.1-3.2**) was adjusted

to match the experimental pressure drop (**Fig. 8.20**). A summary for the parameters used to calculate the relative permeability curves is given in **Table 8.4**.

TABLE 8.4—SUMMARY OF THE PARAMETER USED TO CALCULATE THE RELATIVE PERMEABILITY CURVES FOR THE CARBONATE CORES USED IN THIS STUDY.

Rock Type	k_{rwi}	k_{rCO2i}	S_{wi}	S_{CO2i}	N_w	N_{CO2}
Pink Desert limestone	0.35	0.05	25%	15%	4	1.5
Austin chalk	0.6	0.3	33%	10.3%	1.5	5
High permeability Indiana limestone	0.3	0.04	40%	29%	3	1
Low permeability Indiana limestone	0.28	0.05	34%	8%	2.5	1.2
Silurian dolomite	0.33	0.032	40%	20%	0.5	15

Capillary pressure is a function of porosity, permeability, interfacial tension, and wetting-phase saturation. The model developed by El-Khatib (1995) was used to calculate the capillary pressure curves for the carbonate cores used in the present study (**Eq. 3.3**). The irreducible water saturation (S_{wi}) was obtained from the coreflood experiments given in **Table 8.4**. Contact angle between CO_2 and brine was adjusted in order to match the experimental results. Contact angle of 80° was found to give the best match for all cores used in the current study.

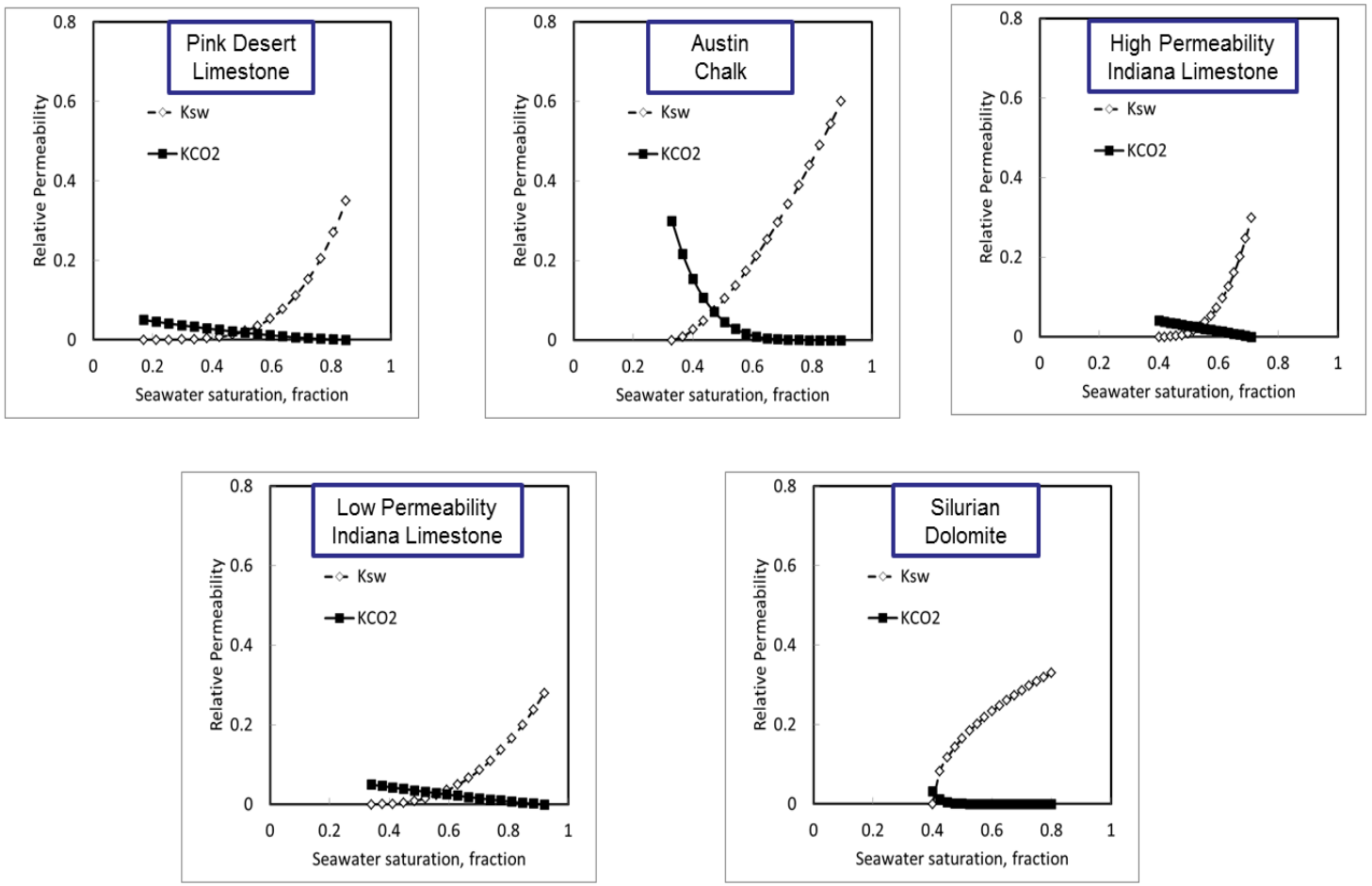

Fig. 8.20—Relative permeability of seawater and CO_2 for the cores used in this study.

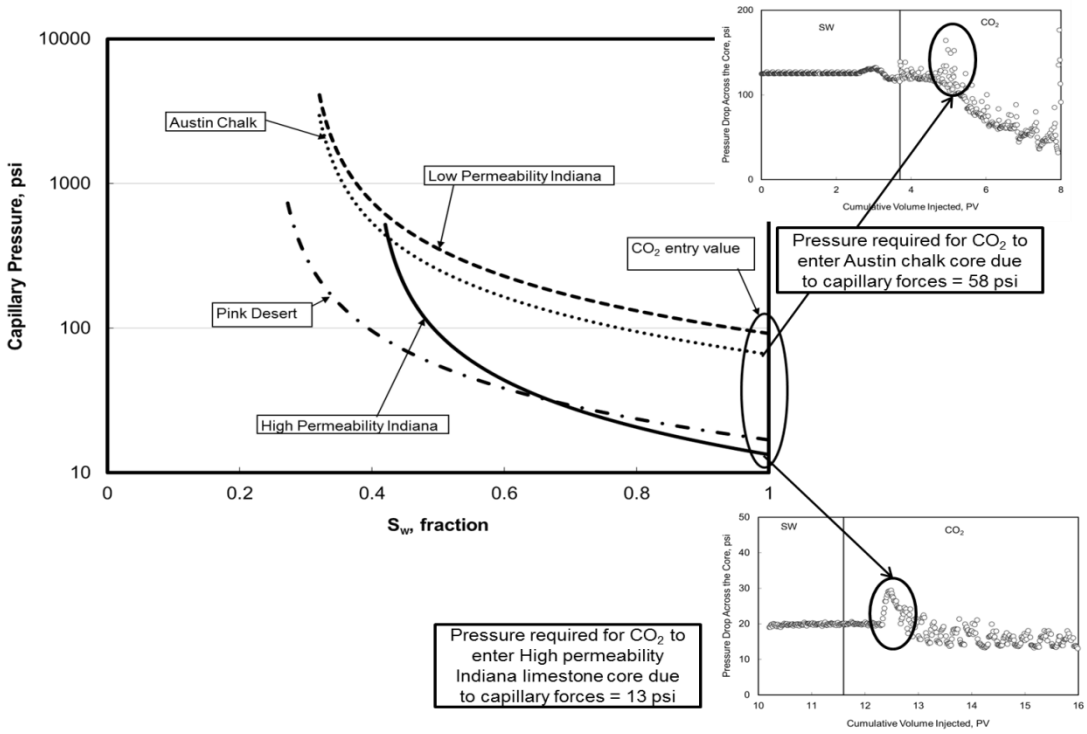

Fig. 8.21—Capillary pressure vs. seawater saturation curves for limestone cores used in this study.

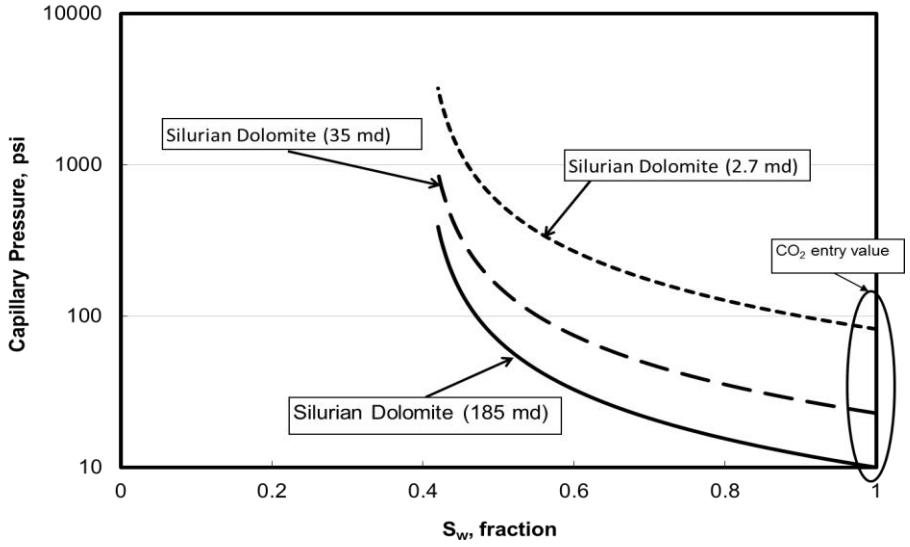

Fig. 8.22—Capillary pressure vs. seawater saturation curves for dolomite cores used in this study.

The capillary pressure curves for limestone cores are given in **Fig. 8.21**. For low permeability Indiana limestone, 92 psi was required for CO_2 to enter the core, compared to 13 and 17 psi to enter the pores of high permeability Indiana and Pink Desert limestone, respectively. For Silurian dolomite cores (**Fig. 8.22**), 82 psi was required for CO_2 to enter core SD3, compared to 10 psi for core SD1.

TABLE 8.5—LIST OF KINETIC RATE PARAMETERS FOR REACTIONS BETWEEN CO_2 AND DIFFERENT MINERALS.

Mineral	Reactive Surface Area cm^2/g	$Log_{10}\ k_{0\beta}$ $mol/m^2.s$	Activation Energy KJ/mole	Reference Temperature °C	Reference
Calcite	9.8	-6.19	62.76	25	Svensson and Dreybrodt (1992)
Dolomite	9.8	-8.9	62.76	25	Xu and Pruess (2004)
Chlorite	9.8	-12.52	88.00	25	Xu et al. (2006)
Albite	9.8	-8.44	69.8	37	Blum and Stillings (1995)

The porosity changes due to mineral dissolution and precipitation are governed by **Eqs. 3.7- 3.8**. The change in porosity will yield a change in the absolute permeability. The power-law (**Eq. 3.9**) and Carman-Kozeny (**Eq. 3.10**) were used to calculate the permeability based on the initial and final permeabilities and porosities. XRD of limestone cores used in this study indicated that all of these cores contained more than 99.7 wt% calcite, while dolomite cores were 98 wt% dolomite and 2 wt% chlorite and

albite. The kinetic rate parameters of CO_2 with various minerals present in these cores are given in **Table 8.5.**

8.5.1 Numerical Simulation

Fig. 8.23 shows the change in the porosity of Pink Desert limestone, due to rock dissolution and precipitation after CO_2 injection. For Core PD1 where WAG injection of CO_2 and seawater without sulfate injected, an increase in the core porosity was noted close to the core inlet due to the dissolution of calcium carbonate. With continuous dissolution of the calcium carbonate, precipitation will take place indicated by the reduction of core porosity (starting after moving 2 in. from the core inlet). Just behind this zone an increase in the core porosity was noted again (4 in. from the core inlet), because the solution has the potential to dissolve more rock after the precipitation occurred in the previous zone. More increase in the rock porosity was noted for core PD1 (**Fig. 8.23A**), compared to more damage observed for core PD2 (**Fig. 8.23B**), which agrees with the experimental results (an increase in permeability was noted for core PD1, and a reduction noted for core PD2). Power-law exponent (n), and Carman-Kozeny exponent (m), were adjusted to match the final absolute permeability measured in the lab with the value calculated from porosity change. For PD1, the match between the two permeabilities with n = 5.17 and m = 4.54. For core PD2, n = 8.14, and m = 7.82. A greater exponent was needed for PD2, calcium sulfate scale will tend to plug the core throats, resulting in less permeability with almost no effect on the porosity.

For Austin chalk cores, a reduction in the porosity was predicted for both cores, with more reduction noted in core AC2. The power-law exponent for core AC1 was found to be 6.2, and Carman-Kozeny exponent was 5.8, which are close to the values calculated for core PD1. For core AC2, larger exponents were needed to adjust the permeability (n = 13.3, m = 12.7) because of the presence of calcium sulfate scale. The exponent for AC2 was larger than in the PD2 case, since the smaller pores in AC2 increase the likelihood of calcium sulfate scale to plug the pore throats.

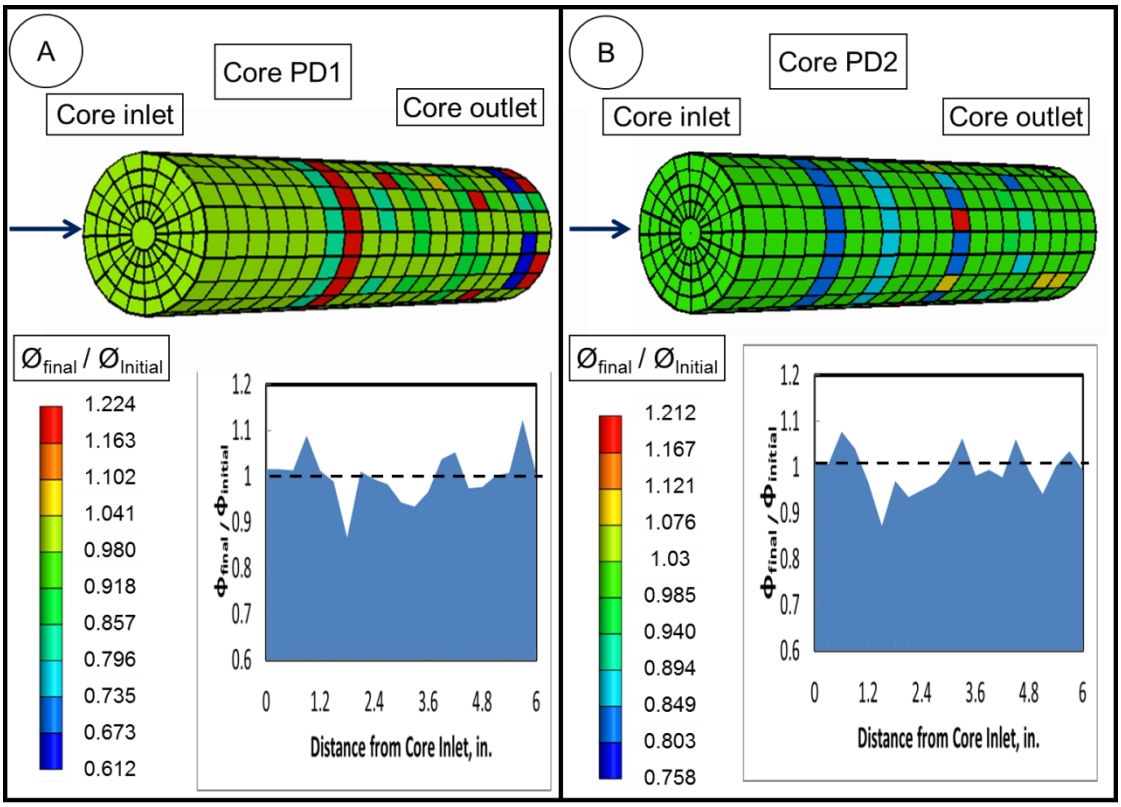

Fig. 8.23—Change in Pink Desert Limestone porosity after CO_2 injection. A) Core PD1, calcium carbonate precipitated after WAG injection of CO_2 and seawater without sulfate. B) Core PD2, calcium carbonate and calcium sulfate precipitated after WAG injection of CO_2 and seawater.

For the high permeability Indiana limestone cores, it is not easy to adjust the exponents for heterogeneous cores, because of the variation of the porosity, pore size and the presence of vugs. The exponents for core HKI1 were n = 44.88, and m = 44.4. Larger exponents were found for HKI2 (n = 129.0, m = 128.5), because of calcium sulfate scale formation. Fig. 25 shows a good match between the pressure drop data obtained from the experimental data and from the numerical simulator.

The numerical solution doesn't capture the instantaneous increase in pressure during injection alternating from one phase to another (from CO_2 to seawater and vice versa). For the case of alternating to CO_2, the core was saturated with seawater, pressure build up occurred when CO_2 reached the core inlet phase to overcome the capillary forces and displace seawater to establish the flow inside the core, the excess pressure dissipation occurred after CO_2 entered the core. The pressure increase was higher during alternation to seawater because of the higher viscosity of seawater (CO_2 viscosity was 0.021 cp, while brine viscosity was 0.36 cp at the experiment conditions, 1300 psi and 200°F) and lower mobility compared to CO_2. That behavior occurred instantaneously as shown by the experimental data (**Fig. 8.24**) and couldn't be captured by the numerical simulator.

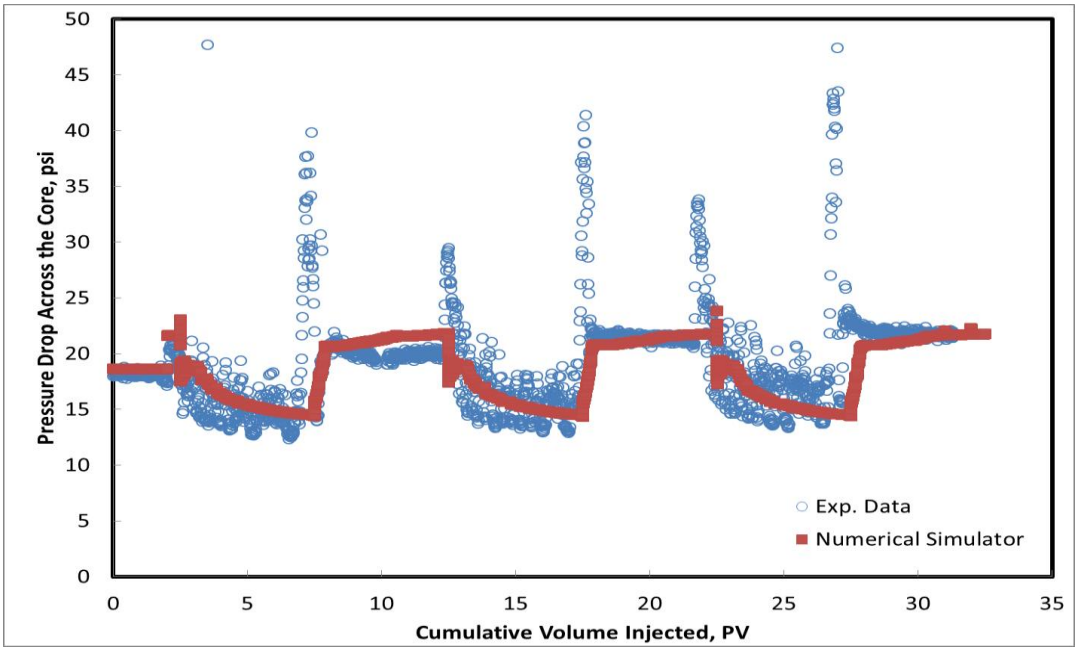

Fig. 8.24—Pressure drop across the high permeability Indiana limestone core. An acceptable match was obtained between the experimental and numerical simulator results.

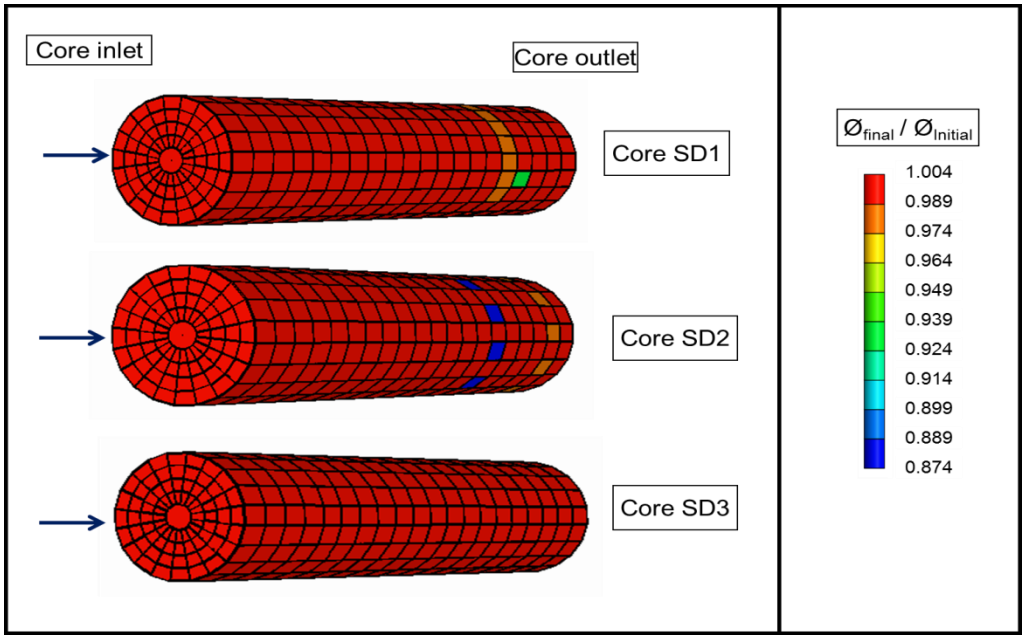

Fig. 8.25—Change in Silurian Dolomite porosity after CO_2 injection.

TABLE 8.6—SUMMARY OF THE POWER-LAW AND CARMAN-KOZENY EXPONENTS.			
	Core	**Power-Law Exponent (n)**	**Carman-Kozeny Exponent (m)**
Homogenous	PD1	5.17	4.53
	PD2	8.14	7.82
	AC1	6.2	5.8
	AC2	13.3	12.7
Heterogeneous	HKI1	44.88	44.4
	HKI2	129.0	128.5
	SD1	421.1	420.6
	SD2	448.2	445.0
	SD3	382.0	380.0

The reaction rate of carbonic acid with dolomite is lower than the reaction rate with calcite (**Table 8.5**). Reduction in the core porosity was noted close to the core outlet, and no significant change in porosity was noted along the core length for the Silurian dolomite cores (SD1, SD2, and SD3) **Fig. 8.25**. A significant change in the cores permeability was noted from the lab experiments, because of the presence of silicate mineral with dolomite rock. Both the power-law and Carman-Kozeny exponent for dolomite cores were around 400. **Table 8.6** Summarizes the exponents for all cases discussed in this study. Izgec et al. (2006) proposed that Carman-Kozeny exponent of 6.5 matches the change in limestone core permeability when injecting CO_2 into NaBr

brine saturated cores, which agrees with our results for homogenous limestone cores with seawater without sulfate.

9. FUTURE WORK

This study presents physical and numerical results/analysis for bench-scale CO_2/brine WAG in a variety of carbonate and sandstone cores. The effects of water composition (sulfate-bearing versus sulfate-free synthetic seawater; high salinity versus low salinity), rock type (carbonate versus sandstone), and rock matrix (low versus high permeability; homogeneous versus heterogeneous) are investigated. The results suggested that homogeneous cores were less susceptible to permeability reduction due to mineral reaction, addition of sulfate increased damage due to calcium sulfate precipitation, and rock composition/mineral distribution affected the magnitude and type of precipitation that occurred, in addition to dissolved species in the effluent. However, further research is desirable to extend the present work, including:

1- Address the effect of CO_2 impurities on the change in formation permeability. In this study pure CO_2 was used in all experiments. However, the presence of impurities (SO_2, H_2S, and NO_x) can significantly change the results. No quantitative study has been conducted before to study the effect of CO_2 contaminants on the formation permeability and the literature shows that H_2S does not alter the results, the addition of SO_2 to the injection results in the precipitation of anhydrite near the well (Knauss et al. 2005; Bacon et al. 2009; Jacquemet et al. 2009).

2- In the current study the core plug length was 6 in. and the experiments were conducted at injection pressure up to 2000 psi and temperature up to 250˚F.

In order to examine the validity of the results to ultra-deep formation, extra experiments need to be conducted at higher pressure and temperature conditions (up to 10,000 psi and 350˚F) and longer core.

3- A synthetic homogenous field model (model proposed by Dahle et al. 2009) was used to run the field scale simulation. A simulation study on actual field data is recommended to address how the reservoir heterogeneity can affect the results obtained in this study.

4- Presence of oil in the core can significantly change the behavior of permeability alteration observed in this study since the solubility of CO_2 in oil is much higher than the solubility in brines. Conducting coreflood experiments in oil saturated cores will simulate the CO_2 injection in enhanced oil recovery project, while the current study applies mostly for saline aquifers.

10. CONCLUSIONS

The WAG technique used in CO_2 sequestration may cause either damage or enhancement in the formation based on several factors. In this study, at a back pressure of 1300 psi, the effects of CO_2 to brine volumetric ratio, CO_2 volume per cycle, temperature, and injection rate were examined. There was no oil in the core and the study pertains mostly to limestone saline reservoirs. A commercial reservoir simulator (CMG-GEM) ran at both core and field scale to confirm the experimental results. Based on the results obtained, the following conclusions can be drawn:

- Change in porosity and permeability was noted just around the wellbore, no changes were noted farther in the aquifer.
- Short WAG cycles resulted in a permeability loss because of the precipitation of $CaCO_3$ scale inside the core. In the field scale no significant changes in porosity and permeability were noted.
- Uniform rock dissolution occurred at the core inlet, which resulted in permeability enhancement at the core inlet; while precipitation occurred farther from the injection face, which resulted in a reduction in permeability.
- Power-law exponent of 3.89, or Carman-Kozeny exponent of 3.4 can be used to relate the change in permeability to the change in porosity of Pink Desert limestone due to CO_2 injection.
- Structural trapping represents the main trapping mechanism in CO_2 sequestration in carbonate aquifers, structural trapping contribution decreases with time, while

residual phase and dissolved phase trapping increases.

Calcium sulfate precipitation during CO_2 sequestration in carbonate cores reduces the rock permeability. In this study, the effect of temperature, injection flow rate, and brine salinity were addressed. A commercial reservoir simulator (CMG-GEM) was used to simulate lab data and predict field results. Based on the results obtained, the following conclusions can be drawn:

- Calcium chloride has the most effect on the limestone cores during sequestration, and increasing calcium chloride concentration caused a significant increase in calcium concentration to be observed in the core effluent samples.
- Higher reaction rate constant ($\log(k_{25})$) predicted as the brine salinity increases to simulate the increase in calcium concentration observed in the core effluent samples
- Field scale simulations showed that a small change in permeability noted during WAG injection of CO_2 with either DI water or seawater without sulfate (up to 5% change in permeability). While injection of seawater will cause up to 10% damage around the wellbore due to calcium sulfate precipitation.
- Brine composition doesn't affect the trapping mechanisms of CO_2.
- Temperature is the main factor that affects calcium sulfate precipitation. The higher the temperature, the more damage is introduced, due to low calcium sulfate solubility. At a low temperature, an enhancement in the core permeability was observed, due to the high solubility of calcium sulfate.

Based on the results of the coreflood experiments conducted on the Silurian dolomite cores, the following conclusions can be drawn;

- The presence of silicate minerals (clays and feldspars) with dolomite rock, even with low concentrations, can impact the core permeability significantly during CO_2 injection.
- There is no clear relationship between injection flow rate, temperature, WAG cycle volume and brine:CO_2 volumetric ratio. The only factor that affects change in core permeability is the initial core permeability.
- Mole ratio of calcium to magnesium less than one noted in the core effluent samples indicated more magnesium dissolved in the brine, while more calcium precipitated inside the cores.

Eleven coreflood experiments were conducted in this study to examine CO_2 injection in sandstone rock. The effect of WAG cycle volume, CO_2:brine volumetric ratio, temperature, and WAG vs. continuous CO_2 injection were addressed in this paper. The cores were initially 100% saturated with brine to simulate a sandstone saline aquifer, with no oil present in the cores. A compositional reservoir simulator (CMG-GEM) was used to simulate the coreflood experiments run in this study. Based on the results obtained, the following conclusions can be drawn:

- Loss of core permeability was noted during continuous CO_2 injection due to the release of clay particles. This was confirmed from the cyclic behavior of the pressure drop across the core.
- Damage during WAG injection caused by the precipitation of the reaction

products (calcium carbonate and iron oxides), and/or the migration of clay particles leached after dissolution of cementing material (carbonates).

- Analysis of core effluent samples indicated that CO_2 dissolved calcite and dolomite. Analysis of the solids highlighted the presence of clays and iron oxides.
- Berea sandstone cores were damaged (21-55% loss in permeability) due to CO_2 injection.
- Carman-Kozeny and power-law equations couldn't be used to predict the change in permeability due to CO_2 injection into sandstone cores.
- The modified Van Baaren's equation can be used to predict the change in core permeability based on the change in core porosity. The Archie cementation exponent obtained in this study ranges between 1.017 and 1.7 at a sorting coefficient of 0.75.
- Increasing the CO_2 volume injected per WAG cycle postpones the precipitation of calcium carbonate.

Ten coreflood experiments were run using different carbonate cores, seawater, and seawater without sulfate, at 200°F, 1300 psi back pressure, and 5 cm^3/min. This study focuses on WAG injection of CO_2 because of the enhancement of residual trapping of CO_2 when compared to continuous CO_2 injection, and less damage occurred to the core when compared to SWAG injection. A numerical simulation study using a compositional reservoir simulator tool (CMG-GEM) was conducted to confirm the experimental results. Based on these results, the following conclusions can be drawn:

- Based on the change in core permeability, damage observed in homogenous carbonate cores (Pink Desert and Austin chalk) was less than the damage observed in the heterogeneous ones (Indiana limestone and Silurian dolomite) after CO_2/WAG injection.
- Aragonite, calcite, and magnisian calcite precipitated from different limestone rocks after CO_2 injection.
- Calcium concentration in the core effluent samples was similar for all limestone cores used in this study, regardless of the core initial permeability.
- High injection pressure was required for CO_2 to overcome the capillary forces in the low permeability cores, which increase the risks of formation fracturing during CO_2 injection.
- For homogenous limestone cores, exponents between 5.0 and 6.0 for power-law and Carman-Kozeny can be used for permeability calculations, based on the final and initial porosities.
- The presence of sulfate scales will tend to increase the exponents used in the power-law and Carman-Kozeny equations.
- The power-law and Carman-Kozeny exponents were larger for heterogeneous carbonate (45 for vuggy Indiana limestone); the presence of silicate minerals will yield in a significant increase in that exponent (400 for Silurian dolomite).

REFERENCES

Alkattan, M., Oelkers, E.H., Dandurand, J.L., Schott.J. 1998. An experimental study of calcite and limestone dissolution rates as a function of pH from -1 to 3 and temperature from 25 to 80°C. *Chemical Geology* **151**(1): 199–214.

Alotaibi, M.B., Nasralla, R.A., Nasr-El-Din, H.A., 2010. Wettability Challenges in Carbonate Reservoirs. Paper SPE 129972 presented at Improved Oil Recovery Symposium held in Tulsa, Oklahoma, 24-28 April.

Bachu, S., and Adams, J.J., 2003. Sequestration of CO_2 in Geological Media in Response to Climate Change: Capacity of Deep Saline Aquifers to Sequester CO_2 in Solution. *Energy Conversion and Management*, May, **44**, pp. 3151- 3175.

Bacon, D.H., Sass, B.M., Bhargava, M., Sminchak, J. and Gupta, N. 2009. Reactive Transport Modeling of CO_2 and SO_2 Injection into Deep Saline Formations and Their Effect on the Hydraulic Properties of Host Rocks. *Energy Procedia* **1** (1) 3283–3290.

Bahara, M.,and Liu, K., 2008. Measurement of the Diffusion Coefficient of CO_2 in Formation Water Under Reservoir Conditions: Implications for CO_2 Storage. Paper SPE 116513 presented at the SPE Asia Pacific Oil & Gas Conference and Exhibition in Perth, Australia, 20-22 October.

Bardon, C., Corlay, P., Longeron, D., and Miller, B., 1994. CO_2 Huff 'n' Puff Revives Shallow Light-Oil-Depleted Reservoirs. Paper SPE 22650. *SPE Reservoir Engineering* **9**(2): 91-100.

Bennion, D.B., and Bachu, S., 2006. Supercritical CO_2 and H_2S Brine Drainage and Imbibition Relative Permeability Relationships for Intergranular Sandstone and Carbonate Formations. Paper SPE 99326 presented at the SPE Europec/EAGE Annual Conference and Exibition held in Vienna, Austria, 12-15 June.

Bennion, D.B. and Bachu, S. 2008. Drainage and Imbibition Relative Permeability Relationships for Supercritical CO_2/Brine and H_2S/Brine Systems in Intergranular Sandstone, Carbonate, Shale, and Anhydrite Rocks. SPE *Reservoir Evaluation & Engineering* **11**(3):487-496.

Bertier, P., Swennen, R., Laenen, B., Lagrou, D., and Dreesen, R. 2006. Experimental identification of CO_2–water–rock interactions caused by sequestration of CO_2 in Westphalian and Buntsandstein sandstones of the Campine Basin (NE-Belgium). *Journal of Geochemical Exploration* **89** (1): 10-14.

Boving, T.B. and Grathwohl, P., 2001, Tracer diffusion coefficients in sedimentary rocks: correlation to porosity and hydraulic conductivity, *Journal of Contaminant Hydrology*, **53**(1): 85-100.

Cantucci, B., Montegrossi, G., Vaselli, O., Tassi, F., Quattrocchi, F., and Perkins E.H. 2009. Geochemical modeling of CO_2 storage in deep reservoirs: The Weyburn Project (Canada) case study. *Chemical Geology* **265** (1) 181–197.

Carroll, J. J., Slupsky, J. D. and Mather, A. E., 1991. The Solubility of Carbon Dioxide in Water at Low Pressure. *J. Phys. Chem. Ref. Data* **20** (6): 1201.

Dahle, H.K., Eigestad, G.T., Nordbotten, J.M., and Pruess K. 2009. A Model-Oriented Benchmark Problem for CO_2 Storage. Workshop on Modeling and Risk of

Assessment of Geological Storage of CO_2 held in Longyearbyen, Svalbard, Norway, 3-7 August.

Delshad, M., Wheeler, M.F., Kong, X., 2011. A Critical Assessment of CO_2 Injection Strategies in Saline Aquifers. Paper SPE 132442 presented at the SPE Western Regional Meeting held in Anaheim, California, USA, 27-29 May.

Dick, M.A., Heinz, T.J., Svoboda, C.F., and Aston, A. 2000. Optimizing the Selection of Bridging Particles for Reservoir Drilling Fluids. Paper SPE 58793 presented at SPE International Symposium on Formation Damage Control, Lafayette, Louisiana, 23-24 February.

Dria, D.E., Pope, G.A., Sepehrnoori, K. 1993. Three-Phase Gas/Oil/Brine Relative Permeabilities Measured Under CO_2 Flooding Conditions. *SPE Reservoir Engineering* **8**(2): 143-150.

Duan, Z., Sun, R., Zhu, C., and Chou, I.M., 2006. An improved model for the calculation of CO_2 solubility in aqueous solutions containing Na^+, K^+, Ca^{2+}, Mg^{2+}, Cl^-, and SO_4^{2-}. *Marine Chemistry* **98** (2): 131–139.

Egermann, P., Bazin, B., and Vizika, O. 2005. An Experimental Investigation of Reaction-Transport Phenomena during CO_2 Injection. Paper SPE 93674 presented at the SPE Middle East Oil & Gas Show and Conference held in Bahrain International Exhibition Centre, Bahrain, 12–15 March.

El-Khatib, N. 1995. Development of a Modified Capillary Pressure J-Function. Paper SPE 29890 presented at Middle East Oil Show, Bahrain , 11-14 March.

Enick, R.M., and Klara, S.M., 1989. CO_2 Solubility in Water and Brine Under Reservoir Conditions. *Chem. Eng. Comm*. **90**(1): 23-33.

EPA, 2008. Recent Climate Change: Atmosphere Changes. Climate Change Science Program. United States Environmental Protection Agency.

Fenghour, A. and Wakeham, W.A., 1997. The Viscosity of Carbon Dioxide. Journal of *Physical Chemistry Reference Data* **27** (1): 31-44.

Fischer, S., Liebscher, A., and Wandrey. M. 2010. CO_2–brine–rock interaction — First results of long-term exposure experiments at insitu P–T conditions of the Ketzin CO_2 reservoir. *Chemie der Erde - Geochemistry* **70**(3): 155-164.

Flett, M., Gurton, R., and Taggart, I., 2004.The Function of Gas-Water Relative Permeability Hysteresis in the Sequestration of Carbon Dioxide in Saline Formations. Paper SPE 88485 proceedings of the SPE Asia Pacific Oil and Gas Conference and exhibition, Australia, Oct. 18-20.

Flint, O., 1967. Increased Solubility of Calcium Sulphate in Sea Water Containing Hydrochloric Acid. *Desalination* **4**(3): 28-335.

Gaus, I., Azaroual, M., and Czernichowski-Lauriol, I. 2005. Reactive transport modeling of the impact of CO_2 injection on the clayey cap rock at Sleipner (North Sea). *Chemical Geology* **217** (3): 319– 337.

Gaus, I., Audigane, P., André, L., Lions, J., Jacquemet, N., Durst, P., Czernichowski-Lauriol, I., and Azaroual, M. 2008. Geochemical and solute transport modeling for CO_2 storage, what to expect from it? *International Journal of Greenhouse Gas Control* **2**(4): 605-625.

Graue, D.J., and Blevins, T.R., 1978. SACROC Tertiary CO_2 Pilot Project. Paper SPE 7090 presented at SPE Symposium on Improved Methods of Oil Recovery held in Tulsa, Oklahoma, 16-17 April.

Grigg, R.B. and Svec, R.K. 2003. Co-Injected CO_2-Brine Interactions with Indiana Limestone. Paper SCA 2003-19 presented at the International Symposium of the Society of Core Analysts held in Pau, France, 21-24 September.

Grigg, R.B., Svec, R.K., Lichtner, P.C., Carey, W., and Lesher C.E. 2005. CO_2/Brine/Carbonate Rock Interactions: Dissolution and Precipitation. Presented at the Annual Conference on Carbon Capture & Sequestration, Alexandria, Virginia, May 2-5.

Grigg, R.B. and Svec, R.K. 2006. CO_2 Transport Mechanisms in CO_2/Brine Coreflooding. Paper SPE 103228 presented at the SPE Annual Technical Conference and Exhibition held In San Antonio, Texas, 24-27 September.

Grigg, R.B., and Svec, R.K., 2008. Injectivity Changes and CO_2 Retention for EOR and Sequestration Projects. Paper SPE 110760 presented at the SPE/DOE Improved Oil Recovery Symposium held in Tulsa, Oklahoma, U.S.A., 19-23 April.

Gruber, N.G. 1996. Water Block Effects in Low Permeability Gas Reservoirs. *Journal of Canadian Petroleum Technology* **38**(13): 99-13-55.

Gunter, W.D., Wiwchar, B., and Perkins, E.H., 1997. Aquifer Disposal of CO_2-Rich Greenhouse Gases: Extension of the Time Scale of Experiment for CO_2-Sequestring Reactions by Geochemical Modeling. *Mineral Petroleum,* **59**, (1-2), pp. 121-140.

Gunter, W.D., Perkins, E.H., and Hutcheon, I. 2000. Aquifer disposal of acid gases: modelling of water–rock reactions for trapping of acid wastes. *Applied Geochemistry* **15**(8): 1085-1095.

Izgec, O., Demiral, B., Bertin, H., and Akin, S. 2005. Experimental and Numerical Investigation of Carbon Sequestration in Saline Aquifers. Paper SPE 94697 presented at SPE/EPA/DOE Exploration and Production Environmental Conference held in Galveston, Texas, 7-9 March.

Izgec, O., Demiral, B., Bertin, H., and Akin, S. 2005. CO_2 Injection in Carbonates. Paper SPE 93773 presented at the SPE Western Regional Meeting held in Irvine, CA, 30 March-1 April.

Izgec, O., Demiral, B., Bertin, H., and Akin, S. 2006. Experimental and Numerical Modeling of Direct Injection of CO_2 into Carbonate. Paper SPE 100809 presented at the SPE Annual Technical Conference and Exhibition held in San Antonio, Texas, 24-27 September.

Jacquemet, N., Le Gallo, Y., Estublier, A., Lachet, V., von Dalwigk, I., Yan, J., Azaroual, M., and Audigane, P. 2009. CO_2 streams containing associated components - a review of the thermodynamic and geochemical properties and assessment of some reactive transport codes. *Energy Procedia* **1**(1): 3739-3746.

Jimenez-Lopez, C., Romanek, C.S., and Caballero, E., 2006. Carbon Isotope Fractionation in Synthetic Magnesian Calcite. *Geochimica et Cosmochimica Acta* **70**(5): 1163–1171.

Juanes, R., Spiteri, E.J., Orr Jr., F.M., Blunt, M.J., 2006. Impact of Relative Permeability Hysteresis on Geological CO_2 Storage. *Water Resources Research* **42**,W12148.

Karl T. R., Trenberth K. E., 2003. Modern Global Climate Change. *Science* **302** (5651): 1719–23.

Kitano, Y., Tokuyama, A., and Arakaki, T., 1979. Magnesian Calcite Synthesis from Calcium Bicarbonate Solution Containing Magnesium and Barium Ions. *Geochemical Journal* **13**(1): 181-185.

Knauss, K.G., Johnson, J.W., and Steefel, C.I. 2005. Evaluation of the impact of CO_2, co-contaminant gas, aqueous fluid and reservoir rock interactions on the geologic sequestration of CO_2. *Chemical Geology* **217** (3): 339–350.

Krumhansl, J., Pawar, R., Grigg, R., Westrich, H., Warpinsk, N., Zhang, D., Jove-Colon, C., Lichtner, P., Lorenz, J., Svec, R., Stubbs, B., Cooper, S., Bradley, C., Rutledge, J., and Byrer C. 2002. Geological Sequestration of Carbon Dioxide in a Depleted Oil Reservoir. Paper SPE 75256 presented at the SPE/DOE Improved Oil Recovery Symposium held in Tulsa, Oklahoma, 13–17 April.

Kuo, C.W., Perrin, J.C., and Benson, S.M., 2010. Effect of Gravity, Flow Rate, and Small Scale Heterogeneity on Multiphase Flow of CO_2 and Brine. Paper SPE 132607 presented at SPE Western Regional Meetingheld in Anaheim, California, 27-29 May.

Lee, Y.-J. and Morse, J.W., 1999. Calcite precipitation in synthetic veins: Implications for the time and fluid volume necessary for vein filling. *Chemical Geology* **156** (1): 151–170.

Li, L., Peters, C.A., Celia, M.A. 2005. Upscaling geochemical reaction rates using pore-scale network modeling. *Advances in Water Resources* **29**(9): 1351-1370.

Linnikov, O.D., and Podbereznyi, V.L., 1995. Prevention of sulfate scale formation in desalination of Aral Sea water. *Desalination* **105** (1): 143-150.

Liu, L., Suto, Y., Bignall, G., Yamasaki, N., and Hashida, T. 2003. CO_2 injection to granite and sandstone in experimental rock/hot water systems. *Energy Conversion and Management* **44**(9): 1399-1410.

Mahmoud, M.A., Nasr-El-Din, H.A., De Wolf, C.A. and Alex, A.K. 2011. Sandstone Acidizing Using A New Class of Chelating Agents. Paper SPE 139815 presented at the SPE International Symposium on Oilfield Chemistry, The Woodlands, Texas, USA. 11-13 April.

Marshall, W.L., and Slusher, R., 1968. Aqueous Systems at High Temperature. Solubility to 200°C of Calcium Sulfate and Its Hydrates in Seawater and Saline Water Concentrates, and Temperature-Concentration Limits, *J. Chem. Eng. Data* **13**(1): 83-93.

Mathis, R.L., and Sears, S.O., 1984. Effect of CO_2 Flooding on Dolomite Reservoir Rock, Denver Unit, Wasson (San Andres) Field, TX. Paper SPE 13132 presented at SPE Annual Technical Conference and Exhibition held in Houston, Texas, 16-19 September.

Meehan, D. N., 1980, Estimating Water Viscosity at Reservoir Conditions, *Petroleum Engineering*: 117-118.

Meggyesy, S.D., Jagucki, P.E., Gerst, J., and Place, M., 2008. Case Study: Evaluation of Regional Lithology for Carbon Dioxide Storage Using a Single Test Well in Southeastern Ohio. Paper SPE 117591 presented at the SPE Eastern Regional/AAPG Eastern Section Joint Meeting held in Pittsburgh, Pennsylvania, USA, 11–15 October.

Meijer, J.A.M. and Van Rosmalen, G.M.,1984. Solubilities and Supersaturations of Calcium Sulfate and its Hydrates in Seawater. *Desalination*, **51** (3): 255-305.

Mito, S., Xue, Z., and Ohsumi, T., 2008. Case study of geochemical reactions at the Nagaoka CO_2 injection site, Japan. *International Journal of Greenhouse Gas Control* **2**(3): 309-318

Morgenthaler, L.N., Lawson, J.B., Faircloth, R.J., Berkshire, D.C., 1993. Scale Prediction and Control in the Denver Unit CO_2 Flood. Paper SPE 26603 presented at SPE Annual Technical Conference and Exhibition held in Houston, Texas, 3-6 October.

Nasr-El-Din, H.A., Lynn, J.D., and Al-Dossary, K.A. 2002. Formation Damage Caused by a Water Blockage Chemical: Prevention Through Operator Supported Test Programs. Paper SPE 73790 presented at the International Symposium and Exhibition on Formation Damage Control, Lafayette, Louisiana ,20-21 February 20.

Nghiem, L., Yang, C., Shrivastava, V., Kohse, B., Hassam M., and Card, C. 2009. Risk Mitigation Through the Optimization of Residual Gas and Solubility Trapping for CO_2 Storage in Saline Aquifers. *Energy Procedia* **1**(1): 3015-3022.

Nighswander, J.A., Kaiogerakis, N., and Mehrotra, A.K., 1989. Solubilities of Carbon Dioxide in Water and 1 wt % NaCl Solution at Pressures up to 10 MPa and Temperatures from 80 to 200°C. *J. Chem. Eng. Data* **34**(3): 355-360.

Nightingale, M., Johnson, G., Shevalier, M., Hutcheon, I., Perkins, E., and Mayer, B. 2009. Impact of Injected CO_2 on Reservoir Mineralogy During CO_2-EOR. *Energy Procedia* **1**(1) :3399-3406.

Omole, O., Osoba, J.S., 1983. Carbon Dioxide - Dolomite Rock Interaction During CO_2 Flooding Process. Paper CIM 83-34-17 presented at the Annual Technical Meeting held in Banff, May 10 – 13.

Partridge, E.P., and White, A.H., 1929. The Solubility of Calcium Sulfate from 0 to 200°, *J. Am. Chem. Soc*., **51;**437-442.

Pauwels, H., Gausa, I., Nindre, Y.M., Pearce, J., and Czernichowski-Lauriol, I. 2007. Chemistry of fluids from a natural analogue for a geological CO_2 storage site (Montmiral, France): Lessons for CO_2–water–rock interaction assessment and monitoring. *Applied Geochemistry* **22**(12): 2817–2833.

Pentland, C.H., El-Maghraby, R., Georgiadis, A., Iglauer, S., Blunt, M.J. 2011. Immiscible Displacements and Capillary Trapping in CO_2 Storage. Energy Procedia 4: 4969-4976.

Perrin , J., Krause, M., Kuo, C., Miljkovic, L., Charoba, E., and Benson, S.M. 2009. Core-scale experimental study of relative permeability properties of CO_2 and brine in reservoir rocks. *Energy Procedia* **1**(1):3515-3522.

Pokrovsky, O.S., Golubev, S.V., Schott, J., and Castillo, A., 2005. Dissolution kinetics of calcite, dolomite and magnesite at 25°C and 0 to 50 atm pCO_2. *Chemical Geology* **217**(3-4): 239-255.

Pokrovsky, O.S., Golubev, S.V., Schott, J., and Castillo, A., 2009. Calcite, dolomite and magnesite dissolution kinetics in aqueous solutions at acid to circumneutral pH, 25 to 150 °C and 1 to 55 atm pCO_2: New constraints on CO_2 sequestration in sedimentary basins. *Chemical Geology* **265**(1-2): 20-32.

Pruess, K., Xu, T., Apps, J., and Garcia, J., 2003. Numerical Modeling of Aquifer Disposal of CO_2. *Society of Petroleum Engineers Journal,* **8** (1): 49-60.

Prutton, C.F., and Savage, R.L. 1945. The Solubility of Carbon Dioxide in Calcium Chloride-Water Solutions at 75, 100, 120° and High Pressures. *J. Am. Chem. Soc*. **67**(9): 1550–1554.

Raistrick, M., Hutcheon, I., Shevalier, M., Nightingale M., Johnson, G., Taylor, S., Mayer, B., Durocher, K., Perkins, E., and Gunter, B., 2009. Carbon dioxide-water-silicate mineral reactions enhance CO_2 storage; evidence from produced fluid measurements and geochemical modeling at the IEA Weyburn-Midale Project. *Energy Procedia* **1** (1): 3149–3155.

Sayegh, S.G., Krause, F.F., Girard, M., DeBree, C. 1990. Rock/Fluid Interactions of Carbonated Brines in a Sandstone Reservoir: Pembina Cardium, Alberta, Canada. Paper SPE 19392, *SPE Formation Evaluation* **5**(4): 399-405.

Shariat, A., Moore, R.G., Mehta, S.A., Van Fraassen, K.C., Newsham, K.E. and Rushing, J.A. 2012. Laboratory Measurements of CO_2-H_2O Interfacial Tension at

HP/HT Conditions: Implications for CO_2 Sequestration in Deep Aquifers. Paper CMTC 150010 presented at the Carbon Management Technology Conference, Orlando, Florida, 7-9 February.

Sorensen, J.A., Holubnyak, Y.I., Hawthorne, S.B., Miller, D.V., Eylands, K., Steadman, E.N., and Harju J.A. 2009. Laboratory and numerical modeling of geochemical reactions in a reservoir used for CO_2 storage. *Energy Procedia, Greenhouse Gas Control Technologies 9* **1**(1): 3391–3398.

Svensson, U., and Dreybrodt, W. 1992. Dissolution kinetics of natural calcite minerals in CO_2–water systems approaching calcite. Equilibrium. *Chemical Geology* **100**(1): 129-145.

Taberner, C., Zhang, G., Cartwright, L., and Xu, T., 2009. Injection of Supercritical CO_2 into Deep Saline Carbonate Formations, Predictions from Geochemical Modeling. Paper SPE 121272 presented at EUROPEC/EAGE Conference and Exhibition held in Amsterdam, The Netherlands. 8-11 June.

Takasawa, T., Kawamura, T., and Arihara, N., 2010. Effects of CO_2 Density and Solubility on Storage Behavior in Saline Aquifers. SPE paper 133743, presented at SPE Aisa Pacific Oil & Gas Conference and Exhibition held in Brisbane, Australia, 18-20 October.

Talash, A.W., Crawford, P.B. 1964. Rock properties computed from random pore size distribution. Paper SPE 790-MS.

Torn, A., Torabi, F., Asghari, K. and Mohammadpoor, M. 2012. Effects of Aquifer Parameters on Long-Term Storage of Carbon Dioxide in Saline Aquifers. Paper

CMTC 151485 presented at the Carbon Management Technology Conference, Orlando, Florida, USA, 7-9 February.

Vernik, L. 2000. Permeability Prediction in Poorly Consolidated Siliciclastics Based on Porosity and Clay Volume Logs. *Petrophysics* **41**(2): 2000-v41n2a1.

Watts, R.J., Gehr, J.B., Wasson, J.A., Evans, D.M., and Locke, C.D. 1982. A Single CO_2 Injection Well Minitest in a Low-Permeability Carbonate Reservoir. *Journal of Petroleum Technology* **34**(8):1781-1788.

Warner Jr., H.R. 1977. An Evaluation of Miscible CO_2 Flooding in Waterflooded Sandstone Reservoirs. Paper SPE 6117, *Journal of Petroleum Technology* **29**(10): 1339-1347.

Warren, J., 2000. Dolomite: Occurrence, evolution and economically important Associations. *Earth-Science Reviews* **52**(1-3):1-81.

Wellman, P.T., Grigg, R.P., McPherson,B.J., Svec, R.K., and Lichtner, P.C., 2003. Evaluation of CO_2-Brine-Reservoir Rock Interaction with Laboratory Flow Tests and Reactive Transport Modeling. Paper SPE 80228 presented at the SPE International Symposium on Oilfield Chemistry held in Houston, Texas, U.S.A., 5–7 February.

Wigand, M., Carey, J.W., Schütt, H., Spangenberg, E., and Erzinger. J. 2009. Geochemical effects of CO_2 sequestration in sandstones under simulated in situ conditions of deep saline aquifers. *Applied Geochemistry* **23**(9): 2735-2745.

Xu, T., Sonnenthal, E., Spycher, N., and Pruess, K. 2006. TOUGHREACT—A simulation program for non-isothermal multiphase reactive geochemical transport in

variably saturated geologic media: Applications to geothermal injectivity and CO_2 geological sequestration. *Computers & Geosciences* **32** (2): 145–165.

Zhou, D., Fayers, F.J., and Orr, F.M., 1994. Scaling of Multiphase Flow in Simple Heterogeneous Porous Media. Paper SPE 27833, *SPE Reservoir Engineering* **12**(3): 173-178.